EXPLOITING GLOBULAR CLUSTER PULSARS AS PROBES OF THEIR ENVIRONMENT

FEDERICO ABBATE

Dottorato di Ricerca in Fisica ed Astronomia
Dipartimento di Fisica 'G. Occhialini'
Scuola di Scienze
Università degli Studi Milano - Bicocca

January 2020

SUPERVISORS:
Prof. Monica Colpi
Prof. Andrea Possenti

LOCATION:
Dipartimento di Fisica 'G. Occhialini'
Università degli Studi Milano - Bicocca
Piazza della Scienza 3, I-20126, Milano, Italy

ABSTRACT

The discovery of pulsars has been revolutionary for astronomy and opened the possibility of performing extremely high precision timekeeping in our Galaxy. The pulsars, with their broadband lighthouse-like emission and stability of their rotation, have the perfect characteristics to probe the potential well and the gaseous environments around them.

The dense globular clusters that surround the Galaxy are some of the most efficient factories of fast pulsars (known as millisecond pulsars) and are extremely fascinating objects to study. In their very centres they are thought to contain intermediate mass black holes (IMBHs), the missing links between the stellar black holes and the supermassive ones that inhabit the centres of galaxies, and the key to understanding the black hole population and evolution. Furthermore, the gas content and magnetic field of the globular clusters is able to probe the large scale magnetic field of the Galaxy, especially in the largely unknown Galactic halo.

The presence of pulsars allows us to study the clusters with unprecedented precision. We can estimate the acceleration felt by the pulsar by measuring the derivative of the rotation period. This allows us to study the mass density profile of the cluster and look for deviations that might be caused by the presence of an IMBH. The effects of a central black hole are visible also in the derivatives of the acceleration that can be measured by timing the pulsar for long periods. The broadband nature of the pulsar emission enables the study of the ionized gas content and the magnetic field through the effects of dispersion and Faraday rotation.

I apply these techniques to globular cluster 47 Tucanae that contains 25 known pulsars and measure the structural parameters of the cluster. I confirm the presence of ionized gas, test different distribution models, and discover, for the first time, a magnetic field in the cluster. No magnetic field has ever been proposed in a globular cluster, but the observations suggest that it is present and is about one order of magnitude stronger than what energy equipartition with the gas would imply. In this thesis I claim that the magnetic field is caused by an interaction of the cluster with a magnetized outflow from the Galactic disk that extends in the halo. Such an outflow has been previously proposed and here finds confirmation.

No IMBH is found in 47 Tucanae with mass higher than 4000 $M_\odot$. However, the study of another cluster returned more exciting results. The globular cluster M62 has three known pulsars close to the centre which have accelerations that are not compatible with the published

density profile. An excess of $\sim$ 3900 $M_\odot$ with a 68% confidence interval of (1200,6000) $M_\odot$ is found in the central region. This excess has a very high mass to light ratio and could be due to an IMBH or a system of stellar mass black holes. Only with more observations and simulations tailored to this cluster, the IMBH can be confirmed.

In my thesis I further explore the possibility of using the knowledge gained from the globular cluster pulsars to probe the formation history of the stellar cluster that surrounds the Galactic centre. One possible formation scenario points towards the tidal disruption of stellar clusters. Although no millisecond pulsars have been found in the region, using simulations, I show what the distribution of pulsars should be and where we should look to find them.

The scientific discoveries possible with globular cluster pulsars are diverse and can extend out of the clusters into the entire Galaxy. The future of this field will be dominated by the next generation radio-telescopes like the new MeerKAT radio telescope in South Africa which promises to revolutionize our knowledge of pulsars. In the final chapter I describe this facility and what it will be able to achieve in the field of globular cluster pulsars.

CONTENTS

ACRONYMS

AGB Asymptotic Giant Branch

ATNF Australia Telescope National Facility

BIPM Bureau International des Poids et Mesures

CMB Cosmic Microwave Background

DM Disperion Measure

FWHM Full Width Half Maximum

GC Globular Cluster

GPS Global Positioning System

GR General Relativity

ICM Intracluster Medium

IMBH Intermediate Mass Black Hole

ISM Insterstellar Medium

LMXB Low Mass X-ray Binary

MCMC Markov Chain Monte Carlo

MEM Measurement Equation Modelling

METM Measurement Equation Template Matching

MSP Millisecond Pulsar

NSC Nuclear Star Cluster

PA Position Angle

PDF Probability Distribution Function

RFI Radio Frequency Interference

RGB Red Giant Branch

RM Rotation Measure

RVM Rotating-Vector Model

SARAO South African Radi Astronomical Observatory

SKA Square Kilometre Array

SMBH Super Massive Black Hole

SNR Supernova Remnant

SSB Solar System Barycentre

S/N Signal to Noise Ratio

TAI International Atomic Time

ToA Time of Arrival

TT Terrestrial Time

UTC Universal Time Coordinated

WD White Dwarf

1 INTRODUCTION

Over 50 years have passed from the discovery of pulsars [175] and while much about these strange objects is still unknown, they have become essential tools for many different branches of physics thanks to their unique properties [126, 228]: the densities and pressures found in the centre of these stars are so extreme that they can't be replicated in any laboratory on Earth and are thus essential to nuclear physicists looking for exotic matter [221]; the highly magnetized and relativistic plasma found in the magnetosphere of pulsars is studied by plasma physicists interested in the emission mechanism [87]; The extreme rotational stability of pulsars and the discovery of binary systems with other compact objects has allowed General Relativity (GR) experts to put some of the strongest constraints on the validity of GR [213] and test alternative theories of gravity [29, 141]; The long term rotational stability of pulsars and the significant number of binary neutron stars in compact orbits has also attracted gravitational waves astronomers interested in the mergers of those objects [7] and in their applicability as clocks to look for very low frequency gravitational waves [104, 214, 251]; finally, the impulsive and broadband nature of the pulsar emission are very important for Galactic astronomers interested in the ionized gas content of the Galaxy and its magnetic field [278].

1.1 NEUTRON STARS

The concept of a star entirely made of neutrons was brought forward soon after the discovery of the neutron itself [33, 34, 219][1]. These stars were thought to be entirely composed of neutrons whose interactions could halt the gravitational collapse giving rise one of the densest stable configuration of matter possible in nature, much denser than white dwarfs and just shy of becoming a black hole. The mass of these stars would be similar to that of the Sun but would be contained in a diameter of a few tens of kilometers and the densities would be close to the ones found in atomic nuclei [282]. The first observational proof of the existence of these stars came in 1967 thanks to Jocelyn Bell, a doctoral student at Cambridge [175]. It was an accidental discovery. The original rationale behind the observations was to observe quasars in the radio band through interplanetary scintillation. A pulsed source was seen repeating every ~ 1.337 s. The source followed sidereal time and not the 24h cycle, so artificial interference was ruled out. After

1 A reconstruction of the history of the period shows that Landau's prediction of neutron stars actually predates the discovery of the neutron by Chadwick [359]

a few months and the discovery of more similar objects it became clear that the pulsed radiation came from a rotating neutron star. The picture became complete more than one year later when a pulsar was discovered inside the Crab nebula [331]. This nebula was associated with the explosion of a supernova which was known to be a possible formation scenario for neutron stars. Because of this discovery, the Nobel prize in Physics was awarded to Jocelyn Bell's supervisor, Anthony Hewish, and Martin Ryle in 1974. It was the first time such a prestigious award was granted to astronomers.

1.1.1 *Observational properties*

Neutron stars are usually observed either as pulsars or as accretion powered sources in binary systems. Thanks to these observations it is possible to test different models was possible measure some properties of these peculiar objects like the mass and the radius.

The mass of such objects can be precisely measured using pulsar timing techniques in binary pulsars (see section 2.2). The distribution of the measured masses is peaked at around 1.4 $M_\odot$ [284], extends at lower values to 1.2 $M_\odot$ [258] and has a long high mass tail to masses above 2.0 $M_\odot$ [17, 99].

The radius of neutron stars can be directly probed using the thermal emission from the surface. Measuring the temperature and estimating the distance of the neutron star it is possible to recover the emitting surface area from the luminosity. The thermal emission is usually observed in X-rays and can be used to put stringent limits on the dimensions of the star. These observations led to measurements of radii between 7 and 14 km [59].

1.2 PULSARS

What characterises a neutron star as a pulsar is the characteristic pulsed emission. The emission originates from a small region in the magnetosphere of the neutron star in the form of a beam that sweeps the sky as it rotates around the rotation axis. The beam intercepts the Earth's line of sight only over small rotational phases and this causes the pulsation that we see. This emission can be observed at different frequencies bands in the electromagnetic spectrum from radio to optical, X-rays and gamma rays. A few hundreds have been observed in X-rays and in gamma rays [9, 246] and only a few have been observed in optical [321]. The large majority of pulsars are observed in the radio band with over 2700 known radio pulsars [250][2]. In what follows I will concentrate on the radio emission of pulsars but there are significant overlaps with other frequency bands.

2 see the following website for an updated list of all known pulsars and their properties: http://www.atnf.csiro.au/people/pulsar/psrcat/

In the radio band the emission is non thermal in nature with a very high brightness temperature. The period varies between 1.4 ms [174] and over 23 s [338]. The period is not constant but is observed to increase in time as the neutron star loses rotational energy. The amount of energy lost can be estimated by measuring the period, P, and the rate of increase of the period, $\dot{P}$, as follows:

$$\dot{E} = \frac{dE_{rot}}{dt} = \frac{dI\Omega^2/2}{dt} = -I\Omega\dot{\Omega} = 4\pi^2 I\dot{P}P^{-3}, \tag{1.1}$$

where I is the moment of inertia of the neutron star, $\Omega = 2\pi/P$ is rotational angular frequency. The moment of inertia of a neutron has not yet been measured directly (although this might be possible in the future [101]) but can be estimated from the typical mass (1.4 $M_\odot$)and radius (10 km) to be $I = kMR^2 = 10^{45} g\, cm^2$ assuming the geometry to be that of a sphere of uniform density ($k = 0.4$). The quantity $\dot{E}$ is called *spin-down luminosity*.

This loss of energy that causes the neutron star to slow down does not come from the observed radiation but from the intense magnetic fields. Neutron stars contain some of the strongest magnetic fields in the universe going from $10^8 - 10^{15}$ G with a dipolar geometry. A strong magnetic dipole in fast rotation, according to classical electrodynamics [190], radiates energy and slows down the rotation. The energy lost by this process can be written as:

$$\dot{E}_{dipole} = \frac{2}{3c^3}|\mathbf{m}|^2\Omega^4 \sin^2\alpha, \tag{1.2}$$

where $\mathbf{m}$ is the magnetic moment and α is the angle between the magnetic axis and the spin axis. In the case of a dipole, the magnetic moment becomes $|\mathbf{m}| = B_p R^3/2$, where B_P is the strength of the magnetic field at the equator, and R is the radius of the neutron star. Equating the energy lost by this process to the spin-down luminosity we obtain:

$$4\pi^2 I\dot{P}P^{-3} = -\dot{E}_{dipole} = -\frac{B_p^2 R^6 \Omega^4 \sin^2\alpha}{6c^3}, \tag{1.3}$$

from which we derive the spin down rate as:

$$\dot{P} = -\frac{2\pi^2 B_p^2 R^6 \sin^2\alpha}{3Ic^3}\frac{1}{P}. \tag{1.4}$$

Since we can measure both the period P and the spin down rate $\dot{P}$ and assuming $\alpha = 90^\circ$, we can use this relation to derive the strength of the magnetic field at the surface of the neutron star:

$$B_p = \sqrt{\frac{3c^3 I}{2\pi^2 R^6 sin^2\alpha}\dot{P}P} \simeq 10^{12}\,\mathrm{G}\left(\frac{\dot{P}}{10^{-15}}\right)^{1/2}\left(\frac{P}{\mathrm{s}}\right)^{1/2}. \tag{1.5}$$

This value of the magnetic field strength must be considered only an order of magnitude estimate given the numerous assumptions in the model.

From eq. 1.4 it is also possible to measure the age of the neutron star by solving the differential equation as a function of time. Assuming that at birth the rotational period was much shorter than it is now, we find a characteristic age of:

$$\tau_c = \frac{P}{2\dot{P}} \simeq 15.8\,\mathrm{Myr} \left(\frac{P}{\mathrm{s}}\right) \left(\frac{\dot{P}}{10^{-15}}\right)^{-1}. \tag{1.6}$$

Estimating this value for the Crab pulsar gives a characteristic age of 1260 yr which is comparable to the real age of 966 yr. This result helped consolidate the theory of magnetic dipole breaking but it is not always consistent with observations. In some cases the discrepancy between the age estimated with the formula above and the real age can be very large, like in the case of pulsar J0538+2817 which has a characteristic age of 620 kyr and an age estimated from proper motion of only 30 kyr [212].

A problem that the model described faces is that it works only in vacuum. This assumption manifests itself in the dependence on the angle α between the magnetic axis and the rotation axis. If the two axes are aligned, the theory prescribes that there should be no losses since the magnetic field geometry is not changing. This assumption breaks down when we try to apply basic equations of electromagnetism to the surface of the neutron star. On the surface there is thin layer where the pressure is low enough that free protons and electron can survive. The very strong magnetic field (around 10^{12} G) on the surface induces an electric field in the vacuum that exerts a force on the particles that can exceed gravity by 10 orders of magnitude. Thus, the particles are extracted from the surface and create a magnetosphere around the pulsar. This magnetosphere will be static with respect to the magnetic field lines and will co-rotate with the surface until the rotation speed exceeds the speed of light. This radius where this speed is achieved is called *light-cylinder radius*. This co-rotating magnetosphere causes an effect similar to the magnetic dipole breaking and is not dependent on the orientation of the magnetic axis. Simulations show that in these conditions the energy loss is comparable to the one of the magnetic dipole in vacuum but does not have a strong dependence on the alignment.

A way to test the described model is to measure the second time derivative of the period. This is a difficult task possible only for a few pulsars (see section 2.2), but it gives us access to the breaking index, n. It is defined as the power law index describing the evolution of the spin frequency $\nu = 1/P$ in the equation:

$$\dot{\nu} = -K\nu^n, \tag{1.7}$$

where K is a constant. From eq. 1.4 we find that in the case of a magnetic dipole $n = 3$. By taking the time derivative of his equation we find:

$$n = \frac{\ddot{\nu}\nu}{\dot{\nu}^2}. \tag{1.8}$$

Measurements of the second period derivative show that the breaking index varies from 0.9 to 2.8 [239] with a record value of 3.15 [30], the only one above the canonical value of 3. Therefore, the assumption that $n = 3$ for all pulsars is not consistent with observations. However, the magnetic breaking model is still essential to define a number of useful quantities and is used regularly by pulsar astronomers.

1.2.1 *Pulsar population*

According to the standard model described above, the properties of pulsars can be estimated by the rotational period P and the time derivative $\dot{P}$. Starting from these two observables we can plot the entire pulsar population on the so called $P - \dot{P}$ *diagram* shown in Figure 1.1. Different types of pulsars can be separated using this diagram. The canonical pulsars are shown in the green circle. They represent the bulk of the populations, have spin periods between a few tenths of a second and a few seconds with a period derivative between 10^{-17} and 10^{-12} s s^{-1}. The magnetic field is between 10^{11} and 10^{13} G and the characteristic age can vary from being very young, 1 kyr to very old 1 Gyr. These pulsars are usually isolated and, when they are young, can be associated with a Supernova Remnant (SNR). The formation scenario of these pulsars is explained in Section 1.3.

The red circle shows the Millisecond Pulsars (MSPs), they have spin periods between 1 ms and a few tens of ms with very low period derivative, around 10^{-20} s s^{-1}. The magnetic field is low, around $10^8 - 10^9$ G and the characteristic age is higher then 1 Gyr and in some cases can be longer than the age of the Universe. They are in large majority in binaries and there are no known SNR association. The formation process can explain all of these properties (see Section 1.4).

Lastly the blue circle shows the so-called *magnetars*. They are very young pulsars, $\tau_c \sim 1$ kyr, with very high magnetic fields, $B_p \sim 10^{14} - 10^{15}$ G, and almost all of them are associated with a SNR. They are some of the slowest known pulsars and while they appear very bright in other frequency bands, only four are seen as transient radio pulsars.

1.2.2 *Pulsar emission*

The radio emission of the pulsars originates in the polar region of the neutron star magnetosphere. It can have very different shapes for different pulsars (see examples in Figure 1.2): in some cases the

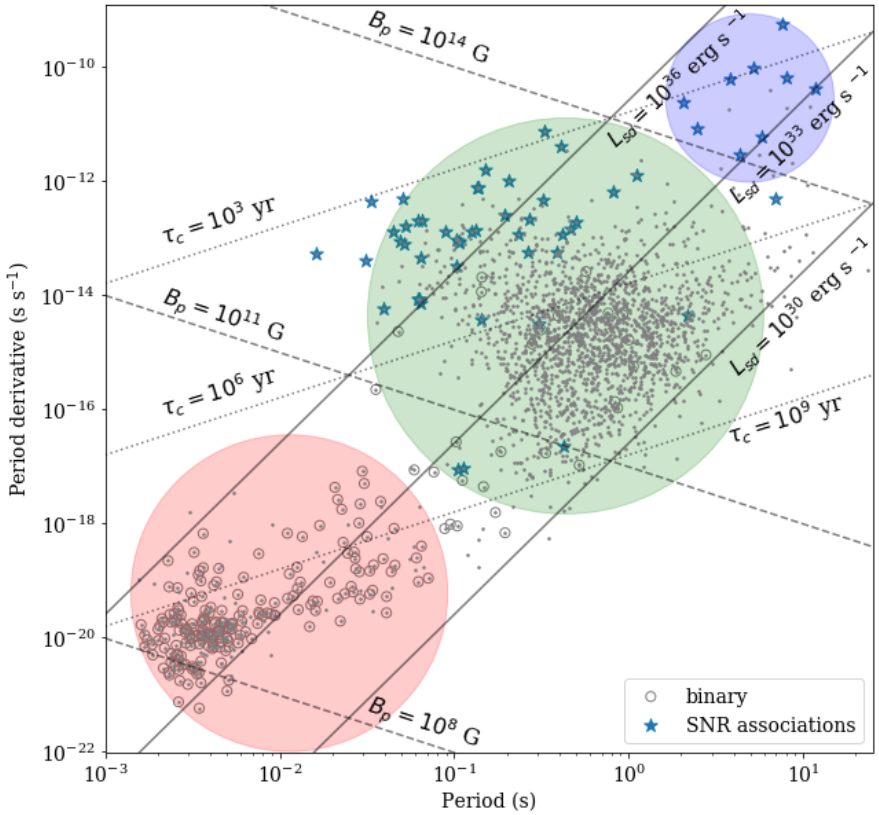

Figure 1.1: $P - \dot{P}$ diagram for for 2259 pulsars present in the PSRCAT catalogue[250]. Lines of constant spin-down luminosity, L_{sd}, magnetic field, B_p and characteristic age τ_c. Pulsars in binary systems have been highlighted with circles and pulsars associated with a supernova remnant with a blue star. The red circle shows the position of the millisecond pulsars, the green circle the position of the canonical pulsars and the blue circle shows the magnetars.

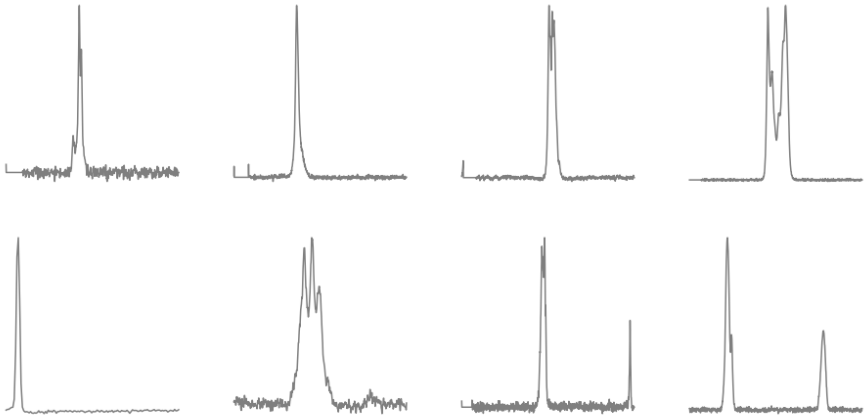

Figure 1.2: Profiles of a selection of pulsars at 1.4 Ghz. The pulsars are: J0147+5922 [317], J0543+2329 [317], J0742-2822 [317], J1239+2452 [317], J1327-622 [193], J1705-1906 [317], J1730-2304 [211], J1939+2134 [211].

profile is simple with a single sharp peak, other times it has multiple components or broader peaks.

In some cases, like the last two profiles in Figure 1.2, it can also have an emission feature in the phase opposite to the main pulse, called an *interpulse*. This is commonly interpreted as coming from the polar region opposite to the main pulse. In these cases the rotation axis is almost orthogonal to the magnetic axis and we see both emission cones point towards Earth during the rotation.

Individual pulses from a pulsar are very weak and can only be observed for the brightest pulsars. The rest of the pulsars require coherent addition of hundreds or thousands of pulses for them to rise above the noise forming an 'integrated profile'. While individual pulses can be quite different one from the other, the integrated profile remains very stable over the years. The emission has a spectrum that can typically be described by a power law with a power law index of ~ -1.8 [257]. A small number of pulsars do not follow this simple relation but have a spectrum peaked at around 1 Ghz [202].

The emission of a pulsar can display some of the highest degrees of polarization; while some can appear unpolarized, others can be almost entirely linearly polarized. Typically more energetic pulsars have higher degrees of linear polarization (around 20 percent for those with $L_{sd} < 5 \times 10^{33}$ and more than 50 percent in those where $L_{sd} > 2 \times 10^{35}$ erg s^{-1}) [158, 356, 373]. Pulsars also display a significant amount of circular polarization ($\sim$ 10 percent).

The high degree of linear polarization allows us to measure the polarization Position Angle (PA). The PA is the angle with respect to the celestial North along which the electric filed of the incoming electromagnetic radiation is oscillating. Determining the PAs and how they vary along the pulse profile can help study the geometry and the

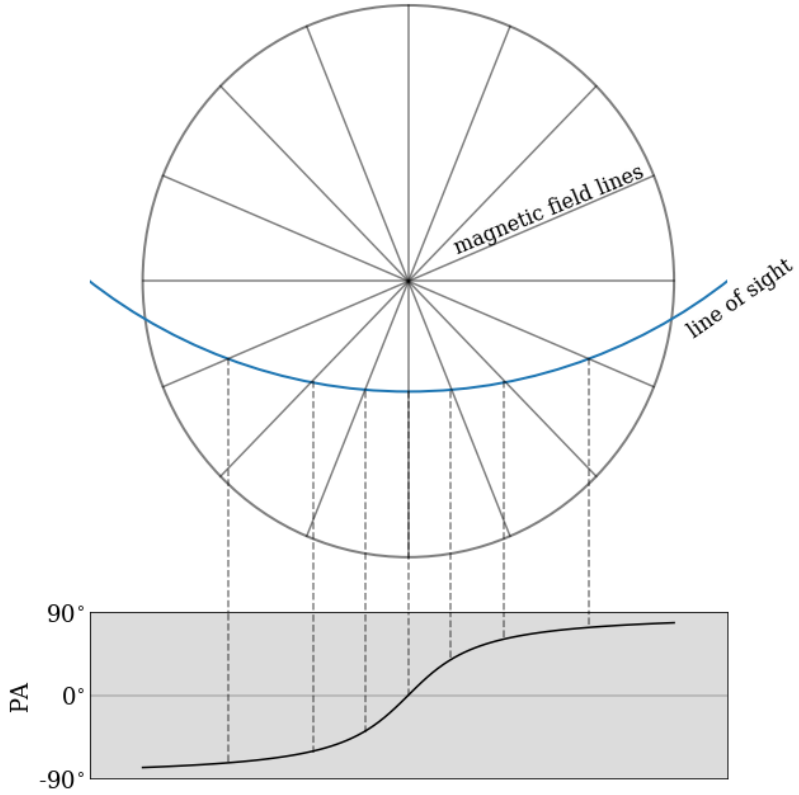

Figure 1.3: Sketch of the RVM. The top panel shows the emission beam and the path crossed by the line of sight (blue line) during a rotation. The magnetic field lines are pointing radially outwards (or inwards depending if we are looking at the North or South pole). The line of sight will cross regions with different magnetic field orientation and the emission from the regions crossed by the line of sight will have polarization parallel to the magnetic field lines. The bottom panel shows the swing in PA along the pulse profile.

emission process of the pulsar. In several pulsars the PA swings along an S-shaped curve over the pulse profile, this is usually explained with the so called Rotating-Vector Model(RVM, [303]). In this model, described in Fig. 1.3, the emission originates in a filled cone over the polar regions. In a dipole, the magnetic field lines are oriented radially outwards from the pole. As the line of sight crosses different parts of the emission cone, the inclination angle between the line of sight and the magnetic field lines changes along an S-shaped curve. If the polarization of the emission is thought to be aligned with the magnetic field, we see the same curve in the PAs . From the maximum difference in PA and the maximum rate of change it is possible to estimate the misalignment between the rotation and the magnetic axis and the impact parameter between the line of sight and the magnetic axis. However, it is rare that the formalism of the RVM can be fully applied

and uniquely derive the geometry. The observed PA profiles can be flat or more complex and sometimes show jumps of about 90°. The jumps are usually explained as the superposition of two orthogonal polarization modes [35, 97]. This mixing of modes is associated with a drop in polarization [199].

1.3 BIRTH OF NEUTRON STARS

The standard picture of the birth of neutron stars [294] is linked to supernova explosion of stars heavier than 8-12 $M_\odot$, the exact value changes depending on the metallicity. A star in this mass range evolves through all of the nuclear burning stages up to iron after which production of heavier elements consumes more energy than what it produces. Once a core of iron of about 1.4 $M_\odot$ (a limit known as the Chandrasekhar mass, [89]) is formed the electrons become ultra-relativistic and are no longer able to balance the gravity of the star and the core starts to collapse.

Two main processes happen that reduce the available energy budget and push the collapse even faster: photodisintegration of atomic nuclei and the inverse beta decay. The first happens when the temperature in the core rises to the level that thermal photons have enough energy to break up heavy nuclei. The iron nuclei are broken first in helium nuclei releasing in the core 4 neutrons. Then, as the temperature rises even further, the helium atoms are broken into protons and neutrons. This process absorbs a significant quantity of energy and accelerates the collapse. Simultaneously, the second process, the inverse beta decay, takes place. When electrons are particularly energetic, they can interact with protons, either unbound or in heavier nuclei, to form a neutron and an electronic neutrino. The neutrinos are very weakly interacting and are free to escape outside the core powering the supernova that is happening outside. At the end of these processes all that is left in the collapsing core are just free neutrons. The collapse continues until the neutrons become degenerate and become able to exert the pressure necessary to halt the collapse. What is left at the centre is a neutron star.

This origin can also help explain the fast rotation and high magnetic field of the neutron stars. In the zero order assumption that the supernova explosion does not remove angular momentum or magnetic momentum from the star, we can try to estimate what the rotation and magnetic field of a normal star would be if we reduce it to the size of a neutron star. For reference we shall take the most well known star, the Sun. The angular momentum of the Sun is $\mathcal{L} = R_\odot M_\odot v_\odot$, where $R_\odot$ is the Solar radius, $M_\odot$ is the Solar mass and $v_\odot$ is the rotational velocity of the Sun. We write the velocity as a function of the rotational period $T_\odot$ using the formula $v_\odot = \frac{2\pi}{T_\odot} R_\odot$. If we reduce the Sun to the dimension of an average neutron star and impose conservation of

angular momentum, we obtain, using $R_\odot \sim 7 \times 10^8$ m, $R_{NS} \sim 10^4$ m and $T_\odot \sim 30$d:

$$T_{NS} = T_\odot \left(\frac{R_{NS}}{R_\odot} \right)^2 \sim 0.5\,\text{ms}, \tag{1.9}$$

which is a reasonable birth period for a pulsar.

If we try to collapse the Sun to the typical size of a neutron star, and we impose conservation of the magnetic moment $BR^3 = \text{const}$, we find, using $B_\odot \sim 1$ G,

$$B_{NS} = B_\odot \left(\frac{R_\odot}{R_{NS}} \right)^3 \sim 2 \times 10^{14}\,\text{G}. \tag{1.10}$$

This magnetic field is high but still compatible with what is observed for some pulsars.

After a neutron star is born, it starts spinning down due to magnetic dipole breaking as described in Section 1.2. It evolves in the $P - \dot{P}$ diagram (Fig. 1.1) following a line of constant magnetic field until it reaches the so called *death line* which corresponds to $L_{SD} = 10^{30}$ erg s^{-1}. Once a pulsar crosses this line, the process that powers the radio emission is supposed to shut down and the pulsar is no longer visible. However, as shown if Fig. 1.1, there a few exception to this rule.

1.4 BIRTH OF MILLISECOND PULSARS

The process described above is able to describe the formation of canonical pulsars and magnetars (which are known to have supernovae associations), but does not work for MSPs. For them, the explanation must be searched in a peculiarity shared by most MSPs, the binarity. When a neutron star is in a binary, matter from the companion can accrete on the surface of the neutron star and, in particular conditions, accelerate or slow down the rotation of the neutron star. If the accreting material has lower angular momentum than the material at the surface of the neutron star, like normal stellar winds, the neutron star will slow its rotation. If, on the other hand, the accreting material has higher angular momentum it will accelerate the pulsar and bring the spin period down to a few milliseconds. This standard formation mechanism [14, 370] is usually linked to strong emission of X-rays from the surface of the neutron star in a Low Mass X-ray Binary (LMXB). In a few systems, the X-ray bright state is seen to alternate with standard MSP emission (eg. [28, 286, 332]). These are the so called *transitional MSPs* and are the direct evidence that accretion on a neutron star is linked to the birth of MSPs.

This model is also capable of accounting for the low magnetic field found in MSPs. While during the isolated evolution of a neutron star the magnetic field does not substantially vary [371], accretion can weaken the magnetic field [337]. Various models have been devised to

explain the decay of the magnetic field. One model by Bhattacharya and Srinivasan [50] assumes that the magnetic field is anchored in flux tubes in the superconducting core of the neutron star. During the spin-down, the flux tubes are brought closer to the surface by outgoing vortices and are dissipated since the surface is conductive. This can happen only when the rotation of the neutron star is slowed to hundreds of seconds. Such slow rotations are difficult to occur in isolated neutron stars but can be reached in the presence of a weak wind from a solar type companion. In the later stages of evolution, when the dimensions of the companion grow and the state of a LMXB is reached the rotation period will decrease but the magnetic field cannot come back.

Thanks to the low magnetic fields, MSPs typically live for several billions of years and the time it would take them to reach the *death line* usually exceeds the Hubble time. The binary companion that recycled the pulsar into an MSP is usually seen as a WD in circular orbits (reached through tidal dissipation of the original eccentricity). In some cases the companion also becomes a neutron star and in other cases we see non degenerate stars as companions. Most of these systems are divided in two categories: *black widow* pulsars with a companion mass $\lesssim 0.1\ M_\odot$ where the strong wind of the pulsar is stripping the outer layers of the star; *redback* pulsars with companions in the mass range $\sim 0.1 - 0.5\ M_\odot$. These systems are usually in tight orbits and, because of the large dimensions of the non degenerate star, they sometimes show regular eclipses of the radio signal. These systems are rare in the Galactic disk but are more common in globular clusters as shown in section 1.9.

According to this model, all MSPs must have accreted matter in order to reach the observed spins and must, therefore, be more massive than canonical pulsars. While mass measurements show that MSPs can be significantly more massive than canonical pulsars [139], it is not always the case [284][3]. According to the spatial distribution of MSPs in globular clusters (more details in Chapter 2) it appears that the general population is less massive than expected. To explain these supposedly very light MSPs, different formation scenarios have been invoked like electron-capture supernovae [187, 189]. This is a collapse that can happen in a ONeMg White Dwarf (WD) if its core reaches a mass of $1.38\,M_\odot$. It is triggered by electron capture on ^{24}Mg and ^{20}Ne before further burning can start. This scenario involves much less energy than a classical core collapse supernova and forms a lighter neutron star with much smaller kick velocity. This type of collapse can happen in an isolated WD in particular conditions or in a binary if the WD accretes enough matter, this scenario is called *accretion induced collapse*, or in a merger between WDs, called *merger induced collapse*. Through

3 A more up to date list of measured masses of neutron stars can be found at the website https://www3.mpifr-bonn.mpg.de/staff/pfreire/NS_masses.html

these scenarios, it has been speculated that MSPs can be formed directly without the need for accretion and recycling [137].

1.5 EFFECTS OF INTERSTELLAR MEDIUM

The radiation of the pulsars, before reaching our telescopes, must cross large sections of the Galaxy filled with a low density plasma called Insterstellar Medium (ISM). As the radiation crosses the ISM a large number of effects can disturb the signal and, at times, conceal the pulsar entirely. These effects are due to frequency dispersion, Faraday rotation, scintillation and scattering [228]. However, if these effects are properly accounted for, they can be used as an invaluable probe of the properties of the ISM in different parts of the Galaxy. The following derivation follows Lorimer and Kramer [228].

1.5.1 *Dispersion Measure*

An important property of ionised plasma is that it will respond differently when interacting with radiation of different frequencies. It will show a frequency dependant index of refraction which will cause a delay in the time of arrival of the pulses at different frequencies. The refractive index in a non-magnetised plasma can be expressed as

$$\mu = \sqrt{1 - \left(\frac{f_p}{f}\right)^2}, \tag{1.11}$$

where f is the frequency of the radiation and f_p is the plasma frequency defined as

$$f_p = \sqrt{\frac{e^2 n_e}{\pi m_e}} \simeq 8.5\,\mathrm{kHz} \left(\frac{n_e}{\mathrm{cm}^{-3}}\right)^{1/2}. \tag{1.12}$$

In the previous equation, e is the electron charge, m_e is the electron mass and n_e is the electron number density. Because of the higher mass of the positive ions, their interaction with radiation is dampened and they do not contribute significantly to the previous equation.

The delay between a radio signal of frequency f and a signal of infinite frequency along a path length d is

$$t = \left(\int_0^d \frac{dl}{v_g}\right) - \frac{d}{c}, \tag{1.13}$$

where $v_g = \mu c$ is the group velocity. In the approximation that the observing frequency is much larger than f_p, we find

$$t = \frac{1}{c}\int_0^d \left(1 + \frac{f_p^2}{2f^2}\right) dl - \frac{d}{c} = \frac{e^2}{2\pi m_e c}\frac{\int_0^d n_e dl}{f^2}. \tag{1.14}$$

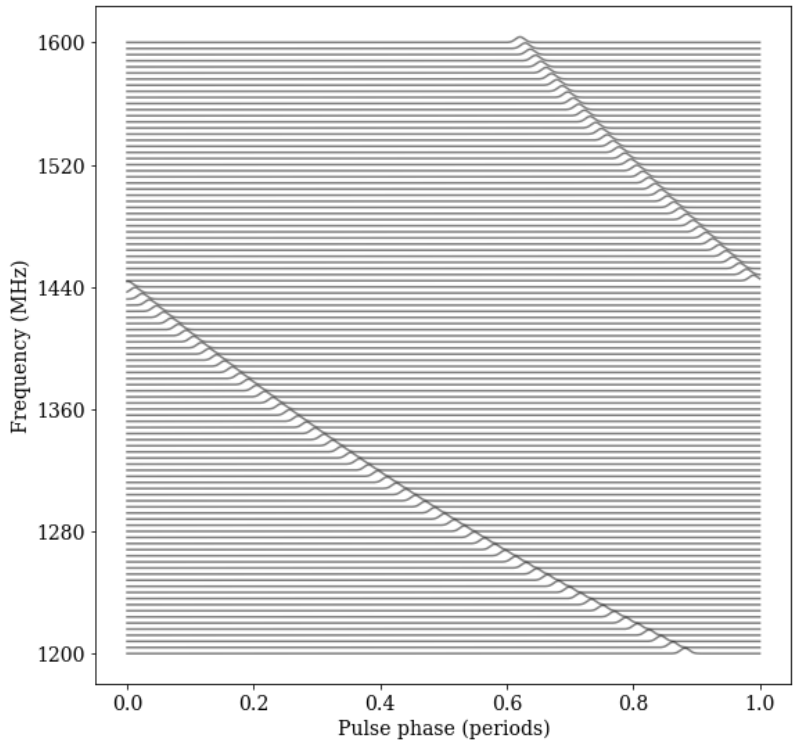

Figure 1.4: Dispersive effects of the ISM on a pulsar in L-band (1200-1600 MHz). The pulsar period is chosen to be 0.1 s and the DM is 100 cm^{-3} pc. Each frequency sees a different refractive index and arrives with a different delay. The quadratic dependence on the frequency is clearly visible.

The integral along the line of sight of the electron number density corresponds to the column density and is called Disperion Measure (DM) and is usually expressed in cm^{-3} pc. The constant in front of eq. 1.14 is called *dispersion constant*, $\mathcal{D}$, can be approximated as 4.15×10^3 MHz^2 pc^{-1} cm^3 s.

A useful expression of the delay between two different frequencies (both expressed in MHz) is

$$\Delta t \simeq 4.15 \times 10^6 (f_1^{-2} - f_2^{-2}) \,\mathrm{DM\,ms}. \tag{1.15}$$

If the frequency band is large, the delay between the top and bottom frequency can easily become larger than the spin period of the pulsar as shown in Fig. 1.4. If this effect is not accounted for using de-dispersion techniques (see Section 2.1), the pulsed signal can appear as a continuous source making the pulsar undetectable.

By measuring the DM for a pulsar we are able to calculate the total column density of electrons in front of the pulsar. Using the DM of different pulsars at different distances in the Galaxy it is possible to estimate distribution of ionised gas in our Galaxy. Alternatively, if the distance along the line of sight of the pulsar is not known, it can be estimated using models of Galactic electron density. The

simplest model assumed a symmetric distribution of electrons [235], while a very successful model was 'NE2001' [96] which incorporated information from pulsars with known distances as calibration. The most recent Galactic electron model is the 'YMW2016' [361]. However, distance estimates obtained using this method can be incorrect if the pulsar is found near high density clouds or in the Galactic halo.

1.5.2 *Rotation Measure*

If the ionised medium is also permeated by magnetic fields, the situation changes slightly. The refractive index becomes

$$\mu = \sqrt{1 - \left(\frac{f_p}{f}\right)^2 \mp \frac{f_p^2 f_B}{f^3}}, \tag{1.16}$$

where the $\mp$ refers to waves of different circular polarisations: left circular polarisation goes with the minus sign while right circular polarisation goes with the plus sign. f_B is the cyclotron frequency and has the form

$$f_B = \frac{eB_\parallel}{2\pi m_e c} \simeq 3\,\mathrm{MHz}\left(\frac{B_\parallel}{\mathrm{G}}\right) \tag{1.17}$$

and depends only on the component of the magnetic field parallel to the line of sight. For typical Galactic magnetic fields ($B \sim 1\,\mu$G) $f_B \sim 3$ Hz. The time difference caused by this difference of refractive indexes between the different polarisations is very small, ~ 1 ns, hence negligible in most cases. It becomes significant only for low frequency observations of pulsars in dense and higly magnetised regions (see Fig. 1 of [336]).

The different propagation speeds for the different polarizations cause a differential phase rotation, known as *Faraday rotation*, of

$$\Delta\Psi_{\mathrm{Faraday}} = \int_0^d (k_R - k_L)dl, \tag{1.18}$$

where k_R and k_L are the wavenumber for the right and left circular polarizations. The wavenumber as a function of frequency, f, can be written as:

$$k(f) = \frac{2\pi}{c}\mu f. \tag{1.19}$$

Substituting the value of the refractive index μ found in 1.16 and 1.17, the phase rotation becomes

$$\Delta\Psi_{\mathrm{Faraday}} = \frac{e^3}{\pi m_e^2 c^2 f^2}\int_0^d n_e B_\parallel dl. \tag{1.20}$$

Usually, the property of the incoming wave that is measured in not the phase itself but the polarisation PA which is the direction in the

plane of the sky where the electric field of the wave is oscillating. This angle is periodic on π rather than 2π, its difference due to the Faraday rotation is

$$\Delta\Psi_{PA} = \Delta\Psi_{\text{Faraday}}/2 = \lambda^2 \text{RM}, \tag{1.21}$$

where λ is the wavelength and RM is the *rotation measure* usually measured in rad m^{-2} defined as:

$$\text{RM} = \frac{e^3}{2\pi m_e^2 c^4} \int_0^d n_e B_\parallel dl. \tag{1.22}$$

A simultaneous measurement of both DM and RM provides the average of the parallel component of the magnetic field in the ISM weighted by the electron density along the line of sight

$$\langle B_\parallel \rangle = \frac{\int_0^d n_e B_\parallel dl}{\int_0^d n_e dl} = 1.23 \mu\text{G} \left(\frac{\text{RM}}{\text{rad m}^{-2}} \right) \left(\frac{\text{DM}}{\text{pc cm}^{-3}} \right)^{-1}. \tag{1.23}$$

The value measured in the previous equation must not be considered a faithful representation of the real magnetic field which can have reversals along the line of sight. However, by measuring RM and DM for many pulsars it is possible to construct and test models of the galactic magnetic field [165, 236, 247, 252, 278, 340]. These studies of the Galactic magnetic field are complementary to the ones performed studying the synchrotron radiation that is sensible to the perpendicular component [74].

1.5.3 *Scintillation*

Like stars in the night sky, point-source radio objects, like pulsars, scintillate. The scintillation is caused by inhomogeneities in the refractive medium that distort the plane of propagation of the radiation and cause interference patterns. If the interference is constructive at the location of the telescope the signal is boosted. On the other hand, if the interference is destructive, the signal is dampened. The presence of scintillation can hide bright pulsars from view and, in favourable condition, reveal very dim pulsars.

Scintillation is stronger for pulsars with small quantities of intervening matter (low DM) and weaker for pulsars with large quantities of intervening matter (high DM). If the radiation has to cross a larger or denser part of the ISM , different parts of it can create constructive and destructive interference patterns and the probability of them being all aligned is very small. Therefore pulsars with high DM are more likely to be flux stable as all interference patterns average out. For pulsars with low DM , on the other hand, the patterns do not average out and the fluctuations are stronger.

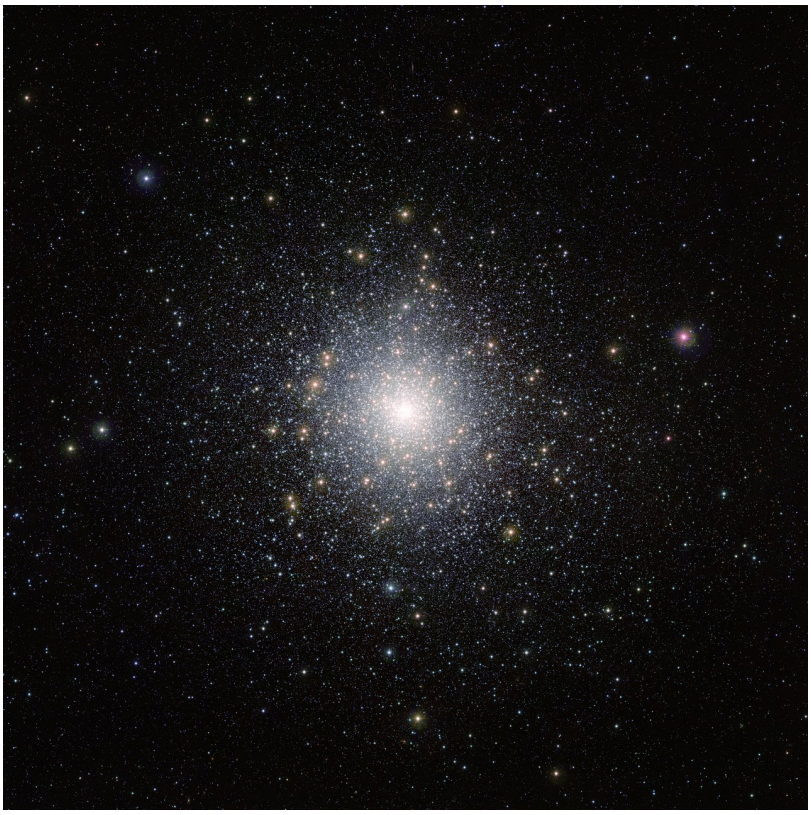

Figure 1.5: Globular cluster 47 Tucanae. Credits: ESO/M.-R. Cioni/VISTA Magellanic Cloud survey.

1.6 GLOBULAR CLUSTERS

Globular Cluster (GC) are usually defined as gravitationally-bound spherical stellar systems which are very old ($\sim$ 10 Gyr), massive ($> 10^5$ $M_\odot$) and with low metallicity. They typically have radii of tens of parsecs and central densities of $\sim 10^3 - 10^6$ $M_\odot$. There are more than 150 GCs in and around our Galaxy and they are located either in the central bulge or in the halo that surrounds the Galactic disk[4]. A key difference between GCs and dwarf galaxies is the absence of star formation and the lack of measurable concentrations of dark matter in the former. A picture of globular cluster 47 Tucanae (also known as NGC 104 hereafter 47 Tuc) is shown in Fig. 1.5.

There are a few exceptions to this definition; a more general and solid definition of GCs has been given by Kruijssen [217]: "A gravitationally-bound, stellar cluster that in terms of its position and velocity vectors does not coincide with the presently star-forming component of its host galaxy."

The term "stellar cluster" excludes dwarf galaxies as they are dark matter-dominated. A GC can pass through a star-forming region of

4 A list of known GCs with their properties can be found at the website: https://people.smp.uq.edu.au/HolgerBaumgardt/globular/

the host galaxy but has a different velocity or it can corotate with the galaxy but outside of star-forming regions.

The stars in a GC are thought to be all coeval, born in a single star-formation episode. Recently precise measurements of the color magnitude diagrams of different GCs have shown that there are multiple populations of stars separated by a few 100 Myr [95, 270]. The stars in the main sequence have a very clear cut-off in mass called *turn-off point*. Measuring the mass of the stars at this point and correlating it to the lifetime of main sequence stars it is possible to find with accuracy the age of the globular cluster. In almost all GCs, there is also a small number of stars in the main sequence with mass higher than the turn-off. They are called *blue stragglers* and have likely formed later in the life of the cluster after mass transfer from a companion or from mergers induced by collisions [124].

The metallicity of the GCs shows a bimodal distribution correlated with the spatial position [364]. GCs that live in the Galactic halo have metallicities $Z < 0.1\,Z_\odot$, while GCs that live in the bulge have $Z > 0.1\,Z_\odot$.

1.6.1 *Radial profile of globular clusters*

The GCs appear spherically symmetric with only a small number showing evidence of rotation or elliptic shape [52]. A good approximation of the surface density distribution is the King profile [204, 205]. This profile is also called a *lowered isothermal profile* because it has the same distribution as an isothermal profile but truncated at the tidal radius, r_t, which corresponds to the radius where the gravitational force of the cluster is equivalent to the one exerted by the Galaxy. The distribution function of a King model[5] is

$$f_K(\mathcal{E}) = \begin{cases} \rho_1 (2\pi\sigma^2)^{-3/2} \left(e^{\mathcal{E}/\sigma^2} - 1\right) & \mathcal{E} > 0 \\ 0 & \mathcal{E} \leq 0 \end{cases}, \tag{1.24}$$

where $\mathcal{E}$ is the relative energy defined as $\mathcal{E} = \Psi - \frac{1}{2}v^2$ and Ψ is the gravitational potential energy, ρ_1 is a reference density and σ is the central one-dimensional velocity dispersion. The condition $\mathcal{E} > 0$ corresponds to considering only the stars that have velocities smaller than the escape velocity of the GC (only the stars gravitationally bound to the GC). Without this condition the GC would expand to infinity and would contain an infinite mass.

5 distribution functions of this form were first introduced by Michie [268]

From this distribution function it is possible to measure the density profile, by integrating it over the velocity space. The result is as follows:

$$\rho_K(\Psi) = \rho_1 \left[e^{\Psi/\sigma^2} \mathrm{erf}\left(\frac{\sqrt{\Psi}}{\sigma}\right) - \sqrt{\frac{4\Psi}{\pi\sigma^2}} \left(1 + \frac{2\Psi}{3\sigma^2}\right) \right], \tag{1.25}$$

where erf is the Gaussian error function. An approximated version of this equation written as a function of radius, r, is [138]

$$\rho_K(r) = \frac{\rho_0}{[1 + (r/r_c)^2]^{3/2}} \tag{1.26}$$

where ρ_0 is the value of the mass density in the centre and r_c is the core radius. This parameter is measured from observations as the radius at which the surface brightness falls to half of its central value. Technically the parameter in the King profile is not exactly the core radius but corresponds to the radius at which the surface brightness falls to 0.5013 of its central value. Because of this similarity the King radius is commonly referred to as the core radius [54]. It must be noted that equation 1.26 is valid only within a few core radii and does not describe the GC in its entirety.

A simple yet powerful relation can be derived by King profile that relates the core radius, the central mass density, and the central stellar velocity dispersion is:

$$r_c = \sqrt{\frac{9\sigma^2}{4\pi G \rho_0}}. \tag{1.27}$$

1.6.2 *Dynamics*

The static model described before is excellent for determining the GC parameters but does not describe its evolution. The dynamics of stars in a GC are affected both by the static gravitational potential and by the gravitational interactions between single stars. These interaction, or *encounters* can be strong enough to alter the orbit of a star so that it loses memory of its original direction. A useful quantity used to check if the dynamics of a stellar system is dominated by the stellar encounters or not is the *relaxation time*. It is defined as the time after which the orbits of the stars change so much that it is impossible to reconstruct the original velocity distribution of the stellar system. If this time is shorter than the system's lifetime, the dynamic of the system is dominated by the stellar encounters and is called *collisional*. For a population of stars of equal mass m, number density n and velocity dispersion σ, this time can be expressed as [54]:

$$\tau_r = 0.34 \frac{\sigma^3}{G^2 m^2 n \ln\Lambda}, \tag{1.28}$$

where $\ln\Lambda \sim 10$ is the Coulomb logarithm. Calculating this time at the half-mass radius for GCs returns $10^8 - 10^9$ yr. Since the life of a GC is $\sim 10^{10}$ yr, the GCs are very collisional systems.

Stellar encounters can influence the dynamics by transferring energy from one part of the cluster to another [94]. This happens either through a series of distant encounters that induce small changes in the energy content of a star or through a few close encounters that can significantly alter the orbit. These encounters can impart on a star enough energy that it becomes unbound to the GC and leaves the cluster. In a GC with stars of the same mass, the escape of stars can have catastrophic consequences. As stars are ejected from the central dense regions of the GC, they remove a significant portion of energy. Because of energy conservation, the core must then contract and become denser. When the core becomes so dense that the local relaxation time is much shorter than it is in the rest of the GC, it decouples dynamically and becomes unable to transfer energy to the outer regions. This dense core becomes *isothermal* and keeps contracting until it collapses in the centre.

Real GCs, however, are not made up of stars of the same mass. They are made up of multiple components like main sequence stars, red giants, blue stragglers, WDs and neutron stars. The presence of multiple components changes the dynamical evolution and introduces the concept of *mass segregation* where stars of different mass populate different parts of the cluster. This is driven by the tendency of stars to reach *energy equipartition* where stars of different mass approach the same energy [330]. To reach this state low-mass stars will have to gain energy and move further away from the centre, while high mass stars will have to lose energy and sink deeper in the cluster. At the end of this process, the core will be populated only by high mass stars while the outer regions by low mass stars. This condition is not stable because as the massive stars move in the centre, their dynamics will become dominated by their self-gravity and will detach dynamically from the outer regions. The core will move away from equipartition and be subjected to the same instability that drives the collapse of single-mass clusters. This is called *Spitzer instability*.

Fortunately, this collapse can be halted by the presence of binaries whose interaction with single stars can release large quantities of energy. The outcomes of the interactions of a binary and an isolated star are hard to predict [94] but, in general, if an isolated star with kinetic energy E_K interacts with a binary with orbital kinetic energy E_O and if $E_k < E_O$, the isolated star will gain energy and the binary will shrink further. The presence of only a few binaries in tight orbits is enough to stabilise the GC.

Even if binaries can halt the collapse, mass segregation will still be present in the GC. This will alter the radial and velocity distribution of stars with different masses. If we assume that full energy equipartition

is reached, the surface density profile of a population of stars of mass m is [231]

$$S_m(r_\perp) = S_{m,0}\left[1+\left(\frac{r_\perp}{r_c}\right)^2\right]^{\alpha/2}, \tag{1.29}$$

where $r_\perp$ is the distance of the star projected on the plane of the sky, $\alpha = 1-3(m/m_*)$ and m_* is the mass of the class of stars that dominate the dynamics. The distribution of the class of stars that dominate the dynamics (corresponding to $\alpha = -2$) is the same as that of a single-mass cluster.

The velocity dispersion becomes smaller for more massive stars and, in the case of full energy equipartition, is:

$$\sigma(m) = \sigma_{m_*}\left(\frac{m}{m_*}\right)^{1/2}, \tag{1.30}$$

where σ_{m_*} is the velocity dispersion of the dominant mass class.

However, in realistic GCs, full equipartition is never reached [53, 345]. The equipartition assumption is valid only for the most massive stars, while stars of mass similar to the dominant mass class have not fully reached this stage. With more realistic assumptions, the velocity distribution can be written as [53]

$$\sigma(m) = \begin{cases} \sigma_0 e^{-\frac{1}{2}\frac{m}{m_{\rm eq}}} & m \le m_{\rm eq} \\ \sigma_{\rm eq}\left(\frac{m}{m_{\rm eq}}\right)^{-1/2} & m > m_{\rm eq} \end{cases}, \tag{1.31}$$

where $m_{\rm eq}$ is the mass of the stars that have reached equipartition, $\sigma_{\rm eq}$ corresponds to the velocity dispersion at $m_{\rm eq}$ and $\sigma_0 = \sigma_{\rm eq}e^{1/2}$.

1.7 INTERMEDIATE MASS BLACK HOLES

GCs are thought to host in their centre an Intermediate Mass Black Hole (IMBH). These are black holes with masses between $10^2 - 10^5$ $M_\odot$ thought to be link between stellar black holes and supermassive black holes and considered the seeds upon which the supermassive black holes form [192, 220, 267, 352]. Very little observational evidence is present but it is suspected that, if they exist, they could be found in GCs [37]. An interesting argument in favour of the the presence of IMBHs in GCs is the relation between the mass of supermassive black holes and the velocity dispersion of the host galaxy [123, 148, 209]. Extrapolating this relation to the velocity dispersion of GCs ($\sim 10-15$ km s^{-1}), we would expect them to host **BH!**s (**BH!**s) of $\sim 1-7\times10^3$ $M_\odot$. This relation suggests that if central black holes are present in the cluster, they would be in the mass range of IMBHs . It must be said, however, that it is not proven that this relation holds down to these black hole masses and the physics describing the co-evolution of a

supermassive black hole and its host galaxy could be different at the scales of GCs.

The formation scenario of an IMBH is unclear and different possibilities have been formulated: collapse from Pop III stars [245]; direct collapse of rapidly inflowing gas in the first metal-free protogalaxies [113, 225, 226]; repeated mergers of stars and stellar black holes [154, 163, 298, 299]. This last formation scenario in particular is supposed to happen only in massive and dense environments like young GCs.

The search for IMBHs in GCs is interesting because they can be sources of gravitational waves if bound to a stellar black hole or a neutron star in close orbit. If present, these systems are likely to be detectable with the next generation of gravitational waves interferometers like the Laser Interferometer Space Antenna and the Einstein Telescope [15, 16, 146, 312].

Even with a lot of theoretical works predicting the existence of IMBHs and placing them at the core of GCs, the observations focused in our Galaxy have led only to upper limits and disputed results. One of the main method used to look for IMBHs in GCs is searching for dynamical effects in the spatial and velocity distribution of the stars in the clusters affected by the presence of an IMBH [38, 147]. Both the surface density and velocity dispersion will rise in the centre if an IMBH is present. The direct influence of the IMBH extends up to the so called *influence radius*. It is defined as the radius at which the Keplerian velocity of a star orbiting the IMBH equates the velocity dispersion of the stars outside [47]:

$$r_i = \frac{GM_{\mathrm{BH}}}{\gamma \langle v_c^2 \rangle}, \tag{1.32}$$

where M_{BH} is the mass of the IMBH and γ is found in simulations to be 2. In an equilibrium situation the density profile will develop a cusp inside this radius described by the power-law distribution [47]:

$$\rho(r) \propto r^{-1.55}. \tag{1.33}$$

The velocity distribution, instead, will show a Keplerian profile inside of the influence radius.

The difficulty of detecting an IMBH with this method is that most of the effects will happen only inside the influence radius which can be small. An IMBH of $M_{\mathrm{BH}} \sim 2000$ $\mathrm{M}_\odot$ in a cluster with velocity dispersion $\sigma = 10$ km s^{-1} has an influence radius of ~ 0.04 pc. If the cluster is found at a distance of 6 kpc, this corresponds to an angular distance of ~ 1.5 arcseconds which is very hard to resolve optically. Because of this difficulty searches have usually resulted in upper limits or tentative claims [263, 279, 372] which have been contested [44].

Another method used to look for IMBH is the search for radiative signatures of accretion on the cluster [240–242]. If an IMBH is present in the centre of a GC it is supposed to accrete the gas present in the region

Name	IMBH mass claim from dynamics ($M_\odot$)	Ref.	Accretion limit on IMBH mass ($M_\odot$)	Ref.
NGC 1904 (M79)	$3 \pm 1 \times 10^3$	[232]	-	-
NGC 5139 (ω Cen)	$4.7 \pm 1.0 \times 10^4$	[281]	<1000	[344]
NGC 5286	$1.5 \pm 1.0 \times 10^3$	[120]	-	-
NGC 6266 (M62)	$2 \pm 1 \times 10^3$	[232]	<1130	[344]
NGC 6388	$2.8 \pm 0.4 \times 10^4$	[233]	<1770	[344]
NGC 6397	600	[196]	<610	[344]
NGC 6715 (M54)	9.4×10^3	[188]	<2990	[344]
NGC 7078 (M15)	$3.9 \pm 2.2 \times 10^3$	[152]	<1530	[344]

Table 1.1: Clusters with reported claims of an IMBH measured through the dynamical effects. For these clusters, no accretion signature has been found and only upper limits have been set. Only for NGC 6397 the upper limit is compatible with the claimed mass of the IMBH .

and radiate in X-rays and in the radio band. The emission strongly depends on the quantity of gas and the accretion efficiencies, but, with reasonable assumptions, only upper limits or controversial claims have been put forward [230, 269, 297, 344]. In Table 1.1 I report several claims of IMBH detections made in GCs. Some of these detections have been contested [44] using detailed N-body simulations. For none of these claims accretion signatures have been seen.

A third method used to look for IMBHs in GCs is through the observations of MSPs [4, 132, 206, 207, 288, 289, 301]. The very precise rotational stability, allows the measurement through Doppler shift of the accelerations and its time derivatives. The idea of using these measurements to map the gravitational potential of the cluster was first proposed by Blandford, Romani, and Applegate [56] and further developed by Phinney [295]. This concept will be explained in greater details in Chapter 5.

At the moment, the only accredited evidence of an IMBH in a GC is from a tidal disruption event that happened in an extra-galactic stellar cluster [223].

1.8 GAS IN GLOBULAR CLUSTERS

The stars in GCs are old and many of them are experiencing the final stages of their lives as Red Giant Branch (RGB) and Asymptotic Giant Branch (AGB) stars. In these stages they are expected to lose $\sim 10^{-9} - 10^{-8}$ $M_\odot$ yr^{-1} [108], while summing all the contributions there should be $\sim 10^{-6}$ $M_\odot$ yr^{-1} of dust [260]. Because of this reason, they release large amounts of gas in the environment forming the Intracluster Medium (ICM). This, together with the lack of star formation, would point to the GCs being rich in gas [350]. However, the only detections of neutral ICM is in M15 where a cloud of H1 of ~ 0.3 $M_\odot$ with $9 \pm 2 \times 10^{-4}$ $M_\odot$ has been found [68, 114, 365]. Searches in other globular clusters have only returned upper limits [41, 327].

The only detection of ionised media has been possible thanks to the pulsars in 47 Tuc [133]. The authors detected significant variations between the DMs of the 20 pulsars known at the time. In very dense environments like GCs, the local acceleration caused by the gravitational potential of the GC can be strong enough to cause detectable Doppler shifts in the spin-down of the pulsars (as shown in Chapter 3). The authors estimated these accelerations and used analytical models to locate the pulsars along the line of sight. They noted that pulsars that were behind the cluster centre had higher DM while pulsars in front of the cluster centre had lower DM . They concluded that the radiation of the pulsar in the back of the cluster had to cross more ionized gas than the rest of the pulsars. They estimated the number density of the ionized ICM to be 0.067 ± 0.015 cm^{-3} corresponding to ~ 0.1 $M_\odot$ of ionized gas in the core of the cluster. More details on how the technique works and on how it was improved in a recent paper [4] can be found in Chapter 3.

A strong evacuation mechanism must be present in order to reconcile theory and observations, different models have proposed some external and other internalmechanisms. External mechanisms require ram pressure stripping either from the Galactic plane when the GC crosses it [310] or from the halo [130]. The first would work but only happens every ~ 100 Myr and the GC would fill with gas between passes, while the second can only work for low mass clusters [302]. Internal mechanisms proposed include stellar collisions [348], novae [316], M-dwarf flaring [93], pulsar winds [328] and main-sequence star winds [326].

When applied to a real GC like 47 Tuc, these mechanisms do not reach the required energy to expel the gas fast enough [259]. However, just a few newly born WDs can provide the thermal energy necessary to eject the gas [259] and the necessary flux of ionizing photons to keep all of the gas ionized as is observed.

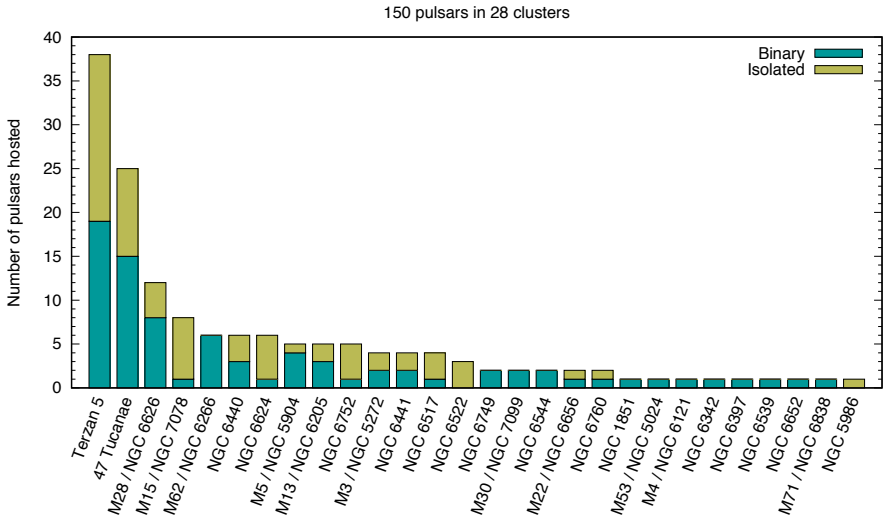

Figure 1.6: HIstogram of the known pulsars in GCs. The different colors represent the number of isolated versus the binary pulsars. Courtesy of Alessandro Ridolfi.

1.9 GLOBULAR CLUSTER PULSARS

In the context of this thesis, GCs are interesting because they host a very large population of pulsars. A total of 150 pulsars are known inside 28 Galactic GCs[6]. An histogram showing the number of known pulsars in GCs is shown in Fig. 1.6. Two clusters dominate the list, Terzan 5 with 38 known pulsars and 47 Tuc with 25. The GCs contribute to about 6% of the total pulsar population while having a small mass compared to the Galactic disk. Per unit of mass, GCs host a population of pulsars about 100 times higher than the Galactic disk. The vast majority of these pulsars are MSPs with only 6 of them having a rotational period longer than 100 ms. This is very peculiar as the slow pulsars dominate the Galactic disk population. Another peculiarity of GC pulsars is that around half of them are in binaries contrary to what is seen in Galactic MSPs which are usually in binaries.

Some binary pulsars have companions that are very hard to explain through the standard formation scenario, like the *black widow* and the *redback* pulsars. The abundance of these kind of systems can only be explained through an exchange of the original companion during a collision. This interpretation is the key to understanding the GC pulsars. Due to the very high densities of the GCs, the neutron stars go through a large number of close encounters that can significantly alter their evolution [79]. Pulsars can therefore increase the eccentricity, exchange companions and even go through different recycling episodes reaching fast rotational velocities. Indeed, the fastest pulsar known is J1748-2446ad located in Terzan 5 with a rotational period of just 1.39 ms

6 The up-to-date list of all known GC pulsars can be found at http://www.naic.edu/ pfreire/GCpsr.html

[174]. Because of these encounters, GC pulsars are more likely to be recycled than Galactic disk pulsars. The fraction of neutron stars that have been recycled as MSPs is about $\geq 10^{-3}$ [357], while for GC pulsars this fraction is about 0.1 [357]. Abbate et al. [5] were able to confirm the value of this fraction using simulations of GCs and Bayesian analysis to estimate the total number of neutron stars and of MSPs as described in Chapter 6. The link between dynamical encounters and pulsars is also supported by the strong correlation between the total rate of encounters and the number of pulsars in each GC [39]. The ratio of binary to isolated pulsars in GCs is also correlated with the encounter rate for a single binary [351] which shows that encounters between binaries and single stars can cause the pulsar to be ejected. The lack of young pulsars can be explained by the absence of on-going star-formation in GCs.

1.9.1 *Formation of pulsars in globular clusters*

The large number of neutron stars in GCs causes some problems for the standard formation scenario of pulsars. Core-collapse supernovae are known to impart also a high kick velocity on the newly born neutron star which can be described by a Maxwellian distribution with a 1D standard deviation of ~ 265 km s^{-1} [179]. The escape velocity from the centre of a typical GC is ~ 50 km s^{-1} [45] meaning that most of the neutron stars would be ejected from the cluster immediately after birth. A way to prevent this escape is if the supernovae happen in a binary system which can absorb part of the kick velocity. Alternatively dynamical models of GC show that during the first period of a GC's life (when most supernovae would happen), its mass would have been higher than it is today [353]. Finally a possibility that could explain the observed population is that there is a formation scenario of neutron stars with low kick velocity.

Another problem that the standard formation scenario runs into is the mass of the pulsars. The standard way to measure pulsar masses is through prolonged timing of relativistic binary pulsars (see section 2.2). Another way is to make use of mass segregation according to which pulsars will sink towards the centre of the GC. Comparing the surface number density of pulsars with respect to the rest of the stars according to Eq. 1.29, will give an estimate of the mass of the pulsar population. This estimate for the pulsars in Terzan 5 returned an average mass of ~ 1.3 M$_\odot$ (this mass includes also the mass of the companion) [301]. The recent evaluation of the mass of the fully recycled pulsar NGC 1851A at 1.25 ± 0.06 M$_\odot$ confirms this idea [308]. This value is smaller than the expected average mass of neutron stars, ~ 1.5 M$_\odot$ [284]. One explanation for this discrepancy is that the assumed mass of the stars that dominate the dynamics in the core is wrong or that the GC pulsars are born less massive than regular

pulsars. These considerations lead to the idea that neutron stars could be born in electron-supernovae from WDs [189]. This scenario can also explain the presence of a few young pulsars despite the lack of star-formation and core-collapse supernovae in the recent past.

1.10 SCIENCE WITH GLOBULAR CLUSTER PULSARS

The pulsars found in GCs are extremely fascinating objects to study because of their unique properties [173]. They can be used individually for studies regarding gravitational physics or the physics of accretion or as an ensamble as probes of the properties of the host clusters.

The measurement of the mass of pulsars through timing (see section 2.2) can help to constraint the equation of state that describes the interior of such stars. GC pulsars play an important role here because many binary systems have high eccentricity which facilitates the measurement of the mass. Furthermore, GC pulsars can undergo different events of recycling which can increase the mass and decrease the rotational period to extreme values. Fast-spinning pulsars can provide additional constraints to the equation of state. GCs are likely to host some of the most massive and fastest pulsars. Indeed, both the fastest [174] and what is likely the most massive pulsar [140] are found in GCs.

Another important field in which GC pulsars play an important role is the physics of eclipses and accretion. Large number of systems with a low-mass main sequence companion can be found in GCs. Many of these systems show eclipses that can be used to probe the gas surrounding the companion. Some of these systems are seen to alternate between standard radio emission and a LMXB phase. Of the three *transitional MSPs* known, one J1824-2452I [286] is found in a GC, in particular in M28. These systems are extremely important to study the relation between LMXBs and MSPs and the phenomenon of recycling.

1.10.1 *Exploring the properties of globular clusters with pulsars*

In this thesis I will focus on the properties of the GCs and of the Galaxy that can be derived by using the entire pulsar population as a whole.

When considered together, the population of pulsars in GCs can act as a probe of the dynamics and of the ICM in GCs. This idea was brought forward by Blandford, Romani, and Applegate [56] even before the first pulsar in a GC was discovered [237] and was further developed in the following years [295]. The gravitational potential of the GC imparts a significant acceleration to the pulsar which affects the derivative of the spin period as is shown in eq. 3.1 and in the subsequent discussion. The second derivative of the period will be instead influenced by the jerk felt by the pulsar. These effects can be

used to determine the structural parameters of the host cluster like the central density and core radius. This effect will depend only on the gravitational mass of the cluster. A comparison between this mass and the luminosity of the cluster allows us to test if some nonluminous matter like an IMBH is present in the centre of the cluster and constrain its mass. This concept will be further developed and applied to GCs 47 Tuc and M62 in Chapters 3 and 5. At the end of Chapter 5 I will describe a new technique to look for IMBHs using the second and third derivatives of the period.

Another way in which pulsars can be used to study the general properties of a GC is through the effects of the interstellar matter. By studying the correlation between the DMs of pulsars in the same cluster we can give constraints on the quantity of ionized gas present inside. Only in one case, 47 Tuc, this method led to a discovery of ionized gas [133]. This cluster was further studied and various distribution models of gas have been tested [4] as described in Chapter 3. The best model consists of a gas of constant density in the central regions of the cluster of number density 0.23 ± 0.05 cm^{-3}. Using this estimate it was possible to further constraint the mass of a possible central IMBH . This constraint is based on the fact that no signatures of accretion of this gas on the IMBH are seen. The presence of detectable quantities of gas opens the question of whether it is magnetized. The study of the RM of the pulsars in this cluster allows the search for such magnetic fields as described in Chapter 4. In this chapter we show how this kind of study can provide unique information on the global properties of the Galactic magnetic field in the largely unknown Galactic halo.

GC pulsars can also play a significant role in the study of the formation of the Nuclear Star Cluster (NSC) that surrounds the central supermassive black hole found in the centre of our Galaxy. One possible formation scenario involves stellar clusters that inspiralled to the Galactic centre, were tidally disrupted and deposited their stars to form what we now observe as the NSC. If this scenario is correct, the stellar clusters would also deposit the pulsar content of the clusters. Discovering these pulsars and determining their spatial distribution can help prove or discredit this hypothesis. The theory and the set-up of the necessary observations is described in Chapter 6.

All of these prospects require the next generation of telescopes to bring the desired scientific results. The future of pulsar astronomy in the next generation will be lead by the Square Kilometre Array (SKA) and its precursor in South Africa MeerKAT. In Chapter 7 I will describe the properties that make the SKA precursor MeerKAT an optimal telescope for carrying out observations of GC pulsars and the main results the collaboration hopes to achieve.

2

RADIO PULSARS OBSERVATIONS

The desire of extreme sensitivity and precision necessary to exploit pulsars for scientific purposes has pushed the technological requirements of the detectors both in hardware and in software to very high levels. Pulsar observations in radio are performed in different frequencies and with different types of telescopes, from simple non-steerable dipole antennas in the frequency range 50 - 300 MHz, to regular dish telescopes from about 600 MHz to about 30 GHz. They can either function as separate telescopes or be connected to form a larger interferometer. In this thesis I will focus on observations in L-band (from 900 MHz to 1.6 GHz) taken with single dish antennas. The data for 47 Tucanae was taken from the Parkes radio telescope in Australia. Part of this thesis uses observations performed at the Green Bank Telescope in West Virginia, USA. In Chapter 7, I will describe shortly the MeerKAT radio telescope, an interferometer recently built in South Africa which I have been involved in. These telescopes are depicted in Fig. 2.1.

2.1 DE-DISPERSION

The effects of dispersion caused by the ionized interstellar medium must be corrected in an early stage of processing to preserve all of the important information. Two main techniques have been used: *incoherent de-dispersion*, a traditionally hardware solution used from the beginning of pulsar astronomy, and *coherent de-dispersion*, a software solution that is gaining popularity thanks to the improvements in technological capabilities [228].

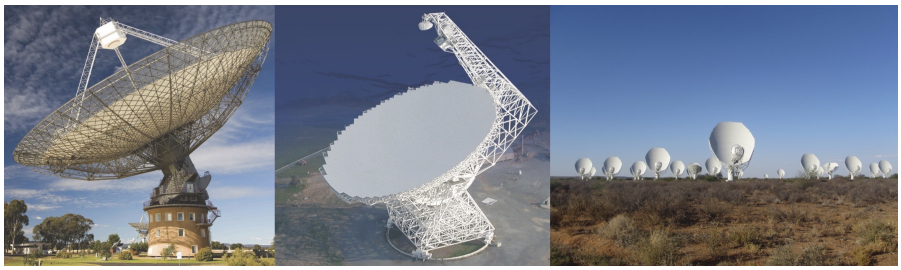

Figure 2.1: Telescopes used for the observations processed in this thesis: Parkes radio telescope (left), Green Bank telescope (centre) and MeerKAT radio telescope (right). Credits: ATNF, Green Bank Observatory, SARAO.

2.1.1 *Incoherent and coherent de-dispersion*

Incoherent de-dispersion consists in dividing the frequency band into a large number of channels, and applying the necessary delay for each channel so that the pulse arrive in each channel at the same time. The delay is measured with equation 1.15. The main limitation of this technique is that the effects of dispersion in each channel are not corrected and this might make MSPs with high DM appear broader than they really are (this has a consequent effect on timing as explained in section 2.2). The choice of the best number of frequency channels must therefore be customized for the sources in the observations.

Coherent de-dispersion is a technique that can completely remove dispersion from the signal without the worry of channelisation. this technique uses both the amplitude and the phase [167] as opposed to incoherent de-dispersion which only looks at the amplitude, hence the name. The principle of coherent de-dispersion is that the dispersive effects can be described as a *phase only* transfer function H, defined in the frequency domain as follows:

$$V(f_0 + f) = V_{\text{int}}(f_0 + f)H(f_0 + f), \tag{2.1}$$

where f_0 is the centre frequency of the band, $V(f_0 + f)$ is the Fourier transform of the voltage measured by the telescope and $V_{\text{int}}(f_0 + f)$ is the Fourier transform of the intrinsic voltage emitted by the pulsar. The transfer function H can be expressed as a function of the dispersion measure through the formula [228]:

$$H(f_0 + f) = e^{i\frac{2\pi\mathcal{D}}{(f_0+f)f_0^2}\text{DM}\,f^2}, \tag{2.2}$$

where $\mathcal{D}$ is the dispersion constant defined in section 1.5.1. By applying the inverse of this function to the complex voltages, it is possible to recover the signal as it was emitted by the pulsar. This method is very computationally demanding and until recently it was impossible to de-disperse coherently observations in real-time.

2.2 PULSAR TIMING

Some of the most important and exciting results in the study of pulsars have come from the technique called *pulsar timing*. This technique consists of measuring the time of arrival, called ToA, of the single pulses and construct timing models that can predict when the pulses will arrive in the future. The Time of Arrivals (ToAs) are affected by many properties of the pulsar, like its position in the sky, its spin period and its derivatives and in case of binary pulsars, the mass and orbit of the pulsar and the companion. Pulsars are extremely stable rotators and in some cases we are able to construct timing solutions that can keep track of every single rotation of the pulsar over decades.

This type of solution is called *phase connected solution*. In particular MSPs are some of the most stable clocks known with a timing stability comparable or even better than atomic clocks [228]. MSPs are more stable than canonical pulsars because they have more stable emission and they do not experience large *glitches*, which are sudden jumps in spin periods that are seen in younger pulsars.

Pulsars are typically weak sources and, even with the most sensitive telescopes, only for a handful of them we can see the emission from every pulse. For the majority of them we need to add a large number of pulses before the signal becomes significantly visible over the noise. The procedure is called *folding* and consists in dividing the time-series in time sections corresponding to the length of a period, and summing the sections together. This way, the pulses will fall at the same phase bins and sum together increasing the statistical significance. The pulse profile obtained with this technique is called *integrated profile*. For some pulsars a few seconds are enough to see the pulse, while other require integration of several minutes. Even if single pulses can have different shapes, the integrated profiles are constant for almost all pulsars (an example of a pulsar which changes profile over the years is B2127+11C in globular cluster M 15 [306]). Since pulsars can have broad profiles, the ToA is measured at a fiducial point of the profile.

2.2.1 *Measuring time of arrivals*

In order to measure precisely the ToAs we must cross-correlate the integrated profiles with a template of the profile. The template can be obtained by summing all of the profiles of earlier observations together in order to increase the Signal to Noise Ratio (S/N) or by synthetically reproducing a noise-free template by representing the profile as a sum of Gaussian profiles [128, 210]. This last method is useful also when considering pulse profile variations as a function of frequencies.

The correlation is performed with a template matching algorithm either in the time domain or in the frequency domain. The frequency domain correlation can reach higher precision as it is not limited by the sampling time of the observation. The precision in time that can be reached with this technique depends both on the S/N of the pulsar (which in turn depends on the integration time) and on the shape of the pulse. The sharper the profile, the more accurate the template matching is. For this reason, coherent de-dispersion systems, which allow for sharper profiles are the best for timing purposes.

The ToAs found this way are measured based on the local observatory time which is usually kept by hydrogen masers. These clocks do not have the stability necessary for timing pulsars for long time-spans and therefore must be corrected. The correction is performed converting to Universal Coordinated Time, UTC(GPS) by using the Global

Positioning System (GPS). This clock does not correspond exactly to UTC because it does not consider the non-uniform rotation of the Earth. The correction is performed by converting to the International Atomic Time (TAI) realization of Terrestrial Time, TT(TAI), which is based on a large number of atomic clocks spread around the Earth. The TT(TAI) is ahead of the UTC by the number of leap seconds that have been added. The TT(TAI) is not perfect and every year the Bureau International des Poids et Mesures (BIPM) publishes corrections, TT(BIPM), that allow precise timing over a large number of years. This is the time format that must be used when timing pulsars. Further information on the different time standard can be found in [180].

2.2.2 *Solar System Barycentre corrections*

The ToAs in this format are measured in a reference frame that is constantly changing as it rotates around the Earth and the Earth orbits around the Sun. A better reference system would be the Solar System Barycentre (SSB). To move the measurement of the arrival time to the SSB we must apply the following corrections [112]:

$$t(\text{SSB}) = t(\text{BIPM}) + \Delta_{\text{DM}} - (\Delta_R^{\odot} + \Delta_E^{\odot} + \Delta_S^{\odot}), \tag{2.3}$$

where $t(\text{BIPM})$ is the ToA in the TT(BIPM) standard, Δ_{DM} is the delay caused by the dispersion in the ISM, $\Delta_R^{\odot}$ is the Solar System Roemer delay, $\Delta_E^{\odot}$ is the Solar System Einstein delay, and $\Delta_S^{\odot}$ is the Solar System Shapiro delay.

In order to remove the delay caused by the dispersion in the ISM, all ToAs are referenced at infinite frequency. If the observation is performed at frequency f, this delay can be expressed using eq. 1.15 as:

$$\Delta_{\text{DM}} = \frac{\mathcal{D}}{f^2}\text{DM}, \tag{2.4}$$

where $\mathcal{D}$ is the *dispersion constant* defined in section 1.5.1. For some pulsars the measure of DM is seen to change with time, in these cases the equation above must be modified accordingly [201].

The Solar System Roemer delay, $\Delta_R^{\odot}$, corresponds to the time difference between the arrival of the pulse at the telescope and at the SSB. In formulas it can be expressed as:

$$\Delta_R^{\odot} = -\frac{(\mathbf{r_{se}} + \mathbf{r_{et}}) \cdot \mathbf{r_{sp}}}{c}, \tag{2.5}$$

where $\mathbf{r_{se}}$ is the vector between the SSB and the centre of the Earth, $\mathbf{r_{et}}$ is the vector between the centre of the Earth and the telescope, $\mathbf{r_{sp}}$ is the vector between the pulsar and the SSB. The geometry is shown in Figure 2.2. This effect is strongly dependant on the position of the

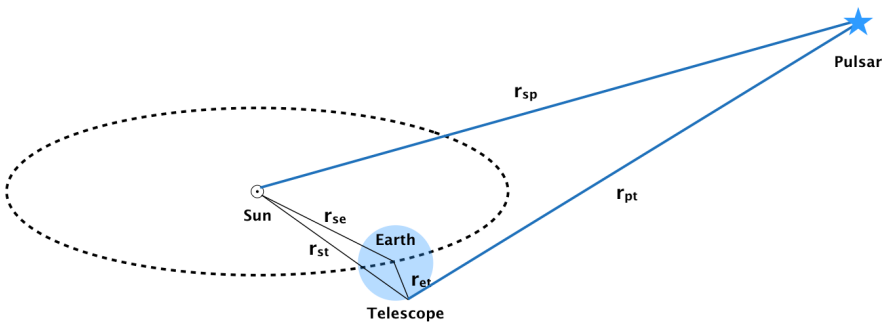

Figure 2.2: Diagram of geometry involved in the Roemer delay.

pulsar in the plane of the sky. An inaccurate determination of the position will lead to sinusoidal delay with a period of exactly one Earth year. The positional precision that can be reached by correcting this effect is of the order of the milliarcsecond or even smaller [132]. If the pulsar has a proper motion in the plane of the sky, the position will change and the correction applied will become wrong. After some years, the delay between the expected ToA and the measured one will have a sinusoidal shape with increasing amplitude. By fitting for this component it is possible to measure the proper motion of the pulsar to accuracies of tenths of milliarcsecond per year.

The Solar System Einstein delay, $\Delta_E^{\odot}$, is the gravitational redshift caused by the deformation of space-time caused by all bodies in the Solar System. In order to estimate the effects caused by the Earth, one must consider its exact geometry.

The Solar System Shapiro delay, $\Delta_S^{\odot}$ [319] accounts for the extra time necessary for the light to cross the space-time deformations caused by Solar System bodies. The greatest contributors are the Sun and Jupiter. In order to account for this effect regularly updated Solar System ephemerides are needed.

Other smaller corrections caused by annual parallax and dispersion caused by the interplanetary medium and the Earth atmosphere are present but usually don't affect the observations.

2.2.3 *Isolated pulsar timing*

It is possible to keep track of each pulse arriving from the pulsar using a Taylor series approximation [228]:

$$N(t) = N_0 + \nu_0(t - t_0) + \frac{1}{2}\dot{\nu}_0(t - t_0)^2 + \frac{1}{6}\ddot{\nu}_0(t - t_0)^3 + \ldots, \quad (2.6)$$

where N_0 is the pulse number at the epoch t_0, $\nu_0 = \nu(t_0)$ is the spin frequency, and $\dot{\nu}_0 = \dot{\nu}(t_0)$ and $\ddot{\nu}_0 = \ddot{\nu}(t_0)$ are the spin frequency derivatives.

Using this formula to fit the observed ToAs we recover the period of the pulsar and its period derivatives. Usually many years of timing

are necessary to measure more than one derivative. The precision with which these derivatives are known increases with longer total observations times. The uncertainty on the period will decrease as $T^{-3/2}$, where T is the total observation time. The first derivative uncertainty will decrease as $T^{-5/2}$, the second period derivative uncertainty as $T^{-7/2}$ and so on.

2.2.4 *Binary pulsar timing*

If the pulsar is in a binary, the equation 2.6 will not hold. The reason is that the pulsar reference frame is not inertial anymore. To use this formula, we need to move in the frame of the orbital barycentre. The correction necessary is similar to the one used for the Solar System and can be written as (including only the most important contributions) :

$$t(\mathrm{BB}) = t(\mathrm{SSB}) + \Delta_R^{\mathrm{bin}} + \Delta_E^{\mathrm{bin}} + \Delta_S^{\mathrm{bin}}, \tag{2.7}$$

where $t(\mathrm{BB})$ is the time in the frame of the binary barycentre, Δ_R^{bin} is the binary Roemer delay, Δ_E^{bin} is the binary Einstein delay, and Δ_S^{bin} is the binary Shapiro delay. For non-relativistic systems, a Kepler's laws can completely describe the system. Instead, for a number of systems post-Keplerian corrections are needed.

To completely describe a system in the Keplerian formalism, five parameters are necessary: orbital period, P_b, the projected semi-major axis $a_p \sin i$, the orbital eccentricity, e, the longitude of periastron ω_p, and the epoch of passage at periastron, T_0. i is the inclination angle between the angular momentum of the binary and the line of sight.

The Keplerian parameters are related to the eccentric anomaly, E (defined in Fig. 2.3), [102] as follows:

$$E - e \sin E = \Omega_b \left[(t - T0) - \frac{1}{2} \frac{\dot{P}_b}{P_b} (t - T_0)^2 \right], \tag{2.8}$$

where $\Omega_b = 2\pi / P_b$ is the mean angular velocity.

These parameters can be used to derive the binary Roemer delay, Δ_R^{bin} which is [55]:

$$\Delta_R^{\mathrm{bin}} = x(\cos E - e) \sin \omega_p + x \sin E \sqrt{1 - e^2} \cos \omega, \tag{2.9}$$

where $x = a_p \sin i / c$. This equation is used to find the Keplerian parameters.

For relativistic systems, the so called *post-Keplerian* parameters become detectable. The five most important post-Keplerian parameters are: the rate of advance of periastron, $\dot{\omega}$, the rate of decay of orbital period, $\dot{P}_b$, the amplitude of the Einstein delay, γ, and the Shapiro delay represented by a *shape* s and a *range* r. The expressions of these

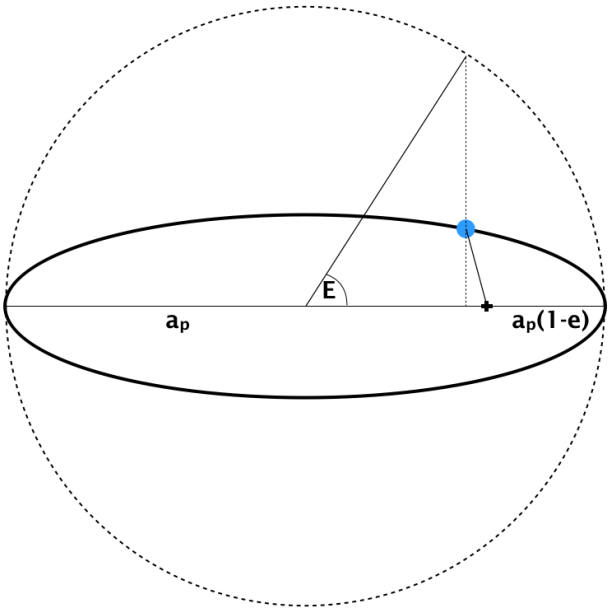

Figure 2.3: Definition of the eccentric anomaly E. The pulsar position is projected on an auxiliary circle with radius a_p.

parameters assuming general relativity is the correct theory of gravity are [228]:

$$\dot{\omega} = 3T_{\odot}^{2/3}\left(\frac{P_b}{2\pi}\right)^{-5/3}\frac{1}{1-e^2}(M_p+M_c)^{2/3} \tag{2.10}$$

$$\gamma = T_{\odot}^{2/3}\left(\frac{P_b}{2\pi}\right)^{1/3} e\frac{M_c(M_p+2M_c)}{(M_p+M_c)^{4/3}} \tag{2.11}$$

$$r = T_{\odot}M_c \tag{2.12}$$

$$s = \sin i = T_{\odot}^{-1/3}\left(\frac{P_b}{2\pi}\right)^{-2/3} x\frac{(M_p+M_c)^{2/3}}{M_c} \tag{2.13}$$

$$\dot{P}_b = -\frac{192\pi}{5}T_{\odot}^{5/3}\left(\frac{P_b}{2\pi}\right)^{-5/3} f(e)\frac{M_pM_c}{(M_p+M_c)^{1/3}}, \tag{2.14}$$

where $T_{\odot} = G\,\mathrm{M}_{\odot}/c^3 = 4.925490947\ \mu$s, all masses are expressed in solar units, G is the gravitational constant and:

$$f(e) = \frac{1+(73/24)e^2+(37/96)e^4}{(1-e^2)^{7/2}}. \tag{2.15}$$

According to these equations the binary Einstein delay, Δ_E^{bin}, is:

$$\Delta_E^{\mathrm{bin}} = \gamma \sin E. \tag{2.16}$$

Instead, the binary Shapiro delay, Δ_S^{bin}, has the following form:

$$\Delta_S^{\mathrm{bin}} = -2r\ln[1-e\cos E - s(\sin\omega(\cos E - e) + \sqrt{1-e^2}\cos\omega\sin E)].$$

(2.17)

In the post-Keplerian formalism other effects will take place like the introduction of two eccentricities e_r and e_θ which will affect the Roemer delay, and aberration. After removing these effects the equation 2.6 can be used again to measure the period and its derivatives.

Thanks to the post-Kelperian parameters we are also able to measure the mass of the pulsar and the companion. The physical unknowns of the system are three: the mass of the pulsar, the mass of the companion, and the inclination angle. The keplerian parameters allows us to establish a relation between these unknowns, the mass function:

$$f(M_p, M_c) = \frac{(M_c \sin i)^3}{(M_p + M_c)^2} = \frac{4\pi^2}{G} \frac{(a_p \sin i)^3}{P_b^2}. \tag{2.18}$$

The measurement of two post-Keplerian parameters of the five in 2.10 will allow us to measure the mass of the pulsar and of the companion. If additional parameters are measured, then it is possible to test whether GR is self-consistent. This has been done in different regimes and provide some of the most stringent tests of GR at strong field regimes [78, 141, 213].

2.3 POLARIZATION CALIBRATION

In radio telescopes, the astronomical signal is received by two orthogonal receivers sensitive to only one polarization (typically linear or circular). These two polarizations are processed in the same way and combined in the final stage. This automatically allows the possibility of conducting polarization studies. Pulsars are often highly polarized sources and the polarization carries important information about the emission and the magnetic field along the line of sight to the pulsar. The use of (carefully calibrated) polarization information can also improve the quality of pulsar timing [367].

2.3.1 *Stokes parameter*

In order to perform any polarization study, the incoming signal is converted in the so-called *Stokes parameters* [335]. If the signal is extracted in two orthogonal linear polarizations, X and Y, with X pointing towards North and Y pointing towards East, and the data is coherently de-dispersed (in order to keep the information on the phase), the Stokes parameters are defined as follows:

$$\begin{cases} I = |X|^2 + |Y|^2 \\ Q = |X|^2 - |Y|^2 \\ U = 2\mathrm{Re}(X^* Y) \\ V = 2\mathrm{Im}(X^* Y) \end{cases}, \tag{2.19}$$

where X^* is the complex conjugate of X. Alternatively two circular polarizations can be extracted, L (left) and R (right). L is chosen so that the electric field rotates clockwise, while for R the electric field rotates counter-clockwise. In this case the Stokes parameters are:

$$\begin{cases} I = |L|^2 + |R|^2 \\ Q = 2\mathrm{Re}(L^* R) \\ U = 2\mathrm{Im}(L^* R) \\ V = |L|^2 - |R|^2 \end{cases} . \tag{2.20}$$

The Stokes parameters can be written as a four-dimensional vector called Stokes vector defined as $S = (I, Q, U, V)$. From the Stokes parameters Q and U it is possible to determine the polarization PA of the incoming radiation as follows

$$\mathrm{PA} = \frac{1}{2} \arctan\left(\frac{U}{Q}\right). \tag{2.21}$$

Another useful quantity easily accessed through the Stokes parameters is the total linear polarization L defined as:

$$\mathrm{L} = \sqrt{Q^2 + U^2}. \tag{2.22}$$

However, The Stokes parameters recovered this way do not faithfully reproduce the real values of the astronomical signal. The data still needs to be calibrated [171, 228].

2.3.2 *Müller matrix*

The calibration is performed through the use of Müller matrix that describes how different effects influence the Stokes parameters on the telescope's receiver. The Stokes vector of the incoming radiation S_{in} is modified into the stokes parameter recorded, S_{out} as follows:

$$S_{\mathrm{out}} = \mathcal{M} \times S_{\mathrm{in}}, \tag{2.23}$$

where $\mathcal{M}$ is the Müller matrix. This matrix can be decomposed as the product of four different matrices each considering a single effect:

$$\mathcal{M} = \mathcal{M}_{\mathrm{amp}} \times \mathcal{M}_{\mathrm{CC}} \times \mathcal{M}_{\mathrm{Feed}} \times \mathcal{M}_{\Pi}. \tag{2.24}$$

Following the order of matrix multiplication the first matrix is $\mathcal{M}_{\Pi}$ which accounts for differences in parallactic angle of the receivers (to be applied only in case the telescope has an alt-azimuthal mount). As the Earth rotates, the feeds of the telescope will rotate with respect to the source and one polarization will leak in the other. The parallactic angle can be measured at any time as follows:

$$\Pi = \arctan\left(\frac{\sin \mathrm{HA} \cos\phi}{\sin\phi \cos\delta - \cos\phi \sin\delta \cos \mathrm{HA}}\right), \tag{2.25}$$

where HA is the hour angle at which the observation is performed, δ is the declination of the source and ϕ is latitude of the telescope. This effect will mix the linear polarization but leave the circular unaltered:

$$\mathcal{M}_{\Pi} = \begin{bmatrix} 1 & 0 & 0 & 0 \\ 0 & \cos 2\Pi & \sin 2\Pi & 0 \\ 0 & -\sin 2\Pi & \cos 2\Pi & 0 \\ 0 & 0 & 0 & 1 \end{bmatrix} \tag{2.26}$$

The second contribution to eq. 2.24 comes from $\mathcal{M}_{\text{Feed}}$ which account for the ideal geometry of the feeds. In the general case, it becomes:

$$\mathcal{M}_{\text{Feed}} = \begin{bmatrix} 1 & 0 & 0 & 0 \\ 0 & \cos 2\alpha & 0 & \sin 2\alpha \\ 0 & 0 & 1 & 0 \\ 0 & -\sin 2\alpha & 0 & \cos 2\alpha \end{bmatrix} \tag{2.27}$$

where α is the angle that reflects the amount of coupling of orthogonal polarizations. In case of linear feeds we have that $\alpha = 0$ and $\mathcal{M}_{\text{feed}}$ becomes the identity matrix.

The next term in eq. 2.24, $\mathcal{M}_{\text{CC}}$ accounts for deviations from the ideal geometry. If the two feeds are not perfectly orthogonal, some polarization will spill-over to the wrong feed. This effect is called *cross-coupling*. If the imperfections are small they can be represented as follows:

$$\mathcal{M}_{\text{CC}} = \begin{bmatrix} 1 & 0 & A & B \\ 0 & 1 & C & D \\ A & -C & 1 & 0 \\ B & -D & 0 & 1 \end{bmatrix} \tag{2.28}$$

where the constants A, B, C, and D depend on the amplitudes, ϵ_1 and ϵ_2, and phases, ϕ_1 and ϕ_2 of the cross couplings:

$$\begin{cases} A &= \epsilon_1 \cos\phi_1 + \epsilon_2 \cos\phi_2 \\ B &= \epsilon_1 \sin\phi_1 + \epsilon_2 \sin\phi_2 \\ C &= \epsilon_1 \cos\phi_1 - \epsilon_2 \cos\phi_2 \\ D &= \epsilon_1 \sin\phi_1 - \epsilon_2 \sin\phi_2 \end{cases} \tag{2.29}$$

The last term of eq. 2.24, M_{amp}, considers differences in the gains and phases for the different polarizations acquired as they are processed. The difference in gain, ΔG, arises from a difference in the amplification mainly caused by slightly different amplifiers in the

first part of the processing. The difference in phase, $\Delta\varphi$, arises from a difference in length of the cables carrying the two polarizations. In the approximation that ΔG is small the Müller matrix can be written as follows:

$$\mathcal{M}_{\text{Amp}} = \begin{bmatrix} 1 & \Delta G/2 & 0 & 0 \\ \Delta G/2 & 0 & 0 & 0 \\ 0 & 0 & \cos\Delta\varphi & -\sin\Delta\varphi \\ 0 & 0 & \sin\Delta\varphi & \cos\Delta\varphi \end{bmatrix} \tag{2.30}$$

The total Müller matrix $\mathcal{M}$ can be recovered after the determination of six parameters: $\epsilon_1, \epsilon_2, \phi_1, \phi_2, \Delta G$, and $\Delta\varphi$. To recover the incoming Stokes vector S_{in}, we need to invert the matrix $\mathcal{M}$ and apply it to the output Stokes vector:

$$S_{\text{in}} = \mathcal{M}^{-1} S_{\text{out}}. \tag{2.31}$$

2.3.3 *Calibration techniques*

The most straight-forward way to calibrate in polarization is to inject an artificial signal (generated by a noise diode) equally in the two polarizations. For linear feeds a noise diode that is 100 percent linearly polarized and with a position angle of 45° is used. This method is useful for correcting a difference in the gains of the amplifiers but does not account for cross-coupling of the feeds.

One way to correct for the cross-coupling is called Measurement Equation Modelling (MEM) described in [366]. This technique requires the observation of a strongly polarized pulsar over a long span of time so that it covers a wide range of parallactic angles and of a source of circular polarization. The difference in response of the feeds at different parallactic angles allows us to measure precisely the cross-coupling parameters.

This method completely calibrates the polarization but requires long tracks of a reference pulsar and is thus very time consuming. A way to still recover the complete solution but at a minimal cost of time is the so-called Measurement Equation Template Matching (METM) [368]. This technique requires a well-calibrated template of a reference pulsar and a recent short observation of the same pulsar. The comparison between the template and the observation is used to measure all of the cross-coupling parameters.

2.4 RM MEASUREMENT

After the data is properly calibrated in polarization, one important property that can be measured is the Faraday Rotation Measure (RM). This parameter is important by itself as it contains information about the magnetic field along the line of sight and for the timing itself. If

the pulsar has a significant amount of Faraday rotation, the polarization position angle at different frequencies will be rotated. When summing all frequencies in order to create a single integrated profile, this rotation will lead to a de-polarization of the signal, which will influence the quality of the timing.

To measure the RM of a pulsar there are different ways: measuring the PA at different frequencies and fitting for equation 1.21; searching for the value of RM that maximizes the linear polarization percentage; RM synthesis [73] which deconvolves the observed polarization in order to re-construct all the Faraday screens the signal crossed.

The first method is the one that will be further developed in this thesis and is described in Chapter 4.1. The second method is implemented in the RMFIT routine in PSRCHIVE [184, 369] and works better with high S/N and high polarization percentage. The RM synthesis technique is shown to obtain similar results than the first method for high S/N sources and worse for low S/N sources (see Fig. 9 in [73]).

3

GLOBULAR CLUSTER 47 TUC: STRUCTURAL PARAMETERS AND GAS

The work described in this Chapter is presented in:
***F. Abbate**, A. Possenti, A. Ridolfi, P. C. C. Freire, F. Camilo, R. N. Manchester, and N. D'Amico "Internal gas models and central black hole in 47 Tucanae using millisecond pulsars." MNRAS, 2018, Vol.481, pp.627–638.*

47 Tuc (depicted in Fig. 1.5) is the second brightest GC in the sky visible to the naked eye in the Southern sky and one of the closest. The main properties of this cluster are reported in Table 3.1. It is located in halo of the Milky Way at a distance from the Galactic plane of about 3.2 kpc. Due to its location close to the South Celestial Pole, it can be observed only by telescopes in the Southern hemisphere. This cluster has been suggested to host an IMBH in the centre. A detailed discussion regarding the presence of the IMBH and a search for its effects on the pulsars in 47 Tuc is carried out in Chapter 5.

In the first part of this chapter I will show how pulsars can be used to probe structural parameters focusing on GC 47 Tuc assuming that there is no IMBH present as is supported by the discussion in Chapter 5. The advantage of using pulsars to probe structural parameters is that they are sensitive also to non-luminous matter and they are not affected by extinction. However, only few clusters have enough pulsars to conduct this type of study. In the second part of the chapter I will focus on the detection of ionized gas and the determination of its density distribution using the observed DM of the pulsars. For this purpose, pulsars are essential as the ionized gas is not visible in any other way.

3.1 47 TUC PULSARS

After two not confirmed claims of detection of pulsars using the Parkes radio telescope [10], the first pulsar was discovered [248] and was followed by many others [80, 208, 249, 285, 311]. Now there are 25 known radio pulsars all of which have a spin period smaller than 8 ms. Over 60 percent of the pulsars are in binary systems, with eight pulsar-WD systems, five *black widow* pulsars, and two *redback* pulsars.

All of the pulsars, with the exception of 47 Tuc P and V, have published phase-connected timing solutions [80, 132, 134–136, 307, 311]. 22 of the pulsars have measured values for the first and second

Table 3.1: Main properties of the globular cluster 47 Tuc.

Parameter	Value	References
Centre RA (J2000)	$00^h24^m05^s.67 \pm 0^s.07$	[263]
Centre Dec (J2000)	$-72°04'52''.62 \pm 0''.26$	[263]
Distance from Sun	4.53 ± 0.04 kpc	[61]
Metallicity	-0.72 dex	[168](2010 edition)
Mass	$(8.4 \pm 0.4) \times 10^5\,M_\odot$	[49]
Tidal radius	119.31 pc	[45]
Core radius	26".5 (0.58 pc)	[49]
Age	10.0 ± 0.4 Gyr	[159]
Escape velocity at core	49.9 km s^{-1}	[45]
Central velocity dispersion	0.574 ± 0.005 mas yr^{-1}	[355]
Central density	$75000 \pm 2000\ M_\odot\ pc^{-3}$	[49, 355]
Central ICM density	$0.067 \pm 0.015\,cm^{-3}$	[133]

period derivative and the proper motion. For 10 of the binary pulsars it was also possible to measure the orbital period derivative. For pulsar 47 Tuc H there is even a 2.3σ detection of a third period derivative. For pulsars 47 Tuc E, H, S, and U there is also a detection of the rate of advance of periastron which allows a determination of the total mass of the system. For pulsar 47 Tuc E, the total mass for the binary system is $2.3 \pm 0.7\ M_\odot$, for 47 Tuc H the mass is $1.61 \pm 0.03\ M_\odot$, for 47 Tuc S the mass is $3.1 \pm 1.1\ M_\odot$, while for 47 Tuc U the total mass is $1.7 \pm 0.7\ M_\odot$. All of the known pulsars, except 47 Tuc X, are located close to the cluster center with a maximum distance of 1.2 arcminute ($\sim$ 3 core radii). This is a consequence of mass segregation, since the pulsar are more massive than the average star in the the GC.

All of the pulsars that have known position have been detected as X-ray sources [51, 58, 60, 161, 162, 172] and the WD companions of 47 Tuc Q, S, T, U, W, and Y have been detected in optical [75, 110, 111, 309].

3.2 STRUCTURAL PARAMETERS

As described in section 1.10, the parameters of the pulsars derived from the timing can be used as probes of the dynamics of the cluster. The period derivative is a probe of the acceleration felt by the pulsars in the gravitational potential of the cluster, the second period derivative is a probe of the jerk felt by the pulsar, while the proper motion (after

subtracting the total proper motion of the GC) gives us the peculiar velocities of the pulsars in the plane of the sky. These parameters can be used to estimate the mass distribution of the GC.

The contributions that affect the measured period derivative can be described as follows:

$$\left(\frac{\dot{P}}{P}\right)_{\text{meas}} = \left(\frac{\dot{P}}{P}\right)_{\text{int}} + \frac{a_c}{c} + \frac{a_g}{c} - \frac{\mu^2 D}{c}, \tag{3.1}$$

where $(\dot{P}/P)_{\text{int}}$ is the spin down caused by magnetic dipole braking, a_c/c is the acceleration along the line of sight caused by the gravitational potential of the GC, a_g/c is the relative acceleration of the cluster with respect to the Solar System in the gravitational potential of the Galaxy, and $\mu^2 D/c$ is the centrifugal acceleration caused by the proper motion of the pulsars called Skhlovskii effect [322], μ is the proper motion of the pulsar, D is the distance of the cluster, and c is the speed of light.

The contribution of the gravitational potential of the Galaxy at the GC's Galactic coordinates a_g/c can be derived from the differential Galactic rotation model [218] and approximately is [275]:

$$a_g = -\cos(b_g)\left(\frac{\Theta_0^2}{R_0}\right)\left[\cos(l_g) + \frac{\beta}{\sin^2(l_g)+\beta^2}\right] \tag{3.2}$$

where $R_0 = 8178 \pm 12_{\text{stat}} \pm 22_{\text{sys}}$ kpc is the distance of the Galactic centre [160], $\Theta_0 = 240 \pm 8$ km s^{-1} [320] and $\beta = (D/R_0)\cos(b_g) - \cos(l_g)$. l_g and b_g are the longitude and latitude of the cluster in Galactic coordinates. In the case of 47 Tuc, the distance from the Solar System is $d = 4.53 \pm 0.08$ kpc [61] and the Galactic coordinates are $l = 305.8953$, and $b = -44.8891$. Thus, we obtain $a_g \simeq -5 \times 10^{-11}$ m s^{-2} which is two orders of magnitude smaller then the measured accelerations.

The average acceleration due to the Shklovskii effect can be estimated by using the proper motion of the cluster measured with data from Gaia Data Release 2 [145]. The measured proper motion is $\mu_{RA} = 5.2477 \pm 0.0016$ mas yr^{-1} and $\mu_{DEC} = -2.5189 \pm 0.0015$ mas yr^{-1}. This average acceleration will therefore be $\simeq 1 \times 10^{-10}$ m s^{-2}.

The most uncertain contribution is the intrinsic spin-down caused by magnetic dipole breaking. It depends on the surface magnetic field as described in equation 1.4 and can vary a lot between pulsars. The distribution of this value can be estimated by looking at the population of MSPs in the Galactic disk taken from the Australia Telescope National Facility (ATNF) catalogue[1] [250]. For them the term a_c/c is not existent and the observed $(\dot{P}/P)_{\text{meas}}$ is dominated by the intrinsic spin down. This value is scattered along a log-normal PDF with

1 The observable parameters for known pulsars can be found at the following webpage: http://www.atnf.csiro.au/people/pulsar/psrcat/

central value $\mu_{\log_{10}(B)} = 8.47$ and sigma $\sigma_{\log_{10}(B)} = 0.33$ [301]. This contribution is of the order of 10^{-9} m s^{-2}.

This contribution, due to its statistical nature, is the main source of uncertainty. In the case of binary pulsars, however, this problem can be avoided. Eq. 3.1 is not strictly applicable only to the spin period but also to other periodic quantities like the orbital period, P_b. For binary pulsars with measured orbital period derivative, we can write the following equation:

$$\left(\frac{\dot{P}_b}{P_b}\right)_{\rm meas} = \left(\frac{\dot{P}_b}{P_b}\right)_{\rm int} + \frac{a_c}{c} + \frac{a_g}{c} - \frac{\mu^2 D}{c}, \tag{3.3}$$

For pulsar-WD binaries the main contribution to $\left(\frac{\dot{P}_b}{P_b}\right)_{\rm int}$ is gravitational wave emission, which is shown to have much smaller effects than the cluster potential. Therefore in these cases, it is possible to estimate directly a_c/c with the main source of error being the observational uncertainty on the orbital period derivative. For black widow systems the situation is different as they usually show large and unpredictable variability of the orbital period [318]. However, black widow pulsars 47 Tuc I and R show small orbital variability and the period derivative can be used to estimate the cluster acceleration[132].

Measuring all the other parameters allows us to probe the contribution a_c/c that depends on the structural parameters of the GC. Thanks to this term we can measure the acceleration felt by each each pulsar in the gravitational potential of the cluster and therefore the mass content and distribution. This value is linked to the structural parameters by equation A.9.

The effects of the cluster potential on the second period derivative can be described as follows [295]:

$$\frac{\ddot{P}}{P} = \frac{1}{c}\dot{\mathbf{a}} \cdot \mathbf{n}, \tag{3.4}$$

where $\mathbf{n}$ is the direction of the line of sight.

The jerks can be due to the mean gravitational potential or the close encounters with nearby stars. The two contributions are of similar magnitude and must be considered together [301]. The jerk due to the mean field is calculated in eq. A.15. The jerk caused by the nearest neighbours, instead cannot be described analytically but only with a statistical description (see section A.4).

To measure both the accelerations and the jerks we need the three dimensional position of the pulsar in the cluster. The components of the position in the plane of the sky are usually known with high accuracy thanks to the timing technique (see section 2.2), while the position along the line of sight is unknown. The measure of the jerks also require the line-of-sight component of the velocity which is not measured for any pulsar. This problem can be solved using

a Markov Chain Monte Carlo (MCMC) algorithm that samples the possible positions and velocities along the line of sight.

3.2.1 *MCMC code*

The MCMC algorithm used to fit for the line-of-sight positions and velocities of the pulsars and the structural parameters has been derived from a work by Prager et al. [301]. The analysis makes use of the EMCEE python package [127] which returns the best fit parameters for the desired model.

The MCMC algorithm works by sampling the parameters in order to look for the set of parameters that maximises the likelihood. The likelihood passed to the algorithm is expressed in logarithms and can be seen as the sum of different log-likelihoods:

$$\mathcal{L} = \mathcal{L}_{x_\perp} + \mathcal{L}_l + \mathcal{L}_{accel} + \mathcal{L}_{jerks} + \mathcal{L}_{vel}, \tag{3.5}$$

where $\mathcal{L}_{x_\perp}$ is the log-likelihood associated with the pulsar position in the plane of the sky, $\mathcal{L}_l$ is the log-likelihood associated to their three-dimensional position, $\mathcal{L}_{accel}$ is the log-likelihood due to the experienced acceleration, $\mathcal{L}_{jerks}$ is the log-likelihood due to the jerk measurements and $\mathcal{L}_{vel}$ is the log-likelihood associated with the velocity measurements.

The log-likelihood associated with the position of the pulsars on the plane of the sky can be found starting from the number density distribution of this stellar component on the plane of the sky (eq. A.1):

$$\mathcal{L}_{x_\perp} \propto \sum_i \log_{10}\left[\left(1 + x_{\perp,i}^2\right)^{\alpha/2}\right], \tag{3.6}$$

where i is the index of the summation over all pulsars.

The log-likelihood associated with the three-dimensional position of the pulsars in the cluster is (eq. A.2):

$$\mathcal{L}_l \propto \sum_i \log_{10}\left[\left(1 + x_{\perp,i}^2 + \frac{l_i^2}{r_c^2}\right)^{(\alpha-1)/2}\right]. \tag{3.7}$$

The acceleration log-likelihood is measured in two different ways depending on whether the pulsar is in a binary system with a measured orbital period derivative. If we know the latter, we can directly probe the acceleration and compare it against the one predicted by the model (eq. A.10). The log-likelihood then becomes:

$$\mathcal{L}_{acc,binary} \propto \sum_i \frac{1}{2\sigma_i}\left(a_{l,i} - a(l|x_\perp, \theta)\right)^2, \tag{3.8}$$

where σ_i is the uncertainty on the measured acceleration, $a_{l,i}$ is the measured acceleration and $a(l|R_\perp, \theta)$ is the predicted acceleration for the set of parameters θ.

If the pulsar is isolated or we has no measurement of the orbital period derivative, we have to estimate the intrinsic spin-down due to magnetic braking. We first subtract the model acceleration from the measured $(\dot{P}/P)$ and then check if the residual acceleration could be due to the intrinsic spin-down. As described in Section 3.2, this quantity can be linked to the surface magnetic field of the pulsar. The magnetic fields of Galactic MSPs follow a log-normal distribution and the log-likelihood becomes:

$$\mathcal{L}_{acc,\,isolated} \propto \sum_i \left[\frac{1}{2\sigma^2_{\log_{10}(B)}} (\log_{10} B_8 - \mu_{\log_{10}(B)})^2 + \log_{10} B_8 \right], \quad (3.9)$$

where B_8 is the magnetic field in units of 10^8 G, whereas $\sigma_{\log_{10}(B)}$ and $\mu_{\log_{10}(B)}$ are the parameters of the lognormal fit performed by Prager et al. [301] on the Galactic MSPs as described in Section 3.2.

As shown in Section A.4, the jerk to which a pulsar is subject is due to both the mean field potential and to nearby stars. The jerk due to the mean field can be estimated directly from the formulas while for the stellar contribution only a statistical description is possible. To estimate the likelihood of measuring a certain value for the jerk we subtract the mean field component and compute the logarithm of the probability that the residual is caused by nearby stars. The log-likelihood becomes:

$$\mathcal{L}_{jerks} = \sum_i \log_{10} \left(\frac{\dot{a}_{nn,i}}{\pi} \frac{1}{[(\dot{a}_{l,i} - \dot{a}_{\mathrm{m}f,i})^2 + \dot{a}^2_{nn,i}]} \right), \quad (3.10)$$

where $\dot{a}_{l,i}$ is the measured jerk, $\dot{a}_{\mathrm{m}f,i}$ is the predicted mean field jerk and $\dot{a}_{nn,i}$ is the scale parameter of the Lorentzian distribution (eq. A.19).

The velocities of the pulsars are distributed according to a Maxwellian distribution, with a velocity dispersion which can be estimated for each pulsar from equation (A.7). Hence the log-likelihood for the velocity is:

$$\mathcal{L}_{vel} \propto \sum_i \left(-3 \log_{10}(\langle v^2 \rangle_i) + 2 \log_{10}(v_{\mathrm{meas},i}) - \frac{3}{2} \frac{v^2_{\mathrm{meas},i}}{\langle v^2 \rangle^2_i} \right). \quad (3.11)$$

As shown in Fig. A.1 it is possible for two different positions along a given line of sight to produce the same line-of-sight acceleration. This generates a bimodal distribution of the line-of-sight position of a pulsar for every measured acceleration. Since the MCMC could get stuck on

one of the two solutions and not explore the parameter space properly, we need to address this problem. We opted for a parallel tempering solution [256] which makes use of chains of different *temperatures* to cover the entire parameter space. The *higher* temperature chains are allowed to move freely while the *colder* chains remain close to the previous values. Combining chains of different temperatures allows us to properly explore the parameter space in order to find the global maximum of the likelihood.

The free parameters used in the fit are: the mass segregation parameter, α, the core radius, r_c, the central density ρ_c, the line-of-sight position of 22 pulsars (47 Tuc P and V do not have a known position and 47 Tuc X is too far from the centre and the approximate equations used are not valid) and the line-of-sight velocity of 21 pulsars. 47 Tuc P, V, and X are excluded for the reasons above and 47 Tuc H has a jerk which has been suggested to be caused by a nearby star so we cannot use it in our fit. The total number of free parameter is thus 46.

The priors on all the parameters are set to be flat except for the core radius for which we used a gaussian prior centred in 0.58 pc and with a standard deviation of 0.03 pc as derived from recent optical observations [49].

The best fit for parameters of 47 Tuc are shown in Fig. 3.1. The results of the fit for the position along the line of sight are reported in Table 3.2. The line of sight velocities are not tightly constrained by our code. They are considered nuisance parameters over which we marginalize.

The posterior distribution of the core radius does not show asymmetries or deviations from the assumed Gaussian prior. This means that the fit is not strongly influenced by this parameter.

The mass segregation parameter, α, is found to be $-2.8^{+0.4}_{-0.7}$. The errors indicate the 68% credible interval of the posterior distribution. This value is consistent with the value of -3.26 ± 0.48 measured in X-rays for the MSPs of 47 Tuc[172]. To check the consistency we also compare, in Fig. 3.2, the cumulative distribution of the pulsars in the plane of the sky with the result obtained with eq. 1.29 using the derived power law index.

The best-fit value for the central density is $\rho_c = 8.6^{+1.3}_{-0.9} \times 10^4$ $M_\odot$ pc^{-3}. This value is compatible with the previously estimated central density of $(7.5 \pm 0.2) \times 10^4$ $M_\odot$ pc^{-3} (Table 3.1).

From the estimates of the core radius and central density we can calculate the velocity dispersion through equation 1.27. We obtain, after converting the result in mas yr^{-1} using the distance estimate of Bogdanov et al. [61], $\sigma_{\mu,0} = 0.60 \pm 0.04$ mas yr^{-1} which is compatible with velocity dispersion measured from the proper motion of the stars [355].

In all models we assumed that the cluster was spherically symmetric. To verify whether this assumption is consistent with the results, we

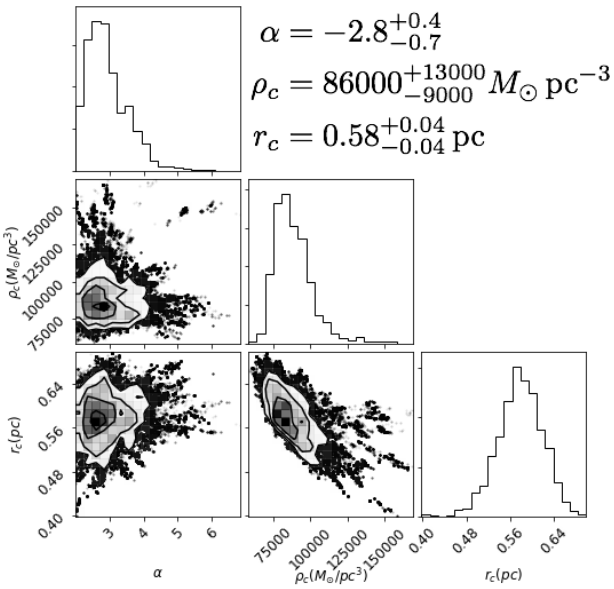

Figure 3.1: Triangle plot showing the marginalized probabilities for the density distribution power law index α, the central density, ρ_c, and the core radius, r_c, for the globular cluster 47 Tuc. The errors indicate the 68% credible intervals.

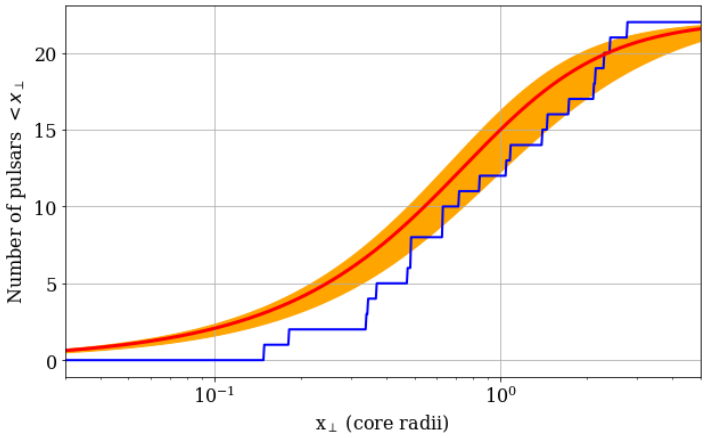

Figure 3.2: Cumulative distribution of the projected offset from the cluster centre. The red line has been obtained integrating eq. (1.26) using the parameter α found in the MCMC fit. The orange area is the 68% credible interval.

Table 3.2: Best-fit parameters for the line-of-sight position of the pulsars. The distance from the centre of the cluster along the plane of the sky, $R_\perp$, is also shown together with the DM values. The errors indicate the 68% credible interval on the posterior distribution.

Pulsar	$R_\perp$ (pc)	DM (pc cm^{-3})	l (pc)
W	0.087	24.4 ± 0.5	$0.40^{+0.29}_{-0.06}$
O	0.106	24.356 ± 0.002	$-0.03^{+0.16}_{-0.03}$
Z	0.198	24.4 ± 0.5	$0.01^{+0.08}_{-0.00}$
R	0.200	24.361 ± 0.007	$-0.22^{+0.08}_{-0.15}$
L	0.214	24.400 ± 0.012	$0.24^{+0.26}_{-0.07}$
ab	0.276	24.373 ± 0.020	$0.02^{+0.12}_{-0.03}$
F	0.283	24.382 ± 0.005	$-0.11^{+0.22}_{-0.07}$
S	0.283	24.376 ± 0.004	$0.58^{+0.17}_{-0.19}$
I	0.365	24.429 ± 0.010	$0.33^{+0.15}_{-0.22}$
G	0.367	24.436 ± 0.004	$0.11^{+0.16}_{-0.03}$
T	0.419	24.411 ± 0.021	$-0.28^{+0.17}_{-0.22}$
Y	0.493	24.468 ± 0.004	$0.19^{+0.03}_{-0.04}$
aa	0.613	24.971 ± 0.007	$0.62^{+0.23}_{-0.18}$
N	0.631	24.574 ± 0.009	$0.17^{+0.28}_{-0.07}$
E	0.818	24.236 ± 0.002	$-0.54^{+0.14}_{-0.12}$
D	0.854	24.732 ± 0.003	$0.04^{+0.11}_{-0.02}$
H	1.012	24.369 ± 0.008	$0.10^{+0.05}_{-0.07}$
U	1.237	24.337 ± 0.004	$-0.80^{+0.26}_{-0.19}$
Q	1.252	24.265 ± 0.004	$-0.33^{+0.13}_{-0.12}$
J	1.342	24.588 ± 0.003	$0.54^{+0.40}_{-0.25}$
M	1.409	24.432 ± 0.016	$0.66^{+0.37}_{-0.19}$
C	1.620	24.600 ± 0.004	$0.75^{+0.78}_{-0.28}$

perform a Kolmogorov-Smirnoff test to check if the measured positions along the line of sight are extracted from the same distribution as the positions along two directions on the plane of the sky. Both tests with right ascension and declination return p-values of ~ 0.6 so the results are consistent with a spherically symmetric cluster.

3.3 GAS MODELS

By using the information (derived in the previous section) about the positions along the line of sight of the pulsars it is possible to investigate which model for the distribution of the internal gas better matches the observed DMs of the 47 Tuc pulsars. We performed a fit to the data presented in Table 3.2 with a Bayesian algorithm without considering pulsars W and Z, because of their imprecise DMs. That allows us to compare models with different parameters through the Bayes factor. This consists of measuring the evidences, which in Bayesian statistics are the integral along the entire parameter space of the likelihood. The evidences can then be compared by calculating the ratio. If the logarithm in base 10 of this ratio is larger than 2, the model with the highest evidence is strongly favoured.

The line-of-sight positions of the pulsars are not normally distributed and therefore standard fitting procedures would not work. To correctly treat their distribution, we extracted the values of the line-of-sight positions at each cycle of the algorithm from the posterior distributions, and built the uncertainty range including the 68% of the posterior density function.

From a given gas density distribution, the contribution $\mathrm{DM_{GC}}$ to the total observed DM due to the globular cluster can be measured with the following integral for each pulsar:

$$\mathrm{DM_{GC}} = \int_{-l_T}^{l} n_g(R_\perp, l')dl', \tag{3.12}$$

where l_T is the tidal radius of the cluster, which is assumed as the maximum radius up to which the gas is present.

3.3.1 *Constant density model*

We first tested the hypothesis of a constant gas density in the region of interest. This is the model that was used by [133] to give the first evidence of ionized gas inside the cluster. Assuming that the region of interest is uniformly permeated by a gas, we do not need to consider the position in the plane of the sky. The total DM for each pulsar is described by the formula:

$$\mathrm{DM} = n_g l + \mathrm{DM_c}, \tag{3.13}$$

where n_g is the value of the gas density and DM_c is the value of the total DM at a plane that passes through the centre of the cluster and is perpendicular to the line of sight (assuming no variation of DM due to the interstellar medium along the various lines of sight to the globular cluster).

Fig. 3.3 shows the best fit with a value of the density $n_g = 0.23 \pm 0.05\,\mathrm{cm}^{-3}$ and $DM_c = 24.38 \pm 0.02\,\mathrm{pc\,cm}^{-3}$. In comparison the values found by [133] are $n_g = 0.067 \pm 0.015\,\mathrm{cm}^{-3}$ and $DM_c = 24.381 \pm 0.009\,\mathrm{pc\,cm}^{-3}$. We find a gas density which is higher than the previous estimate, although with larger uncertainty. The values of the line-of-sight positions of the pulsars and the fits for them are shown in the top panel of Fig. 3.3. The previous values are larger than those found in our analysis. This is probably because of the method used to find the line-of-sight positions of the pulsars. In particular, [133] did not fit for the cluster parameters and took an average value for the intrinsic spin-down. Moreover, since the measurements of the second derivative of the spin period were not available at the time, they had to resolve the ambiguity of the line-of-sight position arbitrarily.

As can be seen in Fig. 3.3 there are some pulsars with DM values very different from the predicted model. We tested whether these outliers had an influence on the fit. We performed the same fitting procedure using randomly chosen subsets of pulsars. In all cases the fits returned values of density and of central DM compatible with the results presented above. So we can conclude that our results are not heavily influenced by the value of some specific millisecond pulsars.

The observed differences of the measured DM from the constant density model have a standard deviation of ~ 0.1 pc cm^{-3}. They can be considered as arising from local over-densities and under-densities inside the cluster or could be due to inhomogeneities in the ISM along the line of sight.

A possible explanation of why pulsar 47 Tuc aa is not well fitted by our model is that it could be located further back than we estimated. The probability of the pulsar being located further than 1.5 pc from the cluster centre is about 4 per cent as measured from the posterior distribution. Statistically, since we have a sample of 22 pulsars, there is a good probability that at least one pulsar would be an outlier at that level.

The region that we are able to probe with the pulsars extends to about 1 pc from the centre. Assuming that this model is valid only in this region we calculate a total mass of gas in the inner 1 pc of $0.023 \pm 0.005\ \mathrm{M}_\odot$.

3.3.2 *King profile distribution*

Another model to be explored is a gas density profile that follows the same King profile as the stars in the globular cluster, suitably scaled.

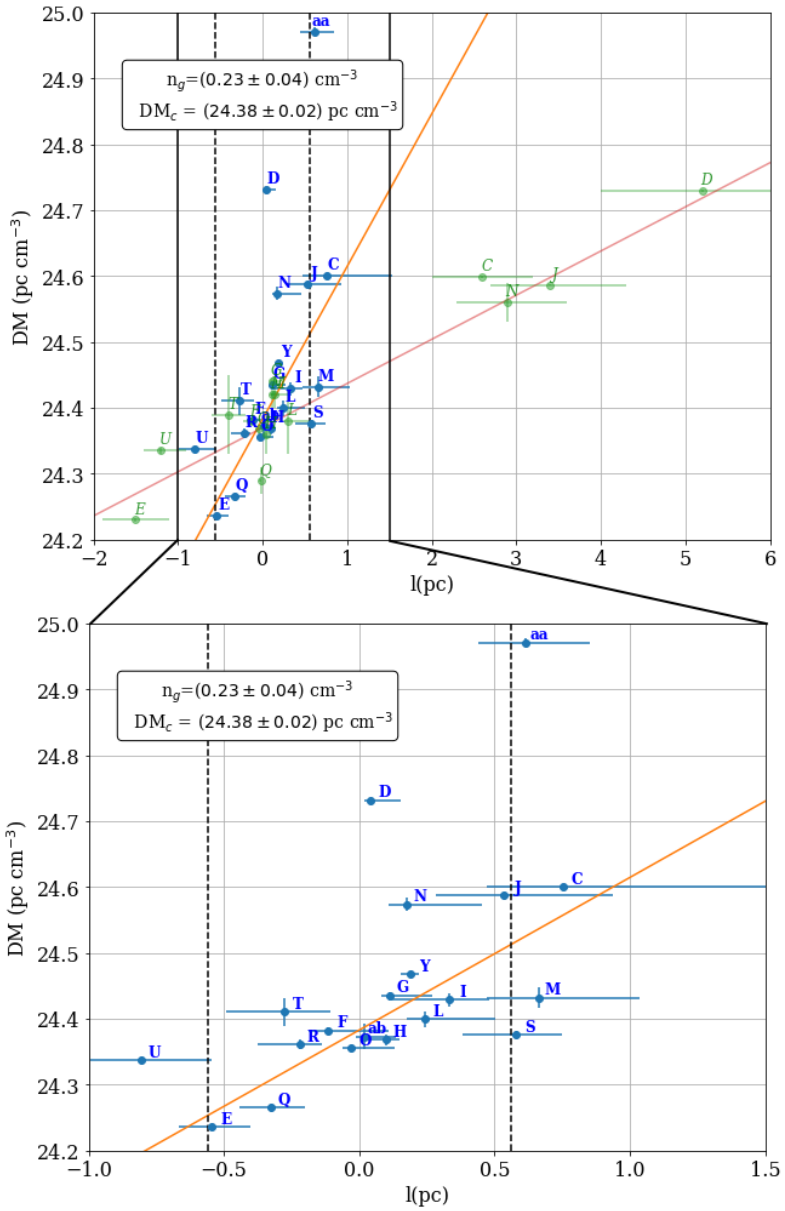

Figure 3.3: Fit of the density of the gas assuming a model of constant density throughout the central regions of the cluster. In the top panel the blue points are associated to the position of the pulsars (l being the distance of each object from the plane passing through the centre and perpendicular to the line of sight) and the error bars indicate the 68% confidence interval on the posterior distribution for the position of the pulsars. The vertical dashed lines correspond to the core radius. The best fit is the orange line. The parameters of the best fit are shown in top left corner of the plot. In the top panel the green points are the distances along the line of sight previously measured [133]. The red line is the best fit found by these authors. The bottom panel is a zoom in the central region of the cluster showing only the new measurements.

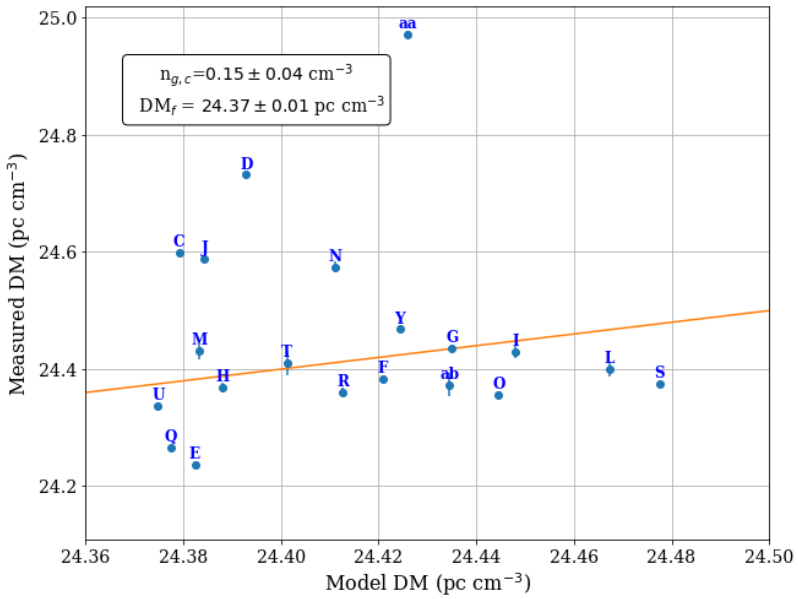

Figure 3.4: Fit of the gas density assuming the gas is distributed following the same King profile as the stars. The plot shows the measured DM versus the DM predicted by the best fit. The orange line represents the unity line. In the case of a perfect fit all the points should fall on the orange line.

This option is motivated by the hypothesis that the observed ionized gas is released by the winds of massive stars. As shown in eq. (A.2) with $\alpha = -2$, the gas density is:

$$n_g(R_\perp, l) = n_{g,c}\left[1 + \left(\frac{R_\perp}{r_c}\right)^2 + \left(\frac{l}{r_c}\right)^2\right]^{-3/2}, \tag{3.14}$$

where $n_{g,c}$ is the density of the gas at the centre of the cluster.

Correspondingly, the total DM for each pulsar should be modelled by the following equation:

$$\mathrm{DM} = \frac{n_{g,c}\, r_c^3}{r_c^2 + R_\perp^2}\left(\frac{l}{\sqrt{l^2 + R_\perp^2 + r_c^2}} + \frac{l_T}{\sqrt{l_T^2 + R_\perp^2 + r_c^2}}\right) + \mathrm{DM}_f, \tag{3.15}$$

where DM$_f$ is the foreground contribution to the total DM.

The best fit for this model is shown in Fig. 3.4. That implies $n_{g,c} = 0.15 \pm 0.04$ cm^{-3} and $\mathrm{DM}_f = 24.37 \pm 0.01$ pc cm^{-3}.

This best fit appears to be much worse than the one reported in the previous section. The logarithm of the Bayes factor K of this model with respect to the constant density model is $\log K \sim 14000 >> 2$. This means that the model with constant gas density is strongly favoured to explain the observed data with respect to a King distribution model for the gas.

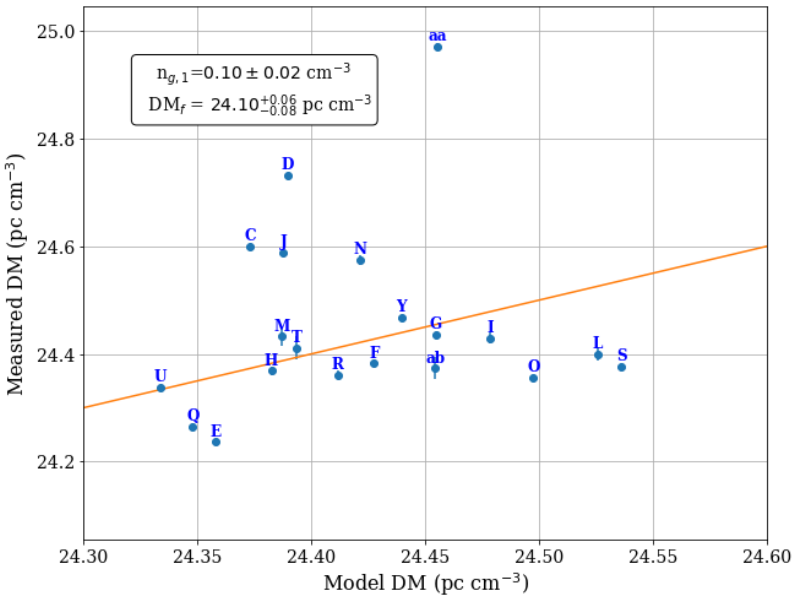

Figure 3.5: Fit of the gas density assuming the distribution of the gas is decreasing as r^{-1}. The plot shows the measured DM versus the DM predicted by the best fit. The orange line represents the unity line. In the case of a perfect fit all the points should fall on the orange line.

3.3.3 *Decreasing model*

It has also been suggested that, in the presence of an IMBH in the centre of the cluster, the gas density profile should be constantly decreasing [287]. We first tested a model in which the gas density drops as $1/r$:

$$n_g(R_\perp, l) = \frac{n_{g,1} r_c}{\sqrt{R_\perp^2 + l^2}}, \tag{3.16}$$

where in this case $n_{g,1}$ corresponds to the density of the gas at one core radius from the centre.

The corresponding total DM for each pulsar is:

$$DM = n_{g,1} r_c \log\left((l^2 + R_\perp^2) + l\right) + \log\left((l_T^2 + R_\perp^2) + l_T\right) + \mathrm{DM}_f, \tag{3.17}$$

where l_T and DM_f are same as in the case of a King profile.

The best fit for this model is reported in Fig. 3.5 with the parameter $n_{g,1} = 0.10 \pm 0.03$ cm^{-3} and $\mathrm{DM}_f = 24.10^{+0.06}_{-0.09}$ pc cm^{-3}.

In this case, the Bayes factor with respect to the constant gas density model and is $\log K \sim 10000 >> 2$. This means that this model with decreasing density is strongly disfavoured to explain the observed data. We repeated the exercise for a gas density scaling as r^{-h} (for

$h = 2, 3$) and always found very large values for the Bayes factor. In summary, it appears that any models in which the gas density decreases within a volume of about 1 pc from the globular cluster centre is significantly disfavoured in comparison with a constant gas density model.

Our analysis confirms the presence of ionized gas in the central regions of 47 Tuc, as it was first reported by [133]. In addition, we have also been able to compare different distributions of gas and one with constant density in the central region is strongly favoured.

3.4 HYDRODYNAMICAL EQUILIBRIUM

McDonald and Zijlstra [259] suggested that the gas might be originating from the winds of evolved RGB and AGB stars in the cluster and it could be completely ionized by the UV radiation of young WD (other kinds of stars are not effective, since they cannot provide enough ionizing photons). According to them, all the ionizing sources in the cluster support a time averaged ionizing flux of 2.43×10^{47} photons s^{-1} with a characteristic temperature of 65000 K. This radiation is enough to heat and ionize all the gas in the cluster. We can check what distribution the gas would follow in this conditions by assuming an equilibrium between the pressure forces and the gravity of the cluster.

The gravitational force on a volume element of gas is expressed by the formula:

$$f_g(r) = -\frac{G\rho_g(r)M_{King}(r)}{r^2}, \tag{3.18}$$

where $\rho_g(r)$ is the density of the gas at radius r and $M_{King}(r)$ is the total mass contained in the cluster assuming a King distribution.

This force must be balanced by the pressure forces. There are two types of pressure: a thermal pressure caused by the temperature of the gas and a radiative pressure driven by the radiation field. This radiation field can interact with the gas since we assume that it is ionized. For an ideal gas the thermal pressure is:

$$P_T(r) = n_g(r)k_B T(r), \tag{3.19}$$

where k_B is the Boltzmann constant. The radiative pressure can be measured from the assumption that the radiation is a blackbody. In this case the pressure at the surface of a star is:

$$P_\star = \frac{4\sigma_{sb}}{3c}T_R^4, \tag{3.20}$$

where T_R is the temperature of the star and σ_{sb} is the Stefan-Boltzmann constant. The radiation pressure has a dependence on the distance r

from the surface as $P_R = P_\star (R_\star / r)^2$, where $R_\star$ is the radius of the star. If we assume that the radiation is coming from WDs, the total radiation pressure at a radius r becomes:

$$P_R(r) = P_\star \left(\frac{R_\star}{r} \right)^2 N_\star(r), \tag{3.21}$$

where $N_\star(r)$ is the number of WDs contained within a radius r and assuming they follow the same King distribution as the normal stars.

Therefore the pressure force per unit volume can be written as:

$$f_P = -\frac{dP}{dr} = -\frac{dP_T}{dr} - \frac{dP_R}{dr} \tag{3.22}$$

All that is needed to solve the differential equation is the temperature of the gas. The latter can be measured by solving the radiative transfer in the cluster with the given radiation field. We did this using the software CLOUDY[2]. For the first run of the code we assumed gas at the constant density of 0.23 cm^{-3} and a metallicity of [Fe/H]$= -0.72$. We used the temperature distribution found this way to solve the equilibrium equation and found the density distribution of the gas. We reiterated the process until convergence. The final temperature and density distributions are shown in Fig. 3.6. The gas density appears to slightly increase in the central parsec and then drop outside. However, this distribution can hardly be distinguished from a constant density profile when looking at pulsar data, owing to the uncertainties on the line-of-sight positions and to the internal scatter of DM. Moreover the set of pulsars is concentrated in the central region where the gas density has not yet decreased. The resulting temperature is able to maintain all the hydrogen and helium completely ionized and keep the heavier elements at a high ionization state.

Many assumptions could affect the results above: e.g. the hypotheses of an ionizing radiation which is constant in time and that is produced only at the centre of the cluster could break down. A more detailed modelling of the equilibrium of the gas, including secular variations in the energy input, must be considered to better understand the behaviour and/or the status of equilibrium of the gas.

3.5 LIMITS ON A POSSIBLE IMBH

Our results about the shape of the gas density in the central region of 47 Tuc (a radially decreasing density profile being disfavoured with respect to a constant density distribution) do not support the presence of an IMBH at the centre but no mass limit can be given using this

2 Version 17.00 of the code is described by [122]. Software can be found at www.nublado.org.

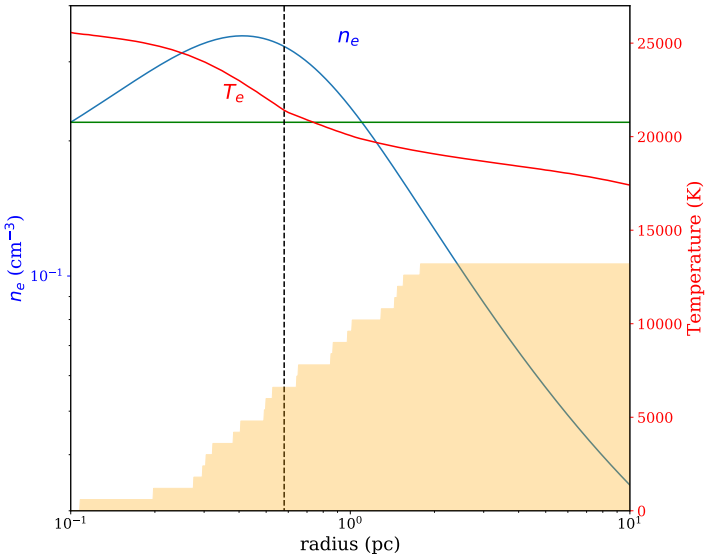

Figure 3.6: Temperature and density profile for the gas in 47 Tuc as obtained from the CLOUDY run and solving the eq. 3.22. The dashed vertical black line is the core radius while the green horizontal line is the estimated value of $n = 0.23$ cm^{-3}. The orange histogram shows the cumulative distribution of the pulsars analysed in this work. See text for more details.

argument as models are not detailed enough [287]. On the other hand, the estimate of the density and the temperature profile of the gas (see previous section) opens also the possibility of putting an independent limit on the mass of the central IMBH. If gas is present around a black hole it should accrete and emit radiation from radio to X-rays. Since only upper limits on such radiation have been derived for 47 Tuc [230, 344], from the theory of accretion we can derive an upper limit on the mass.

This method has been extensively used in the literature [178, 230, 241] and makes use of the Bondi-Hoyle-Lyttleton theory of spherical accretion [64, 65, 185]. According to this model, the mass accretion rate on a black hole of mass M_{IMBH} is:

$$\dot{M}_{BHL} = 4\pi G^2 M_{IMBH}^2 \rho_g c_s^{-3}, \tag{3.23}$$

where ρ_g is the density of the gas far from the black hole and c_s is the sound speed far from the black hole. The sound speed for a thermal gas can be written as $c_s = \sqrt{\gamma k_B T/(\mu_{mol} m_p)}$, where $\gamma = 5/3$ is the adiabatic index and $\mu_{mol} \sim 1.25$ is the mean molecular weight. Rewriting the accretion rate as a function of the mass of the black hole and the density and temperature of the gas we obtain (the same

formula in [240] and in [230] is reported with a mistake in the sign of the exponent of the temperature):

$$\dot{M}_{\rm BHL} = 3.2 \times 10^{17} \left(\frac{\rm M_{BH}}{2000 M_\odot}\right)^2 \left(\frac{n}{0.2\,\rm Hcm^{-3}}\right) \left(\frac{T}{10^4 \rm K}\right)^{-1.5} (\rm g\,s^{-1}). \tag{3.24}$$

The correct value for the accretion rate $\dot{m}$ must account for the accretion efficiency (ϵ) which is around 3% [241], but can be as low as 0.1% [178]: that is because the black hole is supposed to be in a low accretion regime. This regime is prevalent in the cases where the sound speed is higher than the velocity dispersion. In our case the sound speed as measured with the formula reported above is ~ 16 km/s while the velocity dispersion is only ~ 13 km/s.

The X-ray luminosity of the black hole can be measured with the formula $L_X = \eta \dot{m}$, where η is the radiative efficiency, which, for the low luminosity state, can be expressed as $0.5\dot{m}c^4/L_{\rm EDD}$ [241]. In this equation $\rm L_{EDD} = 1.26 \times 10^{38} (M_{BH}/M_\odot)$ erg s^{-1} is the Eddington luminosity.

This luminosity can be compared with the observation to give the maximum possible mass that avoids detection. Usually, however, the most stringent results are obtained from observations in the radio band. The flux density in radio at 5 GHz is in turn linked to the luminosity in X-rays by the following formula [265]:

$$F_{\rm 5GHz} = 10 \left(\frac{L_X}{3 \times 10^{31} \rm erg\,s^{-1}}\right)^{0.6} \left(\frac{\rm M_{BH}}{100\,M_\odot}\right)^{0.78} \left(\frac{d}{10\,\rm kpc}\right)^{-2} (\mu \rm Jy). \tag{3.25}$$

Solving for $\rm M_{BH}$ and expressing all quantities as a function of known parameters we obtain:

$$\begin{aligned} \rm M_{BH} = 44.7\,(F_{5GHz})^{0.39} \left(\frac{n}{0.2\,\rm Hcm^{-3}}\right)^{-0.47} \left(\frac{T}{10^4 \rm K}\right)^{0.7} \\ \times\ \epsilon^{-0.47} \left(\frac{d}{10\rm kpc}\right)^{0.78} (\rm M_\odot). \end{aligned} \tag{3.26}$$

With the values for the density and temperature estimated above, the assumed distance of 47 Tuc and the 3σ upper limit for any radio flux at 5 GHz (11.1 μJy, [344]), we obtain ~ 550 $\rm M_\odot$ for the reference $\epsilon = 3\%$ case, and ~ 2500 $\rm M_\odot$ for the more conservative $\epsilon = 0.1\%$ hypothesis. These values will be compared with the ones obtained dynamically in Chapter 5.

4

GLOBULAR CLUSTER 47 TUC: MAGNETIC FIELD

The work described in this Chapter is presented in:
***F. Abbate**, A. Possenti, C. Tiburzi, E. Barr, W. van Straten, A. Ridolfi, and P. C. C. Freire "Constraints from globular cluster pulsars on the magnetic field in the Galactic halo." Submitted to Nature Astronomy.*

In this chapter we show how measurements of RM of GC pulsars can not only probe the magnetic field of the cluster but also give us precious information on the Galactic halo and on a possible magnetized outflow emitted by the Galactic disk.

The Galactic magnetic field has important effects on the evolution of the Galaxy, by affecting star formation, propagation of cosmic rays and by regulating Galactic winds. However, its origin and precise structure is poorly known [143, 358]. The Galactic magnetic field in the disk is thought to be made of an ordered component at large scales and a random component at small scales with a turbulent nature [170]. The magnetic field in the halo that surrounds the Galaxy is also poorly known [169]; it is usually thought to be predominantly azimuthal [166] but a component perpendicular to the Galactic disk has been suggested [125, 323] and found some support [191, 339, 349]. A possible origin of this component is a magnetized outflow from the disk [347] whose existence is supported by radio observations [86] and by diffuse Galactic X-ray observations [116].

The advantages of using GC pulsars instead of Galactic field pulsars for these kind of studies is threefold: the angular separation of the pulsars is from arcseconds to arcminutes, contrary to field pulsars which are usually separated by more than a degree [278]; the distances to the GCs is very well known from optical studies (e.g. [46]); and a significant fraction of GCs is located in the Galactic halo.

We present the results of polarimetric observations of 47 Tuc. Through these observations we are able to measure the RM of some pulsars and thus probe the magnetic field in front and inside the GC. These measurements show significant fluctuations which we attribute to a magnetic field in the cluster amplified by the interaction with a magnetized Galactic outflow.

4.1 OBSERVATIONS AND RM MEASURE

The observations for this study were taken using the 64m Parkes radio telescope in Australia between April 2014 and March 2015. The total integration time is $\sim$ 80 hours. The observations were carried out with the central beam of the Parkes Multi-Beam Receiver [334] which has a full width half maximum of 14.4′. The backend used is CASPSR (CASPER Parkes Swinburne Recorder) with a central frequency of 1382 MHz and a bandwidth of 400 MHz. Due to interference the observing bandwidth was reduced to 312 MHz. The data was coherently dedispersed and acquired in all four Stokes parameters, 1024 frequency channels and 1024 pulse bins.

The observations were recorded in baseband mode and processed offline separately for each pulsar. The data were reduced and calibrated with the PSRCHIVE software package [184, 369]. Each observation was first cleaned from Radio Frequency Interference (RFI) both in frequency and time. To remove strong RFI at the edges of the observing band, the total bandwidth was reduced from 400 MHz to 312 MHz. The data were calibrated in flux using averaged observations of Hydra A and calibrated in polarization using the METM [368] technique. The pulsars were coherently dedispersed to entirely remove the effects of pulse dispersion caused by the ionised gas along the line of sight and were folded according to the best available timing solutions [132, 307]. Different observations were summed together to obtain integrated profiles with high S/N. The pulsars in 47 Tuc are heavily affected by scintillation so only the best observations for each pulsar were used to produce the integrated profiles. The number of profile bins for each pulsar was reduced in order to smooth the profile. The RM has been measured by fitting for equation 1.21 with a code written in Python following the previous prescriptions of Noutsos et al. [278] and Tiburzi et al. [340].

By looking at the profile, we first select a pulse region where the pulse was present in linear polarization and another off-pulse region dominated by noise. For each frequency channel we measured the average PA along the pulse with the formula:

$$\mathrm{PA} = \frac{1}{2} \arctan \left(\frac{\sum_{i=n_{\mathrm{start}}}^{n_{\mathrm{end}}} U_i}{\sum_{i=n_{\mathrm{start}}}^{n_{\mathrm{end}}} Q_i} \right), \tag{4.1}$$

where U_i and Q_i are the Stokes parameters U and Q for the ith bin of the profile and n_{start} and n_{end} are the start and the end of the pulse region.

To calculate the error on the PAs, we first measured the total linear polarization as:

$$L_{\mathrm{meas}} = \sqrt{\left(\sum_{i=n_{\mathrm{start}}}^{n_{\mathrm{end}}} U_i\right)^2 + \left(\sum_{i=n_{\mathrm{start}}}^{n_{\mathrm{end}}} Q_i\right)^2}. \tag{4.2}$$

Since U and Q are affected by noise and L_{meas} is a positive definite quantity, it is positively biased. To remove the bias [354] we calculated $p_0 = L_{\mathrm{meas}}/(rms(I)\sqrt{n_{\mathrm{pulse}}})$, where $rms(I)$ is the off-pulse root mean square of the total intensity profile and n_{pulse} is the number of bins in the pulse region. The true value of L is:

$$L_{\mathrm{true}} = \begin{cases} 0.0 & \text{if } p_0 < 2.0 \\ \sqrt{L_{\mathrm{meas}}^2 - (rms(I)\sqrt{n_{\mathrm{pulse}}})^2} & \text{otherwise} \end{cases}. \tag{4.3}$$

This is the best correction when $p_0 > 0.7$ [324]. The error of the PAs can be determined by measuring $P_0 = L_{\mathrm{true}}/(rms(I)\sqrt{n_{\mathrm{pulse}}})$; if P_0 is greater than 10, the underlying distribution can be described by a gaussian [115] and therefore the error is:

$$\sigma_{PA} = \frac{1}{2P_0}, \tag{4.4}$$

If instead P_0 is lower than 10, the assumption of a normal distribution is not valid. In this case we need to use the distribution described by [274]:

$$G(\mathrm{PA} - \mathrm{PA}_{true}; P_0) = \frac{1}{\sqrt{\pi}}\left(\frac{1}{\sqrt{\pi}} + \eta_0 e^{\eta_0^2}[1 + \mathrm{erf}(\eta_0)]\right) e^{-P_0^2/2} \tag{4.5}$$

where PA_{true} is the measured value of PA, $\eta_0 = (P_0/\sqrt{2})\cos 2(\mathrm{PA} - \mathrm{PA}_{\mathrm{true}})$ and erf is the Gaussian error function. This distribution is not analytically integrable and to calculate the error we need to numerically integrate this distribution between $\pm\sigma_{\mathrm{PA}}$ in order to obtain 0.683.

Since we are only looking at the pulsed emission, we are sure that all of the polarized emission is coming from the pulsar. Therefore, in the pulsar data we only expect to find a single Faraday component. We performed a least-square fit to find the RM according to the formula:

$$\mathrm{PA}(f) = RMc^2\frac{1}{f^2} + \mathrm{PA}_\infty, \tag{4.6}$$

where PA_∞ is the value of PA at very high frequency.

Almost all pulsars are known to show variations of PA as a function of pulse phase. In these cases, summing together signals over a large

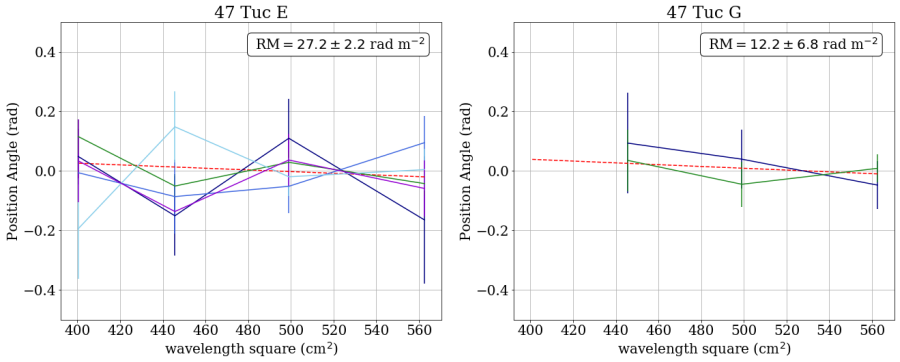

Figure 4.1: Examples of two fits of RM for the pulsars 47 Tuc E and G described in Chapter 4. Both are examples of simultaneous fits over different regions of pulse longitude. In the case of 47 Tuc E we divided the pulse in 5 regions and performed a fit for a single RM for all regions. To facilitate visual inspection of the fit quality, the mean PA was subtracted from each region. The red dashed line shows the best fit. The data have been previously corrected assuming a RM of 30 rad m^{-2} so a straight line with a slope of zero in the plot corresponds to an RM value of 30 rad m^{-2}. For 47 Tuc G we divided the pulse longitude in two regions. The data have been corrected assuming an RM of 15 rad m^{-2}. In both regions the PAs corresponding to the first wavelength squared bin have been removed because the linear polarization is too weak ($p_0 < 2.0$).

rotational phase will lead to a depolarisation of the signal and larger uncertainties. To face this problem, where there is enough S/N, we divide the pulse into regions and perform a simultaneous fit with a single value of RM. The value of PA_∞ can be different for every region and does not influence the measure of RM so we leave it as a free parameter. This way we recover an average value which is close to the real RM. Two examples of these fits are reported in Fig. 4.1.

This approach is also useful when dealing with pulsars with a multi-peaked profile. In pulsars with multi-peaked profile summing all of the polarization information from the pulse together will add a considerable amount of noise which will increase the uncertainty of the measure. Also in this case, this approach leads to a more precise estimate of RM.

Since the error on the PAs is not always Gaussian, the least-square fitting algorithm does not always return the correct uncertainty on RM. To measure it in a more statistically sound way we perform a Monte Carlo simulation. In this simulation we created synthetic profiles of the real pulsars for the U and Q polarization in four frequency bands with the same polarization and added a random Gaussian noise with rms(I) as standard deviation. We calculated the value of RM with the procedure described above for 1000 times and showed that the results followed a Gaussian distribution. We took the standard deviation of

the Gaussian of the simulated results as representative of the error on the RM.

This technique of estimating RM can be affected by the n-π ambiguity. Measuring an angle using the arctangent function always returns a value between -$\pi/2$ and $\pi/2$. If the RM value of the pulsar is such that the PA rotation in the observed frequency band is higher than $\pi/2$, the measured values of PA will be wrong by a factor π and the fit will not return the correct value of RM. To solve this problem, we measured the differences between PAs of neighbouring frequency channels and if these differences are higher than $\pi/2$ we add or subtract π in order to correct the PA. This method has problems if the RM is so high that between two adjacent frequency bins the rotation induced is higher than $\pi/2$. This happens if RM is higher than 247 rad m^{-2} or lower than -247 rad m^{-2}.

The profiles of the pulsars were then corrected for the measured RM and summed at all frequencies. For the pulsars with no measured RM, no correction has been applied.

A source of error for the RM that was neglected is the ionospheric contribution. This is typically between 0.5 and 3 rad m^{-2} and shows strong diurnal variations [341, 360]. Since our measured errors are usually larger, applying this correction would not change much the results.

Other important quantities to measure are the amount of linear polarization and the absolute value of circular polarization. The measured $|V|_{\rm meas}$ is positively biased and it needs to be corrected with the prescription of [198]:

$$|V|_{\rm true} = \begin{cases} 0.0 & \text{if } |V|_{\rm meas}/b < 2.0 \\ \sqrt{|V|^2_{\rm meas} - b^2} & \text{otherwise} \end{cases}, \tag{4.7}$$

where $b = \sqrt{\frac{2}{\pi}} \times \mathrm{rms}(V)$.

In the previous equation $\mathrm{rms}(V)$ is the root mean square of the off pulse region in the Stokes parameter V.

The luminosity and the polarization percentages are measured with:

$$\mathrm{S}_0 = \frac{1}{n_{bin}} \sum_{i=n_{start}}^{n_{end}} I_i \tag{4.8}$$

$$\mathrm{L\,per\,cent} = \frac{1}{n_{bin}} \sum_{i=n_{start}}^{n_{end}} L_{true,i} \times \frac{100}{S_0} \tag{4.9}$$

$$\mathrm{V\,per\,cent} = \frac{1}{n_{bin}} \sum_{i=n_{start}}^{n_{end}} V_i \times \frac{100}{S_0} \tag{4.10}$$

$$|\mathrm{V}|\,\mathrm{per\,cent} = \frac{1}{n_{bin}} \sum_{i=n_{start}}^{n_{end}} |V|_{true,i} \times \frac{100}{S_0} \tag{4.11}$$

where n_{bin} is the total number of bins of the profile and $L_{true,i}$, V_i, $|V|_{true,i}$ are values of linear, circular and absolute circular polarization of the bin i.

4.2 POLARIZATION PROFILES

The pulsars P, V, W, X, Z, aa and ab were not detected in the observations. For the pulsars H, M, R, S and U that were detected it was not possible to measure the value of RM, because of the low S/N and low polarization.

We briefly describe the profiles in total intensity, linear and circular polarization of the analysed pulsars presented in Fig.4.2 and 4.3.

47TUC C This pulsar has a double peaked profile with a dominant leading peak. Both components show distinct linear polarization with the trailing component being the brightest. The circular polarization is similar and has a very dominant trailing component following the trend noted by Johnston et al. [194] and confirmed by Weltevrede and Johnston [356]. The PA doesn't seem to follow a clear trend.

47TUC D This pulsar shows a single asymmetric peak. The linear polarization is only visible in correspondence with the brightest part of the profile. No significant circular polarization is seen.

47TUC E The profile shows three different components with increasing brightness. The first component has very high linear polarization and a very small negative amount of circular polarization. The second component has lower linear polarization and does not show any circular amount. The third component shows very sharp linear and circular polarization. Also this pulsar seems to follow the trend presented by Johnston et al. [194]. The PA is flat in the first component and shows almost orthogonal jumps in the second and third component. A decrease in linear polarization seems to occur in correspondence with the jumps, consistent with what seen by Karastergiou, Johnston, and Manchester [199] that the jump is caused by the mixing of the modes of emission.

47TUC F In the total intensity profile the pulsar shows a large single component. The component is clearly visible with similar fluxes in linear and circular polarization.

47TUC G The pulsar shows two sharp components in total intensity with the leading being the dominant one. The same peaks are visible in the linear polarization profiles but here the trailing component is dominant. There is no significant circular polarization. The PAs of the two peaks appear to be orthogonal.

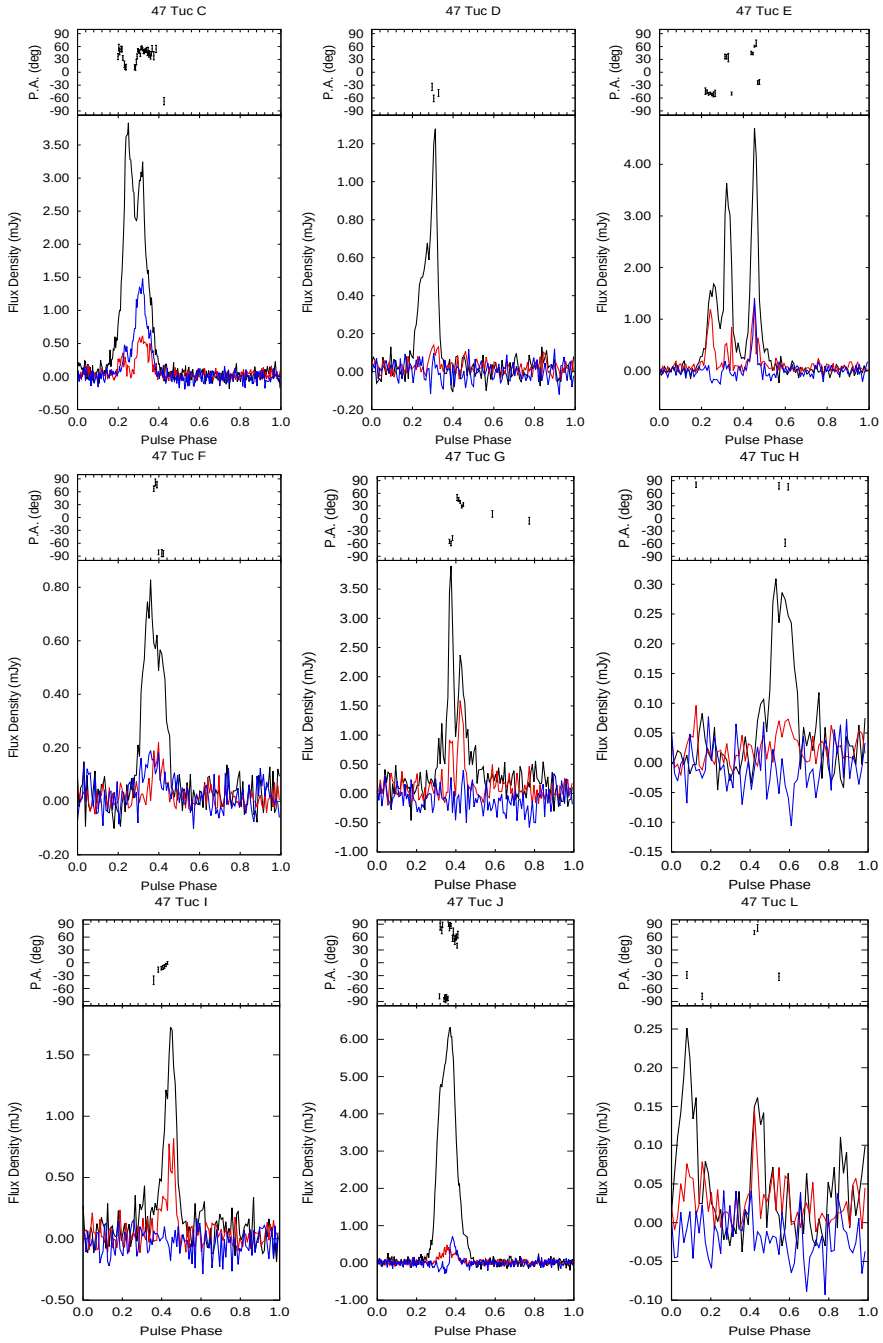

Figure 4.2: Polarization profiles of the pulsars detected in the observations. The top panel of each plot shows the PA variation from the celestial north as a function of pulse phase. The PAs are plotted only if the linear polarization is above 2σ. The bottom plot shows the flux density of the integrated profile. The thick black line is the total intensity, the thin black line is the linear polarization and the dashed line is the circular polarization. The centre frequency of the observations is written on the right of the plot. The profile for the pulsars with measured RM are corrected for the measured value. Each profile is described in details in the text.

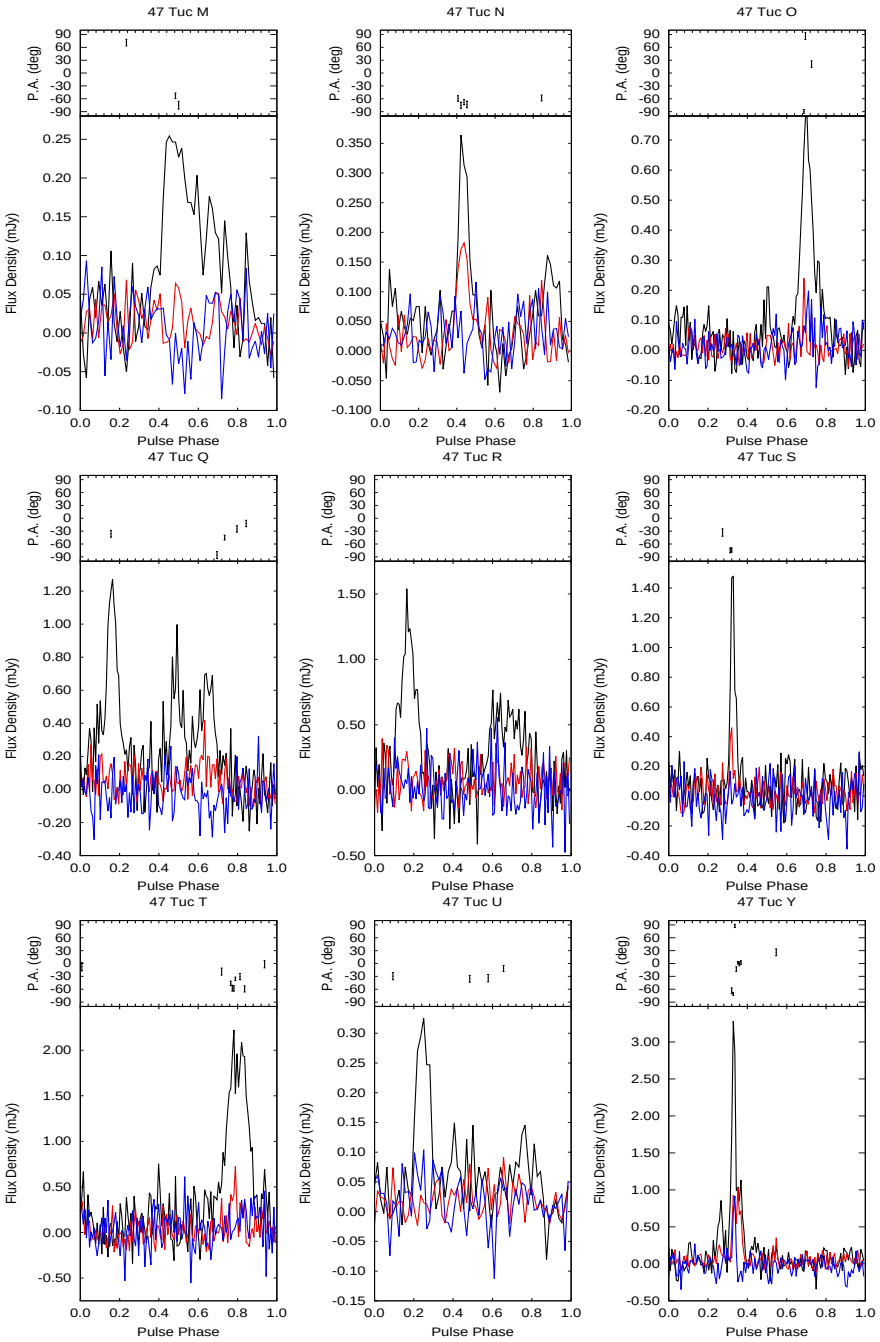

Figure 4.3: Continued.

47TUC H The profile shows a single broad component with no significant polarization.

47TUC I The total intensity profile shows a single peak. The linear polarization is very high while there is no significant circular polarization. the PAs increase linearly along the profile.

47TUC J The profile shows a very bright single component. This component is broad and shows asymmetries that did not appear in the profile presented in [135]. The linear polarization is very small but clearly visible. The circular polarization changes handedness in the centre of the profile from negative to positive. The PA decreases along the profile along a curve that could be described in the context of the RVM [303]. This decrease is in contrast with the model of [304] where the authors suggested that a positive change of handedness of the circular polarization should be accompanied with an increase in PA.

47TUC L The profile of this pulsar is very noisy and shows two clear peaks with the first being brighter. This profile is in contrast with the one shown in [135] where the pulsar shows three components and the two brighter ones have similar flux. This is probably caused by the low S/N of our observations. The second component shows a very high linear polarization fraction. No significant circular polarization is detected.

47TUC M This pulsar shows in total intensity a very broad and asymmetric single component. No significant polarization is detected.

47TUC N The profile shows a bright component and a less bright interpulse. The main component has very high linear polarization but no circular polarization is detected.

47TUC O The profile has a very sharp and symmetrical single component. Only a single spike of linear polarization is clearly seen above the noise. Centred with the total intensity profile is a small amount of circular polarization.

47TUC Q The total intensity profile shows one dominant component and other two smaller components. The first and the second component do not show any significant linear polarization but the third does. No significant circular polarization is detected.

47TUC R This pulsar shows a bright component and, separated by half a rotation, a wider and dimmer component. No significant polarization is seen.

47TUC S The total intensity profile shows a very bright and sharp component. This component is highly linearly polarized but no significant circular polarization is detected.

47TUC T The profile in total intensity shows a single broad component with a small amount of linear polarization near the centre. No circular polarization is detected.

47TUC U This pulsar shows a single component in total intensity. In previous works [80, 135] it showed other two components which are not visible in our observations because of high noise. No linear or circular polarizations are detected.

47TUCY This profile shows a sharp bright component preceded by a smaller component. The leading component does not have any significant polarization. The trailing component, instead, shows a very high degree of linear polarization. The circular polarization is high in the trailing component following the trend noted by [194]. It shows indications of changing handedness near the centre of the profile. The PAs show an almost orthogonal jump in correspondence with the drop of circular polarization.

4.3 RM RESULTS

The measured values of flux, linear polarization, circular polarization, RM and average magnetic field along the line of sight are reported in the table 4.1 and 4.2. The linear polarization of the observed pulsars ranges from begin undetected for 47Tuc U to $\sim$ 60 % for 47Tuc N. The average value is $\sim$ 25 % and the standard deviation is $\sim$ 17 %. The absolute value of circular polarization ranges from being undetected for 47Tuc S to $\sim$ 30 % for 47Tuc C. The average value is $\sim$ 9 % with a standard deviation of $\sim$ 7 %.

Initial results indicated a correlation between the RMs and the spatial distribution of the pulsars. To investigate this, we performed a fit using a Bayesian maximum likelihood algorithm with a linear model described by:

$$\mathrm{RM}_{\mathrm{lin}}(i|m,\theta,\mathrm{RM}_0) = mR_{i,\theta} + \mathrm{RM}_0, \tag{4.12}$$

where $R_{i,\theta}$ is the distance of each pulsar relative to the cluster centre and projected along the axis in the plane of the sky with an inclination angle of θ (measured from North to East) and is defined as $R_{i,\theta} = \mathrm{RA}_i \sin\theta + \mathrm{DEC}_i \cos\theta$, where RA_i and DEC_i are the right ascension and declination of each pulsar after subtracting the right ascension and declination of the cluster centre. The geometry of this model is shown in Fig. 4.4. The free parameters are the magnitude of the

Table 4.1: Summary of the main results of the analysis. The second column (S_0) is the total intensity flux. The columns L per cent, V per cent and $|V|$ per cent are percentages of the the linear, circular and the absolute value for the circular polarizations. The column RM is the value of the Faraday rotation measure. The column $\langle B_{\parallel} \rangle$ is the average value of the parallel component of the magnetic field. For the total intensity flux the error presented is at 3σ, for all the other quantities is at 1σ.

Name	S_0 (mJy)	L (%)	V (%)	$\lvert V \rvert$ (%)	RM (rad m^{-2})	$\langle B_{\parallel} \rangle$ (μG)
C	0.420	15.4	27.1	27.1	33.4	1.36
	(0.010)	(0.4)	(0.2)	(0.3)	(2.4)	(0.10)
D	0.061	13.3	−0.2	2.6	11.8	0.48
	(0.004)	(1.8)	(1.0)	(1.1)	(11.8)	(0.48)
E	0.446	27.4	4.2	9.8	27.2	1.12
	(0.010)	(1.1)	(0.5)	(0.5)	(2.2)	(0.09)
F	0.080	18.7	17.4	17.4	17.4	0.71
	(0.006)	(1.8)	(1.1)	(1.6)	(8.1)	(0.33)
G	0.202	44.1	−1.6	5.7	12.2	0.50
	(0.018)	(2.4)	(1.5)	(1.7)	(6.8)	(0.28)
H	0.036	13.1	−5.1	5.1		
	(0.005)	(4.7)	(2.3)	(3.6)		
I	0.116	46.0	−1.1	1.1	4.9	0.20
	(0.012)	(1.7)	(1.4)	(1.7)	(5.8)	(0.24)
J	0.643	5.9	2.0	4.8	−9.1	−0.37
	(0.007)	(0.2)	(0.1)	(0.2)	(3.1)	(0.13)
L	0.011	55.9	−6.5	6.5	18.7	0.77
	(0.004)	(10.2)	(6.2)	(7.5)	(11.0)	(0.45)

Table 4.2: Continued.

Name	S_0 (mJy)	L (%)	V (%)	$\lvert V\rvert$ (%)	RM (rad m^{-2})	$\langle B_{\parallel}\rangle$ (μG)
M	0.062	12.3	−2.2	12.3		
	(0.010)	(3.7)	(2.0)	(2.6)		
N	0.024	62.7	7.9	15.1	−0.4	−0.02
	(0.005)	(5.4)	(2.6)	(5.2)	(5.6)	(0.23)
O	0.060	9.8	11.6	14.8	23.8	0.98
	(0.006)	(1.6)	(1.1)	(1.7)	(17.0)	(0.70)
Q	0.121	23.5	−1.8	7.3	−9.1	−0.38
	(0.016)	(3.4)	(1.7)	(2.8)	(9.9)	(0.41)
R	0.119	14.4	4.1	4.1		
	(0.019)	(4.9)	(1.2)	(3.8)		
S	0.044	24.3	0.0	0.0		
	(0.009)	(3.7)	(3.0)	(3.5)		
T	0.255	15.7	5.1	5.1	12.2	0.50
	(0.027)	(1.9)	(1.5)	(2.2)	(12.7)	(0.52)
U	0.024	0.0	8.9	8.9		
	(0.006)	(5.1)	(2.2)	(3.8)		
Y	0.110	45.6	9.5	15.9	24.5	1.00
	(0.009)	(2.7)	(1.5)	(2.0)	(3.5)	(0.14)

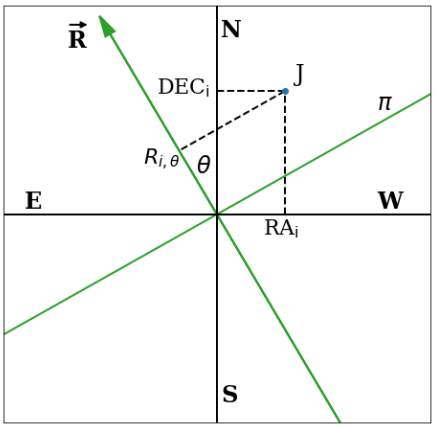

Figure 4.4: Diagram showing the geometry of the linear model used to fit the RM of the pulsars. The pulsar J is shown as an example.

gradient m, the inclination angle θ, and the value of RM at the cluster centre, RM_0.

The Bayesian algorithm minimizes a Gaussian log-likelihood of the form:

$$\mathcal{L} \propto \sum_{i}^{N} -\frac{1}{2\sigma_{\mathrm{RM},i}}(\mathrm{RM}_{\mathrm{meas},i} - \mathrm{RM}_{\mathrm{lin},i}), \tag{4.13}$$

where N is the number of pulsars with measured RM, $\mathrm{RM}_{\mathrm{meas},i}$ is the measured RM for pulsar i and $\sigma_{\mathrm{RM},i}$ is the uncertainty on the measure.

The best-fitting model is shown in Fig 4.5 and represented on top of a map of the cluster in Fig. 4.6. The parameters of the fit and the best-fitting values are the magnitude of the gradient, $m = -0.77 \pm 0.06$ rad m^{-2} arcsec^{-1}, the inclination angle of the gradient measured from Celestial North to East, $\theta = 30 \pm 2$ deg, and the value of RM at the centre of the cluster, $\mathrm{RM}_0 = 20 \pm 1$ rad m^{-2}. The reduced chi-square of the fit is 0.7 with 10 degrees of freedom. We also checked if the linear correlation found could be replicated by a random distribution of RM. To do so we repeated this analysis 10000 times extracting the RMs from a uniform random distribution between -15 and 35 rad m^{-2} making sure the maximum difference between RMs is close to the one observed and with the same uncertainties as the measured values. We calculated the probability of randomly reproducing a fit which is comparable to the measured one by using a Bayesian model selection algorithm based on the Bayes factor. If the ratio of the Bayes factors of the two fits is within 0.01 and 100, then the fits are considered comparable. This happens in 1.5% of the cases but only in 4 cases out of 10000 trials the Bayes factor of the randomly extracted data exceeds the one measured with the observed data. Therefore, the quality of the measured fit cannot be exceeded by random data at the 3.5σ level.

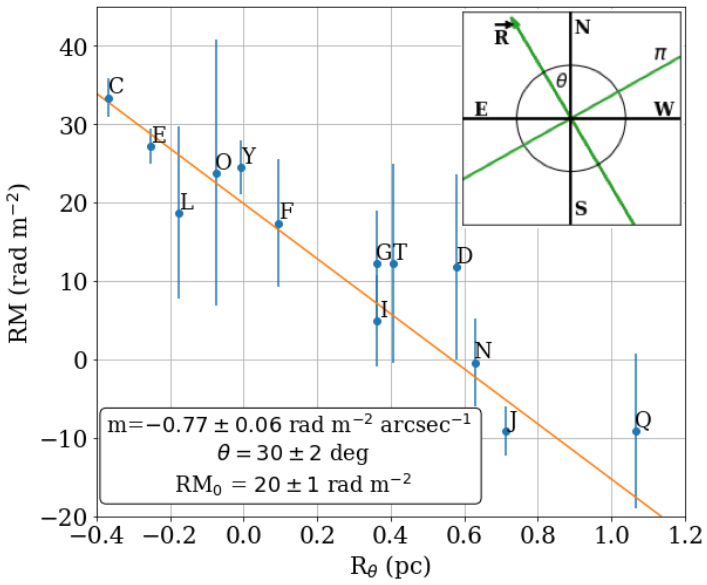

Figure 4.5: RM values as a function of the projected distance of each pulsar from the plane π perpendicular to the axis $\vec{R}$ and intersecting $\vec{R}$ at the centre of the cluster [263]. $\vec{R}$ is oriented with an angle of 30 degrees measured from the North direction to East. The orange line is the best line fit through the data. The panel in the top right shows the direction of the gradient. The box in the bottom left contains the best-fitting parameters. The error bars are at 1σ.

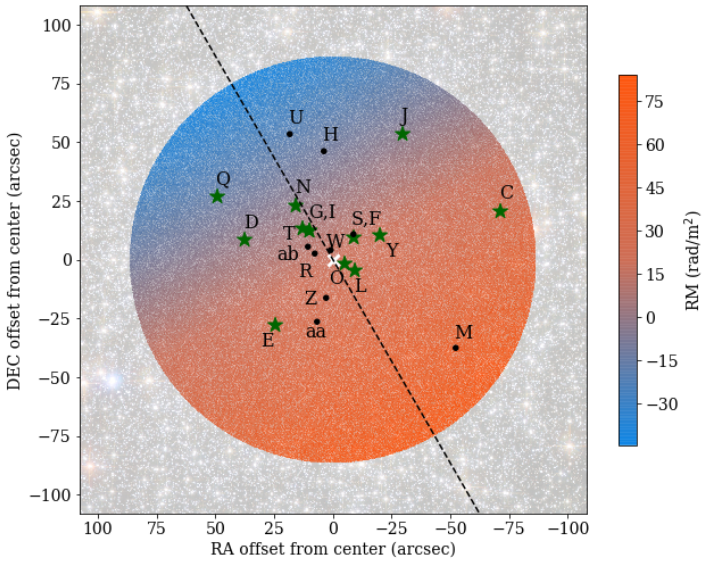

Figure 4.6: Map showing the distribution of pulsars in 47 Tuc. The colour scale shows the RM values predicted by the best-fitting linear gradient model presented in Fig. 4.5. The pulsars for which a measurement of RM was possible are represented by green stars while the pulsars with no measured RM are represented by black dots. The dashed line shows the direction of the $\vec{R}$ axis in Fig. 4.5. A white cross marks the optical centre of the cluster [263]. Credits of background image: NASA, ESA, and the Hubble Heritage (STScI/AURA)-ESA/Hubble Collaboration.

4.4 ORIGIN OF THE RM GRADIENT

If we assume that the RM distribution is caused by differences in the electron density along the line of sight, the latter differences would be reflected in the measured DMs. Assuming that the magnetic field is uncorrelated with the electron density, the relation between magnetic field, RM and DM is given by 1.23:

$$\langle B_{\parallel} \rangle = 1.23 \mu \mathrm{G} \left(\frac{RM}{\mathrm{rad\,m^{-2}}} \right) \left(\frac{DM}{\mathrm{pc\,cm^{-3}}} \right)^{-1}. \tag{4.14}$$

Assuming a constant magnetic field of $\sim 5\mu$G (a typical value for the Galactic magnetic field in the disk [358]), an RM spread of ~ 40 rad m^{-2} would require a DM range of order ~ 10 pc cm^{-3}, much larger than the observed maximum of 0.6 pc cm^{-3}. Therefore, the RM spread cannot be ascribed to fluctuations in the electron density.

Alternatively, the observed broad range of values of RMs could arise from differences in the parallel component of the magnetic field along different lines of sight over the angular scales probed by the pulsars. The magnetic field responsible for that could in turn be located either in the Galactic disk along the line of sight, in the GC itself or in the Galactic halo. In the following we explore these possibilities separately.

4.4.1 *Galactic magnetic field*

At these scales the small-scale magnetic field in the Galactic disk is thought to follow the electron density distribution described consistently by the Kolmogorov theory of turbulence [31, 170].

We tested whether the observed RMs could be described by a turbulent field through the study of the RM structure function, defined as:

$$\mathrm{D}_{RM}(\delta\theta) = \langle [\mathrm{RM}(\theta) - \mathrm{RM}(\theta + \delta\theta)]^2 \rangle_{\theta}, \tag{4.15}$$

where the average is computed between all pairs of pulsars with an angular separation of $\delta\theta$ on the sky. The angular separations between the pulsars in our case go from ~ 0.2 arcsec to ~ 90 arcsec. We first measured the square of the RM difference for each pair of pulsars and averaged them over 7 equally spaced bins each containing around 10 pairs. The spectral index is estimated by performing a straight-line fit through the data in logarithmic units using a Bayesian algorithm with the model:

$$\log \mathrm{D}_{\mathrm{RM}}(i|\alpha, k) = \alpha \log l_i + k, \tag{4.16}$$

where i is the bin number, l_i is the center position of the ith bin, α is the spectral index and k is a normalization parameter. The measured RM structure function is shown in Fig. S6. The value of the best-fitting

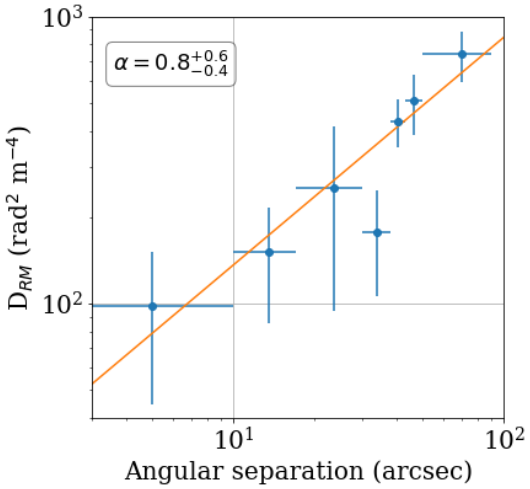

Figure 4.7: Rotation Measure structure function of the pulsars in 47 Tuc. The orange line is the best-fitting power law. The reduced chi-square of the fit is 1.2 with 5 degrees of freedom. The error bars on D_{RM} are at 1σ.

normalization parameter k is $1.3^{+0.7}_{-0.9}$. and the best-fitting spectral index is $\alpha = 0.8^{+0.6}_{-0.4}$ which is lower than the value of 5/3 predicted by the turbulent theory [31] but still consistent with what has been observed in RM studies at larger angular separations [254]. Therefore, this analysis is inconclusive to completely rule out a turbulent magnetic field. The first measure of an RM structure function using the pulsars in a globular cluster was performed by Anna Ho (private communications).

While the standard deviation of RM is comparable with what has been found in previous studies at larger angular separations at similar Galactic latitudes [254, 313], turbulent fluctuations are not expected to show strong correlations with a specific spatial direction. Furthermore, the fluctuations of DM due to the interstellar medium in the Galactic disk, after removing the contribution from the GC gas, have a standard deviation of ~ 0.1 pc cm^{-3} [4]. If the observed RM fluctuations (which have a standard deviation of ~ 13 rad m^{-2}) were due to only the fluctuations of dispersion in the Galactic disk, then the parallel component of the magnetic field would be ~ 150 μG, which is almost two orders of magnitude greater than the expected value.

4.4.2 *Internal magnetic field*

We now explore the second hypothesis that the RM variations on the small scales covered by 47 Tuc pulsars are due to an ordered magnetic field located inside the GC. To obtain an estimate of the required

strength of this magnetic field we start from the definition of the RM 1.22:

$$\mathrm{RM} = \frac{e^3}{2\pi m_e^2 c^4} \int_0^d n_e B_{\parallel} dl, \tag{4.17}$$

where $n_e \sim 0.23$ cm^{-3} [4] is the electron number density, considered constant over the central parts of the cluster, $B_{\parallel}$ is the component of the magnetic field parallel to the line of sight and the integral is extended over the central region of the cluster where the pulsars and the gas are located, about 2 pc [4]. Assuming a constant strength of the magnetic field, the parallel component will have different values depending on where the field lines are pointing. Using the above equation, we find that to explain the observed RM difference of ~ 40 rad m^{-2} we need a difference in the parallel magnetic field component of ~ 100 μG. This value must be compared with the equipartition value of the magnetic field measured using previously determined parameters of the cluster [4] which is ~ 4 μG, making this picture very unlikely.

4.4.3 *Halo magnetic field*

A third option invokes the combined effects of the interaction between the wind released by the Galactic disk and the movement of the GC. In the following we show that in this case a shock front arises providing the needed amplification of the magnetic field transported by the wind. We note that the inclination angle of the gradient, θ, is compatible at 2σ with the direction perpendicular to the Galactic disk, which measured with our conventions would be ~ 26 deg.

The Galactic wind is ejected from the Galactic disk with a velocity of 200 km s^{-1} [116] while the GC is moving towards the Galactic disk with a velocity of ~ 45 km s^{-1} [46]. The total velocity of 47 Tuc with respect to the wind in the direction orthogonal to the Galactic disk is ~ 245 km s^{-1}. This velocity is both superalfvenic ($c_a \sim 175$ km s^{-1}) and supersonic ($c_s \sim 170$ km s^{-1}) with respect to the wind; therefore, a shock forms in front of the cluster. When crossing the shock front, the magnetic field in the wind naturally acquires a component perpendicular to the direction of motion which can be compressed and thus amplified. The geometry of the shock is shown in Fig. 4.8.

To test if this scenario is applicable and could generate a magnetic field comparable with the one observed, we appeal to basic MHD shock equations [91]. We first move in the frame of reference of the shock so that the upstream and unperturbed material (defined with a subscript 1) is moving towards the shock with a speed of U_1, a density of ρ_1 and a magnetic field of B_1. If the magnetic field is aligned with the direction of U_1, the shock can generate a component perpendicular to B_1 in the downstream region (defined with a subscript 2) if $U_1 > c_a$, where c_a is the Alfven speed. In our case $U_1 \sim 250$ km $^{-1}$ while c_a has

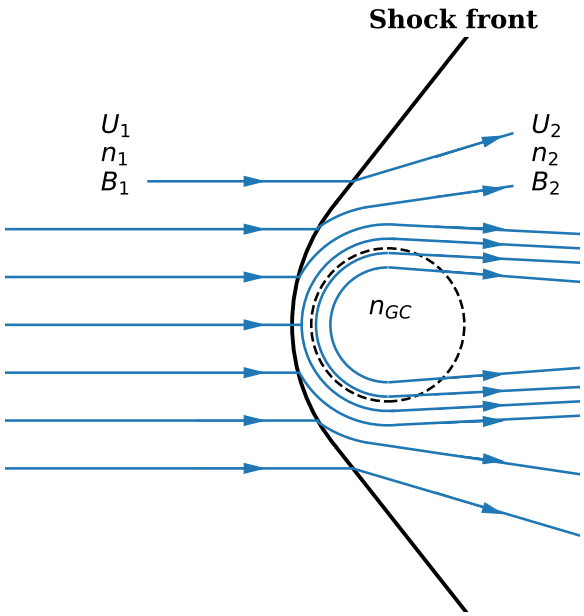

Figure 4.8: Diagram showing the schematic geometry of the shock generated by the superalfvenic motion of the globular cluster. The globular cluster (not in scale) is the dashed circle, the thick black line is the shock front and the blue lines are the magnetic field lines. The quantities denoted with the subscript 1 are the velocity, density and magnetic field of the gas in the upstream region, while the quantities denoted with the subscript 2 are the same in the downstream region. The density of the gas in the cluster is denoted by n_{GC}.

been measured with the formula $c_a = \frac{B_1}{\sqrt{4\pi n_1 m_p}} \sim 175$ km s^{-1}, where $B_1 \sim 3$ μG and $n_1 \sim 1.4 \times 10^{-3}$ cm^{-3} have been derived by scaling the value estimated for the wind [116] at the position of the cluster.

As the gas crosses the shock interface it is compressed, its direction changes away from the normal of the shock and any (even very small) perpendicular component of the magnetic field is enhanced according to the following equations [91]:

$$\frac{n_2}{n_1} = \frac{U_{\parallel 1}}{U_{\parallel 2}} = X_0 \tag{4.18}$$

$$\frac{B_{\perp 2}}{B_{\perp 1}} = \frac{(U_1^2 - c_a^2)X_0}{U_1^2 - X_0 c_a^2}, \tag{4.19}$$

where $U_{\parallel 1}$ and $U_{\parallel 2}$ are the component parallel to the shock normal of the velocities upstream and downstream, $B_{\perp 1}$ and $B_{\perp 2}$ are the perpendicular components to the shock normal in the two regions and X_0 is a factor that must be $1 < X_0 < \frac{u_1^2}{c_a^2} \sim 2$. The component on the x-axis of the magnetic field is conserved through the shock so the direction of the magnetic field changes according to:

$$\frac{B_{\perp 2}}{B_{\parallel 2}} = \tan\theta_2 = \frac{(U_1^2 - c_a^2)X_0}{U_1^2 - X_0 c_a^2} \tan\theta_1, \tag{4.20}$$

where θ_2 is the angle between B_2 and the shock normal and θ_1 is the angle between B_1 and the shock normal. Assuming $X_0 \sim 1.5$ (the central value of the possible interval) we find $n_2 \sim 2 \times 10^{-3}$ cm^{-3}, $u_{x2} \sim 170$ km s^{-1}, and $B_{\perp 2} \sim 3B_{\perp 1}$. For example, if a magnetic field line enters the shock interface at an angle of 5 deg it will come out at ~ 14 deg with a perpendicular component of ~ 0.8 μG.

The density of the plasma inside the cluster is ~ 0.23 cm^{-3}, derived from the electron density [4]. If the magnetic field is to penetrate in the central regions of the cluster, it must be compressed of a factor of ~ 100. This additional compression further amplifies the perpendicular component of the magnetic field which acquires a circular geometry in the half of the cluster that is facing the shock. To estimate how much the perpendicular component of the magnetic field can be amplified by this type of compression, take a cube that is compressed only on one side, called l, with the magnetic field aligned along a direction perpendicular to the compression. Mass conservation implies that $nAl =$ constant where A is the surface area of the face that remains constant. On the other hand, magnetic flux conservation implies that the magnetic flux that crosses the surface of the solid remains constant, in this situation the surface area has a linear dependence with the length of the side that is changing, l, so we have that $Bl =$ constant . Therefore, the magnetic field should grow linearly with the density. Even magnetic field lines that have a perpendicular component of only 0.8 μG (as in the case of a field line that enters the shock with an angle

of 5 deg) are capable of reaching a value of ~ 80 μG which is even higher than the best-fit magnetic field strength that parameterizes our model of the observed RM gradient. This shows that this mechanism is able to reach the required strengths of magnetic fields even if the Galactic wind is less magnetized than we assumed. This compression leaves the parallel component of the magnetic field constant and thus bends the field lines further in a semi-circular shape as depicted in Fig. 4.8.

At first approximation, we can schematically model the magnetic field with a semi-circular geometry as in Fig. 4.9. In this model, the field lines are perpendicular to the Galactic disk and reach the cluster forming an angle θ_H measured from Celestial North to East in the plane of the sky and an angle ϕ with respect to the line of sight. The angle ϕ corresponds to the absolute value of the Galactic colatitude of the cluster. In our case it is expected to be 45 deg. Field lines are circular in the half of the cluster facing the Galactic wind and straight in the other half. The direction in which the field lines rotate changes with respect to the position where they cross the globular cluster. Field lines above the axis H shown in Fig. 4.9 rotate clockwise while field lines under it rotate counter-clockwise.

In order to derive the analytical expression of the magnetic field we first measure the projection of the position of the pulsars on axis R as was done in the linear model: $R_{i,\theta_H} = \mathrm{RA}_i \sin\theta_H + \mathrm{DEC}_i \cos\theta_H$. In the half of the plane R-los that is facing the Galactic wind, the magnetic field is oriented in a circular direction. If we call B the direction of the magnetic field, then it can be described by:

$$\hat{B} = \frac{R_{i,\theta_H}}{\sqrt{x_i^2 + R_{i,\theta_H}^2}}\hat{x} + \frac{x_i}{\sqrt{x_i^2 + R_{i,\theta_H}^2}}\hat{R} \tag{4.21}$$

Where x_i is the distance of each pulsar along the line of sight from a plane parallel to the sky passing through the centre of the cluster and $\hat{B}$, $\hat{x}$, and $\hat{R}$ are the unit vectors respectively along the magnetic field, line of sight and axis $\vec{R}$. In the computation of RM only the component parallel to the line of sight is relevant so we will only consider the component directed along $\hat{x}$. The direction of the magnetic field changes in the two quarters divided by the axis H in panel b) of Fig. 4.9. Above this axis the field lines will be rotating clockwise while under it the field lines will be rotating counter-clockwise. In the half of the cluster that is facing away from the wind, the field lines are straight and only the component along the line of sight enters the equation. The transition between circular and linear field lines happens along the line passing through the centre perpendicular to the direction H that can be parametrized as $x_{H,\perp} = -R_{i,\theta_H} \tan\phi$. Integrating along the line of sight to estimate the contribution to RM, we need to consider

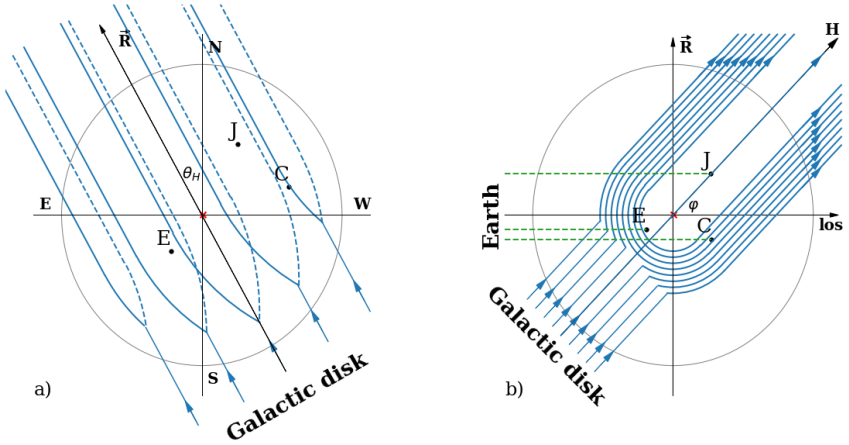

Figure 4.9: Model showing the geometry of the magnetic field lines in the case of an interaction between a Galactic wind and the gas in 47 Tuc. The magnetic field lines, thought to reach 47 Tuc along a direction perpendicular to the Galactic disk, are bent by the presence and the motion of the gas in the cluster. The centre of the cluster is marked with a red cross. Panel a) shows the projection on the plane of the sky in celestial coordinates. The angle θ_H is compatible with the angle θ defined in the linear model in Fig. 4.5. Panel b) shows the same model in the plane defined by $\vec{\mathbf{R}}$ and the line of sight. Three pulsars with precise RM values and known line of sight position [4], 47 Tuc C, E, and J, are also shown. The dashed green lines in panel b) are the lines of sight to the pulsars. The value of RM is influenced only by the component of the magnetic field along these lines of sight. This model of the magnetic field structure inside 47 Tuc produces a RM contribution that is negative for pulsar 47 Tuc J and positive for pulsars 47 Tuc C and 47 Tuc E.

this sign change. The change occurs at the position along the line of sight $x_H = \frac{R_{i,\theta_H}}{\tan\phi}$. The total RM for each pulsar assumes the form:

$$\mathrm{RM}_{wind}(i|B,\theta_H,\mathrm{RM}_{0,H},\phi) =$$

$$\begin{cases} -\frac{e^3}{2\pi m_e^2 c^4} n_e B \int_{x_{max}}^{x_i} \frac{R_{i,\theta_H}}{\sqrt{x^2+R_{i,\theta_H}^2}} dx + \mathrm{RM}_{0,H} & x_i < x_H \text{ and } x_i < x_{H,\perp} \\ -\frac{e^3}{2\pi m_e^2 c^4} n_e B \left(\int_{x_{max}}^{x_H} \frac{R_{i,\theta_H}}{\sqrt{x^2+R_{i,\theta_H}^2}} dx - \int_{x_H}^{x_i} \frac{R_{i,\theta_H}}{\sqrt{x^2+R_{i,\theta_H}^2}} dx \right) + \mathrm{RM}_{0,H} & x_i > x_H \text{ and } x_i < x_{H,\perp} \\ -\frac{e^3}{2\pi m_e^2 c^4} n_e B \left(\int_{x_{max}}^{x_{H,\perp}} \frac{R_{i,\theta_H}}{\sqrt{x^2+R_{i,\theta_H}^2}} dx + \int_{x_{H,\perp}}^{x_i} \cos\phi dx \right) + \mathrm{RM}_{0,H} & x_i > 0 \text{ and } x_i > x_{H,\perp} \\ -\frac{e^3}{2\pi m_e^2 c^4} n_e B \left(\int_{x_{max}}^{x_H} \frac{R_{i,\theta_H}}{\sqrt{x^2+R_{i,\theta_H}^2}} dx - \int_{x_H}^{x_{H,\perp}} \frac{R_{i,\theta_H}}{\sqrt{x^2+R_{i,\theta_H}^2}} dx \right) - & \\ -\frac{e^3}{2\pi m_e^2 c^4} n_e B \left(\int_{x_{H,\perp}}^{x_i} \cos\phi dx \right) + \mathrm{RM}_{0,H} & x_i < 0 \text{ and } x_i > x_{H,\perp} \end{cases} \tag{4.22}$$

Here B is the strength of the magnetic field, assumed to be constant and $\mathrm{RM}_{0,H}$ is the Galactic contribution to RM. The value of x_{max} is set to 10 pc, and we verified that the quality of the fit does not depend strongly on this quantity. The minus sign is added because the line of sight component, x, is positive when the magnetic field points away from Earth while RM must be negative. Solving the integrals, we find the equations of the predicted RM as a function of the physical parameters:

$$\mathrm{RM}_{wind}(i|B,\theta_H,\mathrm{RM}_{0,H},\phi) =$$

$$\begin{cases} \frac{e^3}{2\pi m_e^2 c^4} n_e B R_{i,\theta_H} \log\left(\sqrt{x_{\max}^2 + R_{i,\theta_H}^2} + x_{\max}\right) - & \\ -\frac{e^3}{2\pi m_e^2 c^4} n_e B R_{i,\theta_H} \log\left(\sqrt{x_i^2 + R_{i,\theta_H}^2} + x_i\right) + \mathrm{RM}_{0,\mathrm{H}} & x_i < x_H \text{ and } x_i < x_{H,\perp} \\ \frac{e^3}{2\pi m_e^2 c^4} n_e B R_{i,\theta_H} \left[\log\left(\sqrt{x_{\max}^2 + R_{i,\theta_H}^2} + x_{\max}\right) - 2\log\left(\sqrt{x_H^2 + R_{i,\theta_H}^2} + x_H\right)\right] + & \\ + \frac{e^3}{2\pi m_e^2 c^4} n_e B R_{i,\theta_H} \log\left(\sqrt{x_i^2 + R_{i,\theta_H}^2} + x_i\right) + \mathrm{RM}_{0,\mathrm{H}} & x_i > x_H \text{ and } x_i < x_{H,\perp} \\ \frac{e^3}{2\pi m_e^2 c^4} n_e B \left[-\cos\phi(x_i - x_{H_\perp}) + R_{i,\theta_H} \log\left(\sqrt{x_{\max}^2 + R_{i,\theta_H}^2} + x_{\max}\right)\right] - & \\ -\frac{e^3}{2\pi m_e^2 c^4} n_e B R_{i,\theta_H} \log\left(\sqrt{x_{H,\perp}^2 + R_{i,\theta_H}^2} + x_{H,\perp}\right) + \mathrm{RM}_{0,\mathrm{H}} & x_i > 0 \text{ and } x_i > x_{H,\perp} \\ \frac{e^3}{2\pi m_e^2 c^4} n_e B \left[-\cos\phi(x_i - x_{H_\perp}) + R_{i,\theta_H} \log\left(\sqrt{x_{\max}^2 + R_{i,\theta_H}^2} + x_{\max}\right)\right] - & \\ -2\frac{e^3}{2\pi m_e^2 c^4} n_e B R_{i,\theta_H} \log\left(\sqrt{x_H^2 + R_{i,\theta_H}^2} + x_H\right) + & \\ \frac{e^3}{2\pi m_e^2 c^4} n_e B R_{i,\theta_H} \log\left(\sqrt{x_{H_\perp}^2 + R_{i,\theta_H}^2} + x_{H,\perp}\right) + \mathrm{RM}_{0,\mathrm{H}} & x_i > 0 \text{ and } x_i > x_{H,\perp} \end{cases} \tag{4.23}$$

The free parameters of this model are the strength of the field, B, the inclination angle of the axis in the plane of the sky, θ_H, the foreground

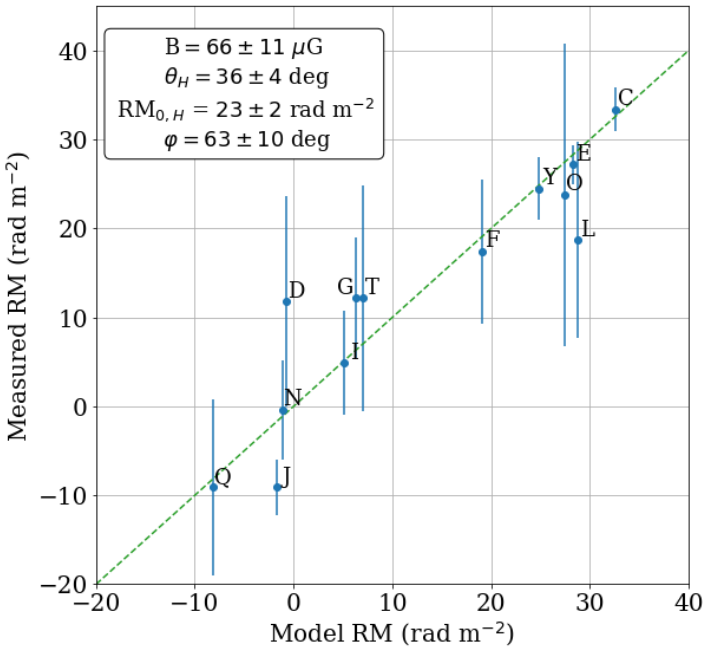

Figure 4.10: Fit of the RM assuming the Galactic wind model described in the text and in Fig. 4.9. The plot shows the measured RM versus the RM predicted by the best fit. The best-fitting values for the parameters are shown in the box. The error bars are at 1σ. For a perfect fit, all points should fall on the dashed green line, which represents the identity function.

contribution to RM, $\mathrm{RM}_{0,H}$ and the inclination angle with respect to the line of sight, ϕ that appears in the definition of x_H.

The best fit to the data is shown in Fig. 4.10 where the RM predicted by the model is plotted versus the measured RM. The reduced chi-square is 1.0 with 9 degrees of freedom while the best-fitting value of the inclination angle θ_H is 36 ± 4 degrees which is compatible at 2.5σ with the direction from the GC to the Galactic disk. The best-fitting value of the foreground contribution to RM is 23 ± 2 rad m^{-2} which is compatible with the values of 30 ± 8 rad m^{-2} [253] and of $16 \sim 10$ rad m^{-2} [283] estimated for this region in extragalactic RM studies. The best-fitting value of the angle ϕ is 63 ± 10 deg, compatible at 2σ with the expected value of 45 deg. In different models [191], the Galactic outflow is not perfectly perpendicular to the Galactic disk so even a marginal compatibility in the direction is acceptable. The intensity of the magnetic field required to explain the observed gradient in RM is 66 ± 11 μG again compatible with the estimated ~ 80 μG.

4.5 CONCLUSIONS

Thus, we conclude that the source of the gradient in RM is likely a magnetic field located inside 47 Tuc and supported by the interaction with a Galactic wind. The required strength means that the magnetic field plays an important role in the internal dynamics of the cluster and must therefore be studied in more details with magnetohydrodynamical simulations. The model can be better tested using observations made with the MeerKAT radio telescope [40] in South Africa, which will be able to determine the RMs of a greater number of pulsars with higher precision. If a Galactic wind permeating the halo is responsible for the observed magnetic field, then similar effects should also be visible in other GCs populating the Galactic halo. Observing these GCs will be helpful in identifying the best model for the halo magnetic field [125].

5

INTERMEDIATE MASS BLACK HOLES IN GLOBULAR CLUSTERS

The work described in this Chapter is presented in:
***F. Abbate**, A. Possenti, A. Ridolfi, P. C. C. Freire, F. Camilo, R. N. Manchester, and N. D'Amico "Internal gas models and central black hole in 47 Tucanae using millisecond pulsars" MNRAS, 2018, Vol.481, pp.627–638.*
***F. Abbate**, A. Possenti M. Colpi, and M. Spera "Evidence of Nonluminous Matter in the Center of M62" The Astrophysical Journal Letters, 2019, Vol. 487*
***F. Abbate**, M. Spera, and M. Colpi "Intermediate mass black holes in globular clusters: effects on jerks and jounces of millisecond pulsars" MNRAS, 2019, Vol. 487, pp. 769-781.*

In this chapter I will focus on the presence of IMBHs in the centre of GCs and on how the pulsars close to the centre can be used to look for them. I will first take in consideration the GC 47 Tuc whose pulsars have been described in Chapter 3. Then, I will present the case for a possible IMBH in M62 using previous observations from the Green Bank Telescope. I will conclude the chapter discussing a new method based on higher derivatives of the spin period and testing it on simulated GCs.

As shown in section 1.7, discovering IMBHs can have important repercussions on the evolution of GCs , the formation of supermassive black holes, and the search of gravitational waves with the next generation of interferometers. One of best places to look for IMBHs are the centres of GCs but, despite many searches with different methods, no clear detection has been made. An important method that has been proposed recently is to use the pulsars' accelerations to search for hidden mass in the centre of GCs . As described in appendix A.3, the acceleration of pulsars in a GC described by a King profile has a maximum given by eq. A.11. If we were able to find a pulsar with an acceleration above this limit, this would imply that the GC contains more mass in the centre than what is accounted for by the king profile. There is good reason to believe that this excess is caused by an IMBH. An alternative hypothesis is that this excess is caused by a system of stellar black holes segregated in the centre [72]. Finally, another possible explanation is that the King profile used to describe the cluster is not good approximation of the real density profile of the cluster.

5.1 47 TUC

A claim of an IMBH in the centre of 47 Tuc has been recently brought forward by Kızıltan, Baumgardt, and Loeb [206] using the information from the pulsars with a suggested mass of 2000 $M_\odot$. This is in contrast with the most recent upper limit derived by searching signatures of accretions, which is 1040 $M_\odot$ [344].

In Abbate et al. [4] we tried to test this claim using the most recent timing solutions derived for the pulsars in 47 Tuc [132, 307] and the MCMC code described in section 3.2.1 used to derive the line-of-sight positions of the pulsars in Chapter 3. We slightly modified the calculation of the likelihood for the acceleration by accounting for the presence of a possible IMBH. The contribution to the acceleration of the IMBH is described in appendix A.3 and takes into consideration both the direct effects of the IMBH and the effects of the overdensity that is created inside the influence radius. Leaving the mass of this possible IMBH as a free parameters brings the total number of free parameters to 47. The prior for this mass was chosen to be logarithmic since it can span over many orders of magnitudes and a flat prior would samples more the high masses.

The posterior distribution of the mass of the IMBH is shown in Fig. 5.1. The peak of the distribution is at zero suggesting that there is no IMBH. We can derive an 99% upper limit by measuring the value that contains 99% of the chains. This limit is $\sim$ 4000 $M_\odot$. In the figure we also report the value of the IMBH claimed by Kızıltan, Baumgardt, and Loeb [207]. Interestingly we find a secondary peak in probability close to this value. The increase in probability contained in this peak in only 4 % if measured by assuming a linearly decreasing background. Measuring the effect of an IMBH of 2000 $M_\odot$ is very difficult since it would have an influence radius of only 0.05 pc in a cluster like 47 Tuc with a central velocity dispersion of $\sim$ 13 km s^{-1} [355]. The closest pulsar to the centre in the plane of sky are 47 Tuc O and W with a distance of only $\sim$ 0.1 pc (see Table 3.2). The effects of a central black hole on the accelerations could be visible only for these pulsars.

The discrepancy between the probability distribution of the mass of the black hole obtained in this work and in Kızıltan, Baumgardt, and Loeb [206] despite being sensitive to the same effects could be caused by different effects: it could be due to different distances of the cluster but it could also be caused by different priors on the mass. In this work we used a logarithmic prior on the mass favouring lower values. If Kızıltan, Baumgardt, and Loeb [206] used different assumptions that favoured higher black hole masses (like a flat prior), the peak at $\sim$ 2000 $M_\odot$ would have gained significance.

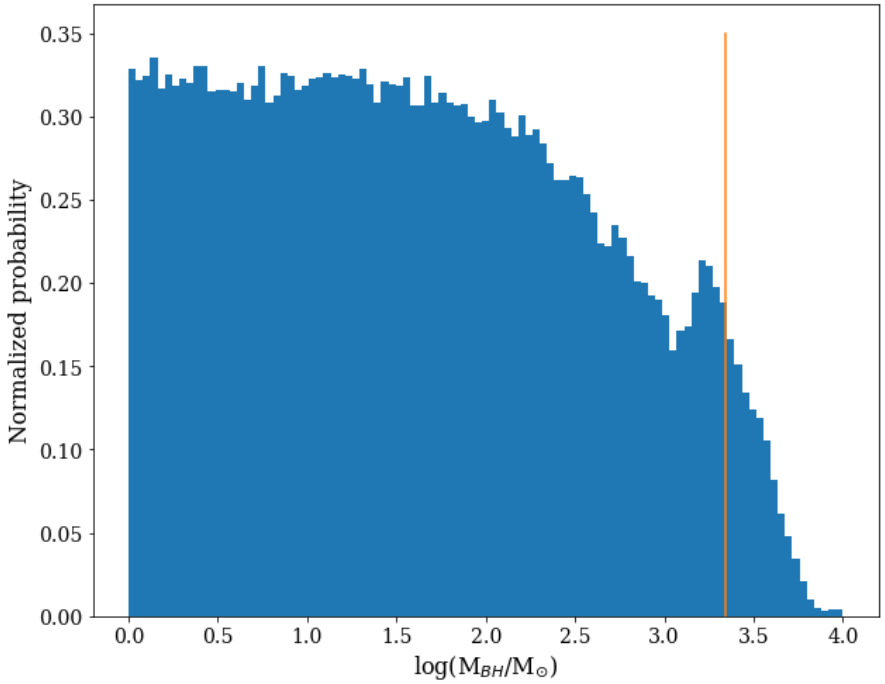

Figure 5.1: Plot of the posterior probability on the mass of the central black hole. The maximum of the distribution is at 0 $M_\odot$ suggesting that a black hole is not necessary to explain the data. The vertical line is at the mass of the black hole of 2200 $M_\odot$ proposed by Kızıltan, Baumgardt, and Loeb [206]. We see an increase in probability close to this value. The upper mass limit above which the black hole is not compatible with our data is $\sim$ 4000 $M_\odot$.

Table 5.1: Properties of the GC M62 using optical data.

Parameter	Value	Reference
Stellar mass		
	$6.74 \pm 0.05 \times 10^5$ $M_\odot$	[45]
Distance		
	6400 ± 180 pc	[46]
Core radius		
	0.36 pc	[45]
Velocity dispersion		
Radial	15.0 ± 1.1 km s^{-1}	[197]
Proper motion	15.3 ± 0.4 km s^{-1}	[355]

5.2 M 62

In this section, we focus on the GC M62, also known as NGC 6266. Using the observed velocity dispersion and surface brightness profiles, McNamara et al. [264] could not exclude the presence of an IMBH while Lützgendorf et al. [232] showed that this cluster may contain an IMBH with mass 2000 $M_\odot$. The latter claim has been recently contested by Baumgardt et al. [46], who showed that the observations are better matched by theoretical models that do not include an IMBH. Furthermore, in a search for radio signatures of accretion from a hypothetical central IMBH, [344] failed in the detection. Instead, they posed an upper limit to the IMBH mass at 1130 $M_\odot$. M62 contains 6 known millisecond pulsars, all of which are in binary systems [100, 234, 300]. Three pulsars are located very close to the centre of the cluster ($\sim$ 0.1 pc). As such, they may bring along crucial information about the possible presence of a central IMBH.

The GC M62 has been observed at different wavelengths over the years in order to measure the parameters of the cluster. The properties important for the present work are shown in Table 5.1.

The most recent distance estimate obtained through *Gaia* observations [46] is 6400 ± 180 pc. This value is smaller than the value found in [168] (2010 edition) which was 6800 pc. Throughout the paper we will use the new distance estimated by Baumgardt et al. [46].

The core radius can be derived from the luminosity density profile with a single-mass King model [205]. Using *Hubble Space Telescope* observations, [272] found 15.4 ± 0.6 arcsec, which corresponds to 0.48 ± 0.02 pc. In contrast, recent *N*-body simulations that match the surface density, the velocity dispersion,and the mass function of M62 suggest a smaller core radius of about 0.36 pc [45].

Using radial velocity measurements, Kamann et al. [197] obtained a value of the central velocity dispersion of 15.0 ± 1.1 km s^{-1}. Using

proper motion data, Watkins et al. [355] estimated a value of 0.504 ± 0.004 mas yr^{-1}, corresponding to that converted to km s^{-1} using the newly determined distance becomes 15.3 ± 0.4 km s^{-1}.

Further information about the dynamical structure of the cluster can be gathered from radio observations of the pulsars. The ephemerides of the pulsars in M62 are taken from [234] and include information on the position of the pulsars in the plane of the sky, their rotational periods (and higher time derivatives), and the binary parameters. Using the position of the centre of gravity as given in [272], pulsars B, E, and F are at about 4 arcseconds from the cluster's centre. At a distance of 6400 pc [44] this corresponds to about 0.1 pc. This distance is comparable with that of the innermost bin in the velocity dispersion profile presented by [355]. The accelerations of these three pulsars are crucial to get insights into the central cluster's mass distribution.

5.2.1 *MCMC fit results*

To perform the fit for the IMBH we need to assume some priors on the parameters. We use the most precise values determined from optical observations. We take the velocity dispersion measured with proper motion data and the core radius as estimated in [45] and the distance measured with *Gaia* data. The priors for the parameters are Gaussians centreed around those values and with the quoted uncertainty as standard deviation. For the core radius the standard deviation was chosen to be 0.01 pc (the same fractional uncertainty as the distance). The corner plot of the core radius, central density, and central dark object mass is shown in Figure 5.2. The comparison between the measured accelerations of the pulsars and the ones predicted by the best-fitting model are shown in Figure 5.3. Only the innermost three pulsars are shown as they are the most affected by the presence of the central object. The posterior distribution function for the mass of the central dark object in logarithmic units is shown in Figure 5.4. We find that an excess mass of 3900 $M_\odot$ is needed in the centre to explain the measured pulsar accelerations. The 68 percent interval is $(1200, 6600)$ $M_\odot$. The posterior distribution becomes compatible with the case of no IMBH ($M_\bullet < 10^2\, M_\odot$) if we consider the 95 percent interval. This excess is on top of the mass distribution estimated for a single-mass King model derived from the observed optical parameters and is located within 0.2 pc (the distance from the centre of the innermost pulsar, F). The central mass density converges to $(3.1 \pm 0.2) \times 10^5$ $M_\odot$ pc $^{-3}$. This value is almost twice than what was estimated through *N*-body simulations in [45], which is 1.6×10^5 $M_\odot$ pc $^{-3}$. This means that an excess of mass in the centre is needed to explain the accelerations of the pulsars. This is also apparent in the lower left panel of the corner plot in Figure 5.2 where we see that if there is no IMBH, the central density must increase in order to compensate for the missing mass.

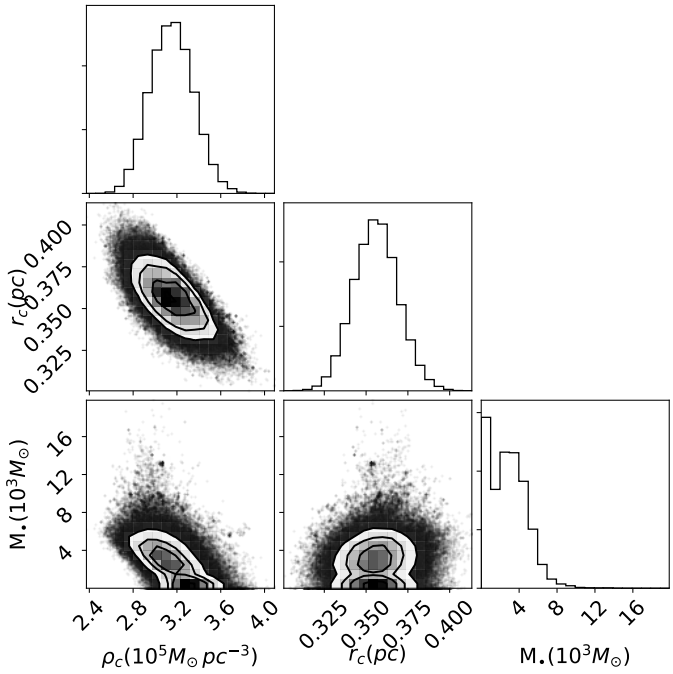

Figure 5.2: Corner plot showing the posterior distribution of the central density, the core radius, and the mass of the central dark object.

To test the nature of the excess of mass, we measure the central mass-to-light ratio. First, we transform the central density in a surface mass density by multiplying it by $2r_c$ [138]. This is compared with the surface brightness density measured in [280] and converted into Solar luminosities per square parsec. The resulting central mass-to-light ratio and the 68 percent interval is $6.4^{+2.1}_{-0.7}$ $M_\odot\, L_\odot^{-1}$. This value is much higher than what is seen at the cluster centres in N-body simulations of different GCs (see Fig. 3 in [44]). Alternatively to an IMBH, the central excess of mass could be explained with a system of stellar dark remnants like massive white dwarfs, neutron stars or black holes. A system of this kind could form in the first evolutionary phases of a GCs and survive up until now if the host cluster has a sufficiently long half-mass relaxation time like M62 ($\sim$ 1 Gyr) [20, 25, 71].

5.2.2 *Uncertainties in the optical parameters*

We have shown that the probability of finding a central excess of mass in M62 is quite high. To check that our finding is not affected by possible systematic errors on the values of the core radius and on the central velocity dispersion, we repeat the MCMC fit by setting the IMBH mass to fixed values, without assuming any priors on the core radius and on the velocity dispersion. Figure 5.5 shows the posterior

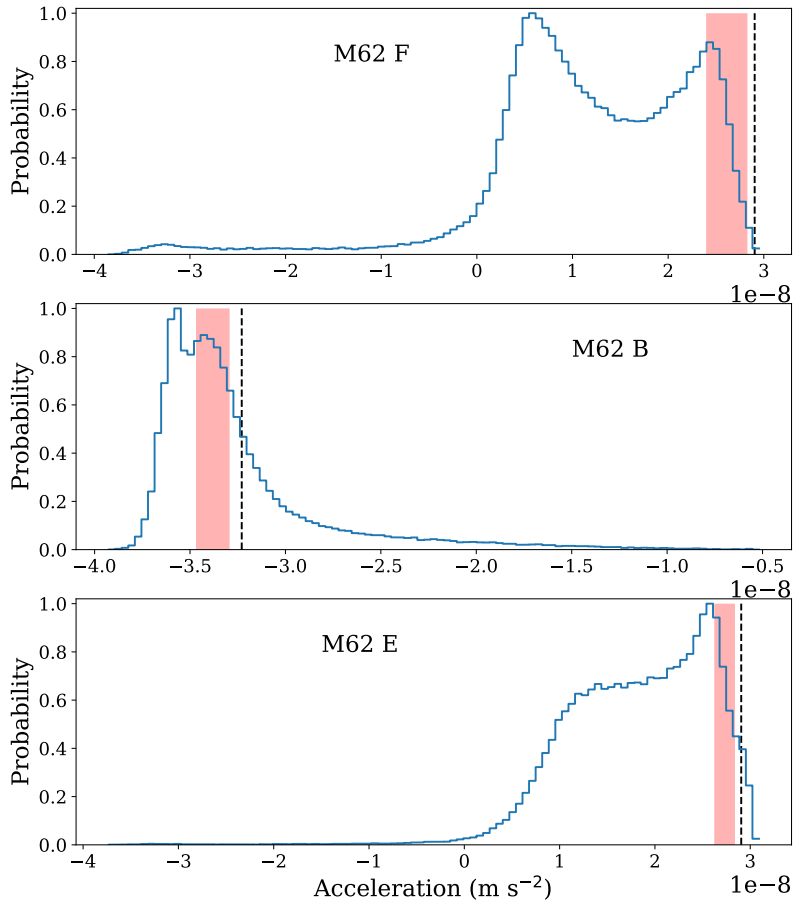

Figure 5.3: Posterior distribution for the accelerations of the pulsars F, B, and E, the three pulsars closer to the centre. The dashed line shows the measured value of $\dot{P}/P$ and the red shaded area is the 1σ interval of the cluster acceleration after removing the Galactic contribution, the Shkolvskii effect and the intrinsic spin-down.

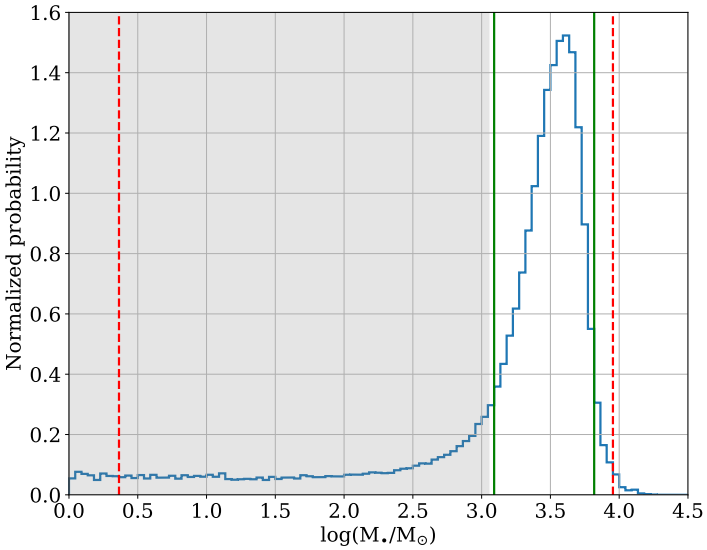

Figure 5.4: Posterior distribution function on the mass of the central dark object in logarithmic units. The green lines show the 68 percent interval and the dashed red lines show the 95 percent interval. The shaded interval is the allowed IMBH mass range from [344]. We assume a core radius of 0.36 pc as in [45].

distribution of the fits for three masses of IMBH, 0 $M_\odot$, 2000 $M_\odot$ and 4000 $M_\odot$. In the same plot we show, with the shaded area, the observed 1σ range for the core radius and velocity dispersion. In the case with no IMBH the shaded interval intersects the 68 percent interval of the posterior distribution only in a very small region (shown in the inset) but, as the mass of the IMBH increases, the region of intersection grows. However, if the real core radius is smaller than the measured one it could be possible to explain the observed pulsar accelerations without the need of an IMBH. The same is true if the true velocity dispersion is higher than what is measured. It is important to note also that in these cases where the IMBH is not needed, the mass to light ratio must remain at the same values.

To test the relation between the mass excess and the core radius and velocity dispersion of the cluster, we run the MCMC code, using two mock GCs ; the first (second) with a core radius of 0.16 pc (0.58 pc) and a total mass of 9×10^4 $M_\odot$ (8.4×10^5 $M_\odot$) simulated in Abbate, Spera, and Colpi [6]. The simulations host IMBHs of different masses in the centre. Here, we show the result of the smallest cluster in the case there is no IMBH in the core. We first run the code with a prior on r_c corresponding to the true value of 0.16 pc inferred from the simulated GC, and later we inject an erroneous value of r_c overestimated by 60 percent to 0.26 pc. This overestimation corresponds to the difference between the largest measured r_c for M62, 0.48 pc [272], and the value it should have to be compatible with no IMBH keeping the same velocity dispersion taken from Figure 5.5, that is $\sim$ 0.3 pc. We extract six

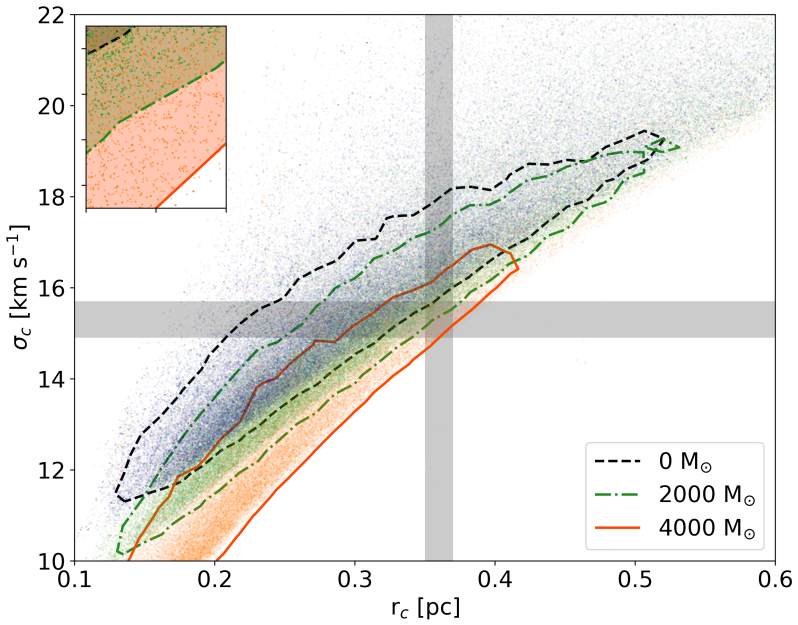

Figure 5.5: Contour plot of the posterior distribution of core radius and velocity dispersion as resulting from the MCMC fit. The shaded grey area shows the 1σ interval of the best determinations of core radius and velocity dispersion. The different sets represent fits with three values of IMBH mass: 0 $M_\odot$ (grey), 2000 $M_\odot$ (green), 4000 $M_\odot$ (orange). The coloured lines show the 68 percent intervals of these distributions. The inset shows a zoom on the central shaded area.

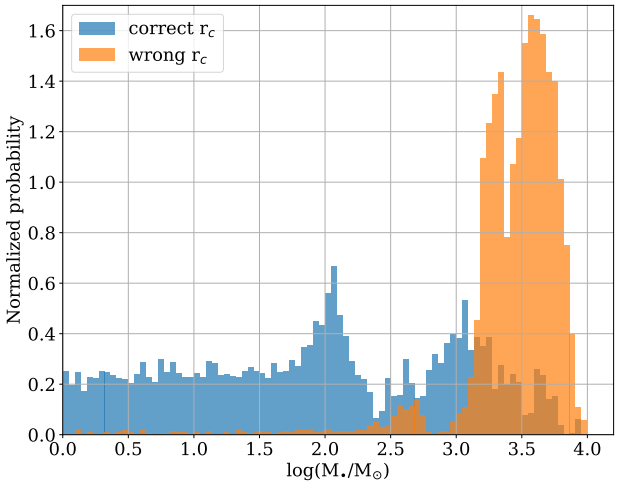

Figure 5.6: Posterior distributions of the mass of the central dark object resulting from a simulated GC with no such mass excess. Assuming the correct value of core radius (blue histogram), the distribution is consistent with a null mass excess. Instead, assuming a core radius overestimated by 60 percent (orange histogram), the distribution indicates a mass excess of ~ 3500 M$_\odot$ which is not present in the simulation.

pulsars (using $\alpha = 3$), and measure their acceleration along the line of sight for the two cases.

Figure 5.6 shows the histograms of the posterior distributions of the central dark object mass from the mock GC. The distribution in orange, corresponding to the incorrect value of r_c, shows a peak at ~ 3500 M$_\odot$ that is incompatible with 0 M$_\odot$ at the 3σ level, whereas the distribution in blue is consistent with the correct assumption of no IMBH, at 1σ level.

We repeat the test using the simulation of the same GC with an IMBH of 1000 M$_\odot$ at the centre and for the more massive GC with a core radius of 0.58 pc. The simulations of both clusters strongly support that an error in the determination of the cluster parameters can lead to an incorrect value of the mass of the IMBH.

5.2.3 *Discussion*

We have used the measured accelerations of the pulsars in M62 and the new distance estimate by *Gaia* to predict the existence of an excess of mass located within the central 4 arcseconds of M62. The existence of a concentration of non-luminous mass is confirmed by looking at the very high central mass-to-light ratio (~ 6). The source of this dark mass excess could be a single IMBH of ~ 3900 M$_\odot$ or a system of massive dark remnants segregated in the centre of similar total mass. This result is obtained strictly assuming the nominal values of the core radius and velocity dispersion from the latest optical observations [45,

355]. We tested the dependence of the result from these assumptions and found important correlations between the aforementioned optical parameters and the mass of the IMBH resulting from the fit. Assuming a smaller core radius or a faster velocity dispersion would result in an IMBH of smaller mass.

We tested the correlation using simulated GCs of known parameters, and we confirmed that an alternate assumption on the core radius can mimic the necessity of an IMBH or can exclude its presence. Thus, more precise estimates of these parameters are needed to uniquely confirm the presence of an IMBH in the cluster.

The optical observations of M62 are compatible with an IMBH of a few thousand $M_\odot$ [264] with a tentative claim of ~ 2000 $M_\odot$ [232] which has been disputed in [44]. According to searches for accretion signatures [344], there is an upper limit on the mass of the IMBH of 1130 $M_\odot$. From the results of our analysis, we cannot either confirm these claims or reduce the upper limits, but, using the published optical parameters of M62, we have found that ~ 4000 $M_\odot$ of low-luminosity matter must be contained within the central 0.2 pc of the cluster. This 'dark' matter can be composed of an unconstrained ratio between one or more IMBHs or a large number of non luminous remnants of stellar origin.

Present-day clusters, with half-mass relaxation times $\gtrsim 1$ Gyr, may have retained many stellar mass dark remnants in their centres [25, 71]. Such subsystems can reach masses of 1000 - 10000 $M_\odot$ for GCs born very massive [20]. Arca Sedda, Askar, and Giersz [26] showed that M62-like GCs build up a subsystem of dark remnants in their centre in about half of the authors' *N*-body realizations. Though highly speculative, some of these stellar remnants might be in the form of binary black holes, which are now observed as powerful gravitational-wave sources [8]. Furthermore, [362] showed that the presence of a large number of black holes in the centre of the clusters should drive out all of the MSPs found inside and would be incompatible with the observed set of pulsars. The stability of this system and the coexistence of stellar black holes and MSPs should be studied with dynamical simulations focused on this cluster.

Further observations of the cluster are necessary to find the source of the excess of mass. Optical observations will help to determine the structural parameters with higher precision, and radio observations will better constrain the accelerations of the pulsars and to look for new pulsars possibly even closer to the centre.

5.3 EFFECTS OF AN IMBH ON JERKS AND JOUNCES OF PULSARS

The effects on the first derivative of the acceleration, referred to as *jerk*, and the second derivative, generally referred to as *jounce* or *snap*, have usually been neglected, despite prolonged timing of MSPs in

GCs shows that jerks and jounces are measurable [132, 224, 289]. In Abbate, Spera, and Colpi [6] we propose a new method of identifying IMBH candidates in Galactic GCs which involves the measurements of high-order time derivatives of the acceleration on an ensemble of MSPs. To this purpose, we carry out a suite of direct N-body simulations of star clusters where we compute self-consistently the high-order derivatives of accelerations, treating MSPs as test particles. We show that the aforementioned derivatives contain crucial information on the mean field gravitational potential as well as on the coarse-grain effects caused by neighbouring stars, both of which are affected by the presence of an IMBH. The equations describing the contributions to the jerks and jounces due to the mean gravitational potential are described in Appendix A.4 and A.5. We show that this method is sensible to IMBHs of lower mass than current standard methods. We apply this technique on a synthetic star cluster to test its capability of detecting a central IMBH, as well as on the GC 47 Tucanae (also known as NGC 104, hereafter 47 Tuc). We also test how the results would improve with longer datasets of observations with both Parkes and MeerKAT radio telescopes.

As described in eq. 3.4, the jerks felt by the pulsars influence the measured second spin derivative. In eq. 3.4, however, we omitted to write the contribution due to the intrinsic spin-down. The complete equation would be:

$$\left(\frac{\ddot{P}}{P}\right)_{meas} = \frac{\dot{a}_c}{c} + \left(\frac{\ddot{P}}{P}\right)_{int}, \tag{5.1}$$

where $\dot{a}_c$ is the jerk due to the GC potential projected along the line of sight. The contribution from the intrinsic spin-down due to magnetic dipole breaking can be estimated following $\dot{\omega}_{int} = -K\omega_{int}^n$ [228], where $\omega = 2\pi/P$, K is a constant and n is the breaking index assumed to be equal to 3. This leads to a second time derivative for the period

$$\left(\frac{\ddot{P}}{P}\right)_{int} = (2-n)\left(\frac{\dot{P}}{P}\right)^2_{int}. \tag{5.2}$$

From the estimate of $(\dot{P}/P)_{int}$ we find that the contribution of the intrinsic spin down on the jerk is of the order of 10^{-27} m s^{-3}. This is completely negligible when compared to the jerk due to the GC which is $\sim 10^{-18} - 10^{-19}$ m s^{-3}. This means that a measure of the second derivative of the period of a pulsar in a cluster corresponds to a direct measure of the jerk of the star.

Furthermore, we have a similar scenario for jounces. The equation for the third period derivative reads

$$\left(\frac{\dddot{P}}{P}\right)_{meas} = \frac{\ddot{a}_c}{c} + \left(\frac{\dddot{P}}{P}\right)_{int}, \tag{5.3}$$

where $\ddot{a}_c$ is the line-of-sight jounce due to the GC potential. Estimating the contribution of the intrinsic spin-down from the time derivative of equation (5.2), we find a value of $\sim 10^{-44}$ m s^{-4}. The latter contribution is negligible compared to the jounce due to the GC, which is $\sim 10^{-28}$ m s^{-4}.

There are also other untreated sources of errors that affect the second and third period derivatives of MSPs. For instance, to compensate for all the delays caused by the Earth's motion, the ToAss of pulses are always referred to the SSB. An imprecise determination of the SSB may lead to inaccurate period derivatives [88]. Other sources of errors like the effects of the velocity both on the plane of the sky and on the line of sight have been discussed in a paper by Liu, Bassa, and Stappers [224].

Quantifying the effect of different sources of errors in the estimation of the second and third time derivative of the period is quite uncertain. As a reference for these uncertainties, we defer to Perera et al. [289] and Freire et al. [132]. Converting the measured period derivatives to acceleration derivatives using the formulae written above, we find that we can measure jerks up to a precision of $\sim 10^{-21}$ m s^{-3} and jounces up to $\sim 10^{-29}$ m s^{-4}. In Section 5.3.2 we will investigate whether this level of accuracy is enough to quantify the effects of a central IMBH.

5.3.1 *Simulations*

We run a set of high-precision N-body simulations of star clusters by means of a new version of the direct summation N-body code HiGPUs[83, 84]. The HiGPUs code implements a Hermite 6th order integration method [277], which uses accelerations, jerks and jounces to advance the positions and velocities of stars over time. The method is implemented using block time steps [2] and written with MPI and OpenCL, to run on different and parallel computing architectures. We also implemented the new AVX-512 instructions to effectively run on the last generation Intel Central Processing Units as well as on Xeon Phi (Knights Landing) coprocessors.

We use the HiGPUs code to evolve a set of star clusters. Each star cluster is composed of $N = 90,000$ stars, whose masses are distributed according to a Kroupa [216] mass function with minimum mass $0.1\,M_\odot$ and maximum mass $2\,M_\odot$[1]. The initial positions and velocities of stars are sampled from a [204] density profile with central dimensionless potential $W_0 = 7$ and a core radius $r_c = 0.16$ pc, similar to the present-day distribution of stars in the GC Terzan 5. We evolved 6 different N-body models of the same star cluster, each one containing a central IMBH with mass $(0, 100, 500, 1000, 5000, 10000)$ $M_\odot$, respectively. The IMBH is initially placed at the centre of the star cluster with zero

1 We use $2\,M_\odot$ as maximum mass of the mass function to mimic the stellar population of a quite old cluster.

velocity, but it can wander during the N-body simulation, since it is treated as a real N-body particle. Furthermore, to minimise statistical fluctuations in our results, we evolve 10 different random realisations of the same star cluster. In our simulations, we do not use a softening parameter to artificially smooth out strong gravitational encounters, we do not include primordial binaries and we do not take into account stellar evolution calculations. All the star clusters start in virial equilibrium with the IMBH and have been evolved for ~ 50 Myr, to ensure that virial equilibrium is preserved and all systems are dynamically stable. The relative variation of the total energy (angular momentum) of each star cluster is kept below 10^{-7} (10^{-8}) for all the simulations.

We also run a set of simulations reproducing the properties of 47 Tuc. The parameters are taken from [49]: the core radius is set to $r_c = 0.58$ pc and the concentration parameter to $C = 1.91$. Each N-body particle represents a single star and the number of particles in the simulations is chosen in order to obtain a total mass of $8.4 \times 10^5\,M_\odot$. We evolved 80 different N-body models of the same star cluster each with an IMBH of different mass chosen randomly between 500 and 8000 $M_\odot$. We focus on this GC as it contains 25 known MSPs [132] and has been subjected to various IMBH searches in the past with negative results [4, 230, 263]. There has been a claim of an IMBH of 2200 $M_\odot$ using the acceleration data from pulsars [206]. However, this claim has not received further support from later studies on the same pulsar dataset [4, 132]. As around 40 percent of these MSPs are isolated, we do not have accurate estimates of the acceleration for them (see section 3.2). This makes the jerks all the more useful when searching for an IMBH in 47 Tuc.

5.3.2 *Results*

Figure 5.7 shows the line-of-sight jerks, and their 1σ interval, as a function of the distance projected along the plane of the sky from the cluster centre. We compare the results from our N-body simulations of a star cluster with an IMBH of $1000\,M_\odot$ and the same star cluster without a central IMBH. The line of sight is chosen to correspond to the z axis of the simulations. The 1σ interval is computed by dividing the projected radius in 25 bins and measuring the 16 and 84 percentile of the jerks of the stars in each bin. The radius up to which the central black hole dominates the dynamics of the system is the influence radius. It is the radius at which the velocity of the Keplerian orbit around the black hole is the same as the stellar velocity dispersion in the core [48]. The effect of the IMBH is clearly visible inside its influence radius and extends further out. All the stars that passed inside the influence radius are affected either directly or indirectly by the IMBH and keep the memory of this interaction even when they leave the

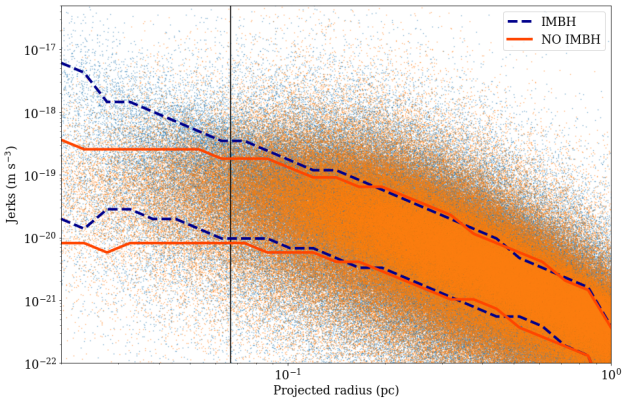

Figure 5.7: Line-of-sight jerks of the stars from the simulations as a function of the projected distance from the cluster centre in presence of a black hole (blue dots) and without (orange dots). The IMBH mass is 1000 $M_\odot$. The dashed blue and the solid red lines are the 1σ interval of the distribution of the jerks measured over 25 radial bins. The vertical line is the influence radius of the IMBH.

influence radius. This way the dynamical effects can extend farther outside.

The IMBH influences both the mean field and the nearest neighbour contribution to the jerks as seen in Figure 5.8. The mean field jerk is measured using equation (A.15), while the nearest neighbours jerk is taken as the difference between the measured jerk and the mean field one. We find that the presence of the IMBH does not change the ratio of the two jerks, but affects their norms. The enhanced gravitational potential and stellar density within the influence radius lead to the increase of the mean field jerks. Likewise, the enhancement in the local velocity dispersion and stellar density lead to the increase of the nearest neighbour jerks, as shown in Figure 5.8.

Jounces projected along the line of sight and their 1σ interval from the simulations are plotted in Figure 5.9 for the case with an IMBH of 1000 $M_\odot$ and without. To create this plot we use the same prescriptions as in the case of jerks (Figure 5.7). The IMBH leads to an increase of the jounces, but less pronounced compared to that for the jerks. If we disentangle the two contributions, jounces from the mean field are affected the most but the contribution of the nearest neighbours is still dominant, as shown in Figure 5.10.

We use MSPs as test particles for detecting the presence of an IMBH through their jerks and jounces. In order to determine the amount of information that can be derived from a single MSP, we map the different distributions in the jerk-radius plane for clusters with the IMBH and without. We repeat this process for all of the IMBH masses in our simulations. We compare the distributions by dividing the projected distance of the stars to the centre into 50 bins up to a maximum of 1 pc. The values of the jerks for these stars were divided into 50

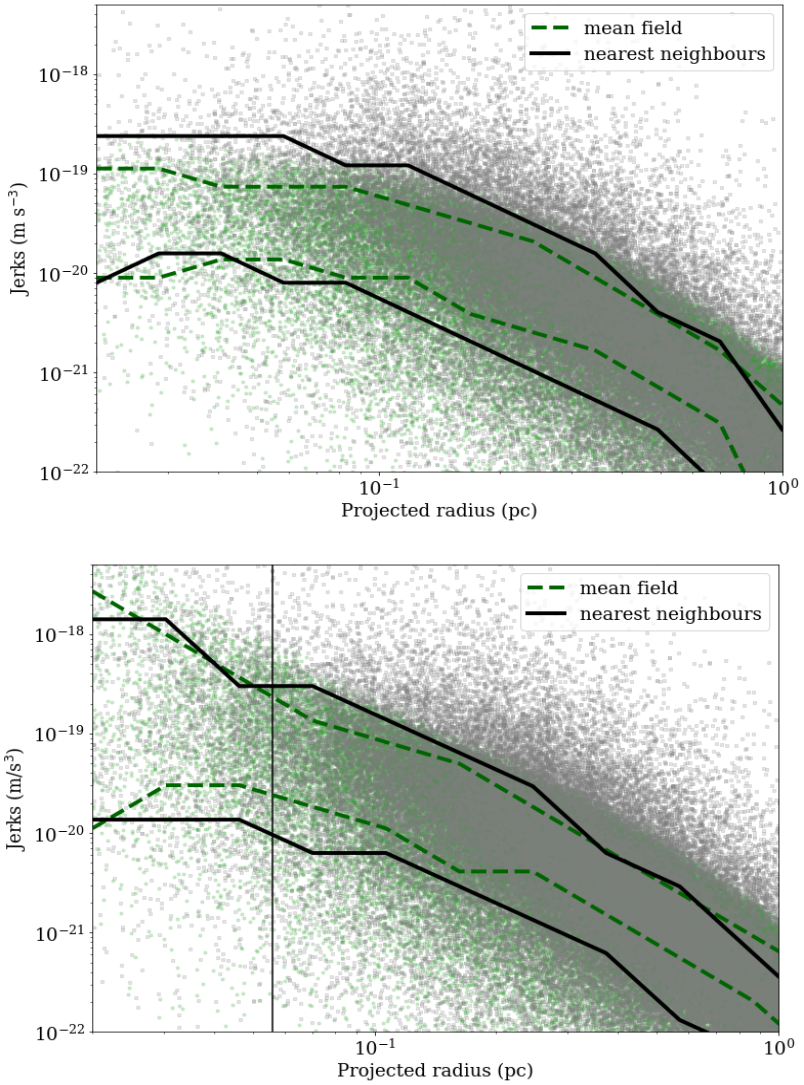

Figure 5.8: Line-of-sight jerks of the stars from the simulations as a function of the projected distance from the cluster centre in the case without the IMBH (top panel) and with an IMBH of 1000 $M_\odot$ (bottom panel). Jerks due to the mean field are plotted with green dots and jerks due to the nearest neighbours are plotted with grey dots. The dashed green and the solid black lines are the 1σ interval of the distribution of the mean field jerks and of the nearest neighbour jerks measured over 12 radial bins. The vertical line shows the influence radius of the IMBH.

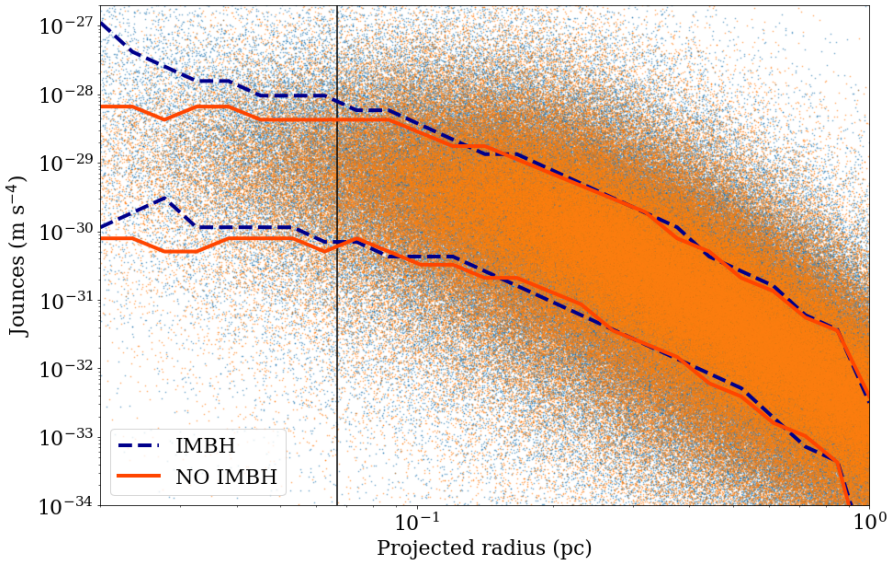

Figure 5.9: Line-of-sight jounces of the stars from the simulations as a function of the projected distance from the cluster centre in presence of an IMBH (blue dots) and without (orange dots). The black hole mass is 1000 $M_\odot$. The dashed blue and the solid red lines are the 1σ interval of the distribution of the jounce measured over 25 radial bins. The vertical line is the influence radius of the black hole.

bins from -2×10^{-18} to 2×10^{-18} m s^{-3}. We show the comparison in Figure 5.11. The colour scale shows in a logarithmic scale the ratio of stars found in each cell in the case with an IMBH and in the case without. If an MSP is found in one of the bright yellow squares, then it is more likely that the parent cluster hosts an IMBH. On the contrary if an MSP is found in one of the dark blue squares it is more likely that it lives in a cluster without an IMBH. Figure 5.12 shows the same probability maps for the jounces created dividing the jounces in 50 bins between -10^{-27} and 10^{-27} m s^{-4}. These maps show that stars close to the centre of the cluster with high values of jerks and jounces are strong indicators of the presence of an IMBH while, if the jerks and jounces are small, the IMBH is likely absent. Even only a few stars located in the bright yellow or dark blue regions of the maps can help discriminate between the different IMBH masses.

We test whether the information gained from these maps is enough to infer the presence of an IMBH and its mass through Bayesian model selection. We assume that each cluster contains 20 MSPs for which accelerations, jerks and jounces have been measured with uncertainty equal to 10^{-21} m s^{-3} for the jerks and to 10^{-29} m s^{-4} for the jounces. Accelerations are measurable only for MSPs in binaries. The fraction of binary MSPs to isolated ones in the Galactic GCs varies form 0.1 for M15, to 0.5 for Terzan 5, and 0.6 for 47 Tuc and can reach 1 for M62. In the simulated cluster we assume that this fraction is 0.5. Therefore of the

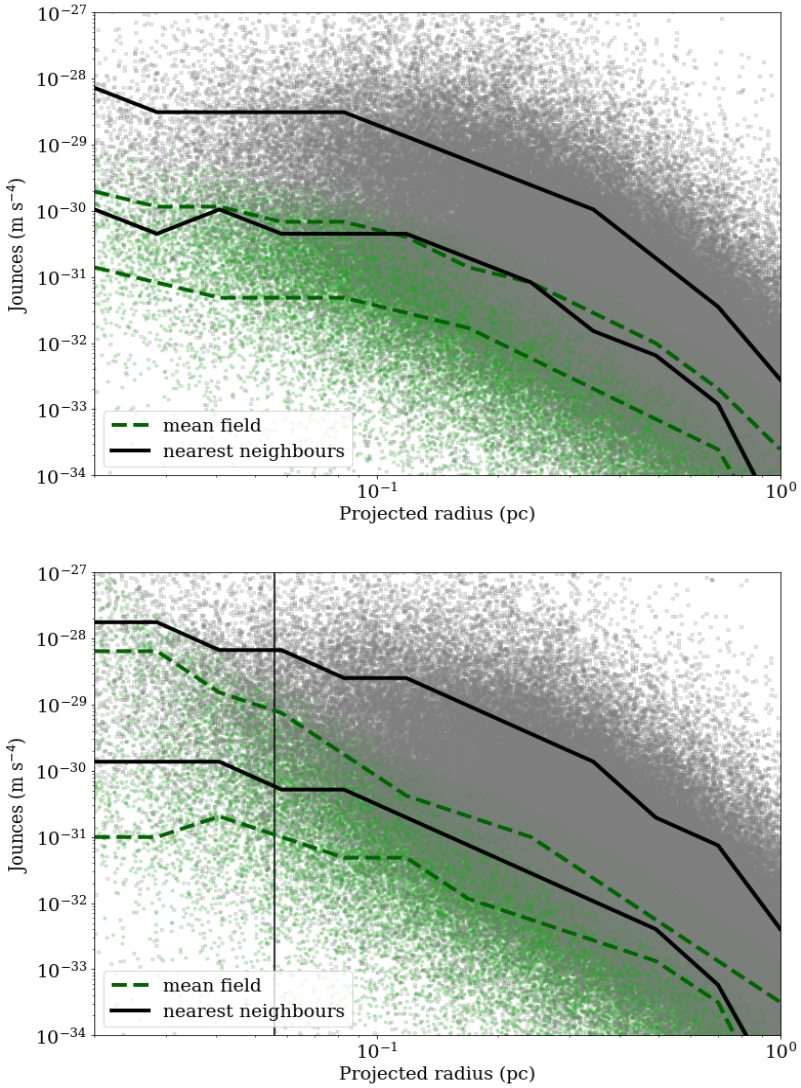

Figure 5.10: Line-of-sight jounces of the stars from the simulations as a function of the projected distance from the cluster centre in the case without a black hole (top panel) and with a black hole of 1000 $M_\odot$ (bottom panel). The jounces due to the mean field are plotted with the green dots and the jounces due to the nearest neighbours are plotted with the grey dots. The dashed green and the solid black lines are the 1σ interval of the distribution of the mean field jounces and of the nearest neighbour jounces measured over 12 radial bins. The vertical line shows the influence radius of the IMBH.

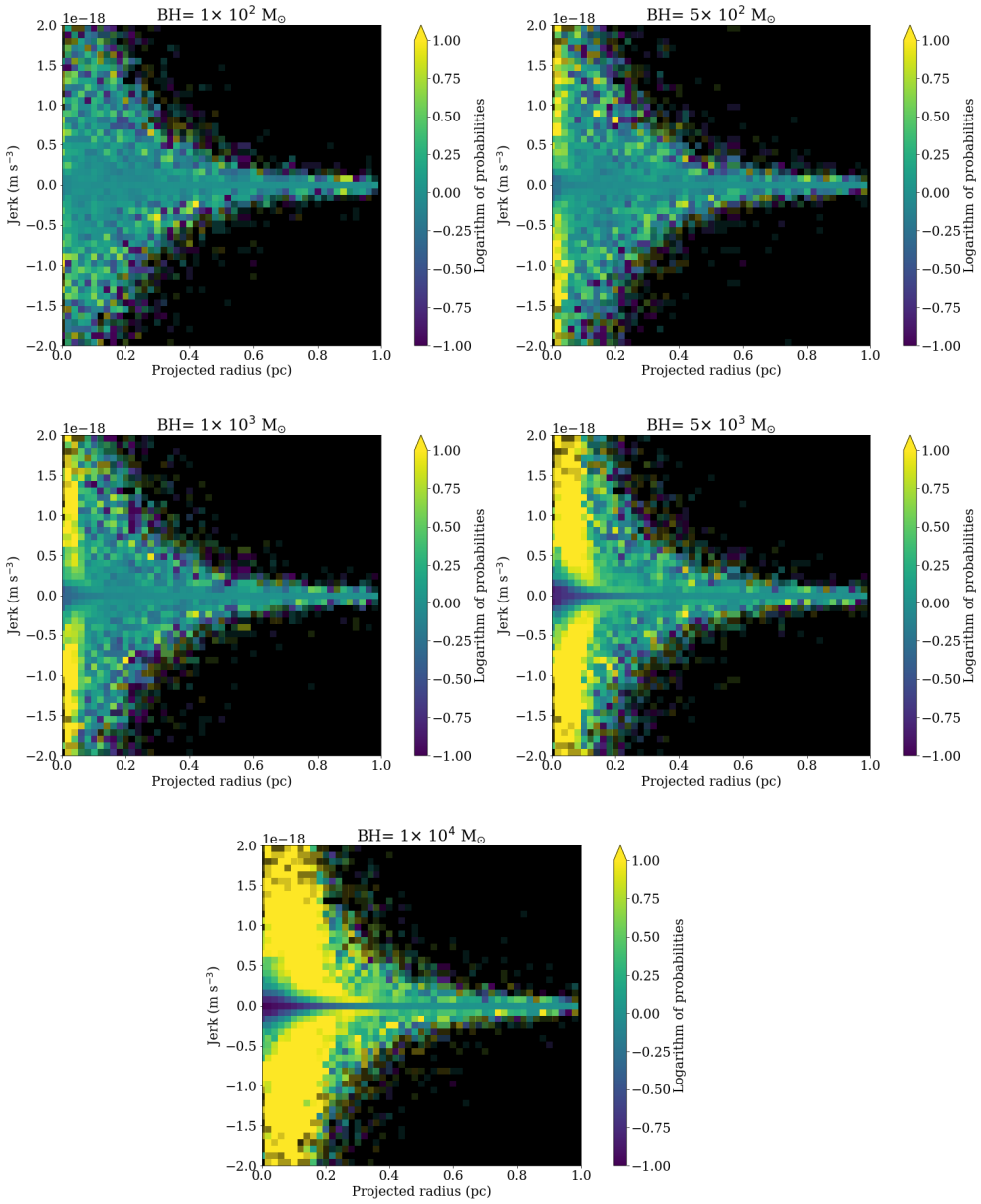

Figure 5.11: Probability of finding an MSP in a given projected radius bin with a given jerk in presence of an IMBH over the probability in the absence of it. The transparency of each pixel qualitatively shows the statistics of the value. Darker pixels have larger uncertainties. Pulsars found in a yellow square indicate that a black hole is likely present, while pulsars in blue square indicate that it is more likely that there is no black hole.

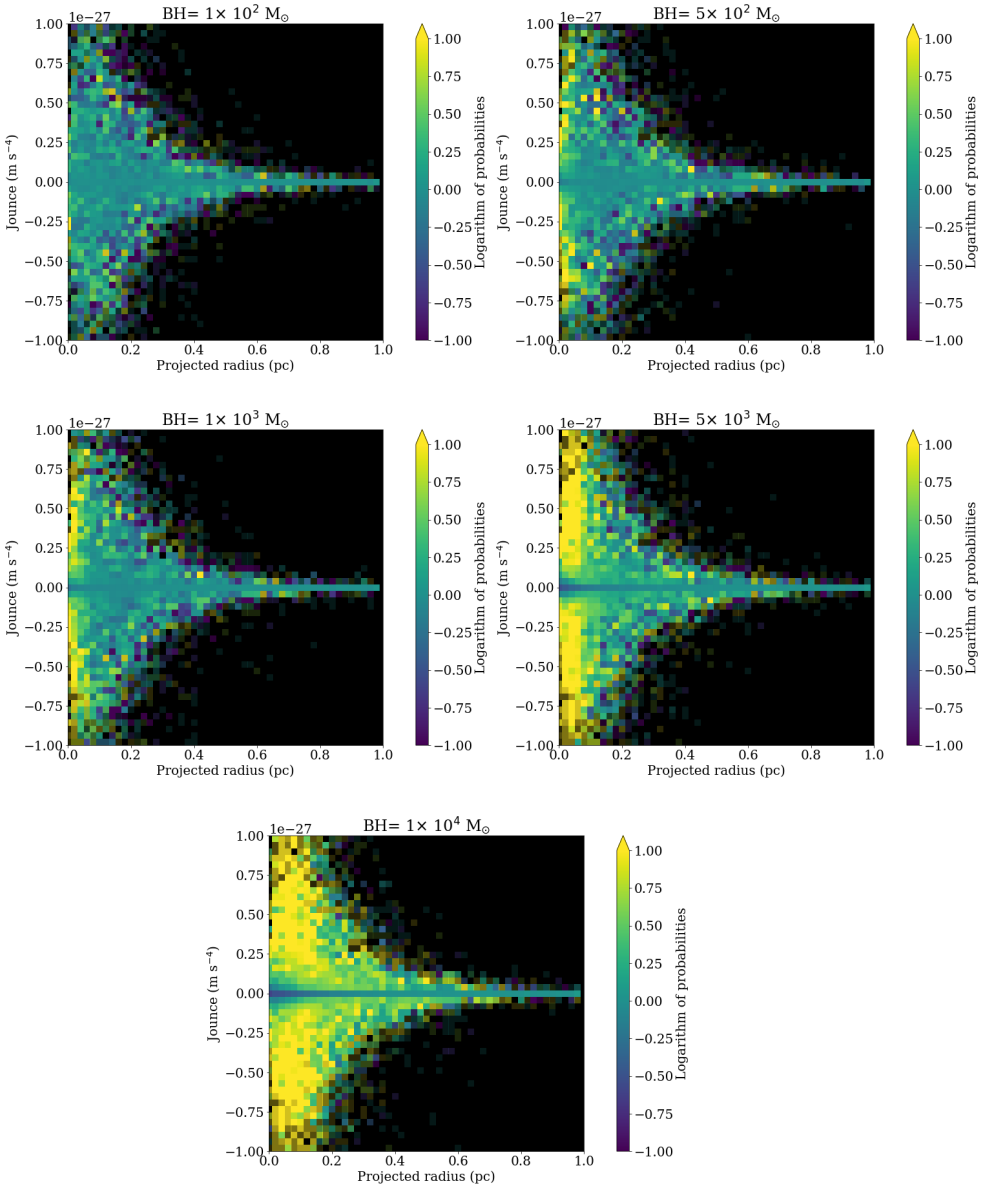

Figure 5.12: Probability of finding an MSP in a given projected radius bin with a given jounce in the presence of an IMBH over the probability in the absence of it. The transparency of each pixel qualitatively shows the statistics of the value. Darker pixels have larger uncertainties. Pulsars found in a yellow square indicate that a black hole is likely present, while pulsars in blue square indicate that it is more likely that there is no black hole.

20 MSPs assumed to be populating our clusters 10 are in a binary. Only for these 10 MSPs it is possible to measure the value of the line-of-sight acceleration. As a reference for the precision of this measurement we take the average uncertainty measured for the binary MSPs in 47 Tuc which is 10^{-9} m s^{-2}. We compare the results obtained using jerks and jounces with the ones obtained using only the accelerations.

Bayesian model selection is a statistical tool that allows us to compare quantitatively different models to find which one best describes the data. This comparison is based on the measures of the evidences which are the likelihoods of obtaining a specific value from the models integrated over the range of the free parameters. Since in our simulations there are no free parameters, the evidences correspond to the likelihoods, i. e. to the probabilities measured in each bin like in the maps of Figure 5.11 and 5.12 (the dimensions of the bins correspond to the errors of the acceleration, jerk and jounce). If there is no reason to prefer a priori one model over the other, the ratio of the evidences returns the Bayes factor which is the quantity used for the comparison. This quantity is usually reported in logarithmic values in base 10. If the Bayes factor is above 2 or below -2 (meaning that the evidence for one model is more than 100 times higher than the other) one model is strongly favoured. If it is between 1 and 2 or between -2 and -1 (with evidences between 10 and 100 times higher) one model is moderately favoured and if it is between -1 and 1 (evidences less than 10 times higher) nothing can be said.

For this test, we consider the simulations described earlier without the IMBH and extract 20 test particles representing MSPs. In Galactic GCs the radial distribution of pulsars does not reproduce the average radial distribution of stars. Since MSPs are more massive than the typical star in the cluster, they are more segregated in the centre and the radial distribution can be described by the following formula (see eq. A.1):

$$N(R_\perp) = N_0 \left(1 + \left(\frac{R_\perp}{r_c}\right)^2\right)^{\alpha/2}, \tag{5.4}$$

where $R_\perp$ is the projected distance from the cluster centre, N_0 is the normalisation and α is the spectral index responsible for the segregation. For the dominant mass stars in a cluster described by a King profile $\alpha = -2$. Typically for MSPs this index is ~ -3 [4, 301]. To reproduce the observed distribution of MSPs, we extract their projected distance from the centre from equation.

We select the stars with projected distance within 0.02 pc of the position of the MSP and we extract the values of the line-of-sight acceleration, jerk and jounce to assign to the MSP from the values of the set of nearby stars. Then, we count the number of stars with projected distance within 0.02 pc of the MSP and with acceleration

within the 1σ interval of the value assigned to MSP, assumed to be 10^{-9} m s^{-2}. This number, divided by the total number of stars corresponds to the likelihood of a star to have that value of projected radius and line-of-sight acceleration. We multiply these likelihoods for each MSP together in order to obtain the total evidence for the set of MSPs. We repeat the same estimate for the jerks and the jounces using as uncertainties 10^{-21} m s^{-3} and 10^{-29} m s^{-4} respectively.

We repeat the measure of the evidence for the same set of MSPs using the simulations with an IMBH described in Section 5.3.1. Finally, we divide the evidence in the case with an IMBH by the evidence in the case without to obtain the Bayes factor. As the set of MSPs is small, this result is severely affected by the random extraction of the parameters. To gain a deeper insight in the result we repeat this calculation 2000 times for each simulation and average the results.

We compute the average Bayes factor for all IMBH masses considered in the simulations, first by taking accelerations into considerations, then jerks, and then jounces. Since accelerations, jerks and jounces are extracted independently of one another, the Bayes factors can be added together (when they are in logarithmic units). The results are summarised in Table 5.2. Since the MSPs were extracted from the simulation without an IMBH the evidences will be higher in the case without an IMBH and the resulting Bayes factors are always negative. At high masses (above 10^3 M$_\odot$) the Bayes factor from the acceleration alone is below -2, so it is enough to affirm whether the IMBH is present. At a mass of 5×10^2 M$_\odot$, the Bayes factor for the acceleration is only -1.6 so we need to incorporate the information from jerks and jounces in order to reach statistically reasonable levels of confidence. At the lowest black hole mass in the simulations (10^2 M$_\odot$) the total Bayes factor is -1 meaning that this mass is below our detection threshold. It is interesting however to look at how the single parameters contribute to this Bayes factor: the accelerations are barely informative about the presence of the IMBH with a Bayes factor of only -0.3 while the Bayes factor of the jerks is lower, -0.6. This shows that for black holes of low masses jerks can be more informative than accelerations. For all IMBH masses, jounces only contribute with a Bayes factor which is much less than that of accelerations or jerks but still jounces carry significant information which helps to bring the Bayes factor over the detection threshold. From these results we state that in order to search for low mass IMBHs in GCs with MSPs, the best approach is to consider the accelerations and their derivatives together.

We test the limits of this technique by changing the number of MSPs in the clusters. We look for the number of MSPs necessary to detect an IMBH of 10^2 M$_\odot$ in the simulations with statistical significance. This number (needed to retain a Bayes factor smaller than -2) is around 40 MSPs with 20 binaries. In this case the Bayes factor from the accelerations would be only -0.7 while the Bayes factor for the jerks

Table 5.2: Logarithm of the Bayes factor between the model with an IMBH and without. The different black hole masses in units of $M_\odot$ and as percentage of the total mass of the simulated cluster are listed in column 1. Columns 2-4 give the Bayes factor using only acceleration, jerks and jounces and the last column give the total Bayes factor.

M_{BH} $M_\odot$	Accelerations ($\log_{10}$)	Jerks ($\log_{10}$)	Jounces ($\log_{10}$)	Total ($\log_{10}$)
1×10^4 (10%)	-5.3	-2.9	-0.9	-9.1
5×10^3 (5%)	-4.4	-2.3	-0.7	-7.4
1×10^3 (1%)	-2.4	-1.0	-0.4	-3.7
5×10^2 (0.5%)	-1.6	-0.8	-0.3	-2.7
1×10^2 (0.1%)	-0.3	-0.6	-0.1	-1.0

would be -1.2 and for the jounces would be -0.2. If the number of MSPs is further reduced to 10 and of binaries to 5, the limit mass of the IMBH measurable goes up to 10^3 $M_\odot$. Also in this case the jerks and jounces play a significant role since the Bayes factor of the lone acceleration is -1.2, while combining the information from jerks and jounces we can reach -2.

5.3.3 *Application to 47 Tuc*

We apply the same technique to our N-body model of 47 Tuc. The parameters of the MSPs were taken from the latest published ephemeris [132, 136, 307]. We used the observed projected distances from the centre, assuming a distance of the GC to the Sun of 4530 pc [61]. For binary MSPs we used the information on the period and orbital period derivatives to measure the acceleration and for all MSPs we used the $\ddot{P}$ to measure the jerk. For these pulsars there is still no clear measure of the jounces. We repeat the analysis described in Section 5.3.2. We first assumed that for isolated MSPs we don't have any information on the accelerations and then we repeat the analysis by estimating the accelerations by subtracting the inferred intrinsic spin-down from the period derivative. The intrinsic spin-down can be modelled by estimating the surface magnetic field inferred from Galactic MSPs with similar properties as those in 47 Tuc (as discussed in section 3.2).

The results of the analysis with and without the acceleration from isolated MSPs are shown in Figure 5.13 where we give the Bayes factor for different IMBH masses. We first show in grey the Bayes factor obtained using only the acceleration from binary MSPs. In this case, high mass black holes look disfavoured but there is not enough

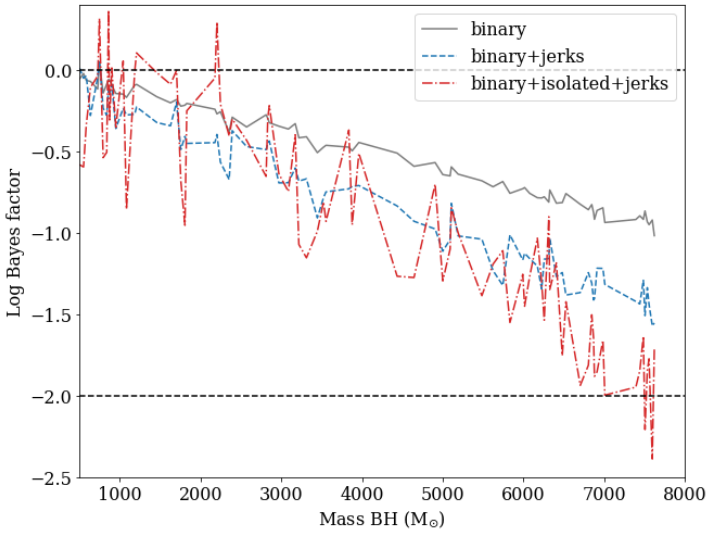

Figure 5.13: Values of the Bayes factor for detecting a central IMBH in 47 Tuc using the parameters of acceleration and jerk measured from the MSPs dataset. The gray line considers only the acceleration from binaries. The dashed blue line considers the acceleration from the binaries and the jerks from all the MSPs. The dot-dashed red line considers also the acceleration of isolated MSPs for which the value of the intrinsic spin-down is extracted from a probabilistic distribution.

statistics to exclude any of the tested IMBH mass. The dashed blue line represents the Bayes factor measured adding the information from the jerks. The situation improves but the Bayes factor never reaches the value of -2. Only when combining also the acceleration from the isolated MSPs, we find a statistically significant upper limit to the mass of the IMBH. This limit is $\sim 7000\ M_{\odot}$. The accelerations for isolated MSPs are measured as described above and add a lot of fluctuations due to the unknown intrinsic spin-down.

The upper limit we obtain here is not as stringent as in [4] where only the accelerations of the MSPs were used. This is because [4] adopted a Monte Carlo Markov Chain algorithm to determine the 3D position of the MSPs. The determination of these positions allowed the authors to estimate analytically the expected line-of-sight accelerations in presence of black holes of different masses. This approach is not feasible for the jerks since we lack the analytical or statistical expressions to calculate the contribution due to nearby neighbours in presence of an IMBH. Therefore, it is not possible to estimate the total jerk felt by a star given the position along the line of sight. However, the focus of the paper is to show the improvement brought by jerks over the accelerations in the search for a central IMBH. In order to do a fair comparison between the accelerations and the jerks, we decided to disregard the 3D positions of the MSPs when measuring the accelerations.

Future observations can lead to a major improvement to the mass measurement of the IMBH. The uncertainty with which the acceleration can be measured decreases with longer observing baselines as $T^{-5/2}$ with T being the total observing timescale [224]. In contrast, the uncertainty on the jerks decreases as $T^{-7/2}$. The uncertainty on the jounces decreases even faster as $T^{-9/2}$ leading to a possible measure of jounces for all MSPs in 47 Tuc in the near future. As the uncertainties on the jerks and jounces of MSPs decrease faster than the ones on the accelerations, a technique to extract information from the jerks and jounces will be necessary to be more sensitive to lower IMBH masses.

To test how the improvements of the measurements of jerks and a first measurement of jounces would influence the sensitivity of the search of a central IMBH, we performed mock simulations of future observations. We used the software TEMPO2 [112] to simulate the ToAs of the pulses supposing that the cluster will be observed on a monthly basis for five more years with the same sensitivity as up to now. With the resulting reduced uncertainties for the jerks and jounces, we apply the same technique explained in Section 5.3.2 again for 47 Tuc.

The blue line in Figure 5.14 shows the Bayes factor as a function of IMBH mass if observations are performed with the Parkes radio telescope. The IMBH upper limit in this case reduces to $\sim 5000\ M_\odot$.

We repeat the same simulations for the MeerKAT radio telescope in South Africa. We first estimate the increase in sensitivity this telescope would have compared with Parkes. MeerKAT is made up of 64 antennas of 13.5 m of diameter, the nominal gain of this telescope is $G_M \sim 2.8\ \mathrm{K\ Jy^{-1}}$ with an observing bandwidth of $\Delta\nu_M = 856$ MHz. The gain of Parkes instead is $G_P = 0.64\ \mathrm{K\ Jy^{-1}}$ and the bandwidth used for these observations is $\Delta\nu_P = 256$ MHz. The signal to noise ratio of an observation with MeerKAT would be $G_M/G_P\sqrt{\Delta\nu_M/\Delta\nu_P} \sim 8$ times higher. This roughly translates into a timing precision with MeerKAT observations 8 times higher than with Parkes. With these improved sensitivities we expect to detect in five years IMBHs of $M_{BH} > 1000\ M_\odot$ as shown in the dashed orange line in Figure 5.14.

Figure 5.14 shows not only the upper limits for non-detections of IMBHs but also the lowest detectable mass of IMBHs in future observations. Any IMBH of mass higher than the upper limits determined above will be detected as the accelerations, jerks and jounces of the MSPs will be inconsistent with the simulation without the IMBH.

5.3.4 *Caveats*

The over-density of stars in the influence radius (see Appendix A) is a stable configuration attained over a large number of relaxation times. Our simulations are not run for such long times to recover the stationary profile, but for the mock cluster used, the relaxation time [54] measured at the core radius is close to the duration of the

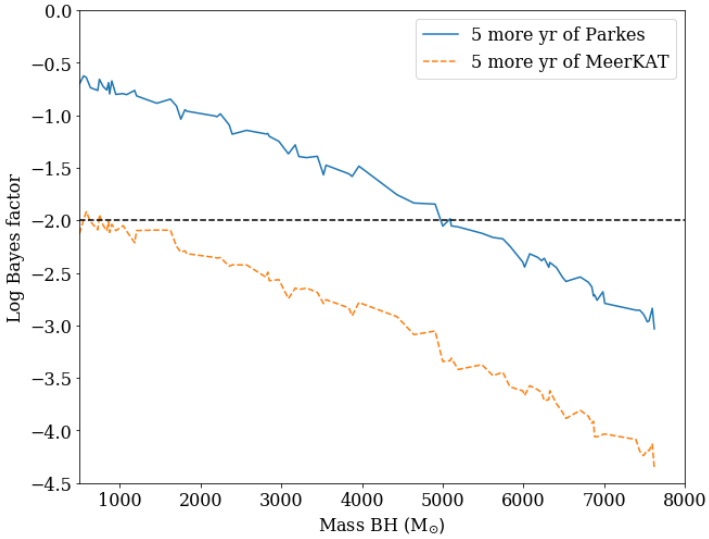

Figure 5.14: Prediction of detectability of a central IMBH in 47 Tuc assuming we have access to 5 more years of timing observations with the Parkes radio telescope (shown in blue) and with the MeerKAT radio telescope (shown in dashed orange). The simulations show that Parkes would allow us to detect IMBHs of mass > 5000 $M_\odot$ and that with MeerKAT of mass > 1000 $M_\odot$. Details of how these simulations were run are found in the text.

simulations, i. e. 50 Myr. For this reason we see an enhanced density in the centre that helps increasing jerks and jounces inside the influence radius.

The situation differs for 47 Tuc. In the simulations we don't see the over-density forming in the centre as the core relaxation time is much longer, ~ 700 Myr. Since the density does not change, the enhanced jerks and jounces that we measured are only caused directly by the gravitational potential of the IMBH and increased velocity dispersion. As jerks and jounces increase in presence of the over-density (as shown in the mock cluster simulations) the results derived in Section 5.3.3 highlighting the importance of jerks in the search of an IMBH will be strengthened by using more evolved simulations.

5.3.5 *Discussion*

IMBHs in Galactic GCs have been searched for extensively, and compelling evidence is still lacking. In particular the discovery of IMBHs of mass below a few thousands solar masses is challenging since their influence is limited to the centre-most region of the star cluster. MSPs have been considered as key probes through their accelerations measured via pulsar timing analysis. In this paper we show that measurements of the second and third derivative of the rotational period of an ensemble of MSPs in a Galactic GCs help in their identification. These derivatives are correlated respectively with the line-of-sight com-

ponent of the first and second derivatives of the acceleration called jerks and jounces.

Direct N-Body simulations of star clusters using the Hermite's 6th order integrator require the computation of higher order derivatives of the star's accelerations to trace with high accuracy the stellar dynamics determined by the mean gravitational field and by neighbouring stars. For the first time, we read off the values of the star's jerks and jounces from a suite of simulations with and without IMBHs.

We demonstrated that a central IMBH modifies the distribution of jerks and jounces within its sphere of influence. We used MSPs as test particles of the gravitational field and, using a Bayesian analysis, we computed the probability of finding MSPs in a given jerk and jounce bin extracted in a suite of simulations with IMBHs over a range of mass between 10^2 and 10^4 $M_\odot$. We showed that the derivatives of the acceleration are more sensitive to the presence of black holes of low masses when compared with just the information taken from the acceleration. A combination of all the kinematic information is shown to be the best method for searching for black holes of all sizes.

We applied this technique to the MSPs in 47 Tuc and obtained an upper limit on the mass of the central IMBH of ~ 7000 $M_\odot$. This result is not as stringent as other upper limits derived for this cluster based only on the acceleration data of the MSPs [4] because it does not take into consideration the position along the line of sight of the MSPs. To include this parameter we need a description of the effects of the IMBH on the jerks and jounces caused by neighbouring stars which is still lacking. However, the inclusion of jerks in the calculation was essential in measuring this mass limit.

As more observations pile up, the accuracy of the measurements of jerks and jounces improves faster than for accelerations. The uncertainty scales as $T^{-7/2}$ for the jerks and $T^{-9/2}$ for the jounces where T being the total length of observations. In contrast the accuracy of accelerations in the case of binary pulsars scales as $T^{-5/2}$. For isolated pulsars the accuracy of the acceleration will not increase since the intrinsic spin down is unknown.

In the near future jerks and jounces might be so precise that they are more informative than accelerations. This has been tested simulating observations for five years with the Parkes radio telescope and with the MeerKAT radio telescope which will observe this cluster in the future. We estimated how the measurements of jerks and jounces can improve and applied the technique to set lower upper limits for IMBHs. With five more years of observations at Parkes the upper limit is ~ 5000 $M_\odot$. With MeerKAT the limit is below 1000 $M_\odot$.

MSPs can become the most precise probes to search for the presence of IMBHs in Galactic GCs . Long observational campaigns are necessary to reach the precision required to achieve this result. Thus, it is important that all these MSPs, even the isolated ones, are regularly observed.

Newly discovered MSPs close to the centre of the clusters would also greatly increase the accuracy of the search.

6

FORMATION OF THE CENTRAL NSC WITH MSPS FROM GLOBULAR CLUSTERS

The work described in this Chapter is presented in:
***F. Abbate**, A. Mastrobuono-Battisti, M. Colpi, A. Possenti, A. C. Sippel, and M. Dotti. "Probing the formation history of the nuclear star cluster at the Galactic Centre with millisecond pulsars." MNRAS, 2018, Vol. 473, pp.927–936*

The fields of astronomy that can be addressed while remaining in the context of GC pulsars are plenty. In chapters 3 and 5 we saw how pulsars can be used to study the properties of the host GCs like the gas content or the presence of an IMBH or black hole system. In chapter 4 we saw that the magnetic field of GCs can be used as a tracer of large scale properties of the Galaxy itself like a magnetized outflow from the disk. In this chapter we show how GC pulsars might help solve the mystery of the formation of the NSC that surrounds the Galactic centre.

We first describe the different possible formation scenarios concentrating on the *cluster-inspiral scenario* that assumes that the NSC was formed by the infall of stellar cluster brought to the Galactic centre by dynamical friction. We show that, in this process, the MSPs present in the clusters will be deposited in the NSC with a peculiar radial profile and finally we test if future surveys of the Galactic centre with radio telescopes will be able to detect the MSPs and infer, from the distribution, the most likely formation scenario.

6.1 GALACTIC NUCLEAR STAR CLUSTER

NSC are dense stellar systems observed in a large fraction of galactic nuclei [62, 85]. They have masses between $10^6 M_\odot$ and $10^7 M_\odot$, effective radii of less than 5 pc [63, 98, 150] and often host a Super Massive Black Hole (SMBH) at their centre [151].

The central parsecs of our Galaxy host a NSC [149, 255] with half-light radius of 4.2 ± 0.4 pc [315], a mass of $2 - 3 \times 10^7$ $M_\odot$ [121, 315] and a central black hole of $4.30 \pm 0.20_{stat} \pm 0.30_{sys} \times 10^6$ $M_\odot$ [155].

The formation mechanism of NSCs is not yet known and two are the main scenarios proposed so far: (1) the *in-situ* formation scenario where infall of gas to the centre of the galaxy and subsequent star formation are responsible for the formation of the cluster and its stellar populations [11, 227, 261, 271]; (2) the *cluster-inspiral* scenario

where stellar clusters spiral into the galactic centre under the action of dynamical friction and slowly accumulate to build up the NSC [18, 19, 21–24, 82, 156, 290, 343]. While the first scenario is dissipative and relies on violent episodic events of gas inflows, the second is dissipationless and regular over the entire lifespan of the NSC.

These two formation processes may not be mutually exclusive, and can work in concert [18]. In particular, the *cluster-inspiral* scenario can account for both the morphological and kinematic properties of the NSC at the Galactic centre [346]. On the other hand the young massive stars in the Galactic NSC [149, 153, 314] show the presence of an ongoing star formation.

The central regions of the Galaxy are thought to host a large population of both ordinary pulsars and millisecond pulsars [MSPs, 292, 357]. The large number of massive and young stars suggests that an abundant population of ordinary pulsars could stem from the ongoing star-formation. Moreover, the Galactic Centre hosts an excess of X-ray sources comparable to the excess measured in GCs [164, 273]. This might be indicative of a large population of MSPs, similar to the ones observed in GCs. This population was for long thought to be unobservable with current telescopes because of the very large expected gas densities in the central regions which would create strong scattering screens [222]. The scattering screens would induce a temporal smearing which would cover completely the pulsed emission of the pulsars.

The discovery of the Galactic Centre magnetar SGR J1745-29 at just 0.1 pc from the central SMBH, Sgr A* indicated that the scattering screen could be up to three orders of magnitude weaker than what expected [329], at least along some favourable lines of sight. Moreover, the angular broadening scale of the magnetar is in excellent agreement with the one measured for Sgr A*, suggesting that the two sources lie behind the same scattering screen [67]. The angular broadening scale is also similar to what measured in masers at $\sim 1 - 50$ pc from the Galactic Centre. Therefore we can argue that the effects of the scattering screen are similar to those seen in SGR J1745−29 over a significant portion of the Galactic Centre region.

In spite of these predictions, the numerous surveys – some of them performed also at relatively high radio frequencies, from 3 GHz to 15 GHz – focused on finding this population of ordinary and millisecond pulsars in the central parsecs of the Galactic region [43, 105, 194, 244] have not detected a single pulsar. This disagreement between predictions and observations is known as *The Missing Pulsar Problem* [106].

In fact, the Galactic Centre pulsar population might also be responsible for the excess that the *Fermi* satellite detected in gamma-ray [103, 157, 181]. This excess peaks at $\sim$ 2 GeV, is roughly spherical and extends to $\sim 10^\circ - 20^\circ$ (1.5-3 kpc) from the Galactic Centre. The

most probable sources of the excess are the annihilation from dark matter particles [103, 181], the emission from diffuse cosmic rays [144] and the emission from a population of MSPs [3, 157]. Wharton et al. [357] estimated that to produce the observed emission the number of MSPs within 1 pc should be $\lesssim 5000$. Brandt and Kocsis [69] suggested, and Arca-Sedda, Kocsis, and Brandt [27] confirmed, that the emission from MSPs from disrupted globular clusters could explain the observed excess. Other authors instead claim that this mechanism could only explain a few percent of the total excess [164, 182, 183].

GCs are known to be breeding grounds for the formation of MSPs [79, 131]. Thus, in the cluster-inspiral scenario, GCs are expected to deposit their population of MSPs which are then inherited by the NSC.

In the *in-situ* formation scenario, ordinary pulsars form out of regular star formation and should be found where young massive stars are observed, ~ 0.5 pc [42, 255, 363]. Field binaries and binaries that form via dynamical interactions in the densest regions of the NSC can produce a population of MSPs [119].

Since ordinary pulsars live only for a few tens of Myr, the current population can not carry any information on the formation scenario. By contrast, MSPs are expected to live and emit radio pulsations for 1-10 Gyr timescales and can be used to disentangle the two formation processes.

This paper is a first attempt to probe the cluster-inspiral scenario using MSPs as tracers of the dynamical formation of the Galactic NSC.

The cluster-inspiral scenario that we refer to in this paper is described in Antonini et al. [19], Perets and Mastrobuono-Battisti [290], and Tsatsi et al. [346]) . In these investigations, NSC form via repeated mergers of dense and massive stellar clusters, which are sinking toward the centre of a Milky Way-like bulge.

In the N-body simulation by Tsatsi et al. [346] used in this investigation, a NSC grows by letting 12 identical stellar clusters fall on the Galactic Centre, one every ~ 0.85 Gyr. The stellar clusters have a mass of $1.1 \times 10^6 M_\odot$ and are represented by a tidally truncated King model [204] with core radius of ~ 0.5 pc, half mass radius of ~ 1.2 pc and the dimensionless King potential W_0 is 5.8. The half mass relaxation time for these clusters is ~ 0.3 Gyr. The Galactic Centre is composed of a nuclear disc of mass $M_{disk} = 10^8$ $M_\odot$ and a central massive black hole of mass 4×10^6 $M_\odot$. The black hole gravitational field acts as attractor and thus contributes to the building up of the NSC. The stellar clusters are released at a distance of 20 pc from the Galactic Centre. The inspiral happens on a timescale of a few tens of Myr, much shorter than the half mass relaxation time. Therefore the internal evolution of the globular clusters can be neglected during the inspiral phase. After the the arrival of the last globular cluster, the system is evolved for 2.2 Gyr, reaching a total simulation time of ~ 12.4 Gyr. Following Tsatsi et al. [346], we analyse three simulations with different initial

conditions on the orbital parameters. In I and II, the longitude of the ascending node Ω and inclination i of the orbits are randomly chosen. In simulation III, the constraint on $i < 90^\circ$ allows to describe the sinking of clusters formed in the central molecular zone of the Milky Way having random offsets with respect to the Galactic plane, but all sharing prograde orbits.

6.2 NEUTRON STARS IN GLOBULAR CLUSTERS

Stellar clusters host a large number of neutron stars that form after a few million year from the core collapse of stars with masses between $9-20\ M_\odot$. In order to determine their spatial distribution and density in every simulated cluster, we focus on the outcome of an N-body simulation of a "reference" star cluster [325]. The cluster is evolved with NBODY6 [1, 2, 276] and has a total initial mass of $1.6\times10^5\ M_\odot$, an initial core radius of ~ 4 pc, an initial half-mass radius of 6.2 pc, and is described by a Plummer density profile. The stars are initially distributed according to the initial mass function of Kroupa, Tout, and Gilmore [215] between $0.1\ M_\odot$ and $50\ M_\odot$. The total number of stars simulated is 262 500 and are evolved accounting for stellar evolution for 12 Gyr as modelled in [186]. In Sippel and Hurley [325], the neutron stars receive kicks at birth whose strength is adjusted in order to obtain a retention fraction of $\sim 10\%$ as is suggested by observations [291, 293]. The simulation is sampled every Gyr, which corresponds to about 0.5 half-mass relaxation times, in order to reconstruct the mass segregation of the neutron stars. The evolution is followed up to 6 half-mass relaxation times. During the evolution of the cluster the half-mass relaxation time remains constant. The positions of the neutron stars as a function of time is shown in Figure 6.1.

The next step consists in rescaling and adapting the outcome of this simulation to our large scale simulation in order to track the position of the neutron stars in each cluster during the assembly of the NSC. To set this correspondence, we divide the stars in radial bins expressed in units of the half-mass radius and measure the mass ratio of neutron stars to normal stars in every snapshot. After obtaining the neutron star mass fraction in every normalised bin, we mark the same fraction in the corresponding stellar clusters used in the simulation of the cluster-inspiral formation scenario. Since every cluster is injected at a different time, the spatial distribution of the neutron stars is modified by mass segregation. The match in time is carried on attributing different spatial distributions according to the time of cluster injection, measured in units of the half-mass relaxation time. Having established these correspondences, we then follow the dismemberment of the host clusters to infer the final position of the neutron star population, at the end of the simulation. The positions and radial distribution of the neutron stars during the simulation of the formation of the NSC

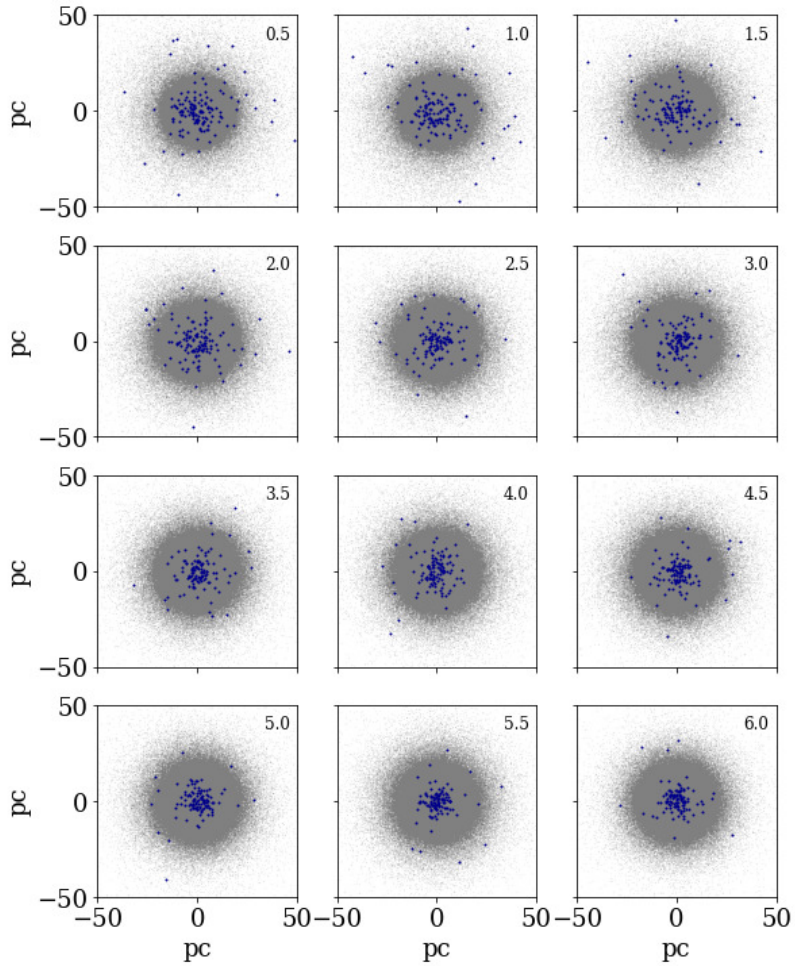

Figure 6.1: Snapshots of the spatial distribution of the neutron stars (blue dots) in the simulated reference cluster by Sippel and Hurley [325] on top the background stellar component (grey dots). The snapshots are taken one every 0.5 half mass relaxation time. The time at which each snapshot is taken is shown in each panel in units of the half mass relaxation time.

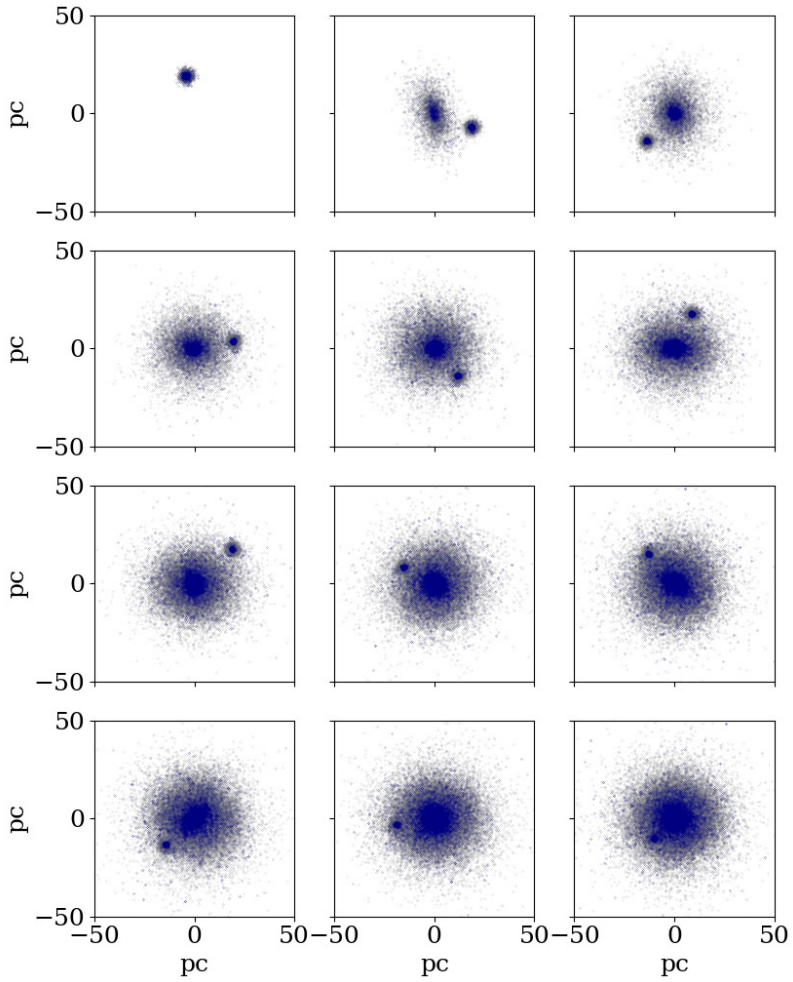

Figure 6.2: Snapshots of the spatial distribution of the neutron stars (blue dots) in the NSC on top the background stellar component (grey dots). Each snapshot is taken when a new globular cluster is injected in the simulation.

are shown in Figure 6.2 and in Figure 6.3. The neutron stars do not cluster in the central regions of the NSC but are scattered throughout a region of 40-50 pc. As these simulations are performed with single mass particles we cannot follow the effect of mass segregation in the NSC.

The radial distributions of the neutron stars deposited by the clusters at the Galactic Centre are shown in Figure 6.4, for the three different simulations. The neutron stars do not cluster within the central parsec. Instead, they are spread over a rather wide volume, with $\sim$ 87% being inside a radius of 20 pc. The peak of the distribution is at 3 pc, close to the gravitational influence radius of the central massive black hole [13, 90, 121, 266]. The first clusters are tidally disrupted closer to the black hole, whereas those sinking at later times have a progressively larger disruption radius, due to the build up of the NSC. This is the

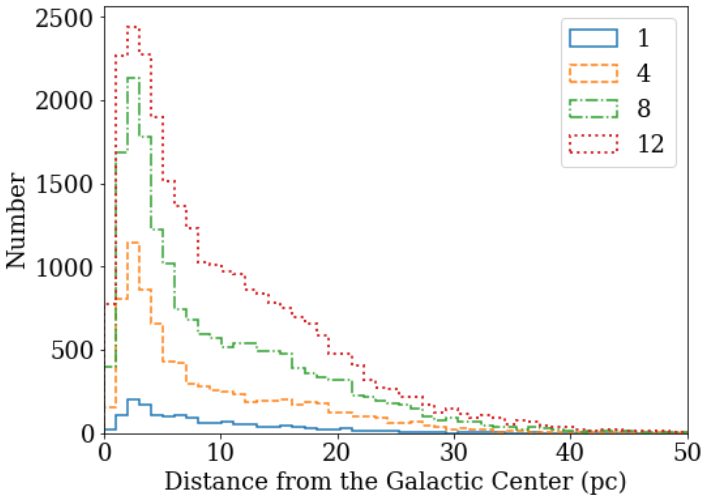

Figure 6.3: Radial distribution of the neutron stars deposited in the NSC during the simulation. The distributions are sampled after the first, forth, eighth and twelfth globular cluster are injected and left to evolve for 0.85 Gyrs. The number of the last globular clusters injected for each distribution is shown in the label. Each bin has a width of 1 pc.

cause of the broad distribution of the neutron stars, in the simulations [290]. The spatial distribution of neutron stars is weakly dependent on the initial conditions of the cluster orbits as is shown in Figure 6.4 where results from the three simulations are plotted. Therefore in our analysis we will use only the simulation I.

So far, the neutron stars of our simulations have been treated as point particles. We lacked in tracing their small-scale dynamics in the cluster and in the NSC leading to their pairing in binaries, and their close interaction with companion stars, which leads to their recycling as MSPs [370]. Thus, in determining the recycling fraction our approach is necessarily statistical, and is based on current observations of MSPs in the field and in globular clusters, and on a comparison with ordinary pulsars. We further note that our simulations do not evolve the stellar population during the NSC growth.

In the Galactic disk (within 3 kpc from the Sun) the ratio of the birthrates of MSPs to ordinary pulsars is found to be $\geq 10^{-3}$ [238]. Using this result Wharton et al. [357] inferred a recycling fraction of $f_{rec} \geq 10^{-3}$. Since the formation mechanism of MSPs is linked to accretion from a companion star, LMXBs have usually been considered the progenitors of MSPs. LMXBs are found to be $\sim$ 100 times more abundant in the globular clusters than in the Galactic field [92, 200]. Based on this information Wharton et al. [357] estimated that the recycling fraction for GCs is $f_{rec} \sim 0.1$.

To determine the number of MSPs that formed from neutron stars, during the time spent in their host cluster, we proceed on with an anal-

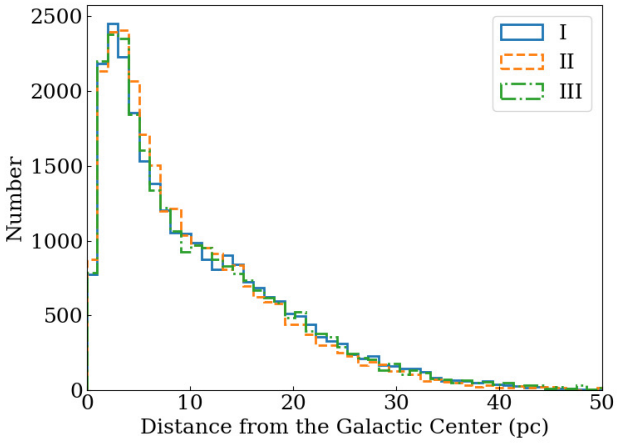

Figure 6.4: Distribution of the neutron stars in the Galactic Centre according to the three simulations. The plots in different colours refer to the three simulations. The distributions are all compatible with one another. Each bin has a width of 1 pc and the distribution peaks at 3 pc.

ysis based on our current knowledge of the MSP luminosity function in the Galactic GCs[1].

We proceed in steps: (i) we first use the luminosity function to infer the number of MSPs in a selected set of Galactic GCs; (ii) for each selected cluster we record the total cluster luminosity and mass-to-light-ratio [as measured in 203, 262] and assign a total stellar mass; (iii) using the value of the neutron star mass fraction inferred from the simulation by Sippel and Hurley [325], we compute the number of neutron stars in each cluster and then the "recycling fraction", defined as the ratio of the number of active MSPs to the number of neutron stars that formed in the cluster; (iv) we then associate to each Galactic globular cluster the "encounter rate" taken from Bahramian et al. [39] which measures the number of close stellar encounters per unit time and is linked to the formation of LMXBs ad MSPs [39, 296]. This quantity is measured as $\Gamma_c \propto \int \rho^2/\sigma$ where ρ is the stellar density and σ is the total velocity dispersion. In this way we explore the dependence of the recycling fraction with the encounter rate.

As far as (i) is concerned we adopt three fits to the MSP luminosity function [36] that will be used also in the analysis on the detectability of the MSPs at the NSC. Following Bagchi, Lorimer, and Chennamangalam [36], we consider three possible log-normal model fits (all

1 From this moment on, we implicitly assume that the NSC at the Galactic Centre formed from the assembly of "globular clusters". The clusters described with a King model then represent replica of the globular clusters of the Milky Way, and MSPs inherit the properties they show in the Galactic globular clusters. One cannot exclude that MSPs form in the high density environment of the newly formed NSC. Our analysis is confined to the populations of MSPs that have been dragged by the dynamical process studied in Tsatsi et al. [346].

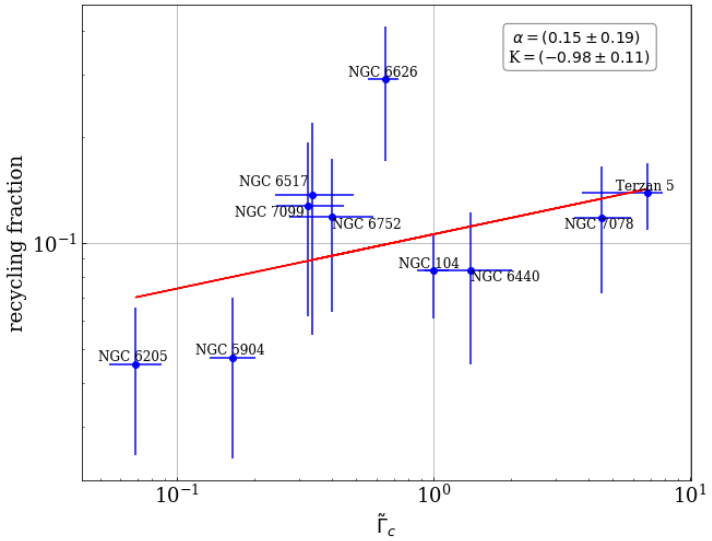

Figure 6.5: Recycling fraction as a function of the normalised encounter rate for a number of Galactic globular clusters measured with Model 1 of Bagchi, Lorimer, and Chennamangalam [36]. The way these quantities are measured is described in the text. The parameters of the best power law fit are shown in the inset.

expressed in unit of mJy kpc^2: Model 1 with mean $\mu = -1.1$ and standard deviation $\sigma = 0.9$, which is the same proposed by Faucher-Giguère and Kaspi [117]; Model 2 with mean $\mu = -0.61$ and standard deviation $\sigma = 0.65$; and Model 3 with mean $\mu = -0.52$ and standard deviation $\sigma = 0.68$.

Figure 6.5 shows the recycling fraction measured using Model 1 of Bagchi, Lorimer, and Chennamangalam [36] as a function of the encounter rate, $\tilde{\Gamma}_c$, normalised to the value obtained for NGC 104. The data is fitted with a power law of the form $\log(f_{rec}(r)) = K + \alpha \log(\tilde{\Gamma}_c)$. The best fit parameters, obtained with a MCMC algorithm, are $K = -0.98 \pm 0.11$ and $\alpha = 0.16 \pm 0.19$ compatible with a straight line fit. The figure shows that over more than two order of magnitudes in $\tilde{\Gamma}_c$ the value of f_{rec} varies weakly. The average value of f_{rec} of all clusters is 0.11. Using Model 2 and Model 3 of Bagchi, Lorimer, and Chennamangalam [36] we see the same weak dependance on $\tilde{\Gamma}_c$. The average value for Model 2 is 0.09 and for Model 3 is 0.06. Based on these results we can also consolidate the order of magnitude estimate of $f_{\rm rec} \sim 0.1$ measured by Wharton et al. [357] in a completely independent way. The value of the normalised encounter rate for the GCs simulated in this work is ~ 20. We assume that, for these values of the encounter rate, the recycling fraction remains the same as that measured for the Galactic ones.

The encounter rate for the NSC can be measured using the density and velocity dispersion profiles with the same procedure used by Bahramian et al. [39] for globular clusters. In this way we obtain a

value, in normalised units, similar to the densest globular clusters, ~ 10 in the scale shown in Figure 6.5. For this reason we assume that the recycling fraction is ~ 0.1 also for the NSC. At the end of the simulations we randomly select the MSPs accordingly to the recycling fraction of the total neutron stars.

6.3 DETECTABILITY OF PULSARS IN THE GALACTIC CENTRE

No MSP has been discovered so far in the Galactic Centre area. In this section we explore the observability of the population of MSPs inferred from the cluster-inspiral scenario, with more sensitive instruments than those available so far.

We have first to select the frequency band at which the surveys should be performed. While the steep radio spectrum would suggest to adopt the low frequencies (1.2-1.8 GHz) at which most of the searches in the Galactic plane have been run so far, the strong scattering of the Galactic Centre would advise to move to higher frequencies. Macquart and Kanekar [243] suggested that the best compromise – for the scattering scenario considered here – is to operate the search experiments around a frequency of $\sim 8-9$ GHz. In view of that, we run our simulations for two reference cases of study. Case 1 assumes to utilise an instrument with characteristics similar to those originally proposed for the high frequency band (8-14 GHz) of the MeerKAT radio-telescope [66]. Case 2 appeals on a much higher instantaneous sensitivity (keeping the other instrumental parameters like those of Case 1), similar to that invoked for the band 5 (4.6-14 GHz) in the context of the SKA1-MID[2] baseline design. In both cases, we simulate surveys performed at a centre frequency of 9 GHz with a bandwidth of 1 GHz.

The MeerKAT telescope is located in South Africa [66]. The SKA1-MID will be the first phase of the medium frequency part of the SKA and will expand around the MeerKAT site [70]. We note that the nominal capabilities of both the instruments at the $\sim 8-9$ GHz band are still under discussion. Hence, our simulations are not aimed at performing any detailed prediction about the MSP yields resulting from them. We used some general properties of the original design of those instruments to check if the order of magnitude of the MSPs discoveries is suitable to probe the formation history of the NSC at the Galactic Centre.

We use the prescriptions described in Macquart and Kanekar [243] to measure the number of detectable MSPs. A pulsar is detected if the pulsed emission is significantly stronger than the background noise, usually a threshold of S/N$=10$ is required, where S/N is the signal to noise ratio. To measure the signal to noise ratio of a pulsar observation

2 www.skatelescope.org/wp-content/uploads/2012/07/SKA-TEL-SKO-DD-001-1_BaselineDesign1.pdf

we use the radiometer equation. This equation states that, in the case of a narrow observing bandwidth, the S/N of a pulsar of flux density S_ν, pulse period P and width W is [229]:

$$\mathrm{S/N} = S_\nu \frac{G\sqrt{n_\mathrm{p}\Delta t \Delta\nu}}{\beta\, T_{sys}} \sqrt{\frac{P-W}{P}}, \tag{6.1}$$

where G is the telescope gain, n_p is the number of polarizations observed, Δt is the total observation time, $\Delta\nu$ is the observing bandwidth and T_{sys} is the total system temperature. The factor $\sqrt{(P-W)/P}$ represents the fraction of power present in the pulse signal. In real surveys devoted to the search of new pulsars this performance in never fully reached. Imperfections caused by the digitisation of the signal and by the improper determination of pulsar properties can reduce the S/N. The factor β in the equation is called *correction fraction* and accounts for these effects. In the worst case scenario it can be as high as 2 and effectively half the observed S/N.

When $\Delta\nu$ is large, the assumption that S_ν, T_{sys} and W are constant breaks down and we must consider their variations across the band. This can be done considering separately the total signal and the total noise received during the observation. The total signal measured can be written as:

$$S = \frac{1}{\beta} n_\mathrm{p}\Delta t \int_{\nu_1}^{\nu_2} S_\nu(\nu')d\nu', \tag{6.2}$$

where ν_1 and ν_2 are the extreme of the observing band. For pulsars, S_ν is usually written in the from $S_\nu(\nu) = L_{1.4} d_{\mathrm{GC}}^{-2} \left(\frac{\nu}{1.4\,\mathrm{GHz}}\right)^\alpha$, where $L_{1.4}$ is the (pseudo-)luminosity of the pulsar at 1.4 GHz in units of mJy kpc^2, d_{GC} is the distance of the Galactic Centre in kpc and α is the spectral index.

The noise per polarization collected over a sampling time, δt in a frequency channel $\delta\nu$ is $n(\nu) = \sqrt{\delta t \delta\nu}\, T_{sys}(\nu)/G \times \sqrt{W(\nu)/(P-W(\nu))}$. The total noise over all sampling times, frequencies and polarization channels adds in quadrature and therefore is:

$$N = \sqrt{n_\mathrm{p}\Delta t \int_{\nu_1}^{\nu_2} \frac{T_{sys}^2(\nu')}{G^2} \frac{W(\nu')}{P-W(\nu')} d\nu'}. \tag{6.3}$$

Therefore, the S/N for the detection of a pulsar is calculated with the formula:

$$\mathrm{S/N} = \frac{1.62\times10^{-5}\sqrt{n_\mathrm{p}\Delta t}\int_{\nu_1}^{\nu_2} L_{1.4}\left(\frac{\nu'}{1.4\,\mathrm{GHz}}\right)^\alpha (\nu')d\nu'}{\beta\sqrt{\int_{\nu_1}^{\nu_2}\frac{T_{sys}^2(\nu')}{G^2}\frac{W(\nu')}{P-W(\nu')}d\nu'}}, \tag{6.4}$$

where we used $d_{GC} = 7.86$ kpc [57].

The telescope system temperature T_{sys} contains contributions from the sky and from the telescope receiver. The contribution from the sky can be divided in different parts: the emission from the the bright Galactic Centre region, the emission from the Earth's atmosphere and from the CMB and the noise of the receiver. Therefore it can be written in the form:

$$T_{sys}(\nu) = T_{GC}(\nu) + T_{CMB} + T_{atm}(\nu) + T_{r} \tag{6.5}$$

The contribution originating from the Galactic Centre can be modelled with the equation:

$$T_{GC}(\nu) = T_0(\nu) \left(\frac{\theta_0^2}{\theta_0^2 + \theta_b^2} \right), \tag{6.6}$$

where $T_0(\nu) = 350(\nu/2.7\,\mathrm{GHz})^{-2.7}$ K [305], $\theta_0 = 0^\circ.33$ [305] and θ_b is the FWHM of the telescope beam, $\theta_b = 1.22\lambda/d$, where d is the diameter of the telescope. The contribution from the CMB is constant at $T_{CMB} \sim 2.7$ K.

The atmospheric emission strongly depends on the telescope site, weather during the observations and on the elevation of the source. For an estimate of the atmospheric emission at the MeerKAT site we looked for the average archival temperature and humidity data for the site and, using past works [12, 176, 177], we recovered the average value at the zenith at the observing frequency. Then we measured the temperature at the different elevations of the Galactic Centre from the telescope and averaged it over the observation. For the MeerKAT and SKA site at 9 GHz we obtained an average atmospheric noise of ~ 5 K. The temperature noise injected by the receiver is taken to be ~ 10 K, assuming performances similar to the current state-of-art systems.

The observed width W of the pulses plays an important role in mock surveys: in fact, when W becomes of the order of the pulse period, the pulsar becomes undetectable even if the flux is very high. W is influenced by different factors: the intrinsic width, W_{int}, the time smearing due to scattering, τ_{scat}, the time smearing due to the dispersive nature of the ISM, τ_{DM}, as well as the sampling time, δt. The resulting width is the sum in quadature of these contributions:

$$W = \sqrt{W_{int}^2 + \tau_{scat}^2 + \tau_{DM}^2 + \delta t^2} \tag{6.7}$$

Following the indications of [107] for a Galactic Centre region of ~ 50 pc radius, the value of τ_{scat} is taken to be the same as the one observed for the magnetar SGR J1745+29 [329]:

$$\tau_{scat} = 1.3 \times \left(\frac{\nu}{1\,\mathrm{GHz}} \right)^{-4} \mathrm{s}. \tag{6.8}$$

The smearing effect due to the dispersive nature of the ISM follows the law:

$$\tau_{DM} = 4.15 \times 10^6 \, \mathrm{DM} (\nu_1^{-2} - \nu_2^{-2}) \, \mathrm{ms}, \tag{6.9}$$

where DM is the dispersion measure in units of pc cm^{-3} and ν_1 and ν_2 are the extremes of the observing bands expressed in MHz. As a reference the magnetar SGR J1745+29 has a DM of 1778 ± 3 [109]. The corresponding time delay is ~ 20 ms at a central frequency of 9 GHz and a bandwidth of 1 GHz, enough to mask most millisecond pulsar. Luckily this effect can be compensated by splitting the data in narrow enough frequency channel and then adding a delay at each frequency channel of the opposite amount than that induced by the DM. This procedure can almost completely correct for this effect, thus making the contribution of τ_{DM} negligible with respect to τ_{scat}. Therefore in our surveys we will assume $\tau_{DM} \sim 0$. The adopted sampling time (see Table 6.1) is similar to what commonly used in current MSP searches.

We simulate surveys with integration times of 10 hours. While long integration times increase the sensibility for isolated MSPs, they might impede the discovery of binary MSPs. Usual binary pulsars search procedures lose efficiency when the orbital period of the binary is shorter than 10 times the total duration of the observation. Therefore binary MSPs with orbits shorter than 100 hours would be difficult to detect. Using the observed population of MSPs in globular clusters, we see that 40% of all MSPs are in binaries with period shorter than this. Thus, these surveys would be sensible to only 60% of the observed MSP population.

Since the simulated survey will be performed at high frequency, ~ 9 GHz, while the luminosity distribution is measured at 1.4 GHz, the spectral index α also plays an important role. Studies directed on MSPs found that the spectral index has a mean value of 1.8 and a standard deviation of 0.6 [257]. Similar values resulted from other studies [e.g. 342].

To simulate the other pulsar properties like period, period derivative, spin-down luminosity and pulse width, we used the measured parameters from the ATNF catalogue [250] for Galactic millisecond pulsars. The width of the pulse for MSP does not show strong variability as a function of frequency, therefore we opted to still use value measured at 1.4 GHz also for observations at very high frequencies.

The period derivative and spin-down luminosity do not enter directly in the process of radio detectability of pulsars, but they become important when considering the gamma ray luminosity. The gamma ray luminosity for pulsars is measured to be $L_\gamma \propto \dot{E}^{1/2}$ [118], where $\dot{E}$ is the spin-down luminosity. If we consider only MSPs this law poorly represents the luminosities [9] and later works use the formula $L_\gamma = \eta \dot{E}$ with $\eta = 0.2$ [182] or $\eta = 0.05$ [183]. As an approximate value we use $\eta = 0.1$.

Table 6.1: Instrumental and observational parameters for simulated surveys. Case 1 refers to a pulsar search with parameters similar to those originally proposed for a Meerkat high frequency band survey. Case 2 refers to a survey with identical properties than Case 1, but for the significantly higher Gain of the telescope. This is meant to reflect the strong enhancement in the sensitivity provided by an experiment using a collecting area similar to that of SKA1-MID.

Parameter	Case 1	Case 2
Central frequency ν (GHz)	9	9
Bandwidth $\Delta\nu$ (GHz)	1	1
Integration time Δt (h)	10	10
Sampling time $t_{\text{samp}}(\mu s)$	40	40
System temperature T_{sys} (K)	32	32
Gain G (K/Jy)	1.75	6.2
Max. baseline (m)	1000	1000
FWHM	8" (0.32 pc)	8" (0.32 pc)

The last parameter we have not yet discussed is the luminosity distribution of the MSPs. Since the most used frequency for observing pulsars is 1.4 GHz, luminosities are usually scaled to this frequency to allow comparisons and are written in units of mJy kpc^2. As has already been discussed in the section 6.2, we will use the three log-normal models described in Bagchi, Lorimer, and Chennamangalam [36]. These models give different predictions about the number and luminosity of the MSPs. While these models are all based on observations of pulsars in globular clusters, the difference between them comes from the different assumptions of low luminosity pulsars which are not observed. However, the low luminosity pulsars in the Galactic Centre would not be detected even with the next generation of radio telescopes. Using the formula 6.3 we can find the lower limit luminosity of the MSPs that can be detected with a S/N higher than 10 in our simulated experiments. They range in the $4 - 13$ mJy kpc^2. Therefore in our survey we consider only the MSPs that are brighter than 1 mJy kpc^2. In the rest of the paper these MSPs will be referred to with the term "radio-bright MSPs". For this radio-bright branch of the luminosity function, all three models result in a comparable number of detections.

The final step is to find the number of radio-bright MSPs deposited in the NSCs. We proceed in the following steps. (i) First we calculate the fraction of radio-bright MSPs to the total number of MSPs using the luminosity function. The desired fraction will be the value of the integral of the luminosity function with luminosities above the

threshold considered (the luminosity function is normalised to one). (ii) Repeating the analysis of section 6.2 we determine the fraction of radio-bright MSPs to neutron stars in the Galactic globular clusters. The average value for this fraction is ~ 0.013. This fraction appears to be independent of the luminosity function model used (as it is expected from the fact that all models give the same number of radio-bright MSPs). The number of radio-bright MSPs is roughly a tenth of all MSPs. (iii) We use this fraction to randomly extract radio-bright MSPs from the population of neutron stars in the NSC at the end of the simulation.

6.4 SIMULATION RESULTS

In order to generate a population of synthetic MSPs in the Galactic Centre we assumed it to have the same properties as the ones observed in the Galactic disk and in the GCs. An important property is the beaming fraction, the fraction of pulsars whose emission crosses our line of sight and therefore becomes visible. In the case of MSPs this fraction is very high, $0.5 - 0.9$ [211].

In order to check for the observability of the population of MSPs, the results of our cluster-inspiral scenario need to be projected along a realistic line of sight. We choose to project along the line of sight that maximises the rotation of the NSC in order to reproduce the observed rotation [346]. The projected distribution maintains the same distribution as is observed in Figure 6.4 but the peak moves to ~ 2 pc.

We divide the central parsecs in bins of width equal to the beam of the telescope, and count the number of radio-bright MSPs in each bin. The width of the beam – which will be obtained from the combination of the voltages collected at the various antennas of the arrays by using a beam-forming procedure – is assumed to match the diffraction limited resolving power; in particular (see Table 1) that implies a width of 8″ which in turn corresponds to ~ 0.32 pc at the distance of the Galactic Centre [assumed to be 7.86 kpc 57]. The map of the intrinsic distribution of the MSPs is displayed in Figure 6.6, using a bin size equal to the beam width of the telescope.

The most sensitive pulsar survey of the Galactic Centre as of today was performed at Green Bank Telescope at a frequency of 14.8 GHz [244]. The telescope has an average diameter of ~ 100 m so the beam of the observation will have a width of 50″, corresponding to ~ 2 pc at the Galactic Centre. Using the recipes described in the previous section, repeated simulations of the aforementioned survey results in the average detection of ~ 1 MSPs. In this case, according to Poissonian statistics, the probability of not observing any MSPs is $\sim 35\%$. The null result of the experiment does not contradict the predictions of our simulations.

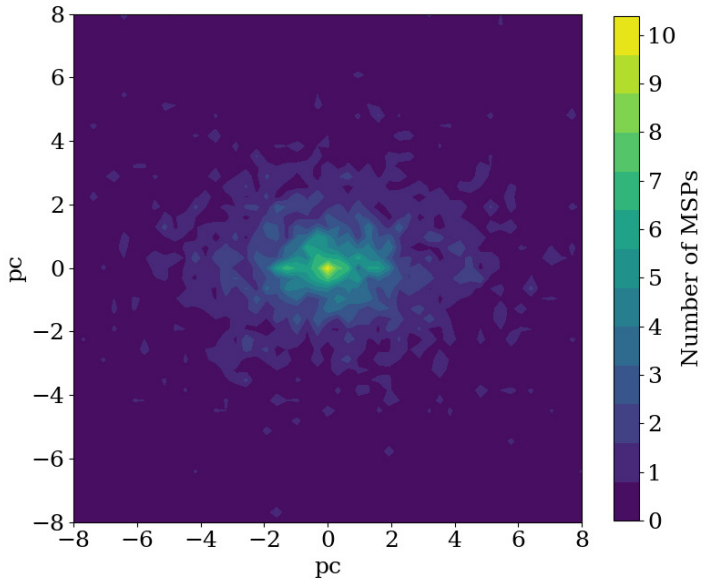

Figure 6.6: Colour-scale map of the distribution of the MSPs at the Galactic Centre. The map is built on a grid of pixels size ~ 0.32 pc, which corresponds to the telescope beam for Case 1 and Case 2.

6.4.1 *Case 1- MeerKAT-like survey*

In Case 1, we simulate the observable sample considering an observation time of 10 hours (see Table 1), in agreement with the observability of the Galactic Centre above the minimum altitude of 15°. For each bin we run the code to determine how many of the radio-bright MSPs are detectable with a MeerKAT-like radio telescope. The result of the simulations is reported in Figure 6.7. There is no single pixel where the detection probability is higher than about 10%. We can potentially detect only ~ 1 MSP within 1 pc, up to ~ 6 in a region with radius of 5 pc, and up to ~ 15 if the search is performed over the entire NSC. In the pessimistic case scenario, where the correction fraction β (see section 6.3) is ~ 2 we obtain a total number of detections of order 10.

6.4.2 *Case 2- SKA1-MID like survey*

In the case of a SKA1-MID-like survey we simulate observations of same duration as for Case 1. The result of the simulations is reported in Figure 6.8. Thanks to the increased collecting area of this telescope the number of detections is significantly larger. Within 1 pc from the Centre, we still detect only ~ 2 MSPs, but the sample increases to ~ 20 in a radius of 5 pc and to ~ 50 if we consider the entire NSC. In the pessimistic case scenario, where the correction fraction β is ~ 2 we obtain a total number of detections of ~ 30.

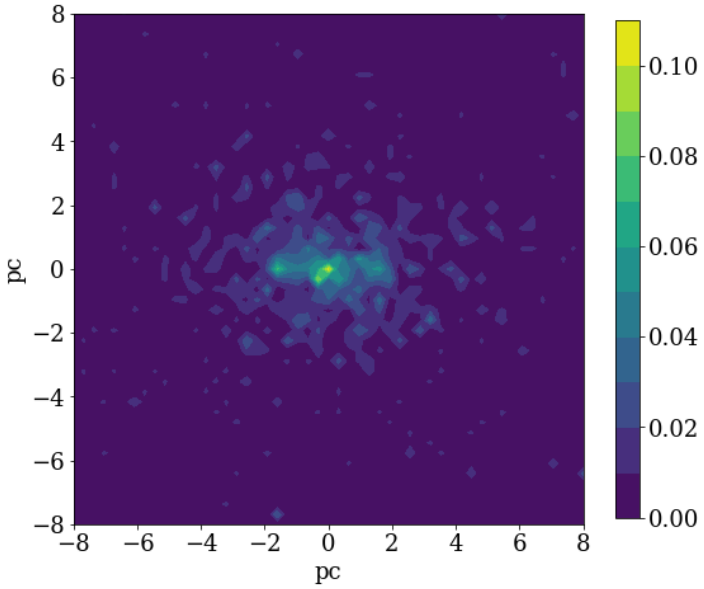

Figure 6.7: Color-scale map reporting the fractional probability of a MSPs at the Galactic Centre to be detected in a Case 1 experiment, averaged over one hundred simulations.

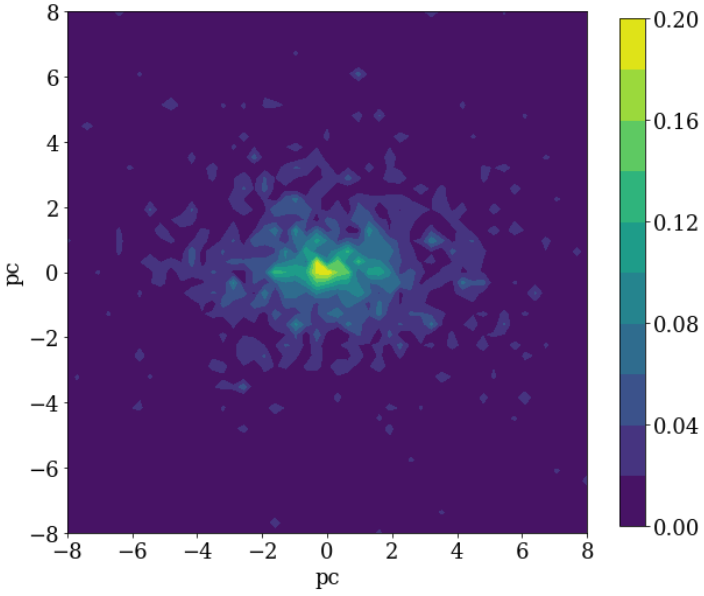

Figure 6.8: Color-scale map reporting the fractional probability of a MSPs at the Galactic Centre to be detected in a Case 2 experiment, averaged over one hundred simulations.

6.5 DISCUSSION

In our cluster-inspiral scenario, about 2700 MSPs are present in the NSC. Only a fraction, $\sim$ 5% are found in the central parsec, and the bulk extends over a region of $\sim$ 20 pc. The aggregation and tidal disruption of globular clusters is a mechanism able to disseminate MSPs over the entire NSC. The mass segregation of neutron stars in the NSC is not included in the simulations during after the assembly of the NSC. We verified that this effect is to first approximation negligible since their mass segregation timescale exceed the Hubble time [142, 266].

Not all MSPs that form in the globular clusters, released in the NSC, will be visible with future radio telescopes. In Case 1 (MeerKAT-like telescope), the detectable MSPs are of order unity within 1 pc, and of order dozen over a spherical volume of $\sim$ 20 pc radius. In Case 2 (SKA1-MID-like telescope) we expect a significant improvement of a factor $\sim$ 3 in the yields.

Wharton et al. [357] considered an in-situ formation scenario for the MSPs at the Galactic Centre, and estimated a number of about 1000 MSPs within the central parsec. Since we don't have enough information to probe the spatial distribution of this population, we only focused on the total number in the central parsec. By simulating a survey, we verified that the Green Bank Telescope would have detected $\sim$ 2 MSPs, consistent with the null result of the recent survey by Macquart et al. [244]. A MeerKAT-like telescope and a SKA1-MID-like telescope would detect $\sim$ 5 and $\sim$ 20 MSPs, respectively in the central parsec. These are much numerous populations than those implied by the cluster-inspiral scenario and a statistically sound discrimination among the *in-situ* and the *cluster-inspiral* hypotheses could be obtained, at least for an experiment of the scale of SKA1-MID (Case 2).

Our estimates depend on the extent of the interstellar scattering at the Galactic Centre, which is the main responsible for smearing the signal from MSPs. In this work, we considered the scattering to be comparable to that inferred from the radio pulses of the magnetar SGR J1745-29. We note that most of the discoverable MSPs in our scenario are indeed outside the central parsec and extend up to $\sim$ 20 pc. These distances are comparable with those of some ordinary pulsars discovered in the Galactic Centre region which show weak scattering of the same entity of the magnetar. Therefore the assumption of a not destroying effect of the scattering at 8-9 GHz is plausible at the positions where we expect to make most of the detections.

However, if the scattering in the central region will turn out to be stronger and close to the values reported in Lazio and Cordes [222], the detections of MSPs will be harder. In this case, effective surveys would have to be conducted at much higher frequencies in order to make the scattering unimportant. Macquart and Kanekar [243] indicated that $\sim$ 25 GHz might be a good choice when finding for a trade-off

among the aim of reducing the scattering smearing and the need of not missing the MSPs due to the weakening of their signal.

6.5.1 *Gamma-ray emission*

We now discuss the possible contribution of the derived population of MSPs to the gamma-ray emission observed by the *Fermi* satellite in the Galactic centre region, limiting the analysis to the MSPs confined within the NSC resulting from the assembly of in-spiralling globular clusters.

We estimate that a population of $\sim$ 2700 MSPs are present in the inner 20 pc of the Galaxy. Some of these MSPs could have been seen as point sources in the *Fermi* map. An approximate estimate of the point source threshold in this region is 5×10^{34} erg s^{-1} [164]. Averaging the result of our simulation over 100 trials we find that, in average, 5 MSPs will exceed this threshold. The null result of current observations are compatible with the predictions only at the 3 sigma level.

However, we note that the majority of the MSPs are located outside the central parsecs of the Galactic Centre. In this region the MSPs will mostly evolve in isolation with very small probabilities of new events of recycling. The MSPs will therefore lose rotational energy through magnetic dipole breaking. The gamma-ray luminosity, as described in 6.3, is linked to the spin-down luminosity and will decrease significantly over the timespan of the simulation. The number of MSPs with luminosities above the threshold will decrease accordingly.

In light of these considerations we limit our discussion of the gamma-ray excess to the central 5 pc of the Galaxy. The total gamma-ray luminosity of the excess is $(2.0 \pm 0.4) \times 10^{37}$ erg s^{-1}, calculated within $\sim$ 1 kpc from the centre [77, 164]. If we rescale the gamma-ray luminosity to account for the emission within the inner 5 pc according to the spatial profile of the excess [76], we find a value of $\sim 1.5 \times 10^{36}$ erg s^{-1}. Since the average gamma-ray luminosity emitted by a MSPs in our model is $\sim 1.4 \times 10^{33}$ erg s^{-1}, the number of required MSPs is $\sim$ 1000. In this region we find $\sim$ 1000 MSPs. We can therefore explain the observed excess in the inner 5 pc of the Galaxy. We note that similar results have been found by Arca-Sedda, Kocsis, and Brandt [27] and Fragione, Pavlík, and Banerjee [129] using different simulations and different methods to estimate the final MSP population. In this work the authors conclude as well that the deposition of MSPs from inspiralling globular clusters can explain the observed central GeV excess.

7 FUTURE PROSPECTS: MEERKAT RADIO TELESCOPE

7.1 SUMMARY

The abundance of recycled pulsars found in GCs and their unique properties make them perfect probes for determining the dynamics and the environment of the GCs. The applications of this technique are not limited to the properties of the host cluster but extend also to the entire Galaxy and can help explore its present state and its evolutionary history.

In this thesis I showed how the information derived from timing these pulsars allows us to determine the 3-D positions in the cluster which in turn allows us to model the distribution of ionized gas and magnetic field. This approach has so far only worked on 47 Tuc where a constant gas density of 0.23 ± 0.05 cm^{-3} and a significant magnetic field of $\sim 60\,\mu$G was found. The presence of such a strong magnetic field was ascribed to the interaction of the gas in the cluster with a Galactic scale magnetic outflow providing strong evidence for its existence and constraints for its density and magnetic field.

I also showed how the same information allows us to determine the structural parameters of the cluster and compare them with the optically derived values to look for discrepancies that could be caused by an IMBH. No significant discrepancy is found in 47 Tuc but instead it is found in M 62. This discrepancy is accompanied by very high values of the M/L ratio in the centre and could be explained by a single IMBH of mass between $1000 - 6000$ M$_\odot$ or by a system of stellar-mass black holes of similar mass. Both these hypotheses would be extremely interesting if confirmed for the implications they would have for gravitational waves astronomy. We showed how the presence of an IMBH can be further constrained by using not only the first derivative of the rotational period but also the second and the third. The prospects opened by these additional probes of the dynamics can extend even further as they might be able to distinguish between an IMBH and a system of stellar-mass black holes of similar mass, but this must be still be tested and verified.

Finally, in Chapter 6, I showed how the current population of GC pulsars can play a significant role in the understanding of the formation history of the nuclear star cluster that surrounds the Galactic centre. It has been suggested that this nuclear star cluster was formed by the disruption of stellar clusters similar to the observed globular clusters. Using simulations of this scenario, that strongly depend on the properties of the GC pulsars, we predict the number and spatial

distribution of the MSP in the Galactic centre. So far no MSP in the Galactic centre has ever been found and potential discoveries might be possible only with the next generation of radio telescopes.

Most of the results presented in this thesis can only be confirmed or discredited with more powerful telescopes. Fortunately, the next generation of telescopes are coming online and they appear to be living up to or even exceed expectations. During my PhD studies I was involved in the scientific commissioning of the MeerKAT radio telescope in South Africa so I will focus on this telescope and describe its capabilities and scientific prospects.

7.2 THE MEERKAT RADIO TELESCOPE

The MeerKAT radio telescope [66, 195] is located deep in the Karoo desert in South Africa and is a precursor of the SKA whose mid-frequency part (SKA-MID) will be built at the same site. Instead, the low-frequency part of the SKA (SKA-Low) will be built in Western Australia. The telescope has an approximate longitude of $-30°43'$, optimal for observing the regions around the Galactic centre and the entire Southern sky. Until this telescope was built, this part of the sky was observable only with the Parkes radio telescope in Australia.

MeerKAT is composed of 64 off-set Gregorian antennas each with an effective primary dish of almost 14 m [32]. Combined with aperture efficiency, the effective area is ~ 7500 m^2, almost three times larger than Parkes. The maximum baseline between antennas is 8 km with 48 antennas located in a core with a radius of 500 m. This guarantees high sensitivity both on the short and on the long baselines.

The receivers are located on an indexer at the focus of the secondary dish (A detailed picture of an antenna can be seen in Fig 7.1). It mounts L-band receivers working between 856-1712 MHz, UHF receivers working between 540-1080 MHz, and is scheduled to have also S-band receivers working between 1750-3500 MHz supplied by the Max-Planck Institute for Radio Astronomy (MPIfR). More details on the specifications of the telescope can be found in a proceeding by Jonas and MeerKAT Team [195] while the pulsar processing pipeline is described by Camilo et al. [81].

7.2.1 *Scientific prospects*

The large collecting area and the wide fractional bandwidth at L-band (the band most traditionally used for pulsar timing) make MeerKAT one of the most exciting upcoming telescopes for pulsar astronomy. There are two major projects focused on pulsars: MeerTIME[1] [40]

1 more details can be found on the website: http://www.meertime.org

Figure 7.1: Close up picture of a MeerKAT antenna. Credits: SARAO

which focuses on timing the known pulsars and TRAPUM[2] [333] which focuses on pulsar searching.

The main targets of MeerTIME are: relativistic binaries useful to measure neutron star masses and test GR and alternative theories of gravity; millisecond pulsars to look for very-low frequency gravitational waves in the context of the pulsar timing array; slow pulsars to study the bulk of the pulsar population focusing on the emission process and the glitches; GC pulsars to look for exotic binary systems, possibly massive neutron stars, and to study the cluster properties as described in this thesis. TRAPUM will look for new pulsars in SNRs, pulsar wind nebulae, unidentified *Fermi* gamma-ray sources, external galaxies, the Galactic centre, the Galactic plane, and GCs. In both projects GCs will be an important target with a significant fraction of reserved time. In the next paragraphs I will focus on how MeerKAT can improve the science results described in this thesis.

The improve in sensitivity of the MeerKAT telescope with respect to the Parkes has already been measured in section 5.3.3. Here we report the calculations and apply them to other clusters. The nominal gain of MeerKAT is $G_M \sim 2.8$ K Jy^{-1} with an observing bandwidth oin L-band f $\Delta\nu_M = 856$ MHz. The gain of Parkes instead is $G_P = 0.64$ K Jy^{-1} and the bandwidth used for these observations is $\Delta\nu_P = 256$ MHz. The signal to noise ratio of an observation with MeerKAT would be $G_M/G_P\sqrt{\Delta\nu_M/\Delta\nu_P} \sim 8$ times higher. This roughly translates into a timing precision with MeerKAT observations 8 times higher than with Parkes. I simulated observations on a monthly bases of several GCs (previously observed by Parkes) taking into considerations this improvement, I found that around 6 months are necessary to measure the orbital period derivatives of the binary pulsars, one to two years for measurements of the second period derivatives, and up to five years for

2 More details can be found on the website: http://www.trapum.org//

the measurements of the third period derivatives. The determination of these parameters would allow for much tighter constraints on the mass of the possible central IMBH.

The larger bandwidth when compared with other telescopes operating in the same band (with the exception of the new ultra wide receiver at Parkes), implies a better determination of RM of the pulsars. This is useful when trying to improve the model describing the magnetic field in 47 Tuc and to search for similar effects in other clusters.

The increased sensitivity of MeerKAT also means that it might be able to discover new pulsars in the clusters. The targets of these searches are various from binaries in eccentric orbits for which to measure the masses to products of exchange interactions. Probably the most interesting pulsars to be found in GCs are those in a binary system with a black hole companion. This black hole might be of stellar mass or of intermediate mass but, in both cases, it would be an unrivalled test of GR in extreme conditions. Additionally these systems would serve as important sources of gravitational waves to be detected with the next generation of gravitational interferometers.

There is a downside, however, in observing a GC with large telescopes. One of the characteristics that make GCs profitable targets for observing pulsars is their compact size and the presence of multiple pulsars in the primary beam of the telescope; this allows us to observe multiple pulsars simultaneously with the same pointing. The size of the beam of a telescope depends on the size of the telescope and the observing wavelength according to the approximate relation $\theta \sim \lambda / D$, where λ is the wavelength and D is the diameter of the telescope (in case of an interferometer like MeerKAT, D is the maximum distance between antennas). The larger the telescope, the smaller the beam. In Figure 7.2 I show the tied array beam of MeerKAT created using a SARAO script called simulate_tab.py [3] observing the GCs 47 Tuc and Terzan 5 in L-band. Even though using only the antennas in the central kilometre ($D = 1$ km), some of the pulsars will be outside the half-power contour and will not be visible. The solution is to simultaneously form different beams centred on each pulsar. This is achievable thanks to the hardware provided by the TRAPUM collaboration. This possibility also allows the search of new pulsars in the entire primary beam of the single antennas which is much larger than the tied array beam formed through interferometry.

While most of the studies of pulsars have made use of L-band observations, the possibility of observing also in UHF (between 540-1080 MHz) further pushes the science results achievable. Pulsars typically have a power-law spectrum with index that is ~ -1.8 [257] so they are brighter at lower frequencies. Usually, in most telescopes, the UHF band is so polluted by interference that it is barely usable. Fortunately,

3 Part of SARAO commissioning software repository for MeerKAT, private communication

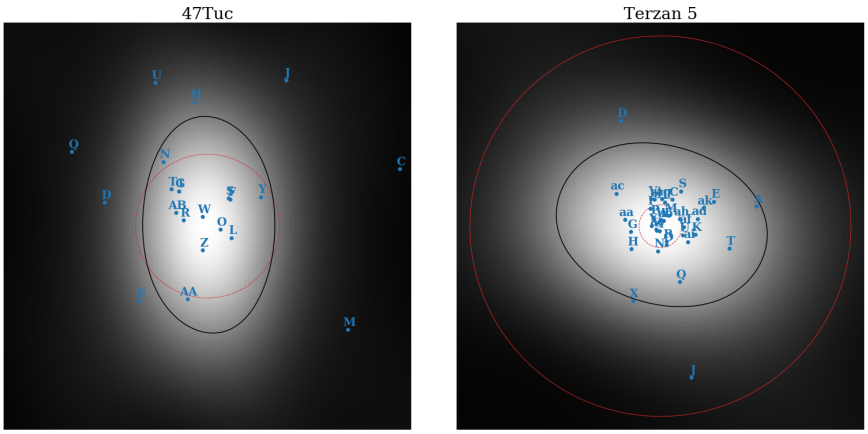

Figure 7.2: Beam of MeerKAT in L-band targeted at GC 47Tuc (left) and Terzan 5(right) using only the antennas in the central kilometre of the array. The black line is the half-power contour of the beam, the dashed red line is the core radius of the cluster and the continuous red line is the half-mass radius of the cluster. In 47 Tuc pulsar X has been omitted as it is far from the centre.

early commissioning tests show that at the MeerKAT site this problem does not exist and the band is very clean. Observing at lower frequencies, not only implies brighter pulsars, but also better determination of DMs and RMs and a bigger beam capable of observing a larger number of pulsars simultaneously in a single beam.

For the search of pulsars in the Galactic centre described in Chapter 6, receivers operating around 9 GHz would be required. Unfortunately, the proposed X-band will not be mounted on the MeerKAT antennas in the near future. The highest observing frequency will be around 3500 MHz of the S-band receivers making the detection of new pulsars harder. The question whether the SKA will eventually mount receivers operating at a frequency of 9 GHz is still being discussed but if approved could lead to significant discoveries.

The fate of future astronomical facilities like the SKA will depend on the discoveries made by MeerKAT. The predicted results listed throughout this thesis and achievable in the near future with MeerKAT are just a small fraction of the science that this telescope will be able to achieve in the field of pulsars and, thanks to the hard work of the South African Radi Astronomical Observatory (SARAO) commissioning team, it looks like our expectations will be met.

Part I

APPENDIX

A

DYNAMICAL PROPERTIES OF PULSARS IN GLOBULAR CLUSTERS

In this appendix I will describe the main dynamical properties of the pulsars (or of any star) in a GC using analitycal formulas, when possible. The quantities are measured both in the absence and in the presence of a central IMBH . The equations are derived assuming the GC can be described by a King profile [205].

A.1 POSITIONS

The column density profile of the pulsars in a globular cluster following a King profile can be well approximated within a few core radii with the formula from [231]:

$$n(x_\perp) = n_0 \left(1 + x_\perp^2\right)^{\alpha/2}, \tag{A.1}$$

where n_0 is the central density, and $x_\perp$ is the distance from the centre in the plane of the sky in units of core radii (r_c), defined as $x_\perp = R_\perp / r_c$. The power law index α is linked to mass segregation and it is related to the mass of the pulsars by the relation $\alpha = 1 - 3q$, where q is the ratio between the mass of the pulsar and the dominant mass class of the cluster ($q = M_p/M_*$). In the case of pulsars having the same mass as the dominant mass class we recover $\alpha = -2$, which is the value for the single-mass analytical King model [205].

The three-dimensional number density has been calculated by [161] and is:

$$n(x) \propto \left(1 + x^2\right)^{(\alpha-1)/2}, \tag{A.2}$$

where $x = r/r_c$ and r is the three-dimensional position of the pulsar. Also in this case, if $\alpha = -2$, we recover the spatial density profile of the single mass King model.

In the case of an IMBH in the centre, the density profile is modified. As described in section 1.7, the presence of the black hole creates a cusp inside the the influence radius described by the power-law distribution [47]:

$$\rho(r) \propto r^{-1.55}. \tag{A.3}$$

A.2 VELOCITIES

The average square velocity of stars in a globular cluster can be obtained from the King distribution function, which is defined as follows:

$$f_K(\mathcal{E}) = \begin{cases} \rho_1 (2\pi\sigma_{\rm vel}^2)^{-3/2} \left(e^{\mathcal{E}/\sigma_{vel}^2} - 1\right) & \mathcal{E} > 0 \\ 0 & \mathcal{E} \leq 0 \end{cases}, \tag{A.4}$$

where $\mathcal{E}$ is the relative energy defined as $\mathcal{E} = \Psi - \frac{1}{2}v^2$, and Ψ is the gravitational potential energy, ρ_1 is a reference density, $\sigma_{\rm vel}$ is the central one-dimensional velocity dispersion and v is the three-dimensional velocity of the star.

The average square velocity can be recovered by the integral:

$$\langle v^2 \rangle = \frac{\int_0^\infty v^4 f_K(\mathcal{E}) dv}{\int_0^\infty v^2 f_K(\mathcal{E}) dv}. \tag{A.5}$$

The limitation of $\mathcal{E} > 0$ can be implemented by limiting the integrals from 0 to $\sqrt{2\Psi}$. In this way we find the solution:

$$\langle v^2 \rangle = \frac{3\sigma_{\rm vel}^2 e^{\Psi/\sigma_{\rm vel}^2} \mathrm{erf}\left(\sqrt{\frac{\Psi}{\sigma_{\rm vel}^2}}\right) - \frac{6}{\sqrt{\pi}}\sqrt{\Psi}\sigma_{\rm vel} - \frac{4}{\sqrt{\pi}\sigma_{\rm vel}}\Psi^{3/2} - \frac{8}{5\sqrt{\pi}}\frac{\Psi^{5/2}}{\sigma_{\rm vel}^3}}{e^{\Psi/\sigma_{\rm vel}^2}\mathrm{erf}\left(\sqrt{\frac{\Psi}{\sigma_{\rm vel}^2}}\right) - \sqrt{\frac{4\Psi}{\pi\sigma_{\rm vel}^2}}\left(1 + \frac{2\Psi}{3\sigma_{\rm vel}^2}\right)}, \tag{A.6}$$

where erf is the Gauss error function.

This expression can be approximated within 20 core radii and with a maximum error of 2 per cent by the formula [6]:

$$\langle v^2 \rangle = \sqrt{3}\sigma_{\rm vel}\left[1 + \left(\frac{x}{6}\right)^2\right]^{-0.2} \tag{A.7}$$

This velocity distribution is valid for the dominant mass class of the cluster. The velocity distribution of heavier will be slower due to energy equipartition as described in eq. 1.31.

In the case of an IMBH in the centre, the velocity distribution will not be altered except inside the influence radius where it will follow a Keplerian profile.

A.3 ACCELERATIONS

The acceleration acting on a pulsar inside a globular cluster is due both to the gravitational potential as modelled by the King profile

and to the perturbations caused by the nearby stars. [301] showed in Terzan 5 that the acceleration from the nearest neighbours is negligible if compared to the mean field acceleration. The same is considered to be valid also the others GCs. The acceleration for the King profile can be derived explicitly starting from eq. 1.26 describing the density profile in a single mass King profile. We first estimate the mass within a certain radius r from the centre [138]:

$$M(r) = \int_0^r \rho(r') 4\pi r'^2 dr' = 4\pi\rho_0 r_c^3 \left[\sinh^{-1}\left(\frac{r}{r_c}\right) - \frac{r}{r_c\sqrt{1+(r/r_c)^2}} \right]. \tag{A.8}$$

The acceleration can then easily be obtained by multiplying the mass by $-G/r^2$ and becomes

$$a(r) = -4\pi G\rho_0 r_c^{-1} \left(\frac{r}{r_c}\right)^{-3} \left[\sinh^{-1}\left(\frac{r}{r_c}\right) - \frac{r}{r_c\sqrt{1+(r/r_c)^2}} \right]. \tag{A.9}$$

This equation is valid only within a few core radii. Projecting this acceleration along the line of sight we obtain:

$$a_r(l,r) = -4\pi G\rho_c \left(\frac{r}{r_c}\right)^{-3} l \left[\sinh^{-1}\left(\frac{r}{r_c}\right) - \frac{r}{r_c\sqrt{1+(r/r_c)^2}} \right]., \tag{A.10}$$

where l is the line-of-sight component of the position of the pulsar relative to the centre of the cluster, in core radii.

For a given position in the plane of the sky, $R_\perp$, the acceleration has a maximum value determined numerically for each line of sight, at the centre ($R_\perp = 0$) this is given by [132]:

$$a_{\mathrm{l,max}}(R_\perp) = 1.5689 \frac{\sigma_{\mu,0}^2 d}{\theta_c}. \tag{A.11}$$

The proper motion central velocity dispersion, $\sigma_{\mu,0}$, is defined as in equation 1.27 and is related to the one-dimensional velocity dispersion defined in Section A.2, σ_{vel}, by the equation: $\sigma_{\mathrm{vel}} = \sigma_{\mu,0}\, d$.

The shape of the acceleration along the line of sight is shown in Figure A.1. For a given acceleration a_l there are two possible line-of-sight positions that are compatible. Therefore using only the measurement of the acceleration it is not possible to determine unequivocally the position of the pulsar.

If a central IMBH of mass M is present, it will influence the acceleration of nearby stars first directly as:

$$\mathbf{a}_M = GM\frac{\mathbf{r}}{r^3} \tag{A.12}$$

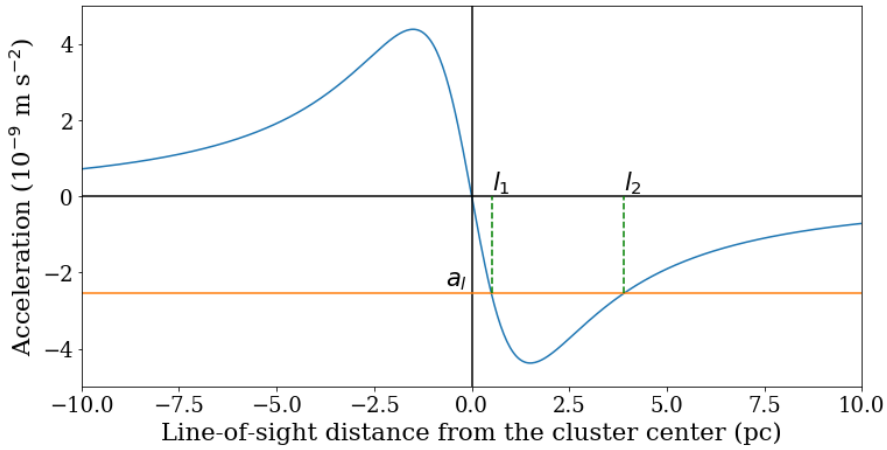

Figure A.1: Plot of the acceleration along the line of sight as a function of the line-of-sight distance from the cluster centre. This plot has been derived for pulsar 47 Tuc C. a_l is the measured acceleration for the pulsar in consideration. To generate this acceleration the pulsar could be located either at l_1 or in l_2.

where $\mathbf{r}$ is the distance from the IMBH and indirectly through the formation of the central over-density as:

$$\mathbf{a}_{\rm cusp} \begin{cases} -\frac{4\pi G}{1.45} r_{\rm i}^{1.55} \rho_i \frac{\mathbf{r}}{r^{1.55}} & r < r_{\rm i} \\ -\frac{4\pi G}{1.45} r_{\rm i}^{3} \rho_i \frac{\mathbf{r}}{r^{3}} & r > r_{\rm i} \end{cases} \tag{A.13}$$

A.4 JERKS

We can estimate the jerk generated by the mean gravitational field by taking the time derivative of the acceleration. Writing eq. A.9 in vectorial form in the following way:

$$\mathbf{a}(r) = -4\pi G \rho_{\rm c} r_{\rm c}^3 \left[\sinh^{-1}\left(\frac{r}{r_{\rm c}}\right) - \frac{r}{r_{\rm c}\sqrt{1+(r/r_{\rm c})^2}} \right] \frac{\mathbf{r}}{r^3} = -|a(r)|\frac{\mathbf{r}}{r}, \tag{A.14}$$

The jerk assumes the form:

$$\dot{\mathbf{a}}_K(r) = -\frac{d|a(r)|}{dt}\frac{\mathbf{r}}{r} - |a(r)|\frac{\mathbf{v}}{r} + |a(r)|\frac{(\mathbf{v}\cdot\mathbf{r})\,\mathbf{r}}{r^3}, \tag{A.15}$$

where $|a(r)|$ is the norm of the acceleration and the time derivative of the norm is

$$\frac{d|a(r)|}{dt} = -2\frac{v|a(r)|}{r} + 4\pi G v \rho_{\rm c} \left(\frac{1}{1+(r/r_{\rm c})^2}\right)^{\frac{3}{2}} \tag{A.16}$$

with v the norm of the velocity.

In the case of GCs , which are collisional stellar systems, jerks are also heavily influenced by neighbouring stars which can be as large as those from the mean field [301]. Specifically, [301] found that the jerk caused by the coarse-grain nature of stellar interactions is distributed with the following probability distribution:

$$P(\dot{\mathbf{a}}) = \frac{1}{\pi^2} \frac{\dot{a}_0}{(\dot{a}^2 + \dot{a}_0^2)^2}, \tag{A.17}$$

where $\dot{a}_0$ is the characteristic jerk given by

$$\dot{a}_0 = \frac{2\pi\xi}{3} G\langle m \rangle \sigma n, \tag{A.18}$$

where $\xi \simeq 3.04$ is a numerical constant, $\langle m \rangle$ is the average mass of the stars, σ is the velocity dispersion, and n is the number density of the stars. The distribution of jerks projected along the line of sight, $\dot{a}_l$ is a Lorentzian distribution

$$P(\dot{a}_l) = \frac{1}{\pi} \frac{\dot{a}_0}{\dot{a}_l^2 + \dot{a}_0^2}. \tag{A.19}$$

If a central IMBH is present in the cluster, the jerk of a pulsar is affected by the central point mass M

$$\dot{\mathbf{a}}_M = -GM \left(\frac{\mathbf{v}}{r^3} - 3 \frac{(\mathbf{v} \cdot \mathbf{r})\, \mathbf{r}}{r^5} \right), \tag{A.20}$$

where $\mathbf{r}$ the distance to the source M and $\mathbf{v}$ is the relative velocity. Additionally, the jerk produced by this over-density of the central cusp takes the form

$$\dot{\mathbf{a}}_{\rm cusp} = \begin{cases} -\frac{4\pi G}{1.45} r_{\rm i}^{1.55} \rho_{\rm i} \left(\frac{\mathbf{v}}{r^{1.55}} - 1.55 \frac{(\mathbf{v}\cdot\mathbf{r})r}{r^{3.55}} \right) & r < r_{\rm i} \\ -\frac{4\pi G}{1.45} r_{\rm i}^{3} \rho_{\rm i} \left(\frac{\mathbf{v}}{r^{3}} - 3 \frac{(\mathbf{v}\cdot r)r}{r^{5}} \right) & r > r_{\rm i} \end{cases} \tag{A.21}$$

where $r_{\rm i}$ is the IMBH influence radius.

The cusp and the increase of the stellar velocity caused by the presence of the IMBH affects also the rate of close encounters between stars. For this reason, even the jerk caused by the nearest neighbours is influenced, but a statistical description of this effect is not available yet. This effect is taken into account in the N-body simulations used in Abbate, Spera, and Colpi [6], because the integration algorithm self-consistently calculates all jerks, at each integration step.

A comparison between the mean field jerks derived using equations (A.15), (A.20) and (A.21) and the ones estimated numerically from the simulations described in section 5.3.1 is shown in Figure A.2.

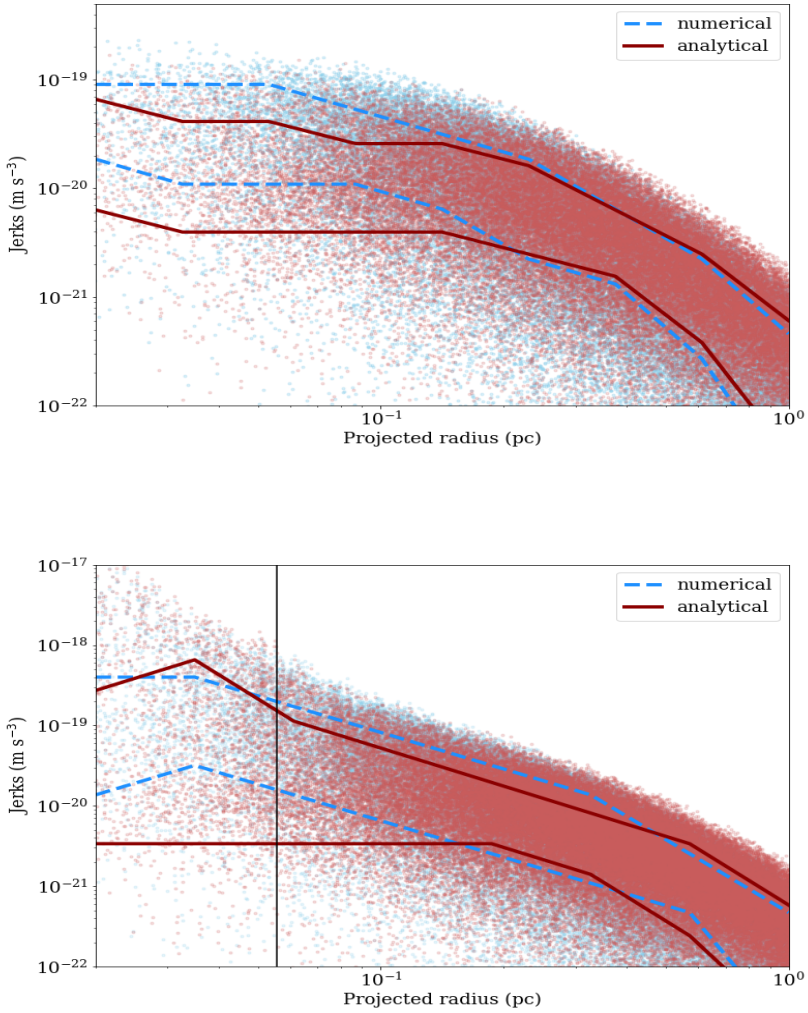

Figure A.2: Values of the mean field jerks measured in the case without (top panel) and with an IMBH of 1000 $M_\odot$ (bottom panel). Blue dots represent the mean field jerks measured numerically from the simulations while red dots are the results of the analytical formulae. The dashed blue and the solid red lines bracket the 1σ interval of the distributions. In the top panel the vertical line shows the influence radius of the IMBH .

The top panel of Figure A.2 shows the case of jerks in the simulation without an IMBH . Red dots refer to the stellar jerks calculated analytically using equation (A.15) while the blue dots show the mean field stellar jerks extracted numerically from the simulation by estimating the mass enclosed within the distance from the centre of each star and using equation (A.20). The jerks calculated analytically are of the same order of magnitude of the ones measured numerically but they appear to be smaller in the centre of the cluster. This discrepancy is caused by stars that are close the centre of the cluster in projection on the plane of the sky but are distant along the line of sight. The analytical equations for stars more distant than a few core radii systematically underestimate the value of the jerks when compared with the numerical value. The top panel of Figure A.2 shows the case of a simulation with a central IMBH of 1000 $M_\odot$. We use equation (A.20) and (A.21) to estimate analytically the jerks. In this case, the analytic estimate appears to be consistent with the numerical one. Inside the sphere of influence of the IMBH the analytical distribution extends to lower values of the jerks because of the same projection effect as in the case without an IMBH .

A.5 JOUNCES

In the case of GC described by a King profile, the jounce due to the mean field gravitational potential is given by

$$\ddot{\mathbf{a}}_K = -\frac{d^2|a(r)|}{dt^2}\frac{\mathbf{r}}{r} - 2\frac{d|a(r)|}{dt}\frac{\mathbf{v}}{r} + 2\frac{d|a(r)|}{dt}\frac{(v\cdot r)r}{r^3} + \\ +5|a(r)|\frac{(v\cdot r)v}{r^3} - 3|a(r)|\frac{(v\cdot r)^2\mathbf{r}}{r^5}, \tag{A.22}$$

where $|a(r)|$ is defined in equation (A.14), $d|a(r)|/dt$ is given by equation (A.16) and $d^2|a(r)|/dt^2$ is

$$\frac{d^2|a(r)|}{dt^2} = -\frac{d|a(r)|}{dt}\frac{|a(r)|}{v} - 4\frac{d|a(r)|}{dt}\frac{v}{r} - 2\frac{|a(r)|v^2}{r^2} - \\ -\frac{4\pi G v^2}{r}\rho_c\left[\frac{1}{(1+(r/r_c)^2)^{3/2}} - \frac{3}{(1+(r/r_c)^2)^{5/2}}\right]. \tag{A.23}$$

Also for the jounce, the contribution from neighbouring stars plays a very important role. [295] shows that this contribution can be much larger than the one from the mean field.

Similarly to the jerks, the presence of an IMBH influences jounces in two ways. It contributes directly as a central point mass

$$\ddot{\mathbf{a}}_M = GM\left(-2a\frac{\mathbf{r}}{r^4} - 6\frac{(\mathbf{v}\cdot r)v}{r^5} - 3\frac{v^2\mathbf{r}}{r^5} + 15\frac{(v\cdot r)^2\mathbf{r}}{r^7}\right), \tag{A.24}$$

and through the cusp over-density. At radial distances $r < r_{\rm i}$ the contribution reads

$$\ddot{\mathbf{a}}_{cusp} = -\frac{4\pi G}{1.45} r_{\rm i}^{1.55} \rho_{\rm i} \left(-0.45 \frac{a\mathbf{r}}{r^{2.55}} - 3.1 \frac{(v\cdot r)v}{r^{3.55}} - 1.55 \frac{v^2\mathbf{r}}{r^{3.55}} + \right. \\ \left. + 5.5 \frac{(v\cdot r)^2 r}{r^{5.55}} \right), \tag{A.25}$$

and for $r > r_{\rm i}$ as

$$\ddot{\mathbf{a}}_{cusp} = -\frac{4\pi G}{1.45} r_{\rm i}^{3} \rho_{\rm i} \left(-2 \frac{a\mathbf{r}}{r^{4}} - 6 \frac{(v\cdot r)v}{r^{5}} - 5 \frac{v^2\mathbf{r}}{r^{5}} + 15 \frac{(v\cdot r)^2 r}{r^{7}} \right). \tag{A.26}$$

Also the jounces caused by nearest neighbours are influenced by the presence of an IMBH but a statistical description of this effect is still missing. It is worth noting that we calculate self-consistently the values of jounces in our N-body simulations.

A comparison between the mean field jounces derived with the above equations (A.22), (A.24), (A.25) and (A.26) and the ones estimated numerically from simulations is shown in Figure A.3.

The top panel of Figure A.3 shows the jounces calculated in a simulation without an IMBH. Red dots show the mean field stellar jounces measured using equation (A.22) while blue dots show jounces computed numerically. The two distributions are compatible with one another showing that equation (A.22) is good analytical approximation of the mean field jounces. The same can be said for the equations describing the effects of the IMBH as is seen on the bottom panel again for a 1000 $M_\odot$ IMBH. In the analytical computation, the IMBH contribution is inferred from equation (A.24) and for the stellar cusp using equation (A.25) and (A.26). In both cases with and without the IMBH the clustering of stars with low jounces at small projected distances is caused by stars that are distant from the centre but appear close in the projection along the line of sight. For these stars the analytical formula is not valid and tends to underestimate the jounces.

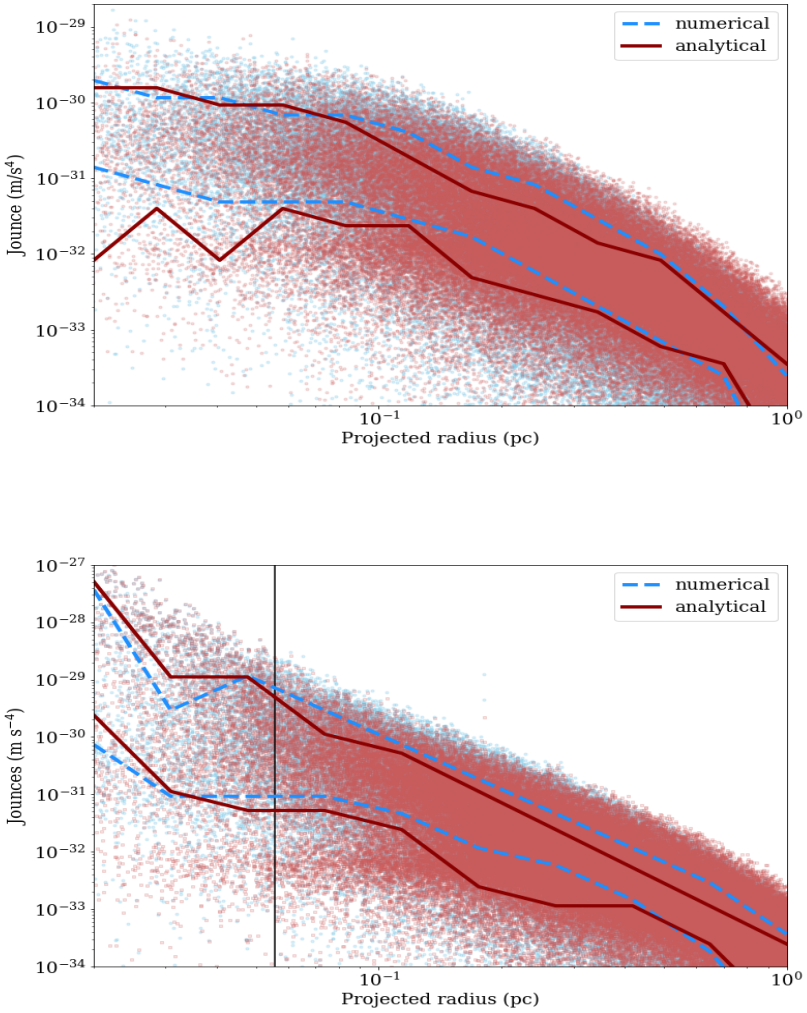

Figure A.3: Values of the mean field jounces measured in the case without (top panel) and with an IMBH of 1000 $M_\odot$(bottom panel). The blue dots represent the mean field jounces measured numerically from the simulations while the red dots are the results of the analytical formulae. The dashed blue and the solid red lines bracket the 1σ interval of the distributions. In the bottom panel the vertical line shows the influence radius of the IMBH.

BIBLIOGRAPHY

[1] S. J. Aarseth. "From NBODY1 to NBODY6: The Growth of an Industry." In: *Publications of the Astronomical Society of the Pacific* 111 (Nov. 1999), pp. 1333–1346. DOI: 10.1086/316455.

[2] S. J. Aarseth. *Gravitational N-Body Simulations*. Cambridge University Press, Oct. 2003, p. 430.

[3] K. N. Abazajian. "The consistency of Fermi-LAT observations of the galactic center with a millisecond pulsar population in the central stellar cluster." In: *Journal of Cosmology and Astroparticle Physics* 3, 010 (Mar. 2011), p. 010. DOI: 10.1088/1475-7516/2011/03/010. arXiv: 1011.4275 [astro-ph.HE].

[4] F. Abbate, A. Possenti, A. Ridolfi, P. C. C. Freire, F. Camilo, R. N. Manchester, and N. D'Amico. "Internal gas models and central black hole in 47 Tucanae using millisecond pulsars." In: *Monthly Notices of the Royal Astronomical Society* 481.1 (Nov. 2018), pp. 627–638. DOI: 10.1093/mnras/sty2298. arXiv: 1808.06621 [astro-ph.HE].

[5] F. Abbate, A. Mastrobuono-Battisti, M. Colpi, A. Possenti, A. C. Sippel, and M. Dotti. "Probing the formation history of the nuclear star cluster at the Galactic Centre with millisecond pulsars." In: *Monthly Notices of the Royal Astronomical Society* 473.1 (Jan. 2018), pp. 927–936. DOI: 10.1093/mnras/stx2364. arXiv: 1708.01627 [astro-ph.GA].

[6] Federico Abbate, Mario Spera, and Monica Colpi. "Intermediate mass black holes in globular clusters: effects on jerks and jounces of millisecond pulsars." In: *Monthly Notices of the Royal Astronomical Society* 487.1 (July 2019), pp. 769–781. DOI: 10.1093/mnras/stz1330. arXiv: 1905.05209 [astro-ph.HE].

[7] Abbott, B. P. et al. "GW170817: Observation of Gravitational Waves from a Binary Neutron Star Inspiral." In: *Physical Review Letters* 119.16, 161101 (Oct. 2017), p. 161101. DOI: 10.1103/PhysRevLett.119.161101. arXiv: 1710.05832 [gr-qc].

[8] B. P. et al. Abbott. "GWTC-1: A Gravitational-Wave Transient Catalog of Compact Binary Mergers Observed by LIGO and Virgo during the First and Second Observing Runs." In: ().

[9] Abdo, A. A. et al. "The Second Fermi Large Area Telescope Catalog of Gamma-Ray Pulsars." In: *The Astrophysical Journal Supplements* 208.2, 17 (Oct. 2013), p. 17. DOI: 10.1088/0067-0049/208/2/17. arXiv: 1305.4385 [astro-ph.HE].

[10] J. G. Abies, D. McConnell, C. E. Jacka, P. M. McCulloch, P. J. Hall, and P. A. Hamilton. "A millisecond pulsar in a 32-minute binary orbit." In: *Nature* 342.6246 (Nov. 1989), pp. 158–161. DOI: 10.1038/342158a0.

[11] D. Aharon and H. B. Perets. "Formation and Evolution of Nuclear Star Clusters with In Situ Star Formation: Nuclear Cores and Age Segregation." In: *The Astrophysical Journal* 799, 185 (Feb. 2015), p. 185. DOI: 10.1088/0004-637X/799/2/185. arXiv: 1409.5121.

[12] C. Ajello, G. Bonelli, and G. Sironi. "Evaluation of Earth's atmospheric brightness temperature at decimetric wavelengths." In: *The Astrophysical Journal Supplements* 96 (Feb. 1995), pp. 643–650. DOI: 10.1086/192132.

[13] T. Alexander. "Stellar processes near the massive black hole in the Galactic center [review article]." In: *Physics Reports* 419 (Nov. 2005), pp. 65–142. DOI: 10.1016/j.physrep.2005.08.002. eprint: astro-ph/0508106.

[14] M. A. Alpar, A. F. Cheng, M. A. Ruderman, and J. Shaham. "A new class of radio pulsars." In: *Nature* 300.5894 (Dec. 1982), pp. 728–730. DOI: 10.1038/300728a0.

[15] P. Amaro-Seoane and L. Santamaría. "Detection of IMBHs with Ground-based Gravitational Wave Observatories: A Biography of a Binary of Black Holes, from Birth to Death." In: *The Astrophysical Journal* 722 (Oct. 2010), pp. 1197–1206. DOI: 10.1088/0004-637X/722/2/1197. arXiv: 0910.0254.

[16] P. Amaro-Seoane et al. "Laser Interferometer Space Antenna." In: *ArXiv e-prints* (Feb. 2017). arXiv: 1702.00786 [astro-ph.IM].

[17] John Antoniadis, Paulo C. C. Freire, Norbert Wex, Thomas M. Tauris, Ryan S. Lynch, Marten H. van Kerkwijk, Michael Kramer, Cees Bassa, Vik S. Dhillon, and Thomas Driebe. "A Massive Pulsar in a Compact Relativistic Binary." In: *Science* 340.6131 (Apr. 2013), p. 448. DOI: 10.1126/science.1233232. arXiv: 1304.6875 [astro-ph.HE].

[18] F. Antonini, E. Barausse, and J. Silk. "The Coevolution of Nuclear Star Clusters, Massive Black Holes, and Their Host Galaxies." In: *The Astrophysical Journal* 812, 72 (Oct. 2015), p. 72. DOI: 10.1088/0004-637X/812/1/72. arXiv: 1506.02050.

[19] F. Antonini, R. Capuzzo-Dolcetta, A. Mastrobuono-Battisti, and D. Merritt. "Dissipationless Formation and Evolution of the Milky Way Nuclear Star Cluster." In: *The Astrophysical Journal* 750, 111 (May 2012), p. 111. DOI: 10.1088/0004-637X/750/2/111. arXiv: 1110.5937.

[20] M. Arca-Sedda. "On the formation of compact, massive subsystems in stellar clusters and its relation with intermediate-mass black holes." In: *Monthly Notices of the Royal Astronomical Society* 455.1 (Jan. 2016), pp. 35–50. DOI: 10.1093/mnras/stv2265. arXiv: 1502.01242 [astro-ph.GA].

[21] M. Arca-Sedda and R. Capuzzo-Dolcetta. "The globular cluster migratory origin of nuclear star clusters." In: *Monthly Notices of the Royal Astronomical Society* 444 (Nov. 2014), pp. 3738–3755. DOI: 10.1093/mnras/stu1683. arXiv: 1405.7593.

[22] M. Arca-Sedda and R. Capuzzo-Dolcetta. "Lack of nuclear clusters in dwarf spheroidal galaxies: implications for massive black holes formation and the cusp/core problem." In: *Monthly Notices of the Royal Astronomical Society* 464 (Jan. 2017), pp. 3060–3070. DOI: 10.1093/mnras/stw2483. arXiv: 1611.01088.

[23] M. Arca-Sedda and R. Capuzzo-Dolcetta. "The MEGaN project - I. Missing formation of massive nuclear clusters and tidal disruption events by star clusters-massive black hole interactions." In: *Monthly Notices of the Royal Astronomical Society* 471 (Oct. 2017), pp. 478–490. DOI: 10.1093/mnras/stx1586. arXiv: 1706.06541.

[24] M. Arca-Sedda, R. Capuzzo-Dolcetta, F. Antonini, and A. Seth. "Henize 2-10: The Ongoing Formation of a Nuclear Star Cluster around a Massive Black Hole." In: *The Astrophysical Journal* 806, 220 (June 2015), p. 220. DOI: 10.1088/0004-637X/806/2/220. arXiv: 1501.04567.

[25] Manuel Arca Sedda, Abbas Askar, and Mirek Giersz. "MOCCA-Survey Database - I. Unravelling black hole subsystems in globular clusters." In: *Monthly Notices of the Royal Astronomical Society* 479.4 (Oct. 2018), pp. 4652–4664. DOI: 10.1093/mnras/sty1859. arXiv: 1801.00795 [astro-ph.GA].

[26] Manuel Arca Sedda, Abbas Askar, and Mirek Giersz. "MOCCA-SURVEY Database I. Intermediate mass black holes in Milky Way globular clusters and their connection to supermassive black holes." In: *arXiv e-prints*, arXiv:1905.00902 (May 2019), arXiv:1905.00902. arXiv: 1905.00902 [astro-ph.GA].

[27] Manuel Arca-Sedda, Bence Kocsis, and Timothy D. Brandt. "Gamma-ray and X-ray emission from the Galactic centre: hints on the nuclear star cluster formation history." In: *Monthly Notices of the Royal Astronomical Society* 479.1 (Sept. 2018), pp. 900–916. DOI: 10.1093/mnras/sty1454. arXiv: 1709.03119 [astro-ph.GA].

[28] Anne M. Archibald et al. "A Radio Pulsar/X-ray Binary Link." In: *Science* 324.5933 (June 2009), p. 1411. DOI: 10.1126/science.1172740. arXiv: 0905.3397 [astro-ph.HE].

[29] Anne M. Archibald, Nina V. Gusinskaia, Jason W. T. Hessels, Adam T. Deller, David L. Kaplan, Duncan R. Lorimer, Ryan S. Lynch, Scott M. Ransom, and Ingrid H. Stairs. "Universality of free fall from the orbital motion of a pulsar in a stellar triple system." In: *Nature* 559.7712 (July 2018), pp. 73–76. DOI: 10.1038/s41586-018-0265-1. arXiv: 1807.02059 [astro-ph.HE].

[30] R. F. Archibald, E. V. Gotthelf, R. D. Ferdman, V. M. Kaspi, S. Guillot, F. A. Harrison, E. F. Keane, M. J. Pivovaroff, D. Stern, and S. P. Tendulkar. "A High Braking Index for a Pulsar." In: *The Astrophysical Journal* 819.1, L16 (Mar. 2016), p. L16. DOI: 10.3847/2041-8205/819/1/L16. arXiv: 1603.00305 [astro-ph.HE].

[31] J. W. Armstrong, B. J. Rickett, and S. R. Spangler. "Electron Density Power Spectrum in the Local Interstellar Medium." In: *The Astrophysical Journal* 443 (Apr. 1995), p. 209. DOI: 10.1086/175515.

[32] K. M. B. Asad et al. "Primary beam effects of radio astronomy antennas - II. Modelling the MeerKAT L-band beam." In: *arXiv e-prints*, arXiv:1904.07155 (Apr. 2019), arXiv:1904.07155. arXiv: 1904.07155 [astro-ph.IM].

[33] W. Baade and F. Zwicky. "Cosmic Rays from Super-novae." In: *Proceedings of the National Academy of Science* 20.5 (May 1934), pp. 259–263. DOI: 10.1073/pnas.20.5.259.

[34] W. Baade and F. Zwicky. "On Super-novae." In: *Proceedings of the National Academy of Science* 20.5 (May 1934), pp. 254–259. DOI: 10.1073/pnas.20.5.254.

[35] D. C. Backer, J. M. Rankin, and D. B. Campbell. "Orthogonal mode emission in geometric models of pulsar polarisation." In: *Nature* 263 (Sept. 1976), pp. 202–207. DOI: 10.1038/263202a0.

[36] M. Bagchi, D. R. Lorimer, and J. Chennamangalam. "Luminosities of recycled radio pulsars in globular clusters." In: *Monthly Notices of the Royal Astronomical Society* 418 (Nov. 2011), pp. 477–489. DOI: 10.1111/j.1365-2966.2011.19498.x. arXiv: 1107.4521 [astro-ph.SR].

[37] J. N. Bahcall and J. P. Ostriker. "Massive black holes in globular clusters." In: *Nature* 256 (July 1975), p. 23. DOI: 10.1038/256023a0.

[38] J. N. Bahcall and R. A. Wolf. "Star distribution around a massive black hole in a globular cluster." In: *The Astrophysical Journal* 209 (Oct. 1976), pp. 214–232. DOI: 10.1086/154711.

[39] Arash Bahramian, Craig O. Heinke, Gregory R. Sivakoff, and Jeanette C. Gladstone. "Stellar Encounter Rate in Galactic Globular Clusters." In: *The Astrophysical Journal* 766.2, 136 (Apr. 2013), p. 136. DOI: 10.1088/0004-637X/766/2/136. arXiv: 1302.2549 [astro-ph.HE].

[40] M. Bailes et al. "MeerTime - the MeerKAT Key Science Program on Pulsar Timing." In: *Proceedings of MeerKAT Science: On the Pathway to the SKA. 25-27 May*. Jan. 2016, p. 11.

[41] Pauline Barmby, Martha L. Boyer, Charles E. Woodward, Robert D. Gehrz, Jacco Th. van Loon, Giovanni G. Fazio, Massimo Marengo, and Elisha Polomski. "A Spitzer Search for Cold Dust Within Globular Clusters." In: *Astronomical Journal* 137.1 (Jan. 2009), pp. 207–217. DOI: 10.1088/0004-6256/137/1/207. arXiv: 0810.1902 [astro-ph].

[42] H. Bartko et al. "Evidence for Warped Disks of Young Stars in the Galactic Center." In: *The Astrophysical Journal* 697 (June 2009), pp. 1741–1763. DOI: 10.1088/0004-637X/697/2/1741. arXiv: 0811.3903.

[43] S. D. Bates et al. "A 6.5-GHz multibeam pulsar survey." In: *Monthly Notices of the Royal Astronomical Society* 411 (Mar. 2011), pp. 1575–1584. DOI: 10.1111/j.1365-2966.2010.17790.x. arXiv: 1009.5873 [astro-ph.SR].

[44] H. Baumgardt. "N -body modelling of globular clusters: masses, mass-to-light ratios and intermediate-mass black holes." In: *Monthly Notices of the Royal Astronomical Society* 464.2 (Jan. 2017), pp. 2174–2202. DOI: 10.1093/mnras/stw2488. arXiv: 1609.08794 [astro-ph.GA].

[45] H. Baumgardt and M. Hilker. "A catalogue of masses, structural parameters, and velocity dispersion profiles of 112 Milky Way globular clusters." In: *Monthly Notices of the Royal Astronomical Society* 478.2 (Aug. 2018), pp. 1520–1557. DOI: 10.1093/mnras/sty1057. arXiv: 1804.08359 [astro-ph.GA].

[46] H. Baumgardt, M. Hilker, A. Sollima, and A. Bellini. "Mean proper motions, space orbits, and velocity dispersion profiles of Galactic globular clusters derived from Gaia DR2 data." In: *Monthly Notices of the Royal Astronomical Society* 482.4 (Feb. 2019), pp. 5138–5155. DOI: 10.1093/mnras/sty2997. arXiv: 1811.01507 [astro-ph.GA].

[47] Holger Baumgardt, Junichiro Makino, and Toshikazu Ebisuzaki. "Massive Black Holes in Star Clusters. I. Equal-Mass Clusters." In: *The Astrophysical Journal* 613.2 (Oct. 2004), pp. 1133–1142. DOI: 10.1086/423298. arXiv: astro-ph/0406227 [astro-ph].

[48] Holger Baumgardt, Junichiro Makino, and Toshikazu Ebisuzaki. "Massive Black Holes in Star Clusters. II. Realistic Cluster Models." In: *The Astrophysical Journal* 613.2 (Oct. 2004), pp. 1143–1156. DOI: 10.1086/423299. arXiv: astro-ph/0406231 [astro-ph].

[49] A. Bellini, P. Bianchini, A. L. Varri, J. Anderson, G. Piotto, R. P. van der Marel, E. Vesperini, and L. L. Watkins. "Hubble Space Telescope Proper Motion (HSTPROMO) Catalogs of Galactic Globular Clusters. V. The Rapid Rotation of 47 Tuc Traced and Modeled in Three Dimensions." In: *The Astrophysical Journal* 844.2, 167 (Aug. 2017), p. 167. DOI: 10.3847/1538-4357/aa7c5f. arXiv: 1706.08974 [astro-ph.GA].

[50] D. Bhattacharya and G. Srinivasan. "The magnetic fields of neutron stars and their evolution." In: *X-ray Binaries*. Jan. 1995, pp. 495–522.

[51] Souradeep Bhattacharya, Craig O. Heinke, Andrey I. Chugunov, Paulo C. C. Freire, Alessand ro Ridolfi, and Slavko Bogdanov. "Chandra studies of the globular cluster 47 Tucanae: A deeper X-ray source catalogue, five new X-ray counterparts to millisecond radio pulsars, and new constraints to r-mode instability window." In: *Monthly Notices of the Royal Astronomical Society* 472.3 (Dec. 2017), pp. 3706–3721. DOI: 10.1093/mnras/stx2241. arXiv: 1709.01807 [astro-ph.HE].

[52] P. Bianchini, A. L. Varri, G. Bertin, and A. Zocchi. "Rotating Globular Clusters." In: *The Astrophysical Journal* 772.1, 67 (July 2013), p. 67. DOI: 10.1088/0004-637X/772/1/67. arXiv: 1305.6025 [astro-ph.GA].

[53] P. Bianchini, G. van de Ven, M. A. Norris, E. Schinnerer, and A. L. Varri. "A novel look at energy equipartition in globular clusters." In: *Monthly Notices of the Royal Astronomical Society* 458.4 (June 2016), pp. 3644–3654. DOI: 10.1093/mnras/stw552. arXiv: 1603.00878 [astro-ph.GA].

[54] James Binney and Scott Tremaine. *Galactic Dynamics: Second Edition*. Princeton Series in Astrophysics, 2008.

[55] R. Blandford and S. A. Teukolsky. "Arrival-time analysis for a pulsar in a binary system." In: *The Astrophysical Journal* 205 (Apr. 1976), pp. 580–591. DOI: 10.1086/154315.

[56] Roger D. Blandford, Roger W. Romani, and James H. Applegate. "Timing a millisecond pulsar in a globular cluster." In: *Monthly Notices of the Royal Astronomical Society* 225 (Apr. 1987), 51P–53. DOI: 10.1093/mnras/225.1.51P.

[57] A. Boehle et al. "An Improved Distance and Mass Estimate for Sgr A* from a Multistar Orbit Analysis." In: *The Astrophysical Journal* 830, 17 (Oct. 2016), p. 17. DOI: 10.3847/0004-637X/830/1/17. arXiv: 1607.05726.

[58] Slavko Bogdanov, Jonathan E. Grindlay, and Maureen van den Berg. "An X-Ray Variable Millisecond Pulsar in the Globular Cluster 47 Tucanae: Closing the Link to Low-Mass X-Ray Binaries." In: *The Astrophysical Journal* 630.2 (Sept. 2005), pp. 1029–1036. DOI: 10.1086/432249. arXiv: astro-ph/0506031 [astro-ph].

[59] Slavko Bogdanov, George B. Rybicki, and Jonathan E. Grindlay. "Constraints on Neutron Star Properties from X-Ray Observations of Millisecond Pulsars." In: *The Astrophysical Journal* 670.1 (Nov. 2007), pp. 668–676. DOI: 10.1086/520793. arXiv: astro-ph/0612791 [astro-ph].

[60] Slavko Bogdanov, Jonathan E. Grindlay, Craig O. Heinke, Fernando Camilo, Paulo C. C. Freire, and Werner Becker. "Chandra X-Ray Observations of 19 Millisecond Pulsars in the Globular Cluster 47 Tucanae." In: *The Astrophysical Journal* 646.2 (Aug. 2006), pp. 1104–1115. DOI: 10.1086/505133. arXiv: astro-ph/0604318 [astro-ph].

[61] Slavko Bogdanov, Craig O. Heinke, Feryal Özel, and Tolga Güver. "Neutron Star Mass-Radius Constraints of the Quiescent Low-mass X-Ray Binaries X7 and X5 in the Globular Cluster 47 Tuc." In: *The Astrophysical Journal* 831.2, 184 (Nov. 2016), p. 184. DOI: 10.3847/0004-637X/831/2/184. arXiv: 1603.01630 [astro-ph.HE].

[62] T. Böker, S. Laine, R. P. van der Marel, M. Sarzi, H.-W. Rix, L. C. Ho, and J. C. Shields. "A Hubble Space Telescope Census of Nuclear Star Clusters in Late-Type Spiral Galaxies. I. Observations and Image Analysis." In: *The Astronomical Journal* 123 (Mar. 2002), pp. 1389–1410. DOI: 10.1086/339025. eprint: astro-ph/0112086.

[63] T. Böker, M. Sarzi, D. E. McLaughlin, R. P. van der Marel, H.-W. Rix, L. C. Ho, and J. C. Shields. "A Hubble Space Telescope Census of Nuclear Star Clusters in Late-Type Spiral Galaxies. II. Cluster Sizes and Structural Parameter Correlations." In: *The Astronomical Journal* 127 (Jan. 2004), pp. 105–118. DOI: 10.1086/380231. eprint: astro-ph/0309761.

[64] H. Bondi. "On spherically symmetrical accretion." In: *Monthly Notices of the Royal Astronomical Society* 112 (1952), p. 195. DOI: 10.1093/mnras/112.2.195.

[65] H. Bondi and F. Hoyle. "On the mechanism of accretion by stars." In: *Monthly Notices of the Royal Astronomical Society* 104 (1944), p. 273. DOI: 10.1093/mnras/104.5.273.

[66] R. S. Booth and J. L. Jonas. "An Overview of the MeerKAT Project." In: *African Skies* 16 (Mar. 2012), p. 101.

[67] G. C. Bower, A. Deller, P. Demorest, A. Brunthaler, R. Eatough, H. Falcke, M. Kramer, K. J. Lee, and L. Spitler. "The Angular Broadening of the Galactic Center Pulsar SGR J1745-29: A New Constraint on the Scattering Medium." In: *The Astrophysical Journal Letters* 780, L2 (Jan. 2014), p. L2. DOI: 10.1088/2041-8205/780/1/L2. arXiv: 1309.4672.

[68] Martha L. Boyer, Charles E. Woodward, Jacco Th. van Loon, Karl D. Gordon, A. Evans, Robert D. Gehrz, L. Andrew Helton, and Elisha F. Polomski. "Stellar Populations and Mass Loss in M15: A Spitzer Space Telescope Detection of Dust in the Intracluster Medium." In: *Astronomical Journal* 132.4 (Oct. 2006), pp. 1415–1425. DOI: 10.1086/506518. arXiv: astro-ph/0606236 [astro-ph].

[69] T. D. Brandt and B. Kocsis. "Disrupted Globular Clusters Can Explain the Galactic Center Gamma-Ray Excess." In: *The Astrophysical Journal* 812, 15 (Oct. 2015), p. 15. DOI: 10.1088/0004-637X/812/1/15. arXiv: 1507.05616 [astro-ph.HE].

[70] R. Braun, T. Bourke, J. A. Green, E. Keane, and J. Wagg. "Advancing Astrophysics with the Square Kilometre Array." In: *Advancing Astrophysics with the Square Kilometre Array (AASKA14)*, 174 (Apr. 2015), p. 174.

[71] Philip G. Breen and Douglas C. Heggie. "Dynamical evolution of black hole subsystems in idealized star clusters." In: *Monthly Notices of the Royal Astronomical Society* 432.4 (July 2013), pp. 2779–2797. DOI: 10.1093/mnras/stt628. arXiv: 1304.3401 [astro-ph.GA].

[72] Philip G. Breen and Douglas C. Heggie. "On black hole subsystems in idealized nuclear star clusters." In: *Monthly Notices of the Royal Astronomical Society* 436.1 (Nov. 2013), pp. 584–589. DOI: 10.1093/mnras/stt1599. arXiv: 1308.4641 [astro-ph.GA].

[73] M. A. Brentjens and A. G. de Bruyn. "Faraday rotation measure synthesis." In: *Astronomy and Astrophysics* 441.3 (Oct. 2005), pp. 1217–1228. DOI: 10.1051/0004-6361:20052990. arXiv: astro-ph/0507349 [astro-ph].

[74] J. C. Brown. "The Magnetic Field of the Milky Way Galaxy." In: *The Dynamic Interstellar Medium: A Celebration of the Canadian Galactic Plane Survey*. Ed. by R. Kothes, T. L. Landecker, and A. G. Willis. Vol. 438. Astronomical Society of the Pacific Conference Series. Dec. 2010, p. 216. arXiv: 1012.2932 [astro-ph.GA].

[75] M. Cadelano, C. Pallanca, F. R. Ferraro, M. Salaris, E. Dalessandro, B. Lanzoni, and P. C. C. Freire. "Optical Identification of He White Dwarfs Orbiting Four Millisecond Pulsars in the Globular Cluster 47 Tucanae." In: *The Astrophysical Journal* 812.1, 63 (Oct. 2015), p. 63. DOI: 10.1088/0004-637X/812/1/63. arXiv: 1509.01397 [astro-ph.SR].

[76] F. Calore, I. Cholis, and C. Weniger. "Background model systematics for the Fermi GeV excess." In: *Journal of Cosmology and Astroparticle Physics* 3, 038 (Mar. 2015), p. 038. DOI: 10.1088/1475-7516/2015/03/038. arXiv: 1409.0042.

[77] F. Calore, M. Di Mauro, F. Donato, J. W. T. Hessels, and C. Weniger. "Radio Detection Prospects for a Bulge Population of Millisecond Pulsars as Suggested by Fermi-LAT Observations of the Inner Galaxy." In: *The Astrophysical Journal* 827, 143 (Aug. 2016), p. 143. DOI: 10.3847/0004-637X/827/2/143. arXiv: 1512.06825 [astro-ph.HE].

[78] A. D. Cameron et al. "The High Time Resolution Universe Pulsar Survey - XIII. PSR J1757-1854, the most accelerated binary pulsar." In: *Monthly Notices of the Royal Astronomical Society* 475.1 (Mar. 2018), pp. L57–L61. DOI: 10.1093/mnrasl/sly003. arXiv: 1711.07697 [astro-ph.HE].

[79] F. Camilo and F. A. Rasio. "Pulsars in Globular Clusters." In: *Binary Radio Pulsars*. Ed. by Fred A. Rasio and Ingrid H. Stairs. Vol. 328. Astronomical Society of the Pacific Conference Series. July 2005, p. 147. arXiv: astro-ph/0501226 [astro-ph].

[80] F. Camilo, D. R. Lorimer, P. Freire, A. G. Lyne, and R. N. Manchester. "Observations of 20 Millisecond Pulsars in 47 Tucanae at 20 Centimeters." In: *The Astrophysical Journal* 535.2 (June 2000), pp. 975–990. DOI: 10.1086/308859. arXiv: astro-ph/9911234 [astro-ph].

[81] F. Camilo et al. "Revival of the Magnetar PSR J1622-4950: Observations with MeerKAT, Parkes, XMM-Newton, Swift, Chandra, and NuSTAR." In: *The Astrophysical Journal* 856.2, 180 (Apr. 2018), p. 180. DOI: 10.3847/1538-4357/aab35a. arXiv: 1804.01933 [astro-ph.HE].

[82] R. Capuzzo-Dolcetta. "The Evolution of the Globular Cluster System in a Triaxial Galaxy: Can a Galactic Nucleus Form by Globular Cluster Capture?" In: *The Astrophysical Journal* 415 (Oct. 1993), p. 616. DOI: 10.1086/173189. eprint: astro-ph/9301006.

[83] R. Capuzzo-Dolcetta and M. Spera. "A performance comparison of different graphics processing units running direct N-body simulations." In: *Computer Physics Communications* 184 (Nov. 2013), pp. 2528–2539. DOI: 10.1016/j.cpc.2013.07.005. arXiv: 1304.1966 [astro-ph.IM].

[84] R. Capuzzo-Dolcetta, M. Spera, and D. Punzo. "A fully parallel, high precision, N-body code running on hybrid computing platforms." In: *Journal of Computational Physics* 236 (Mar. 2013), pp. 580–593. DOI: 10.1016/j.jcp.2012.11.013. arXiv: 1207.2367 [astro-ph.IM].

[85] C. M. Carollo, M. Stiavelli, and J. Mack. "Spiral Galaxies with WFPC2. II. The Nuclear Properties of 40 Objects." In: *The Astronomical Journal* 116 (July 1998), pp. 68–84. DOI: 10.1086/300407. eprint: astro-ph/9804007.

[86] Ettore Carretti, Roland M. Crocker, Lister Staveley-Smith, Marijke Haverkorn, Cormac Purcell, B. M. Gaensler, Gianni Bernardi, Michael J. Kesteven, and Sergio Poppi. "Giant magnetized outflows from the centre of the Milky Way." In: *Nature* 493.7430 (Jan. 2013), pp. 66–69. DOI: 10.1038/nature11734. arXiv: 1301.0512 [astro-ph.GA].

[87] Benoît Cerutti and Andrei M. Beloborodov. "Electrodynamics of Pulsar Magnetospheres." In: *Space Science Reviews* 207.1-4 (July 2017), pp. 111–136. DOI: 10.1007/s11214-016-0315-7. arXiv: 1611.04331 [astro-ph.HE].

[88] D. J. Champion et al. "Measuring the Mass of Solar System Planets Using Pulsar Timing." In: *The Astrophysical Journal Letters* 720 (Sept. 2010), pp. L201–L205. DOI: 10.1088/2041-8205/720/2/L201. arXiv: 1008.3607 [astro-ph.EP].

[89] S. Chandrasekhar. "The Maximum Mass of Ideal White Dwarfs." In: *The Astrophysical Journal* 74 (July 1931), p. 81. DOI: 10.1086/143324.

[90] S. Chatzopoulos, T. K. Fritz, O. Gerhard, S. Gillessen, C. Wegg, R. Genzel, and O. Pfuhl. "The old nuclear star cluster in the Milky Way: dynamics, mass, statistical parallax, and black hole mass." In: *Monthly Notices of the Royal Astronomical Society* 447 (Feb. 2015), pp. 948–968. DOI: 10.1093/mnras/stu2452. arXiv: 1403.5266.

[91] C. Chiuderi and M. Velli. *Basics of Plasma Astrophysics*. Springer-Verlag, 2015.

[92] G. W. Clark. "X-ray binaries in globular clusters." In: *The Astrophysical Journal Letters* 199 (Aug. 1975), pp. L143–L145. DOI: 10.1086/181869.

[93] G. D. Coleman and S. P. Worden. "Large-scale winds driven by flare-star mass loss." In: *The Astrophysical Journal* 218 (Dec. 1977), pp. 792–800. DOI: 10.1086/155736.

[94] Monica Colpi and Bernadetta Devecchi. "Dynamical Formation and Evolution of Neutron Star and Black Hole Binaries in Globular Clusters." In: *Physics of Relativistic Objects in Compact Binaries: From Birth to Coalescence*. Ed. by Monica Colpi, Piergiorgio Casella, Vittorio Gorini, Ugo Moschella, and Andrea Possenti. Vol. 359. Astrophysics and Space Science Library. Jan. 2009, p. 199. DOI: 10.1007/978-1-4020-9264-0_5.

[95] Charlie Conroy and David N. Spergel. "On the Formation of Multiple Stellar Populations in Globular Clusters." In: *The Astrophysical Journal* 726.1, 36 (Jan. 2011), p. 36. DOI: 10.1088/0004-637X/726/1/36. arXiv: 1005.4934 [astro-ph.GA].

[96] J. M. Cordes and T. J. W. Lazio. "NE2001.I. A New Model for the Galactic Distribution of Free Electrons and its Fluctuations." In: *arXiv e-prints*, astro-ph/0207156 (July 2002), astro–ph/0207156. arXiv: astro-ph/0207156 [astro-ph].

[97] J. M. Cordes, J. Rankin, and D. C. Backer. "Orthogonal modes of polarization from pulsar PSR 2020+28." In: *The Astrophysical Journal* 223 (Aug. 1978), pp. 961–972. DOI: 10.1086/156328.

[98] P. Côté et al. "The ACS Virgo Cluster Survey. VIII. The Nuclei of Early-Type Galaxies." In: *The Astrophysical Journal Supplements* 165 (July 2006), pp. 57–94. DOI: 10.1086/504042. eprint: astro-ph/0603252.

[99] H. T. Cromartie et al. "Relativistic Shapiro delay measurements of an extremely massive millisecond pulsar." In: *Nature Astronomy* (Sept. 2019), p. 439. DOI: 10.1038/s41550-019-0880-2. arXiv: 1904.06759 [astro-ph.HE].

[100] N. D'Amico, A. G. Lyne, R. N. Manchester, A. Possenti, and F. Camilo. "Discovery of Short-Period Binary Millisecond Pulsars in Four Globular Clusters." In: *The Astrophysical Journal* 548 (Feb. 2001), pp. L171–L174. DOI: 10.1086/319096. arXiv: astro-ph/0010272 [astro-ph].

[101] T. Damour and G. Schafer. "Higher-order relativistic periastron advances and binary pulsars." In: *Nuovo Cimento B Serie* 101B.2 (Jan. 1988), pp. 127–176. DOI: 10.1007/BF02828697.

[102] Thibault Damour and J. H. Taylor. "Strong-field tests of relativistic gravity and binary pulsars." In: *Physical Review D* 45.6 (Mar. 1992), pp. 1840–1868. DOI: 10.1103/PhysRevD.45.1840.

[103] T. Daylan, D. P. Finkbeiner, D. Hooper, T. Linden, S. K. N. Portillo, N. L. Rodd, and T. R. Slatyer. "The characterization of the gamma-ray signal from the central Milky Way: A case for annihilating dark matter." In: *Physics of the Dark Universe* 12 (June 2016), pp. 1–23. DOI: 10.1016/j.dark.2015.12.005. arXiv: 1402.6703 [astro-ph.HE].

[104] P. B. Demorest et al. "Limits on the Stochastic Gravitational Wave Background from the North American Nanohertz Observatory for Gravitational Waves." In: *The Astrophysical Journal* 762.2, 94 (Jan. 2013), p. 94. DOI: 10.1088/0004-637X/762/2/94. arXiv: 1201.6641 [astro-ph.CO].

[105] J. S. Deneva, J. M. Cordes, and T. J. W. Lazio. "Discovery of Three Pulsars from a Galactic Center Pulsar Population." In: *The Astrophysical Journal Letters* 702 (Sept. 2009), pp. L177–L181. DOI: 10.1088/0004-637X/702/2/L177. arXiv: 0908.1331 [astro-ph.SR].

[106] J. Dexter and R. M. O'Leary. "The Peculiar Pulsar Population of the Central Parsec." In: *The Astrophysical Journal Letters* 783, L7 (Mar. 2014), p. L7. DOI: 10.1088/2041-8205/783/1/L7. arXiv: 1310.7022 [astro-ph.GA].

[107] J. Dexter, N. Degenaar, M. Kerr, A. Deller, J. Deneva, P. Lazarus, M. Kramer, D. Champion, and R. Karuppusamy. "A transient, flat spectrum radio pulsar near the Galactic Centre." In: *Monthly Notices of the Royal Astronomical Society* 468 (June 2017), pp. 1486–1492. DOI: 10.1093/mnras/stx583. arXiv: 1703.02544 [astro-ph.HE].

[108] A. K. Dupree, Graeme H. Smith, and Jay Strader. "Fast Winds and Mass Loss from Metal-Poor Field Giants." In: *Astronomical Journal* 138.5 (Nov. 2009), pp. 1485–1501. DOI: 10.1088/0004-6256/138/5/1485. arXiv: 0909.1558 [astro-ph.SR].

[109] R. P. Eatough et al. "A strong magnetic field around the supermassive black hole at the centre of the Galaxy." In: *Nature* 501 (Sept. 2013), pp. 391–394. DOI: 10.1038/nature12499. arXiv: 1308.3147 [astro-ph.GA].

[110] Peter D. Edmonds, Ronald L. Gilliland, Craig O. Heinke, Jonathan E. Grindlay, and Fernando Camilo. "Optical Detection of a Variable Millisecond Pulsar Companion in 47 Tucanae." In: *The Astrophysical Journal Letters* 557.1 (Aug. 2001), pp. L57–L60. DOI: 10.1086/323122. arXiv: astro-ph/0107096 [astro-ph].

[111] Peter D. Edmonds, Ronald L. Gilliland, Fernando Camilo, Craig O. Heinke, and Jonathan E. Grindlay. "A Millisecond Pulsar Optical Counterpart with Large-Amplitude Variability in the Globular Cluster 47 Tucanae." In: *The Astrophysical Journal* 579.2 (Nov. 2002), pp. 741–751. DOI: 10.1086/342985. arXiv: astro-ph/0207426 [astro-ph].

[112] R. T. Edwards, G. B. Hobbs, and R. N. Manchester. "TEMPO2, a new pulsar timing package - II. The timing model and precision estimates." In: *Monthly Notices of the Royal Astronomical Society* 372.4 (Nov. 2006), pp. 1549–1574. DOI: 10.1111/j.1365-2966.2006.10870.x. arXiv: astro-ph/0607664 [astro-ph].

[113] Daniel J. Eisenstein and A. Loeb. "Origin of Quasar Progenitors from the Collapse of Low-Spin Cosmological Perturbations." In: *The Astrophysical Journal* 443 (Apr. 1995), p. 11. DOI: 10.1086/175498. arXiv: astro-ph/9401016 [astro-ph].

[114] A. Evans, M. Stickel, J. Th. van Loon, S. P. S. Eyres, M. E. L. Hopwood, and A. J. Penny. "Far infra-red emission from NGC 7078: First detection of intra-cluster dust in a globular cluster." In: *Astronomy and Astrophysics* 408 (Sept. 2003), pp. L9–L12. DOI: 10.1051/0004-6361:20031139.

[115] J. E. Everett and J. M. Weisberg. "Emission Beam Geometry of Selected Pulsars Derived from Average Pulse Polarization Data." In: *The Astrophysical Journal* 553.1 (May 2001), pp. 341–357. DOI: 10.1086/320652. arXiv: astro-ph/0009266 [astro-ph].

[116] John E. Everett, Ellen G. Zweibel, Robert A. Benjamin, Dan McCammon, Lindsay Rocks, and III Gallagher John S. "The Milky Way's Kiloparsec-Scale Wind: A Hybrid Cosmic-Ray and Thermally Driven Outflow." In: *The Astrophysical Journal* 674.1 (Feb. 2008), pp. 258–270. DOI: 10.1086/524766. arXiv: 0710.3712 [astro-ph].

[117] C.-A. Faucher-Giguère and V. M. Kaspi. "Birth and Evolution of Isolated Radio Pulsars." In: *The Astrophysical Journal* 643 (May 2006), pp. 332–355. DOI: 10.1086/501516. eprint: astro-ph/0512585.

[118] C.-A. Faucher-Giguère and A. Loeb. "The pulsar contribution to the gamma-ray background." In: *Journal of Cosmology and Astroparticle Physics* 1, 005 (Jan. 2010), p. 005. DOI: 10.1088/1475-7516/2010/01/005. arXiv: 0904.3102 [astro-ph.HE].

[119] C.-A. Faucher-Giguère and A. Loeb. "Pulsar-black hole binaries in the Galactic Centre." In: *Monthly Notices of the Royal Astronomical Society* 415 (Aug. 2011), pp. 3951–3961. DOI: 10.1111/j.1365-2966.2011.19019.x. arXiv: 1012.0573 [astro-ph.HE].

[120] A. Feldmeier, N. Lützgendorf, N. Neumayer, M. Kissler-Patig, K. Gebhardt, H. Baumgardt, E. Noyola, P. T. de Zeeuw, and B. Jalali. "Indication for an intermediate-mass black hole in the globular cluster NGC 5286 from kinematics." In: *Astronomy and Astrophysics* 554, A63 (June 2013), A63. DOI: 10.1051/0004-6361/201321168. arXiv: 1304.4176 [astro-ph.GA].

[121] A. Feldmeier, N. Neumayer, A. Seth, R. Schödel, N. Lützgendorf, P. T. de Zeeuw, M. Kissler-Patig, S. Nishiyama, and C. J. Walcher. "Large scale kinematics and dynamical modelling of the Milky Way nuclear star cluster." In: *Astronomy and Astrophysics* 570, A2 (Oct. 2014), A2. DOI: 10.1051/0004-6361/201423777. arXiv: 1406.2849.

[122] G. J. Ferland et al. "The 2017 Release Cloudy." In: *Revista Mexicana de Astronomia y Astrofisica* 53 (Oct. 2017), pp. 385–438. arXiv: 1705.10877.

[123] Laura Ferrarese and David Merritt. "A Fundamental Relation between Supermassive Black Holes and Their Host Galaxies." In: *The Astrophysical Journal Letters* 539.1 (Aug. 2000), pp. L9–L12. DOI: 10.1086/312838. arXiv: astro-ph/0006053 [astro-ph].

[124] Francesco R. Ferraro, Barbara Lanzoni, Emanuele Dalessand ro, Alessio Mucciarelli, and Loredana Lovisi. "Blue Straggler Stars in Globular Clusters: A Powerful Tool to Probe the Internal Dynamical Evolution of Stellar Systems." In: *Ecology of Blue Straggler Stars*. Vol. 413. Jan. 2015, p. 99. DOI: 10.1007/978-3-662-44434-4_5. arXiv: 1406.3471 [astro-ph.SR].

[125] Katia Ferrière and Philippe Terral. "Analytical models of X-shape magnetic fields in galactic halos." In: *Astronomy and Astrophysics* 561, A100 (Jan. 2014), A100. DOI: 10.1051/0004-6361/201322966. arXiv: 1312.1974 [astro-ph.GA].

[126] Emmanuel Fonseca, Paul Demorest, Scott Ransom, and Ingrid Stairs. "Fundamental Physics with Radio Millisecond Pulsars." In: *Bulletin of the American Astronomical Society* 51.3, 425 (May 2019), p. 425. arXiv: 1903.08194 [astro-ph.HE].

[127] D. Foreman-Mackey, D. W. Hogg, D. Lang, and J. Goodman. "emcee: The MCMC Hammer." In: *Publications of the Astronomical Society of the Pacific* 125 (Mar. 2013), p. 306. DOI: 10.1086/670067. arXiv: 1202.3665 [astro-ph.IM].

[128] R. S. Foster, L. Fairhead, and D. C. Backer. "A Spectral Study of Four Millisecond Pulsars." In: *The Astrophysical Journal* 378 (Sept. 1991), p. 687. DOI: 10.1086/170469.

[129] Giacomo Fragione, Václav Pavlík, and Sambaran Banerjee. "Neutron stars and millisecond pulsars in star clusters: implications for the diffuse gamma-radiation from the Galactic Centre." In: *Monthly Notices of the Royal Astronomical Society* 480.4 (Nov. 2018), pp. 4955–4962. DOI: 10.1093/mnras/sty2234. arXiv: 1804.04856 [astro-ph.GA].

[130] Juhan Frank and Galen Gisler. "The fate of gas in globular clusters." In: *Monthly Notices of the Royal Astronomical Society* 176 (Sept. 1976), pp. 533–538. DOI: 10.1093/mnras/176.3.533.

[131] P. C. C. Freire. "The pulsar population in Globular Clusters and in the Galaxy." In: *Neutron Stars and Pulsars: Challenges and Opportunities after 80 years*. Ed. by J. van Leeuwen. Vol. 291. IAU Symposium. Mar. 2013, pp. 243–250. DOI: 10.1017/S1743921312023770. arXiv: 1210.3984.

[132] P. C. C. Freire et al. "Long-term observations of the pulsars in 47 Tucanae - II. Proper motions, accelerations and jerks." In: *Monthly Notices of the Royal Astronomical Society* 471.1 (Oct. 2017), pp. 857–876. DOI: 10.1093/mnras/stx1533. arXiv: 1706.04908 [astro-ph.HE].

[133] P. C. Freire, M. Kramer, A. G. Lyne, F. Camilo, R. N. Manchester, and N. D'Amico. "Detection of Ionized Gas in the Globular Cluster 47 Tucanae." In: *The Astrophysical Journal Letters* 557.2 (Aug. 2001), pp. L105–L108. DOI: 10.1086/323248. arXiv: astro-ph/0107206 [astro-ph].

[134] P. C. Freire, F. Camilo, D. R. Lorimer, A. G. Lyne, R. N. Manchester, and N. D'Amico. "Timing the millisecond pulsars in 47 Tucanae." In: *Monthly Notices of the Royal Astronomical Society* 326.3 (Sept. 2001), pp. 901–915. DOI: 10.1046/j.1365-8711.2001.04493.x. arXiv: astro-ph/0103372 [astro-ph].

[135] P. C. Freire, F. Camilo, M. Kramer, D. R. Lorimer, A. G. Lyne, R. N. Manchester, and N. D'Amico. "Further results from the timing of the millisecond pulsars in 47 Tucanae." In: *Monthly Notices of the Royal Astronomical Society* 340.4 (Apr. 2003), pp. 1359–1374. DOI: 10.1046/j.1365-8711.2003.06392.x.

[136] Paulo C. C. Freire and Alessandro Ridolfi. "An algorithm for determining the rotation count of pulsars." In: *Monthly Notices of the Royal Astronomical Society* 476.4 (June 2018), pp. 4794–4805. DOI: 10.1093/mnras/sty524. arXiv: 1802.07211 [astro-ph.IM].

[137] Paulo C. C. Freire and Thomas M. Tauris. "Direct formation of millisecond pulsars from rotationally delayed accretion-induced collapse of massive white dwarfs." In: *Monthly Notices of the Royal Astronomical Society* 438.1 (Feb. 2014), pp. L86–L90. DOI: 10.1093/mnrasl/slt164. arXiv: 1311.3478 [astro-ph.SR].

[138] Paulo C. C. Freire, Jason W. T. Hessels, David J. Nice, Scott M. Ransom, Duncan R. Lorimer, and Ingrid H. Stairs. "The Millisecond Pulsars in NGC 6760." In: *The Astrophysical Journal* 621.2 (Mar. 2005), pp. 959–965. DOI: 10.1086/427748. arXiv: astro-ph/0411160 [astro-ph].

[139] Paulo C. C. Freire, Alex Wolszczan, Maureen van den Berg, and Jason W. T. Hessels. "A Massive Neutron Star in the Globular Cluster M5." In: *The Astrophysical Journal* 679.2 (June 2008), pp. 1433–1442. DOI: 10.1086/587832. arXiv: 0712.3826 [astro-ph].

[140] Paulo C. C. Freire, Scott M. Ransom, Steve Bégin, Ingrid H. Stairs, Jason W. T. Hessels, Lucille H. Frey, and Fernando Camilo. "Eight New Millisecond Pulsars in NGC 6440 and NGC 6441." In: *The Astrophysical Journal* 675.1 (Mar. 2008), pp. 670–682. DOI: 10.1086/526338. arXiv: 0711.0925 [astro-ph].

[141] Paulo C. C. Freire, Norbert Wex, Gilles Esposito-Farèse, Joris P. W. Verbiest, Matthew Bailes, Bryan A. Jacoby, Michael Kramer, Ingrid H. Stairs, John Antoniadis, and Gemma H. Janssen. "The relativistic pulsar-white dwarf binary PSR J1738+0333 - II. The most stringent test of scalar-tensor gravity." In: *Monthly Notices of the Royal Astronomical Society* 423.4 (July 2012), pp. 3328–3343. DOI: 10.1111/j.1365-2966.2012.21253.x. arXiv: 1205.1450 [astro-ph.GA].

[142] M. Freitag, P. Amaro-Seoane, and V. Kalogera. "Stellar Remnants in Galactic Nuclei: Mass Segregation." In: *The Astrophysical Journal* 649 (Sept. 2006), pp. 91–117. DOI: 10.1086/506193. eprint: astro-ph/0603280.

[143] B. M. Gaensler, R. Beck, and L. Feretti. "The origin and evolution of cosmic magnetism." In: *New Astronomy Reviews* 48.11-12 (Dec. 2004), pp. 1003–1012. DOI: 10.1016/j.newar.2004.09.003. arXiv: astro-ph/0409100 [astro-ph].

[144] D. Gaggero, D. Grasso, A. Marinelli, M. Taoso, and A. Urbano. "Diffuse cosmic rays shining in the Galactic center: A novel interpretation of H.E.S.S. and Fermi-LAT gamma-ray data." In: *ArXiv e-prints* (Feb. 2017). arXiv: 1702.01124 [astro-ph.HE].

[145] Gaia Collaboration, A. Helmi, F. van Leeuwen, P. J. McMillan, D. Massari, T. Antoja, A. Robin, L. Lindegren, U. Bastian, and 4. coauthors. "Gaia Data Release 2: Kinematics of globular clusters and dwarf galaxies around the Milky Way." In: *ArXiv e-prints* (Apr. 2018). arXiv: 1804.09381.

[146] Jonathan R. Gair, Ilya Mandel, M. Coleman Miller, and Marta Volonteri. "Exploring intermediate and massive black-hole binaries with the Einstein Telescope." In: *General Relativity and Gravitation* 43 (Feb. 2011), pp. 485–518. DOI: 10.1007/s10714-010-1104-3. arXiv: 0907.5450 [astro-ph.CO].

[147] Karl Gebhardt, R. M. Rich, and Luis C. Ho. "An Intermediate-Mass Black Hole in the Globular Cluster G1: Improved Significance from New Keck and Hubble Space Telescope Observations." In: *The Astrophysical Journal* 634.2 (Dec. 2005), pp. 1093–1102. DOI: 10.1086/497023. arXiv: astro-ph/0508251 [astro-ph].

[148] Karl Gebhardt et al. "A Relationship between Nuclear Black Hole Mass and Galaxy Velocity Dispersion." In: *The Astrophysical Journal Letters* 539.1 (Aug. 2000), pp. L13–L16. DOI: 10.1086/312840. arXiv: astro-ph/0006289 [astro-ph].

[149] R. Genzel, F. Eisenhauer, and S. Gillessen. "The Galactic Center massive black hole and nuclear star cluster." In: *Reviews of Modern Physics* 82 (Oct. 2010), pp. 3121–3195. DOI: 10.1103/RevModPhys.82.3121. arXiv: 1006.0064.

[150] I. Y. Georgiev and T. Böker. "Nuclear star clusters in 228 spiral galaxies in the HST/WFPC2 archive: catalogue and comparison to other stellar systems." In: *Monthly Notices of the Royal Astronomical Society* 441 (July 2014), pp. 3570–3590. DOI: 10.1093/mnras/stu797. arXiv: 1404.5956.

[151] I. Y. Georgiev, T. Böker, N. Leigh, N. Lützgendorf, and N. Neumayer. "Masses and scaling relations for nuclear star clusters, and their coexistence with central black holes." In: *Monthly Notices of the Royal Astronomical Society* 457 (Apr. 2016), pp. 2122–2138. DOI: 10.1093/mnras/stw093. arXiv: 1601.02613.

[152] Joris Gerssen, Roeland P. van der Marel, Karl Gebhardt, Puragra Guhathakurta, Ruth C. Peterson, and Carlton Pryor. "Hubble Space Telescope Evidence for an Intermediate-Mass Black Hole in the Globular Cluster M15. II. Kinematic Analysis and Dynamical Modeling." In: *Astronomical Journal* 124.6 (Dec. 2002), pp. 3270–3288. DOI: 10.1086/344584. arXiv: astro-ph/0209315 [astro-ph].

[153] A. M. Ghez, S. Salim, S. D. Hornstein, A. Tanner, J. R. Lu, M. Morris, E. E. Becklin, and G. Duchêne. "Stellar Orbits around the Galactic Center Black Hole." In: *The Astrophysical Journal* 620 (Feb. 2005), pp. 744–757. DOI: 10.1086/427175. eprint: astro-ph/0306130.

[154] Mirek Giersz, Nathan Leigh, Arkadiusz Hypki, Nora Lützgendorf, and Abbas Askar. "MOCCA code for star cluster simulations - IV. A new scenario for intermediate mass black hole formation in globular clusters." In: *Monthly Notices of the Royal Astronomical Society* 454 (Dec. 2015), pp. 3150–3165. DOI: 10.1093/mnras/stv2162. arXiv: 1506.05234 [astro-ph.GA].

[155] S. Gillessen, F. Eisenhauer, S. Trippe, T. Alexander, R. Genzel, F. Martins, and T. Ott. "Monitoring Stellar Orbits Around the Massive Black Hole in the Galactic Center." In: *The Astrophysical Journal* 692 (Feb. 2009), pp. 1075–1109. DOI: 10.1088/0004-637X/692/2/1075. arXiv: 0810.4674.

[156] O. Y. Gnedin, J. P. Ostriker, and S. Tremaine. "Co-evolution of Galactic Nuclei and Globular Cluster Systems." In: *The Astrophysical Journal* 785, 71 (Apr. 2014), p. 71. DOI: 10.1088/0004-637X/785/1/71. arXiv: 1308.0021.

[157] C. Gordon and O. Macías. "Dark matter and pulsar model constraints from Galactic Center Fermi-LAT gamma-ray observations." In: *Physical Review D* 88.8, 083521 (Oct. 2013), p. 083521. DOI: 10.1103/PhysRevD.88.083521. arXiv: 1306.5725 [astro-ph.HE].

[158] D. M. Gould and A. G. Lyne. "Multifrequency polarimetry of 300 radio pulsars." In: *Monthly Notices of the Royal Astronomical Society* 301.1 (Nov. 1998), pp. 235–260. DOI: 10.1046/j.1365-8711.1998.02018.x.

[159] Raffaele G. Gratton, Flavio Fusi Pecci, Eugenio Carretta, Gisella Clementini, Carlo E. Corsi, and Mario Lattanzi. "Ages of Globular Clusters from HIPPARCOS Parallaxes of Local Subdwarfs." In: *The Astrophysical Journal* 491.2 (Dec. 1997), pp. 749–771. DOI: 10.1086/304987. arXiv: astro-ph/9704150 [astro-ph].

[160] Gravity Collaboration, R. Abuter, A. Amorim, M. Bauböck, J. P. Berger, H. Bonnet, W. Brand ner, Y. Clénet, V. Coudé Du Foresto, and P. T. de Zeeuw. "A geometric distance measurement to the Galactic center black hole with 0.3% uncertainty." In: *Astronomy and Astrophysics* 625, L10 (May 2019), p. L10. DOI: 10.1051/0004-6361/201935656.

[161] J. E. Grindlay, F. Camilo, C. O. Heinke, P. D. Edmonds, H. Cohn, and P. Lugger. "Chandra Study of a Complete Sample of Millisecond Pulsars in 47 Tucanae and NGC 6397." In: *The Astrophysical Journal* 581.1 (Dec. 2002), pp. 470–484. DOI: 10.1086/344150. arXiv: astro-ph/0208280 [astro-ph].

[162] Jonathan E. Grindlay, Craig Heinke, Peter D. Edmonds, and Stephen S. Murray. "High-Resolution X-ray Imaging of a Globular Cluster Core: Compact Binaries in 47Tuc." In: *Science* 292.5525 (June 2001), pp. 2290–2295. DOI: 10.1126/science.1061135. arXiv: astro-ph/0105528 [astro-ph].

[163] M. Atakan Gürkan, Marc Freitag, and Frederic A. Rasio. "Formation of Massive Black Holes in Dense Star Clusters. I. Mass Segregation and Core Collapse." In: *The Astrophysical Journal* 604 (Apr. 2004), pp. 632–652. DOI: 10.1086/381968. arXiv: astro-ph/0308449 [astro-ph].

[164] D. Haggard, C. Heinke, D. Hooper, and T. Linden. "Low mass X-ray binaries in the Inner Galaxy: implications for millisecond pulsars and the GeV excess." In: *Journal of Cosmology and Astroparticle Physics* 5, 056 (May 2017), p. 056. DOI: 10.1088/1475-7516/2017/05/056. arXiv: 1701.02726 [astro-ph.HE].

[165] J. L. Han, R. N. Manchester, A. G. Lyne, G. J. Qiao, and W. van Straten. "Pulsar Rotation Measures and the Large-Scale Structure of the Galactic Magnetic Field." In: *The Astrophysical Journal* 642.2 (May 2006), pp. 868–881. DOI: 10.1086/501444. arXiv: astro-ph/0601357 [astro-ph].

[166] Jinlin Han. "Magnetic fields in our Galaxy: How much do we know? (II) Halo fields and the global field structure." In: *Astrophysical Polarized Backgrounds*. Ed. by Stefano Cecchini, Stefano Cortiglioni, Robert Sault, and Carla Sbarra. Vol. 609. American Institute of Physics Conference Series. Mar. 2002, pp. 96–101. DOI: 10.1063/1.1471830.

[167] T. H. Hankins and B. J. Rickett. "Pulsar signal processing." In: *Methods in Computational Physics. Volume 14 - Radio astronomy*. Vol. 14. Academic Press, Jan. 1975, pp. 55–129.

[168] William E. Harris. "A Catalog of Parameters for Globular Clusters in the Milky Way." In: *The Astronomical Journal* 112 (Oct. 1996), p. 1487. DOI: 10.1086/118116.

[169] M. Haverkorn and V. Heesen. "Magnetic Fields in Galactic Haloes." In: *Space Science Reviews* 166.1-4 (May 2012), pp. 133–144. DOI: 10.1007/s11214-011-9757-0. arXiv: 1102.3701 [astro-ph.GA].

[170] M. Haverkorn, J. C. Brown, B. M. Gaensler, and N. M. McClure-Griffiths. "The Outer Scale of Turbulence in the Magnetoionized Galactic Interstellar Medium." In: *The Astrophysical Journal* 680.1 (June 2008), pp. 362–370. DOI: 10.1086/587165. arXiv: 0802.2740 [astro-ph].

[171] Carl Heiles, Phil Perillat, Michael Nolan, Duncan Lorimer, Ramesh Bhat, Tapasi Ghosh, Murray Lewis, Karen O'Neil, Chris Salter, and Snezana Stanimirovic. "Mueller Matrix Parameters for Radio Telescopes and Their Observational Determination." In: *Publications of the Astronomical Society of the Pacific* 113.788 (Oct. 2001), pp. 1274–1288. DOI: 10.1086/323289. arXiv: astro-ph/0107352 [astro-ph].

[172] C. O. Heinke, J. E. Grindlay, P. D. Edmonds, H. N. Cohn, P. M. Lugger, F. Camilo, S. Bogdanov, and P. C. Freire. "A Deep Chandra Survey of the Globular Cluster 47 Tucanae: Catalog of Point Sources." In: *The Astrophysical Journal* 625.2 (June 2005), pp. 796–824. DOI: 10.1086/429899. arXiv: astro-ph/0503132 [astro-ph].

[173] J. Hessels, A. Possenti, M. Bailes, C. Bassa, P. C. C. Freire, D. R. Lorimer, R. Lynch, S. M. Ransom, and I. H. Stairs. "Pulsars in Globular Clusters with the SKA." In: *Advancing Astrophysics with the Square Kilometre Array (AASKA14)*. Apr. 2015, p. 47. arXiv: 1501.00086 [astro-ph.HE].

[174] Jason W. T. Hessels, Scott M. Ransom, Ingrid H. Stairs, Paulo C. C. Freire, Victoria M. Kaspi, and Fernando Camilo. "A Radio Pulsar Spinning at 716 Hz." In: *Science* 311.5769 (Mar. 2006), pp. 1901–1904. DOI: 10.1126/science.1123430. arXiv: astro-ph/0601337 [astro-ph].

[175] A. Hewish, S. J. Bell, J. D. H. Pilkington, P. F. Scott, and R. A. Collins. "Observation of a Rapidly Pulsating Radio Source." In: *Nature* 217.5130 (Feb. 1968), pp. 709–713. DOI: 10.1038/217709a0.

[176] C. M. Ho, S. Slobin, and K. Gritton. *Atmospheric Noise Temperature Induced by Clouds and Other Weather Phenomena at SHF Band (1-45 GHz)*. Tech. rep. Jet Propulsion Laboratory, California Institute of Technology, 2005.

[177] C. M. Ho, Wang C., K. Angkasa, and K. Gritton. *Estimation of Microwave Power Margin Losses Due to Earth's Atmosphere and Weather in the Frequency Range of 3-30 GHz*. Tech. rep. Jet Propulsion Laboratory, California Institute of Technology, 2004.

[178] Luis C. Ho, Yuichi Terashima, and Takashi Okajima. "A Stringent Limit on the Accretion Luminosity of the Possible Central Black Hole in the Globular Cluster M15." In: *The Astrophysical Journal Letters* 587.1 (Apr. 2003), pp. L35–L38. DOI: 10.1086/375042. arXiv: astro-ph/0303061 [astro-ph].

[179] G. Hobbs, D. R. Lorimer, A. G. Lyne, and M. Kramer. "A statistical study of 233 pulsar proper motions." In: *Monthly Notices of the Royal Astronomical Society* 360.3 (July 2005), pp. 974–992. DOI: 10.1111/j.1365-2966.2005.09087.x. arXiv: astro-ph/0504584 [astro-ph].

[180] G. Hobbs et al. "Development of a pulsar-based time-scale." In: *Monthly Notices of the Royal Astronomical Society* 427.4 (Dec. 2012), pp. 2780–2787. DOI: 10.1111/j.1365-2966.2012.21946.x. arXiv: 1208.3560 [astro-ph.IM].

[181] D. Hooper and L. Goodenough. "Dark matter annihilation in the Galactic Center as seen by the Fermi Gamma Ray Space Telescope." In: *Physics Letters B* 697 (Mar. 2011), pp. 412–428. DOI: 10.1016/j.physletb.2011.02.029. arXiv: 1010.2752 [hep-ph].

[182] D. Hooper and T. Linden. "The gamma-ray pulsar population of globular clusters: implications for the GeV excess." In: *Journal of Cosmology and Astroparticle Physics* 8, 018 (Aug. 2016), p. 018. DOI: 10.1088/1475-7516/2016/08/018. arXiv: 1606.09250 [astro-ph.HE].

[183] D. Hooper and G. Mohlabeng. "The gamma-ray luminosity function of millisecond pulsars and implications for the GeV excess." In: *Journal of Cosmology and Astroparticle Physics* 3, 049 (Mar. 2016), p. 049. DOI: 10.1088/1475-7516/2016/03/049. arXiv: 1512.04966 [astro-ph.HE].

[184] A. W. Hotan, W. van Straten, and R. N. Manchester. "PSRCHIVE and PSRFITS: An Open Approach to Radio Pulsar Data Storage and Analysis." In: *Publications of the Astronomical Society of Australia* 21.3 (Jan. 2004), pp. 302–309. DOI: 10.1071/AS04022. arXiv: astro-ph/0404549 [astro-ph].

[185] F. Hoyle and R. A. Lyttleton. "On the accretion theory of stellar evolution." In: *Monthly Notices of the Royal Astronomical Society* 101 (1941), p. 227. DOI: 10.1093/mnras/101.4.227.

[186] J. R. Hurley, O. R. Pols, and C. A. Tout. "Comprehensive analytic formulae for stellar evolution as a function of mass and metallicity." In: *Monthly Notices of the Royal Astronomical Society* 315 (July 2000), pp. 543–569. DOI: 10.1046/j.1365-8711.2000.03426.x. eprint: astro-ph/0001295.

[187] Jarrod R. Hurley, Christopher A. Tout, Dayal T. Wickramasinghe, Lilia Ferrario, and Paul D. Kiel. "Formation of binary millisecond pulsars by accretion-induced collapse of white dwarfs." In: *Monthly Notices of the Royal Astronomical Society* 402.3 (Mar. 2010), pp. 1437–1448. DOI: 10.1111/j.1365-2966.2009.15988.x.

[188] R. Ibata et al. "Density and Kinematic Cusps in M54 at the Heart of the Sagittarius Dwarf Galaxy: Evidence for A 10^4 M $_{sun}$ Black Hole?" In: *The Astrophysical Journal Letters* 699.2 (July 2009), pp. L169–L173. DOI: 10.1088/0004-637X/699/2/L169. arXiv: 0906.4894 [astro-ph.GA].

[189] N. Ivanova, C. O. Heinke, F. A. Rasio, K. Belczynski, and J. M. Fregeau. "Formation and evolution of compact binaries in globular clusters - II. Binaries with neutron stars." In: *Monthly Notices of the Royal Astronomical Society* 386.1 (May 2008), pp. 553–576. DOI: 10.1111/j.1365-2966.2008.13064.x. arXiv: 0706.4096 [astro-ph].

[190] J. D. Jackson. *Classical Electrodynamics*. Wiley, 1962.

[191] Ronnie Jansson and Glennys R. Farrar. "A New Model of the Galactic Magnetic Field." In: *The Astrophysical Journal* 757.1, 14 (Sept. 2012), p. 14. DOI: 10.1088/0004-637X/757/1/14. arXiv: 1204.3662 [astro-ph.GA].

[192] Jarrett L. Johnson and Francesco Haardt. "The Early Growth of the First Black Holes." In: *Publications of the Astronomical Society of Australia* 33, e007 (Mar. 2016), e007. DOI: 10.1017/pasa.2016.4. arXiv: 1601.05473 [astro-ph.GA].

[193] S. Johnston, L. Nicastro, and B. Koribalski. "Scintillation parameters for 49 pulsars." In: *Monthly Notices of the Royal Astronomical Society* 297 (June 1998), pp. 108–116. DOI: 10.1046/j.1365-8711.1998.01461.x.

[194] S. Johnston, M. Kramer, D. R. Lorimer, A. G. Lyne, M. McLaughlin, B. Klein, and R. N. Manchester. "Discovery of two pulsars towards the Galactic Centre." In: *Monthly Notices of the Royal Astronomical Society* 373 (Nov. 2006), pp. L6–L10. DOI: 10.1111/j.1745-3933.2006.00232.x. eprint: astro-ph/0606465.

[195] J. Jonas and MeerKAT Team. "The MeerKAT Radio Telescope." In: *Proceedings of MeerKAT Science: On the Pathway to the SKA. 25-27 May*. Jan. 2016, p. 1.

[196] S. Kamann et al. "MUSE crowded field 3D spectroscopy of over 12 000 stars in the globular cluster NGC 6397. II. Probing the internal dynamics and the presence of a central black hole." In: *Astronomy and Astrophysics* 588, A149 (Apr. 2016), A149. DOI: 10.1051/0004-6361/201527065. arXiv: 1602.01643 [astro-ph.SR].

[197] S. Kamann et al. "A stellar census in globular clusters with MUSE: The contribution of rotation to cluster dynamics studied with 200 000 stars." In: *Monthly Notices of the Royal Astronomical Society* 473 (Feb. 2018), pp. 5591–5616. DOI: 10.1093/mnras/stx2719. arXiv: 1710.07257 [astro-ph.GA].

[198] A. Karastergiou and S. Johnston. "Absolute polarization position angle profiles of southern pulsars at 1.4 and 3.1 GHz." In: *Monthly Notices of the Royal Astronomical Society* 365.2 (Jan. 2006), pp. 353–366. DOI: 10.1111/j.1365-2966.2005.09692.x. arXiv: astro-ph/0509910 [astro-ph].

[199] A. Karastergiou, S. Johnston, and R. N. Manchester. "Polarization profiles of southern pulsars at 3.1 GHz." In: *Monthly Notices of the Royal Astronomical Society* 359.2 (May 2005), pp. 481–492. DOI: 10.1111/j.1365-2966.2005.08909.x. arXiv: astro-ph/0502337 [astro-ph].

[200] J. I. Katz. "Two kinds of stellar collapse." In: *Nature* 253 (Feb. 1975), p. 698. DOI: 10.1038/253698a0.

[201] M. J. Keith et al. "Measurement and correction of variations in interstellar dispersion in high-precision pulsar timing." In: *Monthly Notices of the Royal Astronomical Society* 429.3 (Mar. 2013), pp. 2161–2174. DOI: 10.1093/mnras/sts486. arXiv: 1211.5887 [astro-ph.GA].

[202] J. Kijak, M. Dembska, W. Lewandowski, G. Melikidze, and M. Sendyk. "Spectrum evolution in binary pulsar B1259-63/LS 2883 Be star and gigahertz-peaked spectra." In: *Monthly Notices of the Royal Astronomical Society* 418.1 (Nov. 2011), pp. L114–L118. DOI: 10.1111/j.1745-3933.2011.01155.x. arXiv: 1109.1013 [astro-ph.GA].

[203] B. Kimmig, A. Seth, I. I. Ivans, J. Strader, N. Caldwell, T. Anderton, and D. Gregersen. "Measuring Consistent Masses for 25 Milky Way Globular Clusters." In: *The Astronomical Journal* 149, 53 (Feb. 2015), p. 53. DOI: 10.1088/0004-6256/149/2/53. arXiv: 1411.1763.

[204] Ivan R. King. "The structure of star clusters. III. Some simple dynamical models." In: *Astronomical Journal* 71 (Feb. 1966), p. 64. DOI: 10.1086/109857.

[205] Ivan King. "The structure of star clusters. I. an empirical density law." In: *The Astronomical Journal* 67 (Oct. 1962), p. 471. DOI: 10.1086/108756.

[206] Bülent Kızıltan, Holger Baumgardt, and Abraham Loeb. "An intermediate-mass black hole in the centre of the globular cluster 47 Tucanae." In: *Nature* 542 (Feb. 2017), pp. 203–205. DOI: 10.1038/nature21361. arXiv: 1702.02149 [astro-ph.GA].

[207] Bülent Kızıltan, Holger Baumgardt, and Abraham Loeb. "Corrigendum: An intermediate-mass black hole in the centre of the globular cluster 47 Tucanae." In: *Nature* 545 (May 2017), p. 510. DOI: 10.1038/nature22320.

[208] H. Knight. "Long-term timing of pulsars in globular clusters." PhD thesis. Swinburne University of Technology, Australia, 2007.

[209] John Kormendy and Luis C. Ho. "Coevolution (Or Not) of Supermassive Black Holes and Host Galaxies." In: *Annual Review of Astronomy and Astrophysics* 51.1 (Aug. 2013), pp. 511–653. DOI: 10.1146/annurev-astro-082708-101811. arXiv: 1304.7762 [astro-ph.CO].

[210] M. Kramer, R. Wielebinski, A. Jessner, J. A. Gil, and J. H. Seiradakis. "Geometrical analysis of average pulsar profiles using multi-component Gaussian FITS at several frequencies. I. Method and analysis." In: *Astronomy and Astrophysics Supplements* 107 (Nov. 1994), pp. 515–526.

[211] M. Kramer, K. M. Xilouris, D. R. Lorimer, O. Doroshenko, A. Jessner, R. Wielebinski, A. Wolszczan, and F. Camilo. "The Characteristics of Millisecond Pulsar Emission. I. Spectra, Pulse Shapes, and the Beaming Fraction." In: *The Astrophysical Journal* 501 (July 1998), pp. 270–285. DOI: 10.1086/305790. eprint: astro-ph/9801177.

[212] M. Kramer, A. G. Lyne, G. Hobbs, O. Löhmer, P. Carr, C. Jordan, and A. Wolszczan. "The Proper Motion, Age, and Initial Spin Period of PSR J0538+2817 in S147." In: *The Astrophysical Journal* 593.1 (Aug. 2003), pp. L31–L34. DOI: 10.1086/378082. arXiv: astro-ph/0306628 [astro-ph].

[213] M. Kramer et al. "Tests of General Relativity from Timing the Double Pulsar." In: *Science* 314.5796 (Oct. 2006), pp. 97–102. DOI: 10.1126/science.1132305. arXiv: astro-ph/0609417 [astro-ph].

[214] Michael Kramer and David J. Champion. "The European Pulsar Timing Array and the Large European Array for Pulsars." In: *Classical and Quantum Gravity* 30.22, 224009 (Nov. 2013), p. 224009. DOI: 10.1088/0264-9381/30/22/224009.

[215] P. Kroupa, C. A. Tout, and G. Gilmore. "The distribution of low-mass stars in the Galactic disc." In: *Monthly Notices of the Royal Astronomical Society* 262 (June 1993), pp. 545–587. DOI: 10.1093/mnras/262.3.545.

[216] Pavel Kroupa. "On the variation of the initial mass function." In: *Monthly Notices of the Royal Astronomical Society* 322.2 (2001), pp. 231–246. DOI: 10.1046/j.1365-8711.2001.04022.x. eprint: /oup/backfile/content_public/journal/mnras/322/2/10.1046/j.1365-8711.2001.04022.x/2/322-2-231.pdf. URL: http://dx.doi.org/10.1046/j.1365-8711.2001.04022.x.

[217] J. M. Diederik Kruijssen. "Globular clusters as the relics of regular star formation in 'normal' high-redshift galaxies." In: *Monthly Notices of the Royal Astronomical Society* 454.2 (Dec. 2015), pp. 1658–1686. DOI: 10.1093/mnras/stv2026. arXiv: 1509.02163 [astro-ph.GA].

[218] K. Kuijken and G. Gilmore. "The mass distribution in the galactic disc -II. Determination of the surface mass density of the galactic disc near the Sun." In: *Monthly Notices of the Royal Astronomical Society* 239 (Aug. 1989), pp. 605–649. DOI: 10.1093/mnras/239.2.605.

[219] L. D. Landau. "To the Stars theory." In: *Phys. Zs. Sowjet* 1 (Dec. 1932), p. 285.

[220] Muhammad A. Latif and Andrea Ferrara. "Formation of Supermassive Black Hole Seeds." In: *Publications of the Astronomical Society of Australia* 33, e051 (Oct. 2016), e051. DOI: 10.1017/pasa.2016.41. arXiv: 1605.07391 [astro-ph.GA].

[221] James M. Lattimer and Madappa Prakash. "The equation of state of hot, dense matter and neutron stars." In: *Physics Reports* 621 (Mar. 2016), pp. 127–164. DOI: 10.1016/j.physrep.2015.12.005. arXiv: 1512.07820 [astro-ph.SR].

[222] T. J. W. Lazio and J. M. Cordes. "Hyperstrong Radio-Wave Scattering in the Galactic Center. II. A Likelihood Analysis of Free Electrons in the Galactic Center." In: *The Astrophysical Journal* 505 (Oct. 1998), pp. 715–731. DOI: 10.1086/306174. eprint: astro-ph/9804157.

[223] Dacheng Lin et al. "A luminous X-ray outburst from an intermediate-mass black hole in an off-centre star cluster." In: *Nature Astronomy* 2 (June 2018), pp. 656–661. DOI: 10.1038/s41550-018-0493-1. arXiv: 1806.05692 [astro-ph.HE].

[224] X. J. Liu, C. G. Bassa, and B. W. Stappers. "High-precision pulsar timing and spin frequency second derivatives." In: *Monthly Notices of the Royal Astronomical Society* 478 (Aug. 2018), pp. 2359–2367. DOI: 10.1093/mnras/sty1202. arXiv: 1805.02892 [astro-ph.HE].

[225] Giuseppe Lodato and Priyamvada Natarajan. "Supermassive black hole formation during the assembly of pre-galactic discs." In: *Monthly Notices of the Royal Astronomical Society* 371.4 (Oct. 2006), pp. 1813–1823. DOI: 10.1111/j.1365-2966.2006.10801.x. arXiv: astro-ph/0606159 [astro-ph].

[226] Abraham Loeb and Frederic A. Rasio. "Collapse of Primordial Gas Clouds and the Formation of Quasar Black Holes." In: *The Astrophysical Journal* 432 (Sept. 1994), p. 52. DOI: 10.1086/174548. arXiv: astro-ph/9401026 [astro-ph].

[227] H. H. Loose, E. Kruegel, and A. Tutukov. "Bursts of star formation in the galactic centre." In: *Astronomy and Astrophysics* 105 (Jan. 1982), pp. 342–350.

[228] D. R. Lorimer and M. Kramer. *Handbook of Pulsar Astronomy*. Cambridge, UK: Cambridge University Press, 2005.

[229] D. R. Lorimer et al. "The Parkes Multibeam Pulsar Survey - VI. Discovery and timing of 142 pulsars and a Galactic population analysis." In: *Monthly Notices of the Royal Astronomical Society* 372 (Oct. 2006), pp. 777–800. DOI: 10.1111/j.1365-2966.2006.10887.x. eprint: astro-ph/0607640.

[230] Ting-Ni Lu and Albert K. H. Kong. "Radio Continuum Observations of 47 Tucanae and ω Centauri: Hints for Intermediate-mass Black Holes?" In: *The Astrophysical Journal Letters* 729.2, L25 (Mar. 2011), p. L25. DOI: 10.1088/2041-8205/729/2/L25. arXiv: 1102.1668 [astro-ph.SR].

[231] Phyllis M. Lugger, Haldan N. Cohn, and Jonathan E. Grindlay. "CCD Photometry of Globular Cluster Core Structure. II. U-Band Profiles for 15 Candidate Collapsed-Core Clusters." In: *The Astrophysical Journal* 439 (Jan. 1995), p. 191. DOI: 10.1086/175164.

[232] N. Lützgendorf, M. Kissler-Patig, K. Gebhardt, H. Baumgardt, E. Noyola, P. T. de Zeeuw, N. Neumayer, B. Jalali, and A. Feldmeier. "Limits on intermediate-mass black holes in six Galactic globular clusters with integral-field spectroscopy." In: *Astronomy and Astrophysics* 552, A49 (Apr. 2013), A49. DOI: 10.1051/0004-6361/201220307. arXiv: 1212.3475 [astro-ph.GA].

[233] Nora Lützgendorf, Karl Gebhardt, Holger Baumgardt, Eva Noyola, Nadine Neumayer, Markus Kissler-Patig, and Tim de Zeeuw. "Re-evaluation of the central velocity-dispersion profile in NGC 6388." In: *Astronomy and Astrophysics* 581, A1 (Sept. 2015), A1. DOI: 10.1051/0004-6361/201425524. arXiv: 1507.02813 [astro-ph.GA].

[234] Ryan S. Lynch, Paulo C. C. Freire, Scott M. Ransom, and Bryan A. Jacoby. "The Timing of Nine Globular Cluster Pulsars." In: *The Astrophysical Journal* 745, 109 (Feb. 2012), p. 109. DOI: 10.1088/0004-637X/745/2/109. arXiv: 1112.2612 [astro-ph.HE].

[235] A. G. Lyne, R. N. Manchester, and J. H. Taylor. "The galactic population of pulsars." In: *Monthly Notices of the Royal Astronomical Society* 213 (Apr. 1985), pp. 613–639. DOI: 10.1093/mnras/213.3.613.

[236] A. G. Lyne and F. Graham Smith. "Pulsar rotation measures and the galactic magnetic field." In: *Monthly Notices of the Royal Astronomical Society* 237 (Mar. 1989), pp. 533–541. DOI: 10.1093/mnras/237.3.533.

[237] A. G. Lyne, A. Brinklow, J. Middleditch, S. R. Kulkarni, and D. C. Backer. "The discovery of a millisecond pulsar in the globular cluster M28." In: *Nature* 328.6129 (July 1987), pp. 399–401. DOI: 10.1038/328399a0.

[238] A. G. Lyne, R. N. Manchester, D. R. Lorimer, M. Bailes, N. D'Amico, T. M. Tauris, S. Johnston, J. F. Bell, and L. Nicastro. "The Parkes Southern Pulsar Survey - II. Final results and population analysis." In: *Monthly Notices of the Royal Astronomical Society* 295 (Apr. 1998), pp. 743–755. DOI: 10.1046/j.1365-8711.1998.01144.x.

[239] A. G. Lyne, C. A. Jordan, F. Graham-Smith, C. M. Espinoza, B. W. Stappers, and P. Weltevrede. "45 years of rotation of the Crab pulsar." In: *Monthly Notices of the Royal Astronomical Society* 446.1 (Jan. 2015), pp. 857–864. DOI: 10.1093/mnras/stu2118. arXiv: 1410.0886 [astro-ph.HE].

[240] T. J. Maccarone. "Radio emission as a test of the existence of intermediate-mass black holes in globular clusters and dwarf spheroidal galaxies." In: *Monthly Notices of the Royal Astronomical Society* 351 (July 2004), pp. 1049–1053. DOI: 10.1111/j.1365-2966.2004.07859.x. eprint: astro-ph/0403530.

[241] T. J. Maccarone and M. Servillat. "Radio observations of NGC 2808 and other globular clusters: constraints on intermediate-mass black holes." In: *Monthly Notices of the Royal Astronomical Society* 389 (Sept. 2008), pp. 379–384. DOI: 10.1111/j.1365-2966.2008.13577.x. arXiv: 0806.2387.

[242] T. J. Maccarone and M. Servillat. "Erratum: Radio observations of NGC 2808 and other globular clusters: constraints on intermediate-mass black holes." In: *Monthly Notices of the Royal Astronomical Society* 408 (Nov. 2010), pp. 2511–2512. DOI: 10.1111/j.1365-2966.2010.16948.x.

[243] J.-P. Macquart and N. Kanekar. "On Detecting Millisecond Pulsars at the Galactic Center." In: *The Astrophysical Journal* 805, 172 (June 2015), p. 172. DOI: 10.1088/0004-637X/805/2/172. arXiv: 1504.02492 [astro-ph.HE].

[244] J.-P. Macquart, N. Kanekar, D. A. Frail, and S. M. Ransom. "A High-frequency Search for Pulsars within the Central Parsec of Sgr A*." In: *The Astrophysical Journal* 715 (June 2010), pp. 939–946. DOI: 10.1088/0004-637X/715/2/939. arXiv: 1004.1643.

[245] Piero Madau and Martin J. Rees. "Massive Black Holes as Population III Remnants." In: *The Astrophysical Journal Letters* 551.1 (Apr. 2001), pp. L27–L30. DOI: 10.1086/319848. arXiv: astro-ph/0101223 [astro-ph].

[246] Igor F. Malov and Maria A. Timirkeeva. "On X-ray emission of radio pulsars." In: *Monthly Notices of the Royal Astronomical Society* 485.4 (June 2019), pp. 5319–5328. DOI: 10.1093/mnras/stz612. arXiv: 1808.07361 [astro-ph.HE].

[247] R. N. Manchester. "Pulsar Rotation and Dispersion Measures and the Galactic Magnetic Field." In: *The Astrophysical Journal* 172 (Feb. 1972), p. 43. DOI: 10.1086/151326.

[248] R. N. Manchester, A. G. Lyne, N. D'Amico, S. Johnston, J. Lim, and D. A. Kniffen. "A 5.75-millisecond pulsar in the globular cluster 47 Tucanae." In: *Nature* 345.6276 (June 1990), pp. 598–600. DOI: 10.1038/345598a0.

[249] R. N. Manchester, A. G. Lyne, C. Robinson, N. D'Amico, M. Bailes, and J. Lim. "Discovery of ten millisecond pulsars in the globular cluster 47 Tucanae." In: *Nature* 352.6332 (July 1991), pp. 219–221. DOI: 10.1038/352219a0.

[250] R. N. Manchester, G. B. Hobbs, A. Teoh, and M. Hobbs. "The Australia Telescope National Facility Pulsar Catalogue." In: *The Astronomical Journal* 129.4 (Apr. 2005), pp. 1993–2006. DOI: 10.1086/428488. arXiv: astro-ph/0412641 [astro-ph].

[251] R. N. Manchester et al. "The Parkes Pulsar Timing Array Project." In: *Publications of the Astronomical Society of Australia* 30, e017 (Jan. 2013), e017. DOI: 10.1017/pasa.2012.017. arXiv: 1210.6130 [astro-ph.IM].

[252] Richard N. Manchester and Joseph H. Taylor. *Pulsars*. W. H. Freeman, 1977.

[253] S. A. Mao, B. M. Gaensler, S. Stanimirović, M. Haverkorn, N. M. McClure-Griffiths, L. Staveley-Smith, and J. M. Dickey. "A Radio and Optical Polarization Study of the Magnetic Field in the Small Magellanic Cloud." In: *The Astrophysical Journal* 688.2 (Dec. 2008), pp. 1029–1049. DOI: 10.1086/590546. arXiv: 0807.1532 [astro-ph].

[254] S. A. Mao, B. M. Gaensler, M. Haverkorn, E. G. Zweibel, G. J. Madsen, N. M. McClure-Griffiths, A. Shukurov, and P. P. Kronberg. "A Survey of Extragalactic Faraday Rotation at High Galactic Latitude: The Vertical Magnetic Field of the Milky Way Toward the Galactic Poles." In: *The Astrophysical Journal* 714.2 (May 2010), pp. 1170–1186. DOI: 10.1088/0004-637X/714/2/1170. arXiv: 1003.4519 [astro-ph.GA].

[255] M. Mapelli and A. Gualandris. "Star Formation and Dynamics in the Galactic Centre." In: *Lecture Notes in Physics, Berlin Springer Verlag*. Ed. by F. Haardt, V. Gorini, U. Moschella, A. Treves, and M. Colpi. Vol. 905. Lecture Notes in Physics, Berlin Springer Verlag. 2016, p. 205. DOI: 10.1007/978-3-319-19416-5_6. arXiv: 1505.05473.

[256] E. Marinari and G. Parisi. "Simulated tempering: a new Monte Carlo scheme." In: *EPL (Europhysics Letters)* 19 (July 1992), p. 451. DOI: 10.1209/0295-5075/19/6/002. eprint: hep-lat/9205018.

[257] O. Maron, J. Kijak, M. Kramer, and R. Wielebinski. "Pulsar spectra of radio emission." In: *Astronomy and Astrophysics Supplements* 147 (Dec. 2000), pp. 195–203. DOI: 10.1051/aas:2000298. arXiv: astro-ph/0010233 [astro-ph].

[258] J. G. Martinez, K. Stovall, P. C. C. Freire, J. S. Deneva, F. A. Jenet, M. A. McLaughlin, M. Bagchi, S. D. Bates, and A. Ridolfi. "Pulsar J0453+1559: A Double Neutron Star System with a Large Mass Asymmetry." In: *The Astrophysical Journal* 812.2, 143 (Oct. 2015), p. 143. DOI: 10.1088/0004-637X/812/2/143. arXiv: 1509.08805 [astro-ph.HE].

[259] I. McDonald and A. A. Zijlstra. "Globular cluster interstellar media: ionized and ejected by white dwarfs." In: *Monthly Notices of the Royal Astronomical Society* 446.3 (Jan. 2015), pp. 2226–2242. DOI: 10.1093/mnras/stu2202. arXiv: 1410.5433 [astro-ph.SR].

[260] I. McDonald, M. L. Boyer, J. Th. van Loon, and A. A. Zijlstra. "Dust Production and Mass Loss in the Galactic Globular Cluster 47 Tucanae." In: *The Astrophysical Journal* 730.2, 71 (Apr. 2011), p. 71. DOI: 10.1088/0004-637X/730/2/71. arXiv: 1101.1096 [astro-ph.SR].

[261] D. E. McLaughlin, A. R. King, and S. Nayakshin. "The M-σ Relation for Nucleated Galaxies." In: *The Astrophysical Journal Letters* 650 (Oct. 2006), pp. L37–L40. DOI: 10.1086/508627. eprint: astro-ph/0608521.

[262] D. E. McLaughlin and R. P. van der Marel. "Resolved Massive Star Clusters in the Milky Way and Its Satellites: Brightness Profiles and a Catalog of Fundamental Parameters." In: *The Astrophysical Journal Supplements* 161 (Dec. 2005), pp. 304–360. DOI: 10.1086/497429. eprint: astro-ph/0605132.

[263] D. E. McLaughlin, J. Anderson, G. Meylan, K. Gebhardt, C. Pryor, D. Minniti, and S. Phinney. "Hubble Space Telescope Proper Motions and Stellar Dynamics in the Core of the Globular Cluster 47 Tucanae." In: *The Astrophysical Journal Suppelement Series* 166 (Sept. 2006), pp. 249–297. DOI: 10.1086/505692. eprint: astro-ph/0607597.

[264] Bernard J. McNamara, Thomas E. Harrison, Holger Baumgardt, and Pouria Khalaj. "A Search for an Intermediate-mass Black Hole in the Core of the Globular Cluster NGC 6266." In: *The Astrophysical Journal* 745.2, 175 (Feb. 2012), p. 175. DOI: 10.1088/0004-637X/745/2/175.

[265] A. Merloni, S. Heinz, and T. di Matteo. "A Fundamental Plane of black hole activity." In: *Monthly Notices of the Royal Astronomical Society* 345 (Nov. 2003), pp. 1057–1076. DOI: 10.1046/j.1365-2966.2003.07017.x. eprint: astro-ph/0305261.

[266] D. Merritt. "The Distribution of Stars and Stellar Remnants at the Galactic Center." In: *The Astrophysical Journal* 718 (Aug. 2010), pp. 739–761. DOI: 10.1088/0004-637X/718/2/739. arXiv: 0909.1318.

[267] M. Mezcua. "Observational evidence for intermediate-mass black holes." In: *International Journal of Modern Physics D* 26, 1730021 (2017), p. 1730021. DOI: 10.1142/S021827181730021X. arXiv: 1705.09667.

[268] R. W. Michie. "On the distribution of high energy stars in spherical stellar systems." In: *Monthly Notices of the Royal Astronomical Society* 125 (Jan. 1963), p. 127. DOI: 10.1093/mnras/125.2.127.

[269] J. C. A. Miller-Jones et al. "The Absence of Radio Emission from the Globular Cluster G1." In: *The Astrophysical Journal Letters* 755.1, L1 (Aug. 2012), p. L1. DOI: 10.1088/2041-8205/755/1/L1. arXiv: 1206.5729 [astro-ph.HE].

[270] A. P. Milone et al. "Multiple Stellar Populations in 47 Tucanae." In: *The Astrophysical Journal* 744.1, 58 (Jan. 2012), p. 58. DOI: 10.1088/0004-637X/744/1/58. arXiv: 1109.0900 [astro-ph.SR].

[271] M. Milosavljević. "On the Origin of Nuclear Star Clusters in Late-Type Spiral Galaxies." In: *The Astrophysical Journal Letters* 605 (Apr. 2004), pp. L13–L16. DOI: 10.1086/420696. eprint: astro-ph/0310574.

[272] P. Miocchi, B. Lanzoni, F. R. Ferraro, E. Dalessand ro, E. Vesperini, M. Pasquato, G. Beccari, C. Pallanca, and N. Sanna. "Star Count Density Profiles and Structural Parameters of 26 Galactic Globular Clusters." In: *The Astrophysical Journal* 774, 151 (Sept. 2013), p. 151. DOI: 10.1088/0004-637X/774/2/151. arXiv: 1307.6035 [astro-ph.GA].

[273] M. P. Muno, J. R. Lu, F. K. Baganoff, W. N. Brandt, G. P. Garmire, A. M. Ghez, S. D. Hornstein, and M. R. Morris. "A Remarkable Low-Mass X-Ray Binary within 0.1 Parsecs of the Galactic Center." In: *The Astrophysical Journal* 633 (Nov. 2005), pp. 228–239. DOI: 10.1086/444586. eprint: astro-ph/0503572.

[274] J. Naghizadeh-Khouei and D. Clarke. "On the statistical behaviour of the position angle of linear polarization." In: *Astronomy and Astrophysics* 274 (July 1993), p. 968.

[275] D. J. Nice and J. H. Taylor. "PSR J2019+2425 and PSR J2322+2057 and the Proper Motions of Millisecond Pulsars." In: *The Astrophysical Journal* 441 (Mar. 1995), p. 429. DOI: 10.1086/175367.

[276] K. Nitadori and S. J. Aarseth. "Accelerating NBODY6 with graphics processing units." In: *Monthly Notices of the Royal Astronomical Society* 424 (July 2012), pp. 545–552. DOI: 10.1111/j.1365-2966.2012.21227.x. arXiv: 1205.1222 [astro-ph.IM].

[277] Keigo Nitadori and Junichiro Makino. "Sixth- and eighth-order Hermite integrator for N-body simulations." In: *New Astronomy* 13 (Oct. 2008), pp. 498–507. DOI: 10.1016/j.newast.2008.01.010. arXiv: 0708.0738 [astro-ph].

[278] A. Noutsos, S. Johnston, M. Kramer, and A. Karastergiou. "New pulsar rotation measures and the Galactic magnetic field." In: *Monthly Notices of the Royal Astronomical Society* 386.4 (June 2008), pp. 1881–1896. DOI: 10.1111/j.1365-2966.2008.13188.x. arXiv: 0803.0677 [astro-ph].

[279] E. Noyola, K. Gebhardt, and M. Bergmann. "Gemini and Hubble Space Telescope Evidence for an Intermediate-Mass Black Hole in ω Centauri." In: *The Astrophysical Journal* 676, 1008-1015 (Apr. 2008), pp. 1008–1015. DOI: 10.1086/529002. arXiv: 0801.2782.

[280] Eva Noyola and Karl Gebhardt. "Surface Brightness Profiles of Galactic Globular Clusters from Hubble Space Telescope Images." In: *The Astronomical Journal* 132 (Aug. 2006), pp. 447–466. DOI: 10.1086/505390. arXiv: astro-ph/0604251 [astro-ph].

[281] Eva Noyola, Karl Gebhardt, Markus Kissler-Patig, Nora Lützgendorf, Behrang Jalali, P. Tim de Zeeuw, and Holger Baumgardt. "Very Large Telescope Kinematics for Omega Centauri: Further Support for a Central Black Hole." In: *The Astrophysical Journal Letters* 719.1 (Aug. 2010), pp. L60–L64. DOI: 10.1088/2041-8205/719/1/L60. arXiv: 1007.4559 [astro-ph.GA].

[282] J. R. Oppenheimer and G. M. Volkoff. "On Massive Neutron Cores." In: *Physical Review* 55.4 (Feb. 1939), pp. 374–381. DOI: 10.1103/PhysRev.55.374.

[283] N. Oppermann et al. "Estimating extragalactic Faraday rotation." In: *Astronomy and Astrophysics* 575, A118 (Mar. 2015), A118. DOI: 10.1051/0004-6361/201423995. arXiv: 1404.3701 [astro-ph.IM].

[284] Feryal Özel and Paulo Freire. "Masses, Radii, and the Equation of State of Neutron Stars." In: *Annual Review of Astronomy and Astrophysics* 54 (Sept. 2016), pp. 401–440. DOI: 10.1146/annurev-astro-081915-023322. arXiv: 1603.02698 [astro-ph.HE].

[285] Z. Pan, G. Hobbs, D. Li, A. Ridolfi, P. Wang, and P. Freire. "Discovery of two new pulsars in 47 Tucanae (NGC 104)." In: *Monthly Notices of the Royal Astronomical Society* 459.1 (June 2016), pp. L26–L30. DOI: 10.1093/mnrasl/slw037. arXiv: 1603.01348 [astro-ph.HE].

[286] A. Papitto et al. "Swings between rotation and accretion power in a binary millisecond pulsar." In: *Nature* 501.7468 (Sept. 2013), pp. 517–520. DOI: 10.1038/nature12470. arXiv: 1305.3884 [astro-ph.HE].

[287] C. Pepe and L. J. Pellizza. "Synthetic extinction maps around intermediate-mass black holes in Galactic globular clusters." In: *Monthly Notices of the Royal Astronomical Society* 460.3 (Aug. 2016), pp. 2542–2551. DOI: 10.1093/mnras/stw1095. arXiv: 1605.03536 [astro-ph.GA].

[288] B. B. P. Perera, B. W. Stappers, A. G. Lyne, C. G. Bassa, I. Cognard, L. Guillemot, M. Kramer, G. Theureau, and G. Desvignes. "Erratum: Evidence for an intermediate-mass black hole in the globular cluster NGC 6624." In: *Monthly Notices of the Royal Astronomical Society* 471 (Oct. 2017), pp. 1258–1258. DOI: 10.1093/mnras/stx1236.

[289] B. B. P. Perera, B. W. Stappers, A. G. Lyne, C. G. Bassa, I. Cognard, L. Guillemot, M. Kramer, G. Theureau, and G. Desvignes. "Evidence for an intermediate-mass black hole in the globular cluster NGC 6624." In: *Monthly Notices of the Royal Astronomical Society* 468 (June 2017), pp. 2114–2127. DOI: 10.1093/mnras/stx501. arXiv: 1705.01612 [astro-ph.HE].

[290] H. B. Perets and A. Mastrobuono-Battisti. "Age and Mass Segregation of Multiple Stellar Populations in Galactic Nuclei and their Observational Signatures." In: *The Astrophysical Journal Letters* 784, L44 (Apr. 2014), p. L44. DOI: 10.1088/2041-8205/784/2/L44. arXiv: 1401.1824.

[291] E. Pfahl. "Total Numbers and the NS Retention Problem." In: *KITP Conference: Globular Clusters: Formation, Evolution and the Role of Compact Objects*. Jan. 2003.

[292] E. Pfahl and A. Loeb. "Probing the Spacetime around Sagittarius A* with Radio Pulsars." In: *The Astrophysical Journal* 615 (Nov. 2004), pp. 253–258. DOI: 10.1086/423975. eprint: astro-ph/0309744.

[293] E. Pfahl, S. Rappaport, and P. Podsiadlowski. "A Comprehensive Study of Neutron Star Retention in Globular Clusters." In: *The Astrophysical Journal* 573 (July 2002), pp. 283–305. DOI: 10.1086/340494. eprint: astro-ph/0106141.

[294] A. C. Phillips. *The physics of stars*. John Wiley and Sons, 1994.

[295] E. S. Phinney. "Pulsars as Probes of Globular Cluster Dynamics." In: *Structure and Dynamics of Globular Clusters*. Ed. by S. G. Djorgovski and Georges Meylan. Vol. 50. Astronomical Society of the Pacific Conference Series. Jan. 1993, p. 141.

[296] D. Pooley et al. "Dynamical Formation of Close Binary Systems in Globular Clusters." In: *The Astrophysical Journal Letters* 591 (July 2003), pp. L131–L134. DOI: 10.1086/377074. eprint: astro-ph/0305003.

[297] David Pooley and Saul Rappaport. "X-Rays from the Globular Cluster G1: Intermediate-Mass Black Hole or Low-Mass X-Ray Binary?" In: *The Astrophysical Journal Letters* 644.1 (June 2006), pp. L45–L48. DOI: 10.1086/505344. arXiv: astro-ph/0605049 [astro-ph].

[298] Simon F. Portegies Zwart and Stephen L. W. McMillan. "The Runaway Growth of Intermediate-Mass Black Holes in Dense Star Clusters." In: *The Astrophysical Journal* 576 (Sept. 2002), pp. 899–907. DOI: 10.1086/341798. arXiv: astro-ph/0201055 [astro-ph].

[299] Simon F. Portegies Zwart, Holger Baumgardt, Piet Hut, Junichiro Makino, and Stephen L. W. McMillan. "Formation of massive black holes through runaway collisions in dense young star clusters." In: *Nature* 428 (Apr. 2004), pp. 724–726. DOI: 10.1038/nature02448. arXiv: astro-ph/0402622 [astro-ph].

[300] A. Possenti, N. D'Amico, R. N. Manchester, F. Camilo, A. G. Lyne, J. Sarkissian, and A. Corongiu. "Three Binary Millisecond Pulsars in NGC 6266." In: *The Astrophysical Journal* 599 (Dec. 2003), pp. 475–484. DOI: 10.1086/379190. arXiv: astro-ph/0308372 [astro-ph].

[301] Brian J. Prager, Scott M. Ransom, Paulo C. C. Freire, Jason W. T. Hessels, Ingrid H. Stairs, Phil Arras, and Mario Cadelano. "Using Long-term Millisecond Pulsar Timing to Obtain Physical Characteristics of the Bulge Globular Cluster Terzan 5." In: *The Astrophysical Journal* 845, 148 (Aug. 2017), p. 148. DOI: 10.3847/1538-4357/aa7ed7. arXiv: 1612.04395 [astro-ph.SR].

[302] William Priestley, Maximilian Ruffert, and Maurizio Salaris. "On the evolution of intracluster gas within Galactic globular clusters." In: *Monthly Notices of the Royal Astronomical Society* 411.3 (Mar. 2011), pp. 1935–1952. DOI: 10.1111/j.1365-2966.2010.17822.x. arXiv: 1010.1532 [astro-ph.SR].

[303] V. Radhakrishnan and D. J. Cooke. "Magnetic Poles and the Polarization Structure of Pulsar Radiation." In: *Astrophysical Letters* 3 (Jan. 1969), p. 225.

[304] V. Radhakrishnan and Joanna M. Rankin. "Toward an Empirical Theory of Pulsar Emission. V. On the Circular Polarization in Pulsar Radiation." In: *The Astrophysical Journal* 352 (Mar. 1990), p. 258. DOI: 10.1086/168531.

[305] W. Reich, E. Fuerst, P. Reich, and K. Reif. "A radio continuum survey of the Galactic Plane at 11 CM wavelength. II - The area L = 358-76 deg, B = -5 to 5 deg. III." In: *Astronomy and Astrophysics Supplements* 85 (Oct. 1990), pp. 633–690.

[306] A. Ridolfi. "Long-term timing of pulsars in globular clusters." PhD thesis. Rheinischen Friedrich–Wilhelms–Universität, Bonn, 2017.

[307] A. Ridolfi et al. "Long-term observations of the pulsars in 47 Tucanae - I. A study of four elusive binary systems." In: *Monthly Notices of the Royal Astronomical Society* 462.3 (Nov. 2016), pp. 2918–2933. DOI: 10.1093/mnras/stw1850. arXiv: 1607.07248 [astro-ph.HE].

[308] Alessandro Ridolfi, Paulo C. C. Freire, Yashwant Gupta, and Scott M. Ransom. "Upgraded Giant Metrewave Radio Telescope timing of NGC 1851A: a possible millisecond pulsar-neutron star system." In: *arXiv e-prints*, arXiv:1909.06163 (Sept. 2019), arXiv:1909.06163. arXiv: 1909.06163 [astro-ph.HE].

[309] L. E. Rivera-Sandoval et al. "Discovery of near-ultraviolet counterparts to millisecond pulsars in the globular cluster 47 Tucanae." In: *Monthly Notices of the Royal Astronomical Society* 453.3 (Nov. 2015), pp. 2707–2717. DOI: 10.1093/mnras/stv1810. arXiv: 1508.05291 [astro-ph.SR].

[310] Morton S. Roberts. "Dust and gas in globular clusters." In: *Astronomical Journal* 65 (Oct. 1960), p. 457. DOI: 10.1086/108288.

[311] Clive Robinson, A. G. Lyne, R. N. Manchester, M. Bailes, N. D'Amico, and S. Johnston. "Millisecond pulsars in the globular cluster 47 Tucanae." In: *Monthly Notices of the Royal Astronomical Society* 274.2 (May 1995), pp. 547–554. DOI: 10.1093/mnras/274.2.547.

[312] Sathyaprakash, B. et al. "Scientific Potential of Einstein Telescope." In: *ArXiv e-prints* (Aug. 2011). arXiv: 1108.1423 [gr-qc].

[313] D. H. F. M. Schnitzeler. "The latitude dependence of the rotation measures of NVSS sources." In: *Monthly Notices of the Royal Astronomical Society* 409.1 (Nov. 2010), pp. L99–L103. DOI: 10.1111/j.1745-3933.2010.00957.x. arXiv: 1011.0737 [astro-ph.GA].

[314] R. Schödel, T. Ott, R. Genzel, A. Eckart, N. Mouawad, and T. Alexander. "Stellar Dynamics in the Central Arcsecond of Our Galaxy." In: *The Astrophysical Journal* 596 (Oct. 2003), pp. 1015–1034. DOI: 10.1086/378122. eprint: astro-ph/0306214.

[315] R. Schödel, A. Feldmeier, D. Kunneriath, S. Stolovy, N. Neumayer, P. Amaro-Seoane, and S. Nishiyama. "Surface brightness profile of the Milky Way's nuclear star cluster." In: *Astronomy and Astrophysics* 566, A47 (June 2014), A47. DOI: 10.1051/0004-6361/201423481. arXiv: 1403.6657.

[316] E. H. Scott and R. H. Durisen. "Nova-driven winds in globular clusters." In: *The Astrophysical Journal* 222 (June 1978), pp. 612–620. DOI: 10.1086/156177.

[317] J. H. Seiradakis, J. A. Gil, D. A. Graham, A. Jessner, M. Kramer, V. M. Malofeev, W. Sieber, and R. Wielebinski. "Pulsar profiles at high frequencies. I. The data." In: *Astronomy and Astrophysics Supplements* 111 (June 1995), p. 205.

[318] G. Shaifullah et al. "21 year timing of the black-widow pulsar J2051-0827." In: *Monthly Notices of the Royal Astronomical Society* 462 (Oct. 2016), pp. 1029–1038. DOI: 10.1093/mnras/stw1737. arXiv: 1607.04167 [astro-ph.HE].

[319] Irwin I. Shapiro. "Fourth Test of General Relativity." In: *Physical Review Letters* 13.26 (Dec. 1964), pp. 789–791. DOI: 10.1103/PhysRevLett.13.789.

[320] S. Sharma, J. Bland-Hawthorn, J. Binney, K. C. Freeman, M. Steinmetz, C. Boeche, O. Bienaymé, B. K. Gibson, G. F. Gilmore, and E. K. Grebel. "Kinematic Modeling of the Milky Way Using the RAVE and GCS Stellar Surveys." In: *The Astrophysical Journal* 793.1, 51 (Sept. 2014), p. 51. DOI: 10.1088/0004-637X/793/1/51. arXiv: 1405.7435 [astro-ph.GA].

[321] A. Shearer and A. Golden. "Why study pulsars optically?" In: *Neutron Stars, Pulsars, and Supernova Remnants*. Ed. by W. Becker, H. Lesch, and J. Trümper. Jan. 2002, p. 44. arXiv: astro-ph/0208579 [astro-ph].

[322] I. S. Shklovskii. "Possible Causes of the Secular Increase in Pulsar Periods." In: *Soviet Astronomy* 13 (Feb. 1970), p. 562.

[323] Anvar Shukurov, Luiz Felippe S. Rodrigues, Paul J. Bushby, James Hollins, and Jörg P. Rachen. "A physical approach to modelling large-scale galactic magnetic fields." In: *Astronomy and Astrophysics* 623, A113 (Mar. 2019), A113. DOI: 10.1051/0004-6361/201834642. arXiv: 1809.03595 [astro-ph.GA].

[324] J. F. L. Simmons and B. G. Stewart. "Point and interval estimation of the true unbiased degree of linear polarization in the presence of low signal-to-noise ratios." In: *Astronomy and Astrophysics* 142.1 (Jan. 1985), pp. 100–106.

[325] A. C. Sippel and J. R. Hurley. "Multiple stellar-mass black holes in globular clusters: theoretical confirmation." In: *Monthly Notices of the Royal Astronomical Society* 430 (Mar. 2013), pp. L30–L34. DOI: 10.1093/mnrasl/sls044. arXiv: 1211.6608.

[326] Graeme H. Smith. "Globular Cluster Winds Driven by Main-Sequence Stars." In: *The Publications of the Astronomical Society of the Pacific* 111.762 (Aug. 1999), pp. 980–985. DOI: 10.1086/316410.

[327] Graeme H. Smith, Peter R. Wood, D. J. Faulkner, and Alan E. Wright. "Parkes H i Observations of Southern Globular Clusters: Implications for Stellar Mass Loss." In: *The Astrophysical Journal* 353 (Apr. 1990), p. 168. DOI: 10.1086/168603.

[328] D. N. Spergel. "Evacuation of gas from globular clusters by winds from millisecond pulsars." In: *Nature* 352.6332 (July 1991), pp. 221–222. DOI: 10.1038/352221a0.

[329] L. G. Spitler et al. "Pulse Broadening Measurements from the Galactic Center Pulsar J1745-2900." In: *The Astrophysical Journal Letters* 780, L3 (Jan. 2014), p. L3. DOI: 10.1088/2041-8205/780/1/L3. arXiv: 1309.4673 [astro-ph.HE].

[330] Lyman Spitzer. *Dynamical evolution of globular clusters*. Princeton Univeristy Press, 1987.

[331] David H. Staelin and III Reifenstein Edward C. "Pulsating Radio Sources near the Crab Nebula." In: *Science* 162.3861 (Dec. 1968), pp. 1481–1483. DOI: 10.1126/science.162.3861.1481.

[332] B. W. Stappers et al. "A State Change in the Missing Link Binary Pulsar System PSR J1023+0038." In: *The Astrophysical Journal* 790.1, 39 (July 2014), p. 39. DOI: 10.1088/0004-637X/790/1/39. arXiv: 1311.7506 [astro-ph.HE].

[333] B. Stappers and M. Kramer. "An Update on TRAPUM." In: *Proceedings of MeerKAT Science: On the Pathway to the SKA. 25-27 May*. Jan. 2016, p. 9.

[334] L. Staveley-Smith et al. "The Parkes 21 CM multibeam receiver." In: *Publications of the Astronomical Society of Australia* 13.3 (Nov. 1996), pp. 243–248.

[335] G. G. Stokes. "On the Composition and Resolution of Streams of Polarized Light from different Sources." In: *Transactions of the Cambridge Philosophical Society* 9 (Jan. 1851), p. 399.

[336] A. Suresh and J. M. Cordes. "Induced Polarization from Birefringent Pulse Splitting in Magneto-ionic Media." In: *The Astrophysical Journal* 870.1, 29 (Jan. 2019), p. 29. DOI: 10.3847/1538-4357/aaf004. arXiv: 1808.09471 [astro-ph.HE].

[337] R. E. Taam and E. P. J. van den Heuvel. "Magnetic Field Decay and the Origin of Neutron Star Binaries." In: *The Astrophysical Journal* 305 (June 1986), p. 235. DOI: 10.1086/164243.

[338] C. M. Tan, C. G. Bassa, S. Cooper, T. J. Dijkema, P. Esposito, J. W. T. Hessels, V. I. Kondratiev, M. Kramer, D. Michilli, and S. Sanidas. "LOFAR Discovery of a 23.5 s Radio Pulsar." In: *The Astrophysical Journal* 866.1, 54 (Oct. 2018), p. 54. DOI: 10.3847/1538-4357/aade88. arXiv: 1809.00965 [astro-ph.HE].

[339] Philippe Terral and Katia Ferrière. "Constraints from Faraday rotation on the magnetic field structure in the Galactic halo." In: *Astronomy and Astrophysics* 600, A29 (Apr. 2017), A29. DOI: 10.1051/0004-6361/201629572. arXiv: 1611.10222 [astro-ph.GA].

[340] C. Tiburzi et al. "The High Time Resolution Universe survey - IX. Polarimetry of long-period pulsars." In: *Monthly Notices of the Royal Astronomical Society* 436.4 (Dec. 2013), pp. 3557–3572. DOI: 10.1093/mnras/stt1834. arXiv: 1310.1823 [astro-ph.SR].

[341] Jaap Tinbergen. *Astronomical Polarimetry*. Cambridge University Press, 1996.

[342] M. Toscano, M. Bailes, R. N. Manchester, and J. S. Sandhu. "Spectra of Southern Pulsars." In: *The Astrophysical Journal* 506 (Oct. 1998), pp. 863–867. DOI: 10.1086/306282. eprint: astro-ph/9805241.

[343] S. D. Tremaine, J. P. Ostriker, and L. Spitzer Jr. "The formation of the nuclei of galaxies. I - M31." In: *The Astrophysical Journal* 196 (Mar. 1975), pp. 407–411. DOI: 10.1086/153422.

[344] Evangelia Tremou et al. "The MAVERIC Survey: Still No Evidence for Accreting Intermediate-mass Black Holes in Globular Clusters." In: *The Astrophysical Journal* 862.1, 16 (July 2018), p. 16. DOI: 10.3847/1538-4357/aac9b9. arXiv: 1806.00259 [astro-ph.HE].

[345] Michele Trenti and Roeland van der Marel. "No energy equipartition in globular clusters." In: *Monthly Notices of the Royal Astronomical Society* 435.4 (Nov. 2013), pp. 3272–3282. DOI: 10.1093/mnras/stt1521. arXiv: 1302.2152 [astro-ph.GA].

[346] A. Tsatsi, A. Mastrobuono-Battisti, G. van de Ven, H. B. Perets, P. Bianchini, and N. Neumayer. "On the rotation of nuclear star clusters formed by cluster inspirals." In: *Monthly Notices of the Royal Astronomical Society* 464 (Jan. 2017), pp. 3720–3727. DOI: 10.1093/mnras/stw2593. arXiv: 1610.01162.

[347] R. Tüllmann, R. J. Dettmar, M. Soida, M. Urbanik, and J. Rossa. "The thermal and non-thermal gaseous halo of NGC 5775." In: *Astronomy and Astrophysics* 364 (Dec. 2000), pp. L36–L41. arXiv: astro-ph/0010267 [astro-ph].

[348] Stefan Umbreit, Sourav Chatterjee, and Frederic A. Rasio. "Clearing the Dust from Globular Clusters." In: *The Astrophysical Journal Letters* 680.2 (June 2008), p. L113. DOI: 10.1086/590080. arXiv: 0805.2358 [astro-ph].

[349] M. Unger and G. R. Farrar. "Uncertainties in the Magnetic Field of the Milky Way." In: *35th International Cosmic Ray Conference (ICRC2017)*. Vol. 301. International Cosmic Ray Conference. Jan. 2017, p. 558. arXiv: 1707.02339 [astro-ph.GA].

[350] D. A. Vandenberg and D. J. Faulkner. "Gas in globular clusters. II. Time-dependent flow models." In: *The Astrophysical Journal* 218 (Dec. 1977), pp. 415–430. DOI: 10.1086/155695.

[351] Frank Verbunt and Paulo C. C. Freire. "On the disruption of pulsar and X-ray binar ies in globular clusters." In: *Astronomy and Astrophysics* 561, A11 (Jan. 2014), A11. DOI: 10.1051/0004-6361/201321177. arXiv: 1310.4669 [astro-ph.SR].

[352] Marta Volonteri. "Formation of supermassive black holes." In: *Astronomy and Astrophysics Review* 18 (July 2010), pp. 279–315. DOI: 10.1007/s00159-010-0029-x. arXiv: 1003.4404 [astro-ph.CO].

[353] Long Wang, Rainer Spurzem, Sverre Aarseth, Mirek Giersz, Abbas Askar, Peter Berczik, Thorsten Naab, Riko Schadow, and M. B. N. Kouwenhoven. "The DRAGON simulations: globular cluster evolution with a million stars." In: *Monthly Notices of the Royal Astronomical Society* 458.2 (May 2016), pp. 1450–1465. DOI: 10.1093/mnras/stw274. arXiv: 1602.00759 [astro-ph.SR].

[354] J. F. C. Wardle and P. P. Kronberg. "The linear polarization of quasi-stellar radio sources at 3.71 and 11.1 centimeters." In: *The Astrophysical Journal* 194 (Dec. 1974), pp. 249–255. DOI: 10.1086/153240.

[355] Laura L. Watkins, Roeland P. van der Marel, Andrea Bellini, and Jay Anderson. "Hubble Space Telescope Proper Motion (HSTPROMO) Catalogs of Galactic Globular Cluster. II. Kinematic Profiles and Maps." In: *The Astrophysical Journal* 803.1, 29 (Apr. 2015), p. 29. DOI: 10.1088/0004-637X/803/1/29. arXiv: 1502.00005 [astro-ph.GA].

[356] Patrick Weltevrede and Simon Johnston. "Profile and polarization characteristics of energetic pulsars." In: *Monthly Notices of the Royal Astronomical Society* 391.3 (Dec. 2008), pp. 1210–1226. DOI: 10.1111/j.1365-2966.2008.13950.x. arXiv: 0809.2438 [astro-ph].

[357] R. S. Wharton, S. Chatterjee, J. M. Cordes, J. S. Deneva, and T. J. W. Lazio. "Multiwavelength Constraints on Pulsar Populations in the Galactic Center." In: *The Astrophysical Journal* 753.2, 108 (July 2012), p. 108. DOI: 10.1088/0004-637X/753/2/108. arXiv: 1111.4216 [astro-ph.HE].

[358] Lawrence M. Widrow. "Origin of galactic and extragalactic magnetic fields." In: *Reviews of Modern Physics* 74.3 (Jan. 2002), pp. 775–823. DOI: 10.1103/RevModPhys.74.775. arXiv: astro-ph/0207240 [astro-ph].

[359] Dmitrii G. Yakovlev, Pawel Haensel, Gordon Baym, and Christopher Pethick. "Lev Landau and the concept of neutron stars." In: *Physics Uspekhi* 56.3, 289-295 (Mar. 2013), pp. 289–295. DOI: 10.3367/UFNe.0183.201303f.0307. arXiv: 1210.0682 [physics.hist-ph].

[360] W. M. Yan et al. "Rotation measure variations for 20 millisecond pulsars." In: *Astrophysics and Space Science* 335.2 (Oct. 2011), pp. 485–498. DOI: 10.1007/s10509-011-0756-0. arXiv: 1105.4213 [astro-ph.SR].

[361] J. M. Yao, R. N. Manchester, and N. Wang. "A New Electron-density Model for Estimation of Pulsar and FRB Distances." In: *The Astrophysical Journal* 835.1, 29 (Jan. 2017), p. 29. DOI: 10.3847/1538-4357/835/1/29. arXiv: 1610.09448 [astro-ph.GA].

[362] Claire S. Ye, Kyle Kremer, Sourav Chatterjee, Carl L. Rodriguez, and Frederic A. Rasio. "Millisecond Pulsars and Black Holes in Globular Clusters." In: *The Astrophysical Journal* 877.2, 122 (June 2019), p. 122. DOI: 10.3847/1538-4357/ab1b21. arXiv: 1902.05963 [astro-ph.HE].

[363] F. Yusef-Zadeh, M. Royster, M. Wardle, R. Arendt, H. Bushouse, D. C. Lis, M. W. Pound, D. A. Roberts, B. Whitney, and A. Wootten. "ALMA Observations of the Galactic Center: SiO Outflows and High-mass Star Formation near Sgr A*." In: *The Astrophysical Journal Letters* 767, L32 (Apr. 2013), p. L32. DOI: 10.1088/2041-8205/767/2/L32. arXiv: 1303.3403.

[364] R. Zinn. "The Globular Cluster System of the Galaxy. IV. The Halo and Disk Subsystems." In: *The Astrophysical Journal* 293 (June 1985), p. 424. DOI: 10.1086/163249.

[365] Jacco Th. van Loon, Snežana Stanimirović, A. Evans, and Erik Muller. "Stellar mass loss and the intracluster medium in Galactic globular clusters: a deep radio survey for HI and OH." In: *Monthly Notices of the Royal Astronomical Society* 365.4 (Feb. 2006), pp. 1277–1282. DOI: 10.1111/j.1365-2966.2005.09815.x. arXiv: astro-ph/0511118 [astro-ph].

[366] W. van Straten. "Radio Astronomical Polarimetry and Point-Source Calibration." In: *The Astrophysical Journal Supplements* 152.1 (May 2004), pp. 129–135. DOI: 10.1086/383187. arXiv: astro-ph/0401536 [astro-ph].

[367] W. van Straten. "Radio Astronomical Polarimetry and High-Precision Pulsar Timing." In: *The Astrophysical Journal* 642.2 (May 2006), pp. 1004–1011. DOI: 10.1086/501001. arXiv: astro-ph/0510334 [astro-ph].

[368] W. van Straten. "High-fidelity Radio Astronomical Polarimetry Using a Millisecond Pulsar as a Polarized Reference Source." In: *The Astrophysical Journal Supplements* 204.1, 13 (Jan. 2013), p. 13. DOI: 10.1088/0067-0049/204/1/13. arXiv: 1212.3446 [astro-ph.IM].

[369] Willem van Straten, Paul Demorest, and Stefan Oslowski. "Pulsar Data Analysis with PSRCHIVE." In: *Astronomical Research and Technology* 9.3 (July 2012), pp. 237–256. arXiv: 1205.6276 [astro-ph.IM].

[370] E. P. J. van den Heuvel. "The Formation and Evolution of Relativistic Binaries." In: *Physics of Relativistic Objects in Compact Binaries: From Birth to Coalescence*. Ed. by Monica Colpi, Piergiorgio Casella, Vittorio Gorini, Ugo Moschella, and Andrea Possenti. Vol. 359. Astrophysics and Space Science Library. Jan. 2009, p. 125. DOI: 10.1007/978-1-4020-9264-0_4.

[371] E. P. van den Heuvel, J. A. van Paradijs, and R. E. Taam. "Evidence for an asymptotic lower limit to the surface dipole magnetic field strengths of neutron stars." In: *Nature* 322.6075 (July 1986), pp. 153–155. DOI: 10.1038/322153a0.

[372] R. P. van der Marel and J. Anderson. "New Limits on an Intermediate-Mass Black Hole in Omega Centauri. II. Dynamical Models." In: *The Astrophysical Journal* 710 (Feb. 2010), pp. 1063–1088. DOI: 10.1088/0004-637X/710/2/1063. arXiv: 0905.0638 [astro-ph.GA].

[373] A. von Hoensbroech, H. Lesch, and T. Kunzl. "Natural polarization modes in pulsar magnetospheres." In: *Astronomy and Astrophysics* 336 (Aug. 1998), pp. 209–219. arXiv: astro-ph/9804318 [astro-ph].

ACKNOWLEDGMENTS

I acknowledge the support from the Ministero degli Affari Esteri della Cooperazione Internazionale - Direzione Generale per la Promozione del Sistema Paese - Progetto di Grande Rilevanza ZA18GR02. Part of this work has also been funded using resources from the research grant “iPeska” (P.I. A. Possenti) funded under the INAF national call Prin-SKA/CTA approved with the Presidential Decree 70/2016. The author would like to acknowledge the use of software created by the staff of the South African Radio Astronomy Observatory, a facility of the National Research Foundation (the "NRF"). It contains intellectual property owned by the NRF and the information contained herein is to be used exclusively for the purpose for which it was disclosed and may not be disclosed to anyone or be used for any purpose other than as set out above, without the NRF’s prior written consent. The author is indebted to the communities behind the multiple open-source software packages on which this work depended.

In the three long years that have passed since the start of my PhD I have been able to travel around the world, meet many new people and learn many new things. I am grateful for all of this to many people.

In particular, I would like to thank my tutor Monica Colpi for wanting me as her student and for pushing for many new collaborations that culminated in several published papers and for others that didn’t. Her enthusiasm for science is truly contagious, I hope that some of it will stick with me in the future.

The person that made all of this work possible was my supervisor Andrea Possenti. Starting from the Master’s thesis, he introduced me to the science of pulsars, envisioned the PhD research project and allowed me to collaborate with the MeerKAT telescope even going to South Africa several times to work with the team. To him I am indebted for passing on the love of pulsars.

I am grateful to the Astrophysics department in Bicocca who introduced me to climbing and organise every year very nice events for the European Researchers’ Night challenging me with fun and elaborate builds. Without any specific order, I would like to thank Alberto, Davide, Mery, Om, Claudio, Tullia, Massimo, Michela, Federico and many others.

The group at the Astronomical Observatory of Cagliari is fantastic. The group is filled with capable, passionate, and extremely friendly people. I owe a lot to them and would like to thank in particular

Alessandro R. Marta, Sabrina, Alessandro C., Maura, Elise, Delphine, Valentina, Francesca and the entire administrative office.

I would like to thank the South African Radio Astronomical Observatory for their hospitality during the many visits in these years, they are incredible people and highly skilled at their job. The success of the MeerKAT telescope is all thanks to their hard work and I am grateful to them for letting me participate. Some of the wonderful people I would like to thank are Mandy, Sarah, Marisa and Maciej.

In closing, I wanted remember with what I consider the best experience of my PhD: the visit to the MeerKAT telescope. It was an amazing experience. After a two days drive across dirt roads in the South African desert, seeing the antennas shine in the first rays of a dawning Sun was truly unforgettable. Thank you, Mandy for making it possible and thanks to all the members of the expedition: Alessandro, Paulo, Isabella, and Abu.